



HAL
open science

Design of algorithms for the automatic characterization of marine dune morphology and dynamics

Julien Ogor

► **To cite this version:**

Julien Ogor. Design of algorithms for the automatic characterization of marine dune morphology and dynamics. Ocean, Atmosphere. ENSTA Bretagne - École nationale supérieure de techniques avancées Bretagne, 2018. English. NNT : 2018ENTA0005 . tel-02354454

HAL Id: tel-02354454

<https://theses.hal.science/tel-02354454>

Submitted on 7 Nov 2019

HAL is a multi-disciplinary open access archive for the deposit and dissemination of scientific research documents, whether they are published or not. The documents may come from teaching and research institutions in France or abroad, or from public or private research centers.

L'archive ouverte pluridisciplinaire **HAL**, est destinée au dépôt et à la diffusion de documents scientifiques de niveau recherche, publiés ou non, émanant des établissements d'enseignement et de recherche français ou étrangers, des laboratoires publics ou privés.



université de bretagne
occidentale

UNIVERSITE
BRETAGNE
LOIRE

THESIS / ENSTA Bretagne

Under the seal of Bretagne Loire

To obtain the title of

DOCTOR of ENSTA Bretagne

Branch : Signal and Image Processing

Doctoral school MathSTIC - ED601

Presented by

Julien OGOR

Prepared at Ensta Bretagne (Lab-STICC,FR)

Design of algorithms for the
automatic characterization of marine
dune morphology and dynamics

Thesis to be defended on 11th June 2018

Before the jury composed of:

- **Luc Jaulin**, president of the jury
Professor, Lab-STICC, Brest, FR
- **Brian Calder**, reporter
Professor, CCOM, Durham, NH, USA
- **Frédéric Cazals**, reporter
Professor, Inria, Sophia Antipolis, FR
- **Carole Nahum**, examiner
PhD, DGA/DS/MRIS, Manager Domain Environment and
Geosciences, Bagneux, FR
- **Thierry Garlan**, examiner
Director of research, SHOM, Brest, FR
- **Marc Roche**, examiner (invited)
PhD, FPS Economy, Brussels, BE
- **Benoit Zerr**, thesis director
Professor, Lab-STICC, Brest, FR



École Doctorale MathSTIC - ED601

THÈSE DE DOCTORAT DE L'ENSTA BRETAGNE

Présentée par

Ogor Julien

Pour obtenir le titre de Docteur de l'ENSTA Bretagne

**Design of algorithms for the automatic
characterization of marine dune morphology and
dynamics.**

Travaux préparés au laboratoire STIC/OSM(Ocean Sensing and Mapping)
ENSTA Bretagne, Brest

September 14, 2018

Résumé

Les dunes marines sont de grandes structures sédimentaires qui, ensemble, couvrent de larges zones appelées champs de dunes. Des dunes ont été découvertes dans tous les océans, de la côte jusqu'aux talus continentaux. Leur forme et mobilité sont des témoins du lien étroit qui existe entre le transport sédimentaire, l'hydrodynamique (courants marins) et la topographie du fond. L'étude des dunes est intéressante scientifiquement parlant, mais elle est également motivée par des enjeux économiques et environnementaux. Les dunes peuvent être étudiées de deux manières: La modélisation et l'analyse de données de terrain (granulométrie, courantométrie, données sismiques, données bathymétriques). Ces deux approches sont très différentes mais complémentaires.

Avec l'amélioration des données Sondeur Multi-Faisceaux (SMF), il est maintenant possible de visualiser la morphologie des dunes et de suivre leur évolution de manière plus détaillée. Plusieurs méthodes automatiques d'analyse de la morphologie et de la dynamique des dunes ont été développées pour analyser les Modèles Numériques de Terrain (MNTs) construits à partir de ces données SMF. Pourtant, aucun ne permet d'estimer les valeurs de descripteurs morphologiques et dynamiques pour chaque dune. L'analyse et l'évaluation de ces descripteurs restent régionales avec le découpage des MNTs en régions rectangulaires. Seul un traitement manuel permet d'estimer ces descripteurs pour chaque dune.

L'objectif de cette thèse est de développer des algorithmes automatiques permettant de quantifier la morphologie et la dynamique de chaque dune. Pour ce faire, une représentation des données SMF sous forme d'une tessellation triangulaire a été préférée au classique MNT régulier. Tout d'abord, les dunes doivent être extraites de la topographie du fond marin.

Un algorithme par accroissement de régions avec adaptation de l'échelle d'analyse, issu de la géomorphométrie est proposé. Les crêtes de dunes sont d'abord extraites en combinant un algorithme de simplification de tessellations avec un algorithme d'extraction de lignes de crête. La résolution de la tessellation est adaptée par l'algorithme de simplification afin de faciliter l'extraction des lignes de crête. Les lignes de crête sont des objets bien définis en géométrie différentielle. Leur extraction s'appuie sur l'interprétation de cette définition appliquée à des modèles discrets du fond (tessellations). Les crêtes servent d'embryons à l'algorithme d'extraction des dunes.

L'estimation des paramètres morphologiques des dunes (longueur, largeur, hauteur, *etc.*) découle de l'extraction automatique des dunes. L'utilisation d'une méthode de recalage non rigide (isométrique) pour la quantification de la dynamique est discutée. Des tessellations représentant la topographie d'un même champ de dunes à différents moments sont analysées par l'algorithme d'extraction des dunes. Ensuite, une dune est associée à une dune d'une autre tessellation qui lui correspond (même dune à un autre instant). La dynamique de chaque dune est quantifiée à partir des résultats de l'algorithme de recalage: les transformations permettant d'aligner différentes représentations d'une dune.

Mots clés: Dunes marines, morphologie des dunes, dynamique des dunes, algorithmes automatiques, données SMF, tessellation triangulaire, géomorphométrie, recalage non rigide.

Abstract

Marine dunes are large sedimentary mounds often organized in dunefields. They have been discovered in oceans all around the globe, from continental rises to nearshore areas. These mobile seafloor structures reflect the unique and complex relationship between the sediment, the seafloor topography and the hydrodynamics (currents). Dunes are not only interesting at a scientific level. In fact, their study is also motivated by economic, safety and environmental reasons. The study of dunes can be divided into two complementary approaches: Modelling and analysis of *in situ* data (granulometry, current, bathymetric data).

The increased quality of MultiBeam EchoSounder (MBES) data allows scientists to monitor and visualize the complexity of, both, dune morphology and dynamics. Automatic methods to characterize dune morphology and dynamics using Digital Terrain Models (DTMs) have already been proposed. But, none does it at the dune scale. Morphological and dynamical descriptors are estimated for patches of the dunefield. Today, the evaluation of such descriptors for each dune can only be achieved manually.

The objective of this thesis is to design automatic algorithms for the quantification of dune morphology and dynamics. A representation of MBES data as triangular meshes has been preferred to the usual gridded DTMs. The first stage consists of delineating dunes in the seafloor. A scale adaptative, region growing algorithm based on geomorphometry is proposed. The combination of mesh simplification and crest extraction algorithms enables to accurately recover dune crest lines. The mesh simplification facilitates the crest extraction by adapting the mesh resolution. Crest extraction is based on the discrete interpretation of the definition of crest lines in differential geometry. The crests are, then, used as seed regions by the dune extraction algorithm.

The evaluation of dune morphological attributes (length, width, height, *etc.*) naturally derives from the automatic dune extraction. The quantification of dune dynamics is realized using a non-rigid (isometric) registration approach. Datasets of a same dune-field acquired at different times are analyzed with the dune extraction algorithm. Each dune is paired with the corresponding dune in the other set. The dynamics of each dune is quantified from the results of the algorithm: the alignment transformations.

Keywords: Marine dunes, dune morphology, dune dynamics, automatic algorithms, MBES data, triangular meshes, geomorphometry, non-rigid registration.

Acknowledgements

First, I would like to thank Direction Générale de l'Armement (DGA) and Region Bretagne for their financial support.

I am also grateful to my supervisor Benoit Zerr for his guidance, time and advice. In general, I would like to thank all members of the OSM (Ocean Sensing and Mapping) team for the interesting discussions and the great work atmosphere during these three years.

I want to express my gratitude to Michel Legris, Irène Mopin and Simon Rohou for their suggested corrections of this manuscript.

I would also like to thank the Federal Public Service (FPS) Economy Continental Shelf Service as well as Service Hydrographique et Océanographique de la Marine (SHOM) for sharing their data. Without data, this work would not have been possible. In particular, many thanks are due to Thierry Garlan and Marc Roche for sharing their data, answering my requests and my interrogations about dunes or the data.

Finally, I want to thank my loving family and Hélène for their unconditional support of my work and their constant encouragement.

Contents

Résumé	iii
Abstract	v
Acknowledgements	vii
Contents	ix
List of Figures	xv
List of Tables	xxi
1 Introduction	1
1.1 Thesis context	2
1.2 Objectives	7
1.3 Contributions	9
1.4 Plan	10
2 Dunes	13
2.1 Introduction	14
2.2 Dunes	15
2.2.1 Definition of the term "dune"	15
2.2.2 Morphological descriptors	16
2.2.3 Dune types	21

2.2.4	Classifications of sand waves	27
2.3	Dune morphology analysis	28
2.3.1	Traditional dune descriptive analysis	29
2.3.2	Automatic morphological analysis methods	32
2.4	Dune dynamics and automatic algorithms	37
2.5	Dune numerical modelling	39
2.6	Conclusion	40
3	Database	43
3.1	Introduction	44
3.2	MBES Data and DTM construction	44
3.3	SHOM and Belgian Databases	48
3.3.1	Belgian data	48
3.3.2	SHOM data	51
3.4	Benchmark	53
3.5	Conclusion	58
4	Geomorphometry	59
4.1	Introduction	60
4.2	Basic concepts of geomorphometry	60
4.3	Common metrics	64
4.3.1	Estimation techniques	66
4.3.2	Metrics estimation on dunefields	70
4.4	Classic terrain characterization algorithms	77
4.4.1	Pixel classification	78
4.4.2	Disparity line algorithms	83
4.4.3	Drainage algorithms	83
4.4.4	OBIA algorithms	85
4.4.5	Region growing algorithms	86

4.5	First dune extraction algorithm	87
4.5.1	Principles	87
4.5.2	Results and discussion	88
4.6	Surface Representation	93
4.7	Conclusion	96
5	Differential Geometry and triangular mesh	99
5.1	Introduction	100
5.2	Useful notions of differential geometry	100
5.3	Curvature estimation on meshes	107
5.3.1	Discrete methods	108
5.3.2	Fitting methods	111
5.3.3	Tensor estimation methods	112
5.4	Comparison of curvature estimation	113
5.4.1	Comparisons on benchmark zone 2	116
5.4.2	Comparisons on benchmark zone 7	121
5.5	Conclusions	124
6	Crest line extraction	125
6.1	Introduction	126
6.2	Surface characteristic lines	126
6.3	Crest line extraction methods	128
6.4	A new quantitative comparison procedure	134
6.4.1	Comparisons on benchmark zone 1	135
6.4.2	Comparisons on benchmark zone 2	143
6.4.3	Analysis of the dune crest descriptors	144
6.5	Crests and mesh resolution	154
6.6	Conclusion	156

7	Mesh simplification	157
7.1	Introduction	158
7.2	Requirements for the extraction of dune crests	158
7.3	State of the art	159
7.4	Proposed mesh simplification algorithm	165
7.4.1	Description	165
7.4.2	Results	168
7.5	Conclusion	172
8	Dune extraction algorithm	173
8.1	Introduction	174
8.2	Description	174
8.2.1	Mesh simplification	175
8.2.2	Crest extraction	178
8.2.3	Dune extraction	181
8.2.4	Assessment of the dune descriptive parameters	191
8.3	Results	192
8.3.1	Benchmark zone 8	192
8.3.2	Part of SHOM zone 1	193
8.3.3	Periodic dunes	195
8.3.4	Dunes on Ouessant bank	197
8.4	Conclusion	198
9	Dune dynamics	201
9.1	Introduction	202
9.2	State of the art	203
9.2.1	Iconic algorithms	203
9.2.2	Symbolic algorithms	209
9.3	Proposed algorithm for the study of dune dynamics	212

9.3.1	Dune dynamics	212
9.3.2	Correspondence	216
9.3.3	Transformation estimation	218
9.3.4	Quantification of dune dynamics	219
9.4	Conclusion	227
10	Conclusion	229
10.1	Summary of the thesis	230
10.2	Contributions	231
10.3	Future work	233
	Bibliography	235

List of Figures

1.1	Variety of dune locations.	3
1.2	Interactions between sediment transportation, seafloor morphology and hydrodynamics.	5
1.3	Bathymetry of the Belgian continental shelf.	6
2.1	Ambiguous definitions of 2D dune parameters.	17
2.2	3D dune descriptors.	19
2.3	Bathymetry of "Langoustiers" zone surveyed in 2016.	21
2.4	A dune field located few kilometers North of Portsall surveyed in 2016.	22
2.5	Dunes at the border of the French continental shelf.	23
2.6	DTM of an exceptional dunefield.	23
2.7	A dune field surveyed in 2013 off the coast of Brittany.	24
2.8	Bathymetry of R2 monitoring area in 2012.	25
2.9	Example of barchan dunes and barchanoid ridges.	26
2.10	Trochoidal dunes off the coast of Brittany.	26
2.11	Base function of most fitting techniques.	33
2.12	Seafloor variations on Ouessant bank between 2012 and 2016.	38
3.1	Diagram of the processing steps to transform raw data into a DTM.	45
3.2	Representation of a dune ($750 \times 250 \times 4$ m) as a cloud of soundings.	46
3.3	DTM of the dune created from the soundings.	47
3.4	Locations of the 11 Belgian control zones	49

3.5	Locations and names of the monitoring areas	50
3.6	Bathymetric data recorded during the 2013 dune campaign.	52
3.7	Locations of the available SHOM boxes.	52
3.8	Bathymetry of the Benchmark zones 1 to 6.	54
3.9	Bathymetry of the Benchmark zones 7 to 11.	55
4.1	Notion of scale.	63
4.2	Notations used for the discrete estimations of morphometric parameters.	68
4.3	BPI estimation with a 3×3 neighborhood.	71
4.4	Slope map of SHOM zone 1 estimated with a 5×5 neighborhood.	71
4.5	Slope estimation on two different dune types.	72
4.6	Comparison of aspect maps on benchmark zone 2 measured at two scales.	72
4.7	Profile curvature maps.	73
4.8	Plan curvature maps.	74
4.9	Minimal curvature maps.	74
4.10	Maximal curvature estimation on benchmark zone 1.	75
4.11	Gaussian curvature estimation on benchmark zone 1.	76
4.12	Mean curvature estimation on benchmark zone 1.	77
4.13	Wood's pixel classification.	80
4.14	Application of Wood classification to SHOM zone 2.	81
4.15	Zoom on dune classification of subfigure (E).	82
4.16	Example of drainage network algorithm.	84
4.17	Catchment segmentations of SHOM zone 2.	85
4.18	Minimum curvature (m^{-1}).	88
4.19	Slope estimation.	89
4.20	Comparison between the seed regions (black) and manually extracted (red lines) dune crests with zooms on failure cases.	90
4.21	Results of the region growing algorithm in SHOM zone 6.	91

4.22	Seed regions with the initial algorithm.	91
4.23	Seed regions using the region size parameter.	92
4.24	Extraction results with a 0.8 slope threshold.	92
4.25	Extraction results with a 0.5 slope threshold.	93
4.26	Extraction results with a 0.5 slope threshold and a maximum distance of 70 m.	93
4.27	Three types of surface approximations: (1): Cloud of soundings; (2): gridded DTM; (3): Triangular mesh.	94
4.28	Decomposition of the mesh into three types of elements.	94
4.29	Mesh construction from a DTM.	96
5.1	Osculating circle and definition of the curvature at a point of a at least C^2 curve.	101
5.2	Link between a curvature and the corresponding normal curvature. . . .	101
5.3	Example of a Darboux frame at a crest point.	105
5.4	Link between a curvature and the corresponding normal curvature. Drawn from Do Carmo (1976).	106
5.5	Discrete methods applied to benchmark zone 2.	117
5.6	Minimum curvature and associated direction by Chen's algorithm.	118
5.7	Influence of the neighborhood size on the Hamann curvature and direction.	119
5.8	Principal curvatures and directions in benchmark zone 2 with discrete tensor estimation methods.	120
5.9	Minimum curvatures and directions of benchmark zone 7 with fitting methods.	122
5.10	Principal curvatures and directions of benchmark zone 7 with fitting met- hods.	123
6.1	Classification of ridge lines.	127
6.2	Bathymetry of Belgian zone R2.	133
6.3	Influence of the vertical exaggeration on our perception of dunes.	133
6.4	Examples of usual test surfaces.	134

6.5	Crest lines detected by the four algorithms.	136
6.6	Differential quantities deriving from the osculating jet method.	137
6.7	Failure case of Hildebrandt's algorithm.	139
6.8	Set of crest lines detected by Hildebrandt's algorithm after modification.	141
6.9	Failure case of Ohtake's algorithm.	142
6.10	Detected lines by the four algorithms on benchmark zone 2.	144
6.11	Cazals1 extracted crests on benchmark zones.	148
6.12	Sinuosity of the crests on benchmark zones.	149
6.13	Height of the crests on benchmark zones.	150
6.14	Strength of the crests on benchmark zones.	151
6.15	Sharpness of the crests on benchmark zones.	152
6.16	Third mathematical descriptor values of the crests on benchmark zones.	153
6.17	Crest lines extracted with Cazals1 algorithm on meshes of benchmark zone 8 with various resolutions.	155
7.1	Simplification by vertex removal.	163
7.2	Three types of edge collapse procedures.	164
7.3	Principle of a triangle removal algorithm.	164
7.4	Five main steps of the mesh simplification algorithm.	166
7.5	Forbidden retriangulation.	167
7.6	Particular case at the border of the surface.	168
7.7	Simplification output mesh of zone 8 with a 4m resolution threshold.	168
7.8	Comparison between the input and output meshes.	169
7.9	Sets of extracted lines before and after simplification on zone 1.	170
7.10	Set of lines extracted on the simplified representation of zone 1.	171
7.11	Set of lines extracted on the simplified representation of zone 4.	171
8.1	Main steps of the dune extraction algorithm.	175
8.2	End condition of the mesh simplification algorithm.	176

8.3	Output mesh of the simplification algorithm of benchmark zone 7. Minimum dune width = 60 m.	177
8.4	Coarse crests detected in benchmark zone 7.	178
8.5	Link between the vertices of the fine and coarse meshes.	179
8.6	Definition of the areas of interest for reconstructing fine crests.	179
8.7	Regions of interest around rough crests on the fine mesh of zone 7.	180
8.8	The set of fine crests included in the crest regions of zone 7.	181
8.9	Final set of dune crests on benchmark zone 7 with a Vertical Exaggeration (VE) = 20.	182
8.10	Initialisation of the Lee and Stoss face boundaries for zone 7.	183
8.11	Comparisons between the direction of the slope vector and dune side direction for a dune on a bank.	184
8.12	Propagation of the information about the local orientation of the dune sides.	184
8.13	Initialisation of the direction of the dune sides from crest segments.	186
8.14	Results of the propagation of the directions of the dune sides.	186
8.15	Observations on the slope of the dune sides.	187
8.16	Extracted dunes when setting the threshold from slope near the crest for benchmark zone 7. VE = 20.	188
8.17	Results of the dune extraction algorithm on benchmark zone 7.	189
8.18	Estimation of smoothed surface normals for an improved growth.	190
8.19	Dunes extracted in benchmark zone 8.	192
8.20	Comparisons between the new algorithm, the one presented in Chapter 4 and manually extracted crests.	194
8.21	Location of the selected dataset in SHOM zone 1.	195
8.22	Extracted dunes on the area.	196
8.23	Plot of the estimated height against the length.	196
8.24	Location of the selected dataset with respect to Ouessant bank.	197
8.25	Extracted dunes on the flank of the bank.	198

9.1	Test of the code validity with a simple image.	207
9.2	Part of a DTM of SHOM zone 2.	208
9.3	Masked Normalized Cross-Correlation (MNCC) maps on real data with translations of: (a): (-10, 17) pixels; (b): (0,0) pixels.	208
9.4	Juxtaposition of DTMs of Belgian zone R2 respectively surveyed in March 2012, September 2012 and March 2014.	214
9.5	Simultaneous visualization of dunes in zone R2 acquired in March 2012 and 2014.	215
9.6	Simultaneous visualization of dunes in SHOM zone 2 acquired in 2012 and 2015.	215
9.7	Comparative visualization of dunes in the flat seafloor part of SHOM zone 2.	216
9.8	Dune correspondence process.	217
9.9	Diagram of the main steps of Huang's algorithm	219
9.10	Dune segmentation and associated vectorial information.	220
9.11	Area for the test of the dynamic algorithm in Ouessant bank. Data acquisitions: 2012 and 2016.	221
9.12	Sample of correspondences between two meshes.	222
9.13	Simultaneous visualisation of the two meshes before and after the alignment procedure.	223
9.14	Histograms of the distances between the corresponding vertices before (left) and after (right) alignment.	223
9.15	Map of distances between the vertex pairs after registration.	224
9.16	Vertex clusters colored by migrating distance.	225
9.17	Migration and deformation vectors for each vertex cluster.	226

List of Tables

2.1	Usual dune morphological descriptors and the level of ambiguity of their definitions	20
2.2	Ashley’s classification of marine dunes under unidirectional and/or alternative currents. H_{mean} : Dune mean height.	27
3.1	Information about the data acquisition of the eleven benchmark zones. . .	56
3.2	Locations and dune properties of the benchmark zones.	57
4.1	Thresholds setting of Figure 4.14.	82
6.1	Comparisons of the crests detected by the four algorithms on zone 1. . .	138
6.2	Closeness of the detected crests on zone 2.	139
6.3	Characteristics of the set of crest lines obtained with the modified Hildebrandt’s algorithm.	140
6.4	Tracing similarities between modified Hildebrandt’s crests and the others.	140
6.5	Quantitative comparisons on zone 2.	144
6.6	Comparisons of the strength values according to the mesh resolution on benchmark zone 8.	147
6.7	Number of extracted lines according to the degree of the fitted jet and the neighborhood size.	155
8.1	Estimated morphological descriptors for the two dunes of zone 7.	191

Glossary

- ADCP** Acoustic Doppler Current Profiler. 23
- BPI** Bathymetric Position Index. 59, 63
- CAGD** Computer aided geometric design. 88
- CGAL** Computational Geometry Algorithms Library. 96
- CHRT** CUBE with Hierarchical Resolution Techniques. 40
- CUBE** Combined Uncertainty and Bathymetry Estimator. 40
- DGA** Direction Générale de l'Armement. vii
- DGPS** Differential GPS. 12
- DTM** Digital Terrain Model. xv, xvi, 8, 16, 19, 29, 36, 38–41, 44, 46, 49, 51, 54, 55, 57–59, 62, 63, 65, 70, 77–79, 82, 83, 85, 95, 146
- EEZ** Exclusive Economic Zone. 14, 41
- FFT** Fast Fourier Transform. 28, 29
- FPS** Federal Public Service. vii, 8, 38, 41
- GIS** Geographic Information System. 44, 54, 71, 144, 145
- GPS** Global Positioning System. 6, 12, 29, 39
- IMU** Inertial Motion Unit. 39
- MARID** Marine and River Dune Dynamics. 35
- MBES** MultiBeam EchoSounder. 6, 8, 12, 23, 29, 38–41, 43, 44, 46, 51, 79
- OBIA** Object Based Image Analysis. 75–77
- PCA** Principal Component Analysis. 100, 108

PPP Precise Point Positioning. 12

RTK Real Time Kinematic. 12

SBES SingleBeam EchoSounder. 29

SHOM Service Hydrographique et Océanographique de la Marine. vii, xv, xvi, 8, 15, 17–19, 35, 38, 41, 44, 71, 79, 81, 198

WT Wavelet Transform. 28

Chapter 1

Introduction

Contents

1.1	Thesis context	2
1.2	Objectives	7
1.3	Contributions	9
1.4	Plan	10

1.1 Thesis context

Today the topography of Mars and the Moon is, in some places, more accurately described than in the deepest parts of the oceans. Most of the ocean is still to be thoroughly explored. The most detailed global map of the ocean has a 30-arc second resolution (~ 1 km)¹. In this context, marine sciences are trying to cope with our lack of knowledge from different standpoints. Bathymetry is the discipline aiming at mapping the seafloor and analyzing its topography. The acquisition of bathymetric data is generally achieved using sonar systems². Bathymetric maps, named DTMs, are generated from this data to visualize and analyze the seafloor topography. A DTM is generally a georeferenced rectangular grid of square cells with a single depth or elevation value associated to each cell.

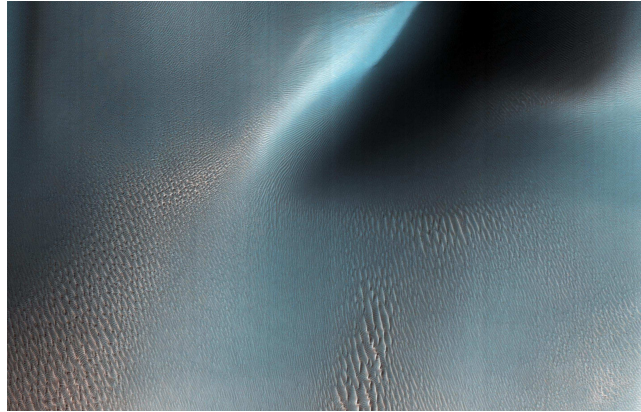
The display of bathymetric data revealed the existence of dunes on the seafloor. Generally, people think about dunes in the deserts, at the beach or even on Mars. These dunes are wind-generated and so called eolian dunes. The existence of marine dunes maintained by currents is not as widely known. Marine dunes are underwater sediment mounds shaped by currents. The currents induced by the tide, the wind or the waves move mobile sediment that agglomerates to form sedimentary structures. These structures have extremely variable sizes as it goes from ripples to banks and dunefields. For example, ripples are visible at the beach and are few centimeters high. Banks can be kilometers long and tens of meters high as visible on Figure 1.3. Dunes are intermediate size structures that can be superimposed on top of banks and have ripples superimposed on them.

A dune has two sides. The one exposed to the current is called the Stoss side and the other one is named the Lee side. The currents push the sand up the Stoss side, then, it slips down the Lee side. The displacement of sediment causes the migration and deformation of the dune.

Dunes are ubiquitous (see Figure 1.1) as they can be found any place where there is mobile sediment. This remark is valid for marine dunes too. As the reader will see in the next chapter, there are also numerous dunes in rivers, on continental shelves and rises across the world.

1. This bathymetric map was produced by General Bathymetric Chart of the Oceans (GEBCO) and is available to download at <https://www.gebco.net/>.

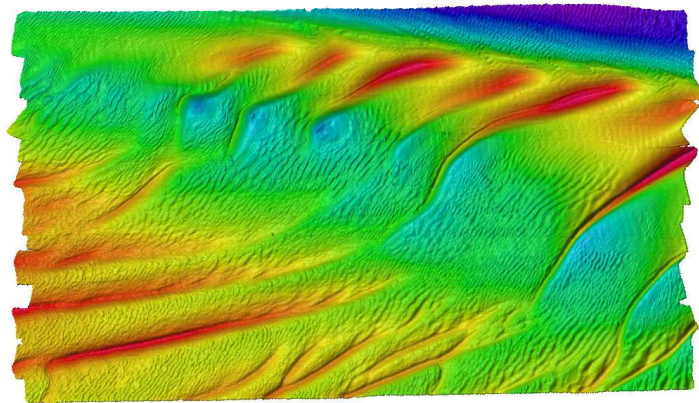
2. Laser scanning systems called LIDAR may now be used in shallow waters as well as airborne and satellite imagery.



(A)



(B)



(C)

FIGURE 1.1: Variety of dune locations. (A): Dunes and ripples observed by NASA's Mars Reconnaissance Rover (MRO) in Proctor crater, Mars (October 7, 2017), this is part of the NASA's Mars Reconnaissance Orbiter Project: <https://www.jpl.nasa.gov/spaceimages/details.php?id=pia22040>; (B): star dunes in Rub Al Khali desert, Saudi Arabia, photographed by George Steinmetz: <http://ngm.nationalgeographic.com/2012/11/sand-dunes/steinmetz-photography#/07-rub-al-khali-star-dune-670.jpg>; (C): Sand dunes and ripples off the coast of Belgium. This area is called KBMA and is a monitoring area of the central part of the Kwintebank, and this dataset was collected in March 2013.

Since the 1970s, with the advances in the acquisition and positioning systems, researchers' interest in marine dunes has not stopped growing. The improvements of the data accuracy and density allow to see more details of dune morphology and even to analyze short-term dynamics. New regions are being explored, steadily revealing the diversity of dunes. If most marine dunes are long, narrow and parallel sand hills organized in dunefields, other dune types have been discovered. This diversity can be explained by the fact that they are unique structures resulting from the complex interaction between mobile sediment and a flow.

The dune formation, growth and evolution are mechanisms that are not fully explained yet. Indeed, their understanding requires deep knowledge about the seafloor morphology, the sediment transportation and the hydrodynamics (currents). Figure 1.2 illustrates how changes on one of these three elements impact the others. The transported sediment comes from the seafloor. Thus, the transported sediments reshape the seafloor. The current adjusts to the topographic modifications and the sediment transport gets impacted. These couplings enable dunes to grow, maintain, transform and migrate. A small change in the system can lead to major modifications on the shape of dunes. Actually, the shape of a dune reflects the fine balance between the elements of the system at a particular time: this is what explains the diversity of dunes. Moreover, this lack of understanding of the mechanisms controlling the dune growth and movement is what makes dunes interesting, challenging on a scientific level. Two main approaches are followed by scientists to study these mechanisms: *in situ* data analysis and modelling.

These two approaches are complementary and share the same goal of understanding dune dynamics. Therefore, a Marine and River Dune Dynamics (MARID) community has been created to the initiate of SHOM and University of Lille 1 in 2000. Since then, MARID³ conferences exclusively dedicated to the study of dunes are organized.

3. More information about MARID community can be found at <https://marid.net/>.

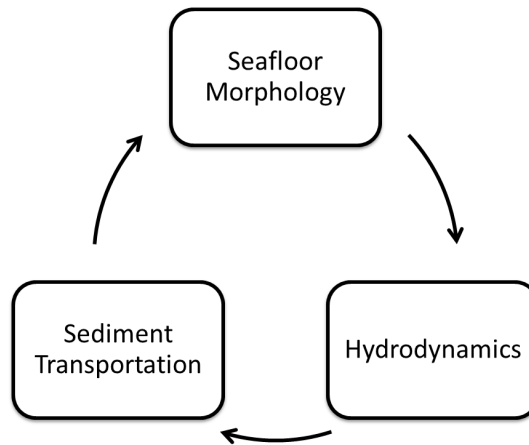


FIGURE 1.2: Interactions between sediment transportation, seafloor morphology and hydrodynamics.

But, the interest in dunes cannot be reduced to scientific purposes/curiosity. Other reasons brought dunes to the front stage. To understand these reasons, it is preferable to look at dunes, dune fields and banks. Figure 1.3 shows the bathymetry of the entire Belgian continental shelf. The observation of the area depicted in this figure highlights most of the reasons that justify the monitoring of dune fields.

Dunes are large, mobile structures which is problematic for navigation safety. Currently, maritime transport is the principal shipping means. Ships are always built larger⁴. Dunes can cover extensive areas. And, dunes can also be found nearshore. In the figure, the depth varies from 0 to 50 m and these variations are mostly due to sandy bedforms. This means that shipping routes necessarily cross dunefields and sand banks and especially nearshore to access harbours. Consequently, dune dynamics needs to be closely monitored and nautical charts must be updated regularly to avoid ship groundings and worse.

Dunes and sand banks are gigantic structures that can reach a height of 20, 30 meters or even more. It is common to observe dunes that are few hundred meters long. At last, these sedimentary structures (dunes) migrate as they are made of mobile sediment put into motion by currents. The mobility of dunes can interfere with other human activities such as buried communication cables or pipelines with risks of free spanning or snapping under the weight of sediment. Furthermore, the installation sites of marine renewable energy infrastructures must be carefully picked. The study of dune

4. For general information, the current biggest ship is a 460m long oil tanker with a 24m draught. cf. https://en.wikipedia.org/wiki/Seawise_Giant

dynamics is essential for the prediction of countermining too. Buried mines periodically show with dune migration and so countermining must be planned accordingly.

Dunes and banks are also a tremendous, easy-access source of aggregate. Indeed, the sedimentary structures may be found close to shore. It is particularly true in Belgium and in the Netherlands where aggregate extraction is a prime economic activity. Besides, these sandy bedforms provide natural coastal protection and are biodiversity hotspots. Coastal management policies can be defined from the study of dunes if required. For instance, aggregate extraction is controlled by law in Belgium.

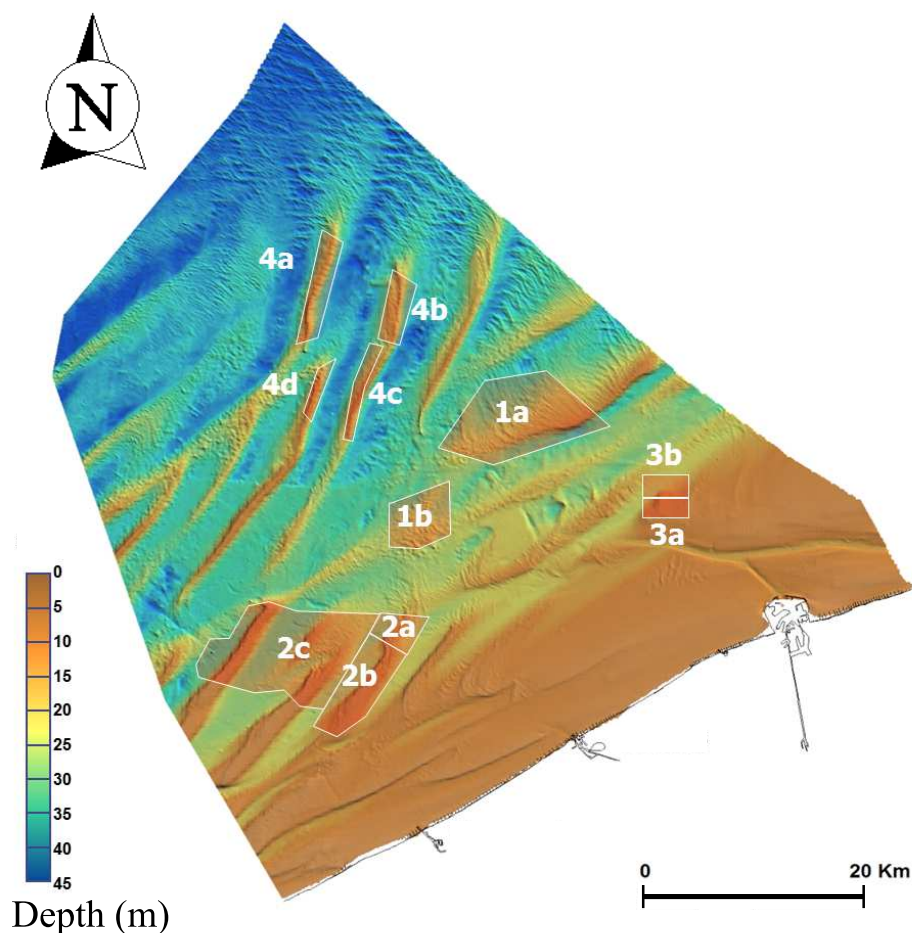


FIGURE 1.3: Bathymetry of the Belgian continental shelf⁴. The numbered areas are used by the Belgian government to control the impact of dredging on the bathymetry.

For all these reasons, study of dunes, especially automatically - the subject of this thesis - is therefore essential.

4. Data available on the website of the Flemish hydrographic office <http://www.afdelingkust.be/en/bathymetric-database>.

1.2 Objectives

The main objective of this thesis is to focus on the quantitative study of dune morphology (shape) and dynamics. More specifically, the objective is to design automatic algorithms in order to quantify dune morphology and dynamics. The proposed algorithms will take as input bathymetric data recorded on dunefields and provide information about the dune morphology and dynamics. In practice, each dune will be described by a limited set of easily-understandable morphological and dynamical descriptors. As dunes are particular variations of the seabed topography, the input data to these algorithms is the bathymetry resulting from the processing of MBES soundings. Moreover, the changes in the morphology of a dune (displacement and deformation) give information about its dynamics. Automated algorithms to tracks these dune changes in location and shape at different times allow for an accurate quantification of the dynamics of dunes.

Dune morphology and dynamics are tightly-linked. Yet, no automatic methods consider both aspects. Furthermore, to this day, there is no dune classification encompassing morphological and dynamical aspects. In fact, existing dune classifications are based on simple morphological descriptors and are not capable of discriminating the different types of dune. The automation of the quantification of dune morphology and dynamics could lead to a new dune classification in line with the observed diversity of dunes.

The first step of the process is to detect the occurrence of dunes in the bathymetric data and to determine the spatial extent of each detected dune. This delimitation task as well as the evaluation of the morphological metrics are systematically made manually by an operator visualizing the data on a screen. This process suffers from a number of disadvantages (tedious, time consuming, subjectivity, inaccuracy, repeatability). Besides, manual analysis is less and less suited to face the incoming data flow. Henceforth, the evaluation of the values of these metrics supposes the development of automatic algorithms.

The automatic or semi-automatic algorithms presented in the literature are inspired from manual analysis and do not exploit the full potential of three-dimensional (3D) MBES bathymetry. The analysis of dune morphometry and dynamics are characterised at a regional scale. Indeed, these techniques are sliding window procedures. Therefore, the analysis is dependent of the window size. In order to further examine dune

characteristics, the best solution is to determine the positions of dunes in the bathymetric data. With dunes considered as individual entities of the seafloor, the problem of their quantitative description could be addressed more thoroughly. But, there is no automatic algorithm proposed in the literature for automatically delineating dunes in DTMs. Besides, the individual dune extraction leads to the common estimation of dune and dunefield properties and specificities (variability of dune characteristics and spatial organization (orientation, spacing, *etc.*)).

During last MARID conference, all dune experts, regardless of their main scientific interest (real data processing and analysis or modelling), agreed on the fact that geomorphometry and related automatic techniques are the future of dune analysis. Geomorphometry is the science of terrain descriptive and quantitative analysis. Therefore, our problem falls in the scope of geomorphometry. Automated methods for the extraction of terrain specific features (drumlins, volcanoes, gullies, pockmarks, mountains) already exist but none is dedicated to marine dunes. Each feature has its geomorphometric signature. This is what makes it recognizable, different from the others. The existing algorithms of extraction of terrain features have to be modified in order to take into account dune signature. Dunes are characterized by a long crest line surrounded by two narrow sides. The dune signature is the set of geomorphometric metrics that will describe this specificity. Once this set of metrics has been figured out, dunes could be automatically delineated. This will lead to the automatic quantification of dune morphology and dynamics. Many descriptors already exist to quantify dune morphology, but, this is not true for dune dynamics.

Dune dynamics is often confined to the assessment of dune migration rate. Yet, this is a simplification of the reality. Indeed the time evolution of dune morphology can be decomposed into two components: migration and deformation. If a dune does not migrate, it does not mean it does not move or change. Deformation is the component of dune dynamics that includes all the local changes of dune morphology whereas migration is related to global dune displacements. Furthermore, dune migration is generally reduced to a simple translation of the entire dune. But, in reality, dune migration is not necessarily homogenous at a dune scale as dune parts migrate independently in several directions or at different speeds. The automated dynamics assessment algorithm will have to avoid these usual assumptions as every aspect of the dynamics of a dune reflects physical phenomena and so may help identifying their mechanisms.

1.3 Contributions

The investigations carried out in the course of this thesis have led to the following major contributions:

- A new quantitative method of comparison of crest line detection algorithms. This method turned to be essential in the next steps towards the development of a combined dune morphological and dynamical analysis method. In fact, the crest detection is the starting point of the entire analysis and so required specific care;
- The development of an automatic dune extraction algorithm leading to a quantitative description of dune morphology. It is based on a region growing approach coupled with a mesh simplification procedure;
- An algorithm for quantitatively assessing dune dynamics. This algorithm makes no assumptions about the complexity of dune dynamics.

The algorithms presented in this thesis gather knowledge for numerous research domains to address the issues related to the study of marine dunes. These algorithms differ from the algorithms in the literature at several levels:

- The input is a 3D representation of the seafloor surface: a triangular mesh⁵;
- The resolution of the surface representing the seafloor is adapted to the dune scale in order to facilitate their delineation. A mesh simplification method has been developed in this prospect;
- The analysis of dunes is not regional as they are considered as individual entities. And, the estimation of individual morphological and dynamical descriptors will enable highlighting the variability of dune characteristics and focusing on the organization of dune fields;
- Dune dynamics is characterized as the combination of migration and deformation.

5. Explanations about what triangular meshes are and the way they are constructed are given in Chapter 4.

1.4 Plan

This dissertation is divided into nine chapters:

- Chapter 2 aims at presenting dunes and dune analysis. A definition of the term "dune" is provided to explain what the proposed algorithms will extract and analyze. The usual dune descriptors and their multiple definitions are listed. The different dune types are also shown in order to highlight the fact that the existing classifications are inadapted. The manual processing and its drawbacks are explained. A review of the automated methods of quantification of dune morphology and dynamics is made and their limitations are discussed. Dune analysis can also be achieved via modelling. So, the capabilities of dune models are presented.
- Chapter 3 introduces the data shared by SHOM and FPS Economy continental shelf service. The impact of MBES acquisition and processing on the bathymetric surface (DTMs) are discussed bearing in mind the next objective: the design of an algorithm for locating dunes in the seafloor. Besides, benchmark zones are defined in order to test the algorithm robustness with respect to data quality and dune diversity.
- Chapter 4 is dedicated to geomorphometry and how the existing landform extraction algorithms can be adapted for dune extraction. It starts with the introduction of key concepts such as the geomorphometric signature. The estimation of usual geomorphometric metrics on DTMs helps figuring out which are capable of revealing the presence of dunes. Then, the automatic algorithms for landform extraction are reviewed and the question of their applicability to dunes is examined. A first dune extraction algorithm is designed, tested and its results are discussed. The main conclusions are that the extraction of dunes starts with a good extraction of their crests and that the use of DTMs to model the seafloor is not the most suited. The advantages of triangular meshes over DTMs are given.

-
- Chapter 5 shows how the geomorphometric metrics (*e.g.* curvatures) can be estimated on triangular meshes. These metrics quantify the variations of the seafloor surface. They are defined in differential geometry. Numerous notions and definitions of differential geometry have been generalized to study triangular meshes. They are explained in this chapter. The estimation of geomorphometric metrics influences the crest extraction. That is why the choice of the estimation method the most suited for the later dune crest extraction is of major importance. The algorithms of estimation of these differential quantities are presented and tested. The conclusions enable determining the method that will be used later for estimating geomorphometric metrics.
 - Chapter 6 aims at comparing the performance of existing crest extraction algorithms for dune crest line extraction. The tested algorithms are based on the differential geometry definition of crests. First, the crest extraction algorithms are presented. Metrics have been defined to quantitatively compare these methods with the goal of selecting the most appropriate for dune crest extraction. These algorithms are designed to extract all crest lines of the mesh. The problem is that the extracted crests can correspond to sand ripples or data artifacts and not only to dunes. Attempts for discarding these undesired crest lines are made by using thresholds on the usual crest line attributes. None worked but a solution came for geomorphometry with the notion of scale. The idea is that the extraction of dune crests will be simpler at dune scale. This suggests the adaptation of the mesh resolution.
 - Chapter 7 introduces mesh simplification algorithms as it was concluded in Chapter 6 that the mesh resolution must be adapted for a correct analysis and extraction of dunes. The simplified mesh will be used during the dune crest extraction process. A list of the requirements that must be met by the mesh simplification is established. After, the different simplification schemes existing in the literature are presented and discussed with regard to the previous criteria. Finally, a simplification procedure in accordance with the previous criteria is proposed and tested to confirm that it has the expected impact on the set of extracted crest lines.

- Chapter 8 presents the proposed automatic dune extraction algorithm combining geomorphometry concepts (signature, scale) and the crest line definition drawn from differential geometry. The algorithm is explained in details and each step is justified. The results of the analysis of datasets showing various dune types are discussed and compared to manual extraction.
- Chapter 9 focuses on the analysis of dune dynamics with automatic algorithms. The problem of quantification of the changes in the morphology of a dune is assimilated to a problem of registration. After a review of registration methods (iconic and symbolic), an algorithm dedicated to the study of dune dynamics is proposed. The symbolic approach to the registration between two successive measurements of the dunes has shown better results than iconic methods. The input of the algorithm is the result of the dune extraction. After estimating the transformation between the two measurements of the dunes, an attempt to quantify dune dynamics is proposed and tested. The results obtained on experimental data are discussed.
- Chapter 10 recalls the main achievements in the automatic extraction of dunes and in the analysis of their dynamics. It also explains how the thesis results will help studying dunes in future work. Finally, modifications or improvements of the proposed algorithms are suggested in order to integrate aspects of dune analysis that might have been discarded.

Chapter 2

Dunes

Contents

2.1	Introduction	14
2.2	Dunes	15
2.2.1	Definition of the term "dune"	15
2.2.2	Morphological descriptors	16
2.2.3	Dune types	21
2.2.4	Classifications of sand waves	27
2.3	Dune morphology analysis	28
2.3.1	Traditional dune descriptive analysis	29
2.3.2	Automatic morphological analysis methods	32
2.3.2.1	Bathymetric profile analysis	32
2.3.2.2	Model fitting techniques	33
2.3.2.3	Frequency analysis	35
2.4	Dune dynamics and automatic algorithms	37
2.5	Dune numerical modelling	39
2.6	Conclusion	40

2.1 Introduction

The aim of this chapter is to introduce dunes, their diversity of shape and the way they are described and studied. This is essential to understand what our work will bring to dune analysis. Dunes are not easy to define as the readers will see, but, an attempt to provide a definition is made in this chapter. A number of descriptive parameters have been defined by the scientific community to describe the morphology and dynamics of dunes. However, only the morphological descriptors are used by existing sand wave classifications. These classifications do not account for dune dynamics and are too simplistic to distinguish between all the different types of dunes. In this regard, there is no satisfactory dune classification.

There are two main ways to study dunes. Some researchers have chosen to describe dune morphology and dynamics through the thorough analysis of miscellaneous measurements (current, bathymetry, sediment samples and cores)(Ernstsen et al., 2004, Ferret et al., 2010, Hardy et al., 2006, Mosher et al., 2000, Van Landeghem et al., 2013). Others rather model these mechanisms (Besio et al., 2004, Blondeaux et al., 2001, Carling et al., 2000, Hulscher et al., 1993, Idier, 2002, Nabi, 2008, Németh et al., 2000) and/or observe dunes generated in flumes¹ (Cataño-Lopera et al., 2009, Dohmen-Janssen & Hulscher, 2008). The comparison and analysis of the models are out of the scope of this thesis. But, they are mentioned to inform the readers of their existence and to explain the mechanisms they try to model. Modelling helps understanding the several phases of the life of a dune and the forcings that shape them. Data analysis and modelling are two different approaches to study the same intricate system. In this regard they are complimentary.

A review of the literature on the study of marine dunes is provided. The aim is not to make an exhaustive list of all research conducted on this topic. Here, the focus will be on presenting how dunes are being studied and what are the limitations of these techniques. The interest behind this review is to conclude on how our algorithms can avoid the shortcomings of the existing techniques, and, therefore, how they can have a true added value for the scientific community.

1. Flumes are laboratory tanks or channels where scientists recreate the *in situ* conditions in a controlled environment in order to understand the mechanisms of the dunes.

2.2 Dunes

The role of this section is to familiarize the readers with the notions related to the study of dunes, to illustrate the complexity of dunes (sediment composition, size, dynamics, shape, environment) and to show how dunes are classically described.

2.2.1 Definition of the term "dune"

Ripples, megaripples, sandwaves, dunes (medium, large, very large, giant), sandbanks, dunefields, all these terms constitute a taxonomy specific to sandy bedforms. Many references to these terms may be found in the literature, in the classifications and even in this thesis. Nevertheless, no clear definition has been provided. The major difficulty is to translate the types of bedforms that have been observed into values of descriptive parameters. In practice, sedimentary bedforms cover a wide range of sizes (*e.g.* height from 10cm to 50m). In some cases, they may interfere with each other and create very complex structures. If the spatial scale differs from one bedform to another, their timescale is different too. Bigger structures are more persistent, that is to say that, their morphology does not proportionally change as fast as the one of smaller structures. For instance, the small ripples at the beach will not be the same in few hours or days whereas it takes months or years for a bank to visually change. This thesis intends to characterize dunes. Therefore, it seems primordial to explain what the term of "dune" designates in a practical manner.

The proposed definition will rely on observations. Generally, dunes and ripples are commonly distinguished on the basis of their scaling or non-scaling with flow depth as well as dimensional criteria such as wavelength. Ripples are defined as small bedforms (length, $L < 0.6$ m) which do not scale with water depth, whereas dunes are larger and generally considered to scale with water depth (Bartholdy et al., 2005). Unfortunately, it is impossible to convert this observation into quantitative morphological requirements. However, what ought to be recalled is that dunes are the second largest marine sand structures after the banks. After a close analysis of the available datasets and discussions with dune specialists², it was concluded that a 1m height³ threshold was appropriate to differentiate dunes from smaller-scale sandy structures. Although the 1m height threshold is used by our dune extraction algorithm presented in Chapter 8, this value

2. Thierry Garlan and Marc Roche who provided me with bathymetric data presented in the next chapter.

3. The height of a dune is one of the descriptors that are presented in the next section.

could be changed if it does not correspond to the reality of a particular dunefield. It is to note that there are cases where ripples are as long as dunes or where dunes slowly turn into ripples or are connected by ripples. Henceforth, the reality is not as simple as it appears but the height threshold is the only way to differentiate these sedimentary structures. Sandbanks are larger-scale structures; the top of a bank is smoother than a dune crest so that both are very distinct. The dune extraction must be adapted to the dune scale in order to avoid extracting banks in addition to dunes. In this regard, geomorphometry-based algorithms will be of major interest and well-suited.

In this thesis, dunes are only considered as sedimentary structures that modify the surface of the seafloor so that they can be extracted from bathymetric data. The study of dune morphology and dynamics is our main concern. But, dunes could also be characterized by their type of sediment, the variability of the grain size, the hydrodynamical forcings (types of currents), *etc.*

In the end, the characterization of dunes by their morphology requires using crisp thresholds (cf. sand wave classifications in Section 2.2.4). A 1m height threshold is chosen to distinguish dunes from smaller sand waves. But, we are aware that it is not ideal and that two nearby sandy bedforms with heights of 0.99 m and 1.01 m are, in fact, very similar. To sum up, there is only a continuum of sandy bedforms covering a wide range of scales. Dunes are the second-largest after sandbanks.

2.2.2 Morphological descriptors

Dune morphology can be measured with morphometrical metrics. In the remainder of this manuscript, they will be referred to as dune descriptors. Descriptors have been used by researchers to quantify dune morphology and especially for comparison purposes. Their values are comparable between dunes and dunefields but also to estimate dune shape evolution through time. The first descriptors were defined when bathymetric profiles were the only morphological information available. Bathymetric profiles are plots of the seafloor depth along a section. It is a two-dimensional representation of the seafloor topography.

Figure 2.1 illustrates these basic descriptors (Height, width, wave length, *etc.*) and their multiple definitions. Descriptors such as the dune depth (see Figure 2.1) have proven to be important thanks to dune modelling (Bartholdy et al., 2005). The depth of the crest of a dune is linked to its height. It is necessary to calculate and save these descriptors in databases in order to highlight links between them.

Sea surface

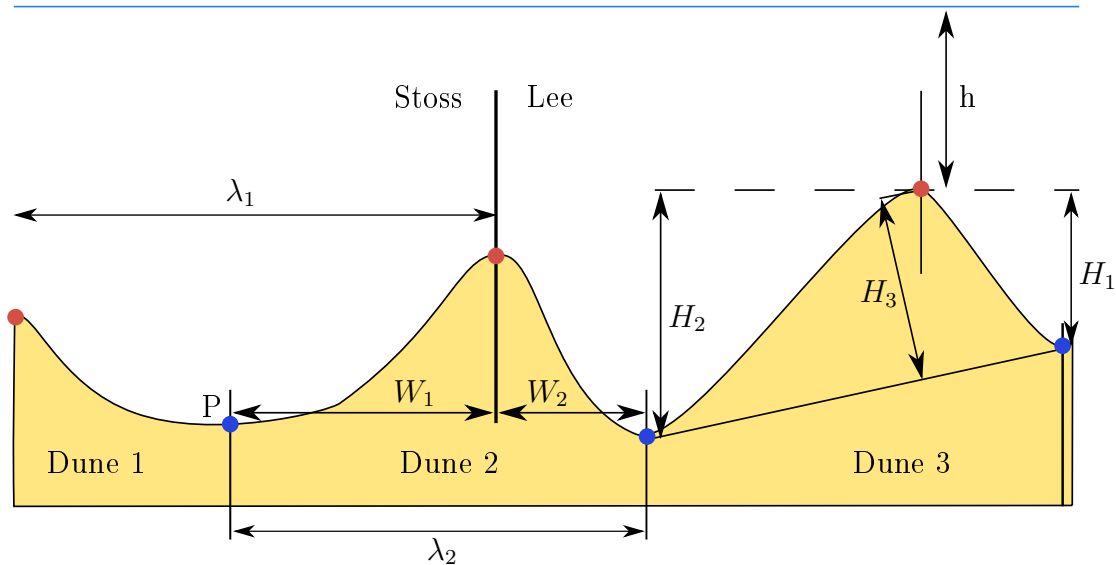


FIGURE 2.1: Ambiguous definitions of 2D dune parameters. The crest points are in red and trough points in blue. $\mathbf{H}_1, \mathbf{H}_2, \mathbf{H}_3$: Potential heights; $\mathbf{W}_1, \mathbf{W}_2$: widths of the Stoss and Lee sides; \mathbf{h} : Dune depth; λ_1, λ_2 : Wavelengths.

Modelling aspires at figuring out the dune mechanisms explaining these observations. Yet the definition of these basic metrics is not as simple as it seems. Researchers need to use consistent definitions of the descriptors, which is not yet the case. In fact, the used definition is rarely mentioned in the literature.

The height (cf. Figure 2.1) can be defined as the depth difference between the crest point (red point on the figure) and a trough point (blue points on the figure). There are two trough points per dune on a profile so two height values (H_1 and H_2). An average of the two gives another value. It is also possible to draw a line passing by the two trough points and the height either being the vertical or perpendicular distance of the crest point above the line (H_3).

Likewise, the definition of the dune width is ambiguous. Sometimes, width and wave length share the same definition. Lee (W_1) and Stoss (W_2) side widths may be considered. The wave length might seem relevant on a profile, but the 3D visualization of dunefield (*e.g.* case of Figure 2.6, shows it is not suited for dune morphology. Indeed, dunes are not equally spaced 2D structures. That is to say that dunes are not all linear and are not always parallel. Dune spacing would be a more correct terminology than wave length. And, the dune spacing is not even constant between two dunes and even less at the scale of a dunefield.

Moreover, these definitions depend on the location of the trough and crest points. It suggests that dune boundaries are known prior to the estimation of the morphological descriptors. Hence, it seems logical to develop an automatic algorithm for delineating dune crests and boundaries. The dune descriptors can next be estimated. If crest points are easily found, this is not true for trough ones. The changes of slope is larger at crest points than at trough points. The depth variations are sometimes so gentle around the foot of a dune that its location is very uncertain. To illustrate the idea, a slight shift of point P on Figure 2.1 would not be shocking whereas the locations of the crest (red) points is less discussable.

The above-mentioned descriptors are generally defined from bathymetric profiles. So, the orientation of the profile modifies the perception of the dune morphology. Running a line perpendicular to the dune crests enables appreciating the true morphology of dunes. The worst case is to survey lines parallel to the dunes and then to observe little depth variations. This could lead to the wrong conclusion that an area is free of dunes. The sectional views of dunes have long limited dune perception. These basic descriptors can be simply qualified in 2D profiles. But dunes are mostly 3D structures. This means that the shape of a dune is susceptible of changing along the crest. Consequently, the values of these descriptors also change along the crest. Hence, clear and consistent definitions have to be found to help in comparing the observations.

In order to describe the 3D morphology of dunes, other descriptors exist. They can be called "3D descriptors" (cf. Figure 2.2). The definitions of these descriptors are not as open to debate as these of 2D descriptors. For instance, the definition of the length of a dune as the length of its crest line is intuitive. The orientation of a dune is defined as the direction of the line passing through the extremities of the dune.

All these descriptors have been combined to propose new metrics bringing additional knowledge on dune morphology. These metrics being defined from the other descriptors, their values depend on the chosen definitions of the 2D/3D descriptors. This can complicate the comparisons of the values between studies. To facilitate comparisons, a first step would be to specify the used definitions.

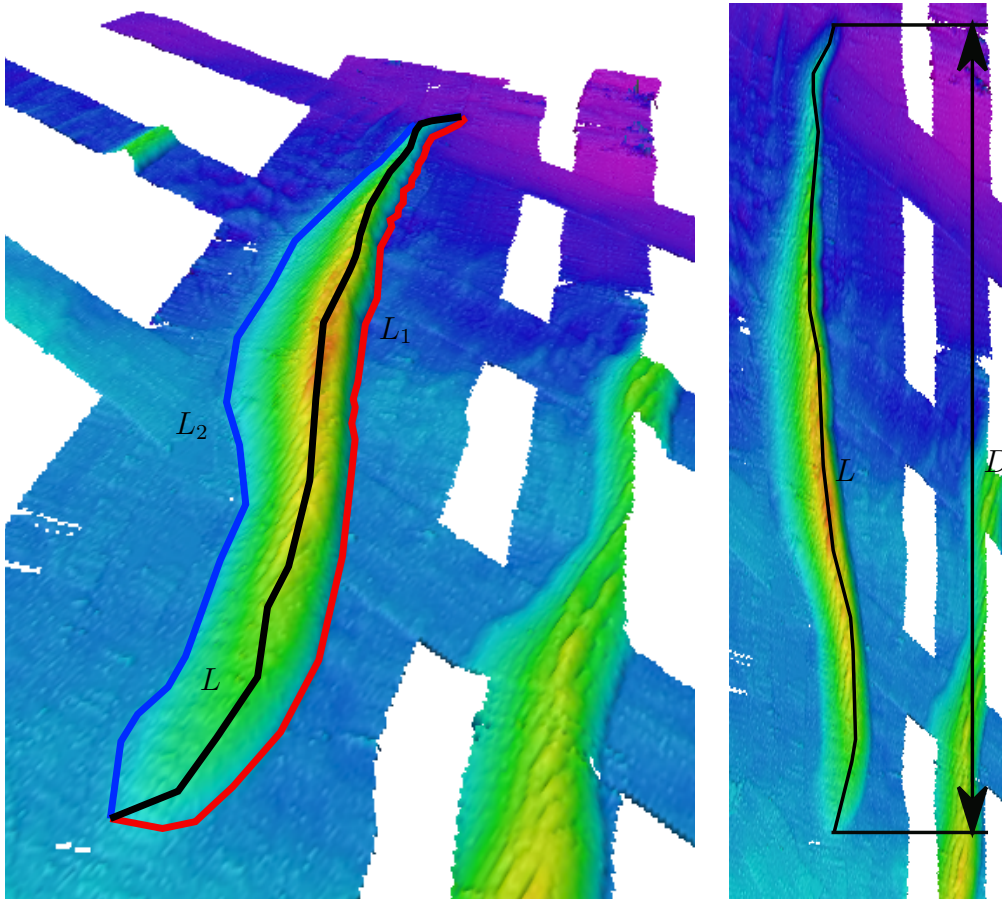


FIGURE 2.2: 3D dune descriptors. L : Crest length; L_1 : Stoss side length; L_2 : Lee side length; D : Geodesic distance between dune extremities.

Here are examples of such combined metrics:

— Steepness index:

$$SI = \frac{H}{W},$$

where H is the dune height and W correspond to the width.

— Asymmetry:

Definition 1:
$$A = \frac{W_2}{W_1}$$

Definition 2:
$$A = \frac{W_2 - W_1}{W_1 + W_2}$$

Definition 3:
$$A = \frac{\lambda - 2L_s}{\lambda},$$

Definition 4: Definition based on the slopes of the Lee and Stoss sides.

with L_2 the Stoss side width, L_1 the Lee side width and λ the wavelength. The readers may find the respective definitions in Franzetti et al. (2013), Knaapen (2005), Xu et al. (2008)).

— Sinuosity:

$$S = \frac{L}{D},$$

where L is the dune length and D the distance between dune extremities.

These new descriptors complement the first and provide information about the symmetry of dune crest, dune "saliency" or linearity. Yet, some might also have multiple definitions.

Table 2.1 sums up information about morphological descriptors and depicts the difficulty of having consistent definitions.

Parameter	2D/3D	Single definition (Y/N)
Length	3D	No
Height	2D	No
Wave length	2D	No
Lee side slope	2D	No
Stoss side slope	2D	No
Asymmetry	2D	No
Maximum slope	2D	No
Volume	3D	Yes
Sinuosity	3D	Yes

TABLE 2.1: Usual dune morphological descriptors and the level of ambiguity of their definitions

Descriptors are meant for quantifying dune morphology. Yet, they have not been used to quantitatively identify different types of dunes. The qualification is left to human expertise and so is purely empirical and visual.

To summarize, clear definitions of the morphological descriptors have to be adopted to make thorough comparisons between studies. Consequently, the definitions used should be included. Numerous descriptors exist and it would be interesting to exploit all of them to describe the outstanding diversity of dune shapes.

2.2.3 Dune types

In order to differentiate the diverse dune morphologies, scientists have developed an appropriate vocabulary. This terminology is widely used to characterize dunes (linear, sinuous, trochoidal, barchan, barchanoidal, transverse, longitudinal, (a)symmetric, bifurcated, isolated, 2D/3D, *etc.*). These adjectives could be referred to as "dune types". This subsection aims at describing and visualizing these dune types and explaining why it is difficult to create a classification encompassing all of them.

The bathymetry of the area named "Langoustiers" is shown on Figure 2.3. In the bottom-right corner, dunes are several meters high, linear and parallel. A linear dune has a straight crest line. In the top-right corner, it seems that dunes are fragments of an old bigger dune. And, in the left part of the image, there is a mix of high, shorter, sinuous (not straight), linear, splitting and merging dunes. This dunefield perfectly illustrates the diversity of dune morphologies and how the spatial organization and nature of dunes can vary even on short distances. The use of an automated dune extraction algorithm will enable an improved quantification of dune morphology for similar, complex areas.

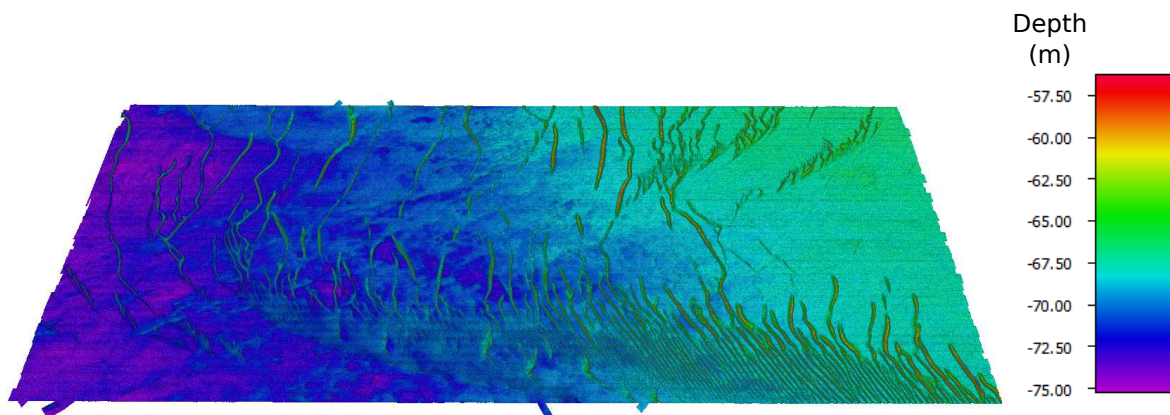


FIGURE 2.3: Bathymetry of "Langoustiers" zone surveyed in 2016 (dimensions: 20×7.5 km).

Figure 2.4 is an example of a dunefield disturbed by a shipwreck. The dunes are linear and almost identical except upstream and downstream of the wreck. The way the dunes are affected by the obstacle is hard to explain and it makes this dataset an interesting study case. It highlights the fact that the changes in the topography impact the hydrodynamics. The modified currents disturbed the sediment transport and changed the dunefield morphology. Moreover, this dataset shows that other features

lie on the seabed. And, the dune extraction algorithm will have to make the distinction between dunes and the other seabed features.

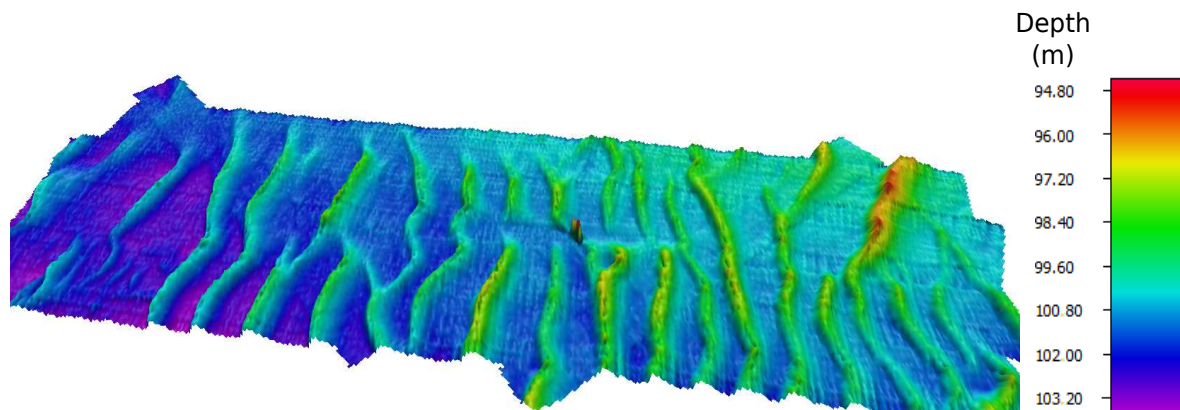


FIGURE 2.4: A dune field located few kilometers North of Portsall surveyed in 2016 (dimensions: 3.5×1 km).

If the previous area is classical (apart from the wreck) with parallel dunes, some areas are so complex that they cannot be precisely described. The area of Figure 2.5 is located hundreds of kilometers to the West of Brest. It is on the French Exclusive Economic Zone (EEZ) border. Despite the high depth, there are dunes and even on the shelf slope as one can see in the southwestern corner. By zooming in, it can be noticed that the entire area is covered by dunes. But they all seem different and some are hard to describe. With hindsight, this is a typical case where a human expert will hesitate on the extraction of dunes. It is difficult to know where a dune crest starts and ends. It is even more difficult to determine their boundaries. The manual dune analysis is almost impossible on this area. Therefore, it may also be difficult for an automatic algorithm to characterize these dunes and its results will probably exceed our expectations. In such a situation, an automatic procedure might be a great support for analyzing dunes.

Another example of particular spatial organization of dunes is shown on Figure 2.6. The dunefield of Figure 2.6 contains linear dunes of various lengths (150 m to 2 km) and heights (1.5 to 5 m). The smallest dunes are organized in a way that suggests that they are fragments of former long dunes. In the bottom-left corner, the dunes are strongly asymmetric (different in the slopes of the Lee and Stoss sides). Another specificity of this dunefield is that the variations in the dune orientation is abnormally large. Hence, the spatial organization is the most interesting aspect of this dataset.

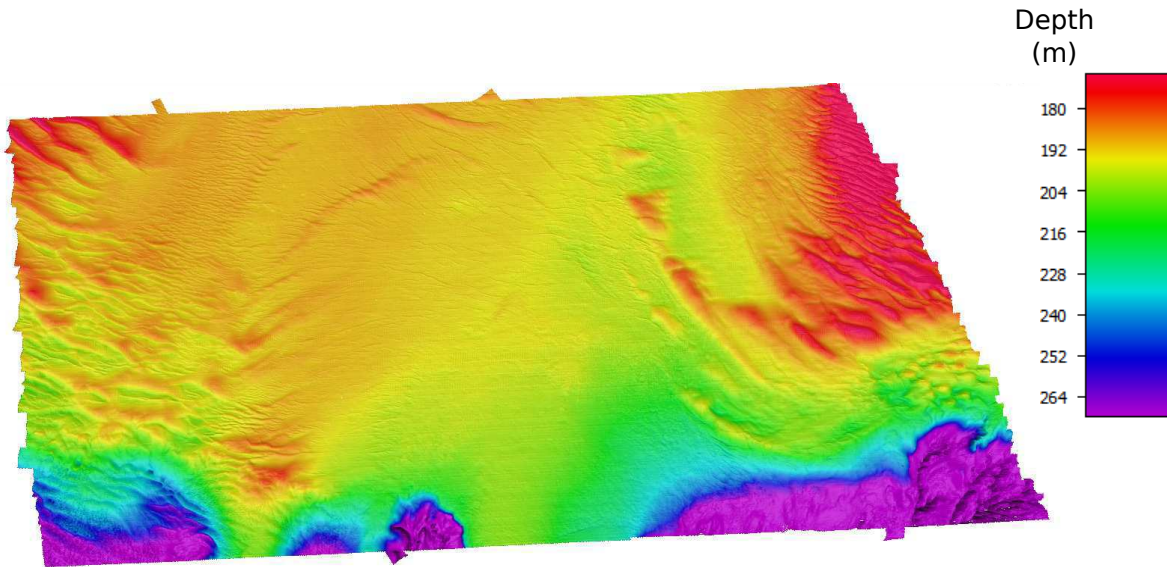


FIGURE 2.5: Dunes at the border of the French continental shelf discovered during 2016 SHOM campaign (dimensions: 40×18 km).

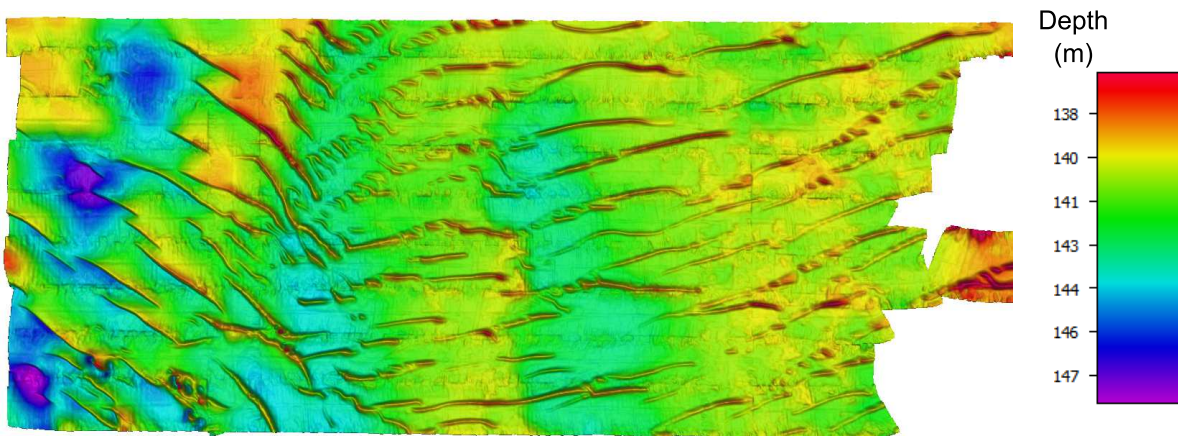


FIGURE 2.6: DTM of an exceptional dunefield (dimensions: 14×6.5 km). This dunefield will be called SHOM zone 6 in the remainder of this manuscript.

More classical dunefields might be simpler to analyze. Figure 2.7 illustrates another dunefield where dunes are parallel with is a usual pattern. Yet, this dunefield is also original. Some dunes are much higher than other (\sim four meter high vs \sim 12 meter high). The dune spacing varies from a few hundred meters between the smallest dunes to more than one kilometer between the largest. In the North, there is a rocky area where dunes are split by rock heads. This is a case where the extraction of dunes will be delicate. After the wreck, rocks are another type of seabed features that the dune extraction algorithm will have to distinguish from dunes.

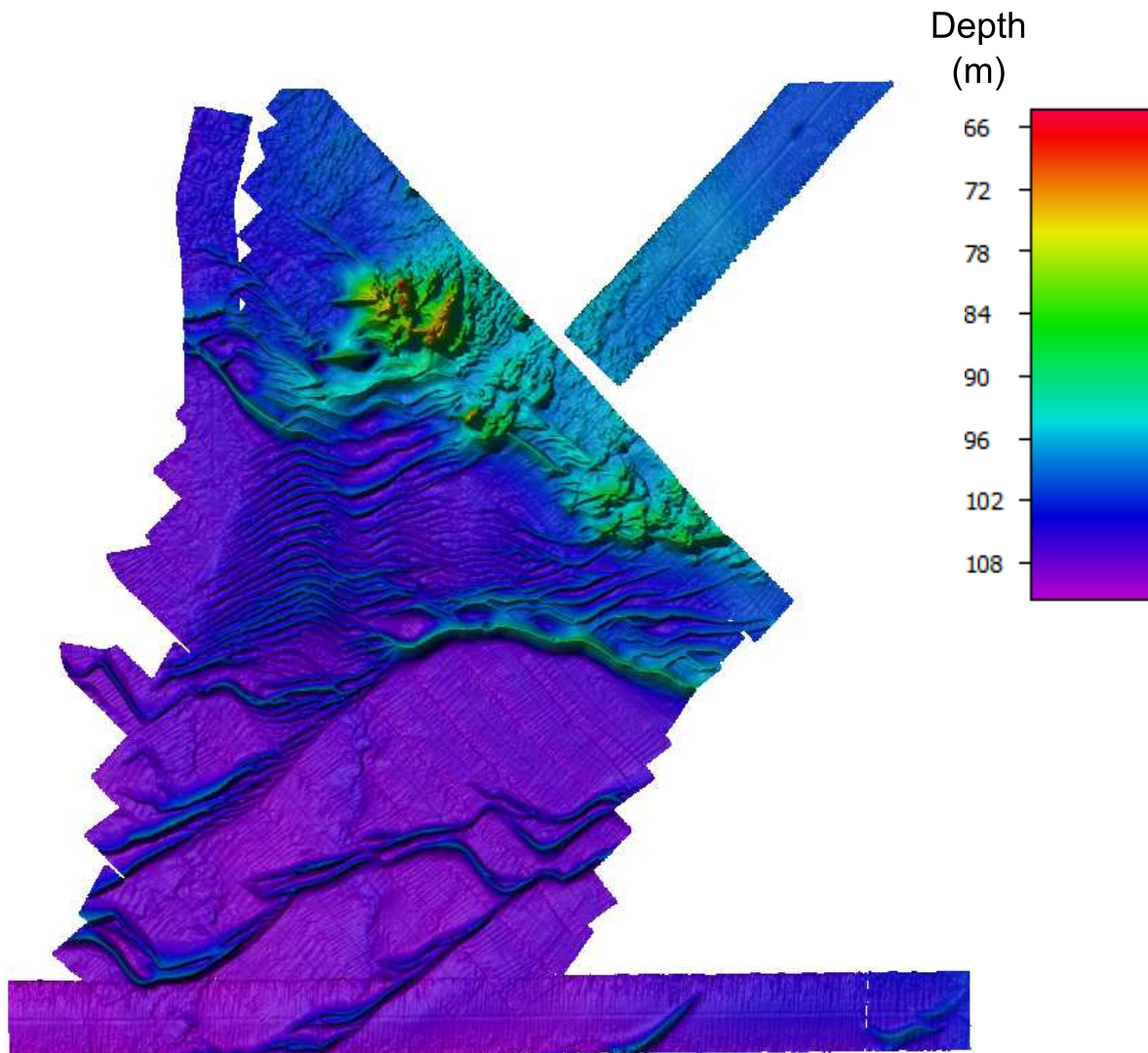


FIGURE 2.7: A dune field surveyed in 2013 off the coast of Brittany (dimensions: 10×10 km). I will be referred to as SHOM zone 1 in the following.

The bathymetry of Figure 2.8 displays a typical shallow dunefield. The dunes are crossed by sand ripples. Although sandy bedforms show a continuum of shapes and sizes, it is still possible at the scale of a dunefield to differentiate ripples and megaripples from dunes due to the difference of dimensions (width, wave length, height). The observations of a large panel of dunefields yield the determination of the 1m height threshold mentioned in Subsection 2.2.1. These ripples have different orientation to the dunes. The presence of ripples will complicate the dune extraction as it modifies the bathymetry and distorts the dune crests. Besides, ripples may be as long as dunes. The mobility of the dunes added to their height and the low depth make this area dangerous for navigation safety. The analysis of the dynamics of such an area is therefore of major importance.

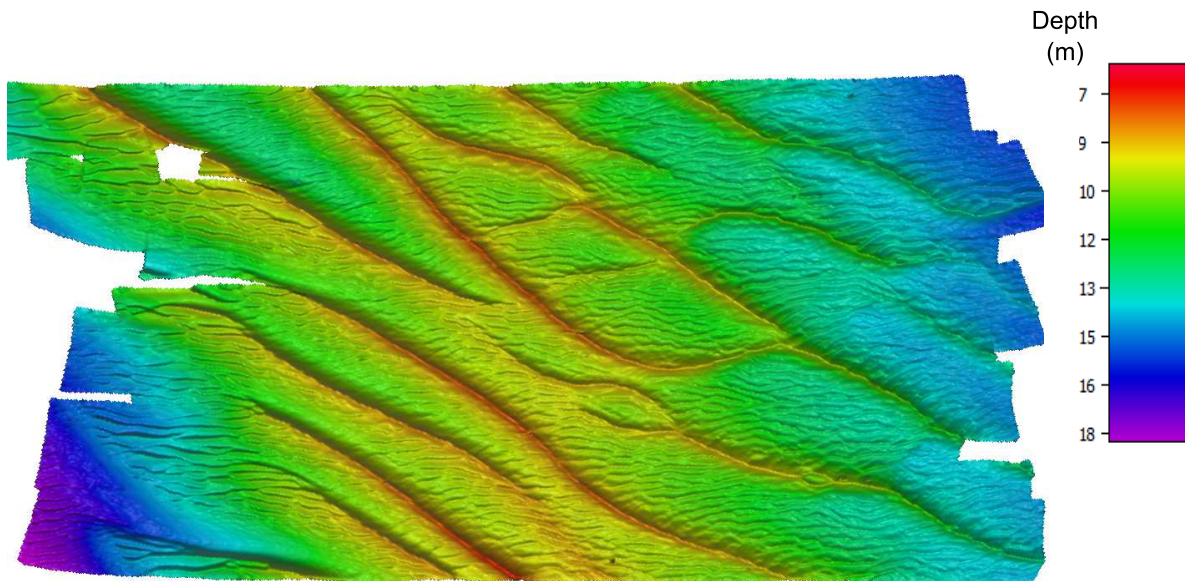


FIGURE 2.8: Bathymetry of R2 monitoring area in 2012 (dimensions: 1.7×1.2 km).

If dunefields may be diverse in terms of spatial organization, their composition is another aspect of their complexity. Although linear, parallel dunes are typical, other dune types exist. Figure 2.9 shows a mix of barchan dunes (isolated dunes) and barchanoidal ridges. The barchan dunes have a characteristic crescent shape. Barchanoidal ridges are approximately lined up, connected barchan dunes. They are long and sinuous since barchans are not straight dunes. Barchanoidal ridges are parallel and seem to connect with barchan dunes as if they were merging (extending). Other dune geometries are visible. They look like transitional dunes between barchanoidal ridges, and connect barchanoidal ridges in the left of the area with these in the right part. This area reflects the complexity of dune and dunefield geometry. It is rather unclear what should be defined as a dune in this dataset except for the barchans. Therefore, it would be interesting to see how an automatic dune extraction algorithm performs on this dataset.

Another special dune type is trochoidal dunes. Figure 2.10 shows a dunefield composed of trochoidal dunes up to fifteen meter high. The typical scar marks at the extremities of these specific dunes are to be noted. Compared to other dune types, trochoidal dunes are narrow and high. Their crests have a parabolic shape.

All figures¹ presented in this subsection give an overview of dune diversity. The human eye is capable of catching all these subtle differences. That is probably why the data analysis is still mostly visual. Yet, a visual description of a dunefield is not sufficient to make comparisons between datasets. The morphology of dunes and dunefields must be quantified in order to reveal potential specificities.

1. The locations of these dunefields are shown on Figures 3.5 and 3.7.

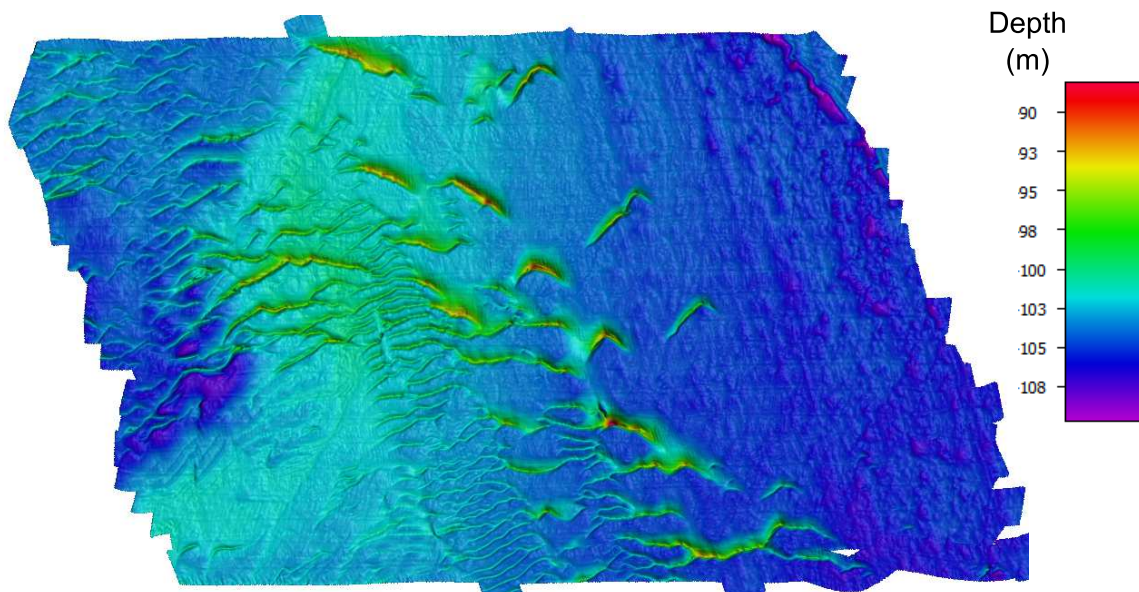


FIGURE 2.9: Example of barchan dunes and barchanoid ridges (dimensions: 19×11 km). From now on, this area will be named SHOM zone 4.

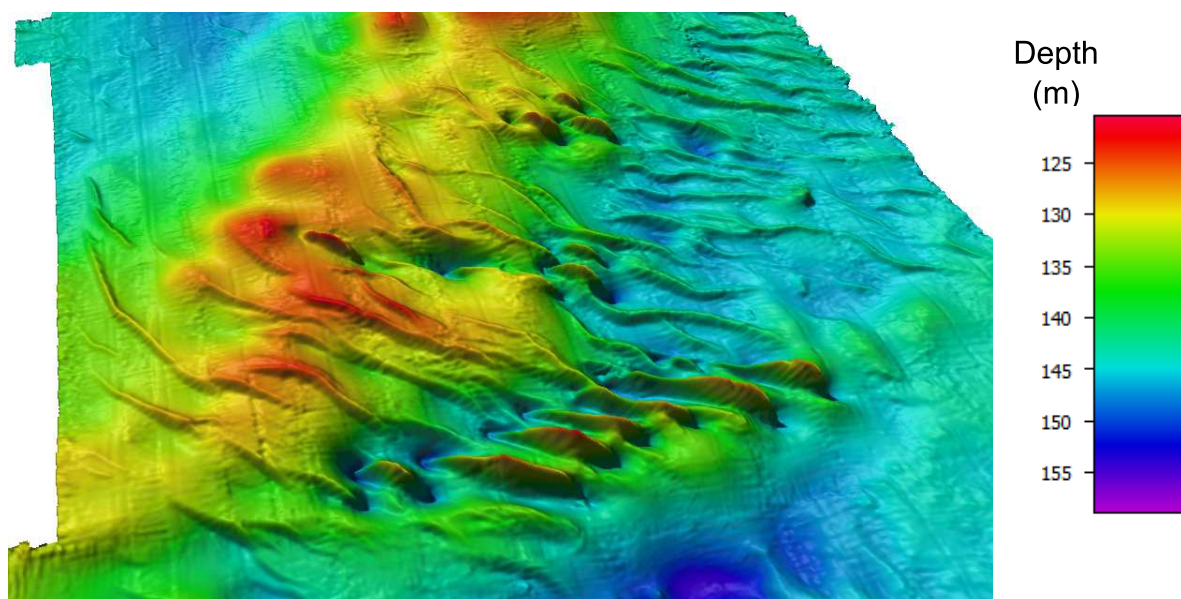


FIGURE 2.10: Trochoidal dunes off the coast of Brittany (dimensions: 13×13 km). This area will be denoted by SHOM zone 5.

The existing dune taxonomy allows description of dune types, but some dune types are overlapping. For instance, a dune can be both linear and asymmetric. Furthermore, some dune types come from classifications of eolian dunes (barchans, transverse, longitudinal (McKee, 1979)) and their definition is originally based on the orientation of the dune with respect to the current direction. Others are simply derived from dune morphology (linear, sinuous, asymmetric, *etc.*). Sometimes, there are small distinctions between two types. A barchan dune is isolated whereas barchanoidal dunes are close

barchan dunes forming a ridge. Thus, the dune types may also involve the immediate dune environment. Hence this characterization in dune type remains qualitative as it is inspired from human observations. Consequently, it has not been translated in terms of dune morphological properties (criteria on the height, length, width, *etc.*).

To add to the terminology of dune types, a dune can be isolated (with no other dunes in its close vicinity) or not, stand on a base such as a bank, interact with ripples, rocks, wrecks or with other dunes. A good way to appreciate the difficulty of studying dunes is to visualize the bathymetry of dune areas. The link between morphological descriptors and dune types is missing. In this regard, a dune extraction algorithm will allow analysis of each dune. Afterwards, more specific descriptors could be proposed to determine the type of a dune and even to analyze its environment.

2.2.4 Classifications of sand waves

A relevant classification with regard to the field observations needs to integrate dune morphology and dynamics. Other classifications exist and are based on hydrodynamical environment and sediment properties (Kleinhans, 2004, Southard & Boguchwal, 1990). The first sand wave classifications only took into account the nearshore structures. For a long time, these structures were the only ones easily accessible and monitored. A classification of bedforms in a tidal environment has been defined Robert W. Dalrymple & Lambiase (1978). Another classification compares sandwave morphology to tidal range (Boothroyd & Hubbard, 1974, 1975).

The most commonly adopted classification is Ashley's (Ashley, 1990). It was mostly based on flume dunes and is valid for dunes generated by unidirectional and/or alternate currents.

Class	Wave length λ (m)	Estimated height H_{mean} (m)
Small dunes	$0.6 < \lambda < 5$	$0.075 < H_{mean} < 0.4$
Medium dunes	$5 < \lambda < 10$	$0.4 < H_{mean} < 0.75$
Large dunes	$10 < \lambda < 100$	$0.75 < H_{mean} < 5$
Very large dunes	$\lambda > 100$	$H_{mean} > 5$

TABLE 2.2: Ashley's classification of marine dunes under unidirectional and/or alternative currents. H_{mean} : Dune mean height.

Even though higher dune diversity has been discovered since the definition of this classification, it is still endorsed by the scientific community. The classes are defined with wavelength and height criteria (see Table 2.2). All the dunes presented in this thesis are classified as large or very large dunes. It shows that this classification is not sufficient to distinguish between dune morphologies. A proposal for modifying the classification was made by Garlan in Garlan (2009). The last class is divided into a "very large dunes" class and a "giant dunes" class.

Migration speed and evolution timescale are elements that can be considered in periodic bedforms classifications (Dodd et al., 2003, Dyer & Huntley, 1999).

A good classification must comply with basic rules:

- It must be based on descriptive parameters with a clear definition;
- The classes must be exclusive;
- The classes boundaries must be quantitatively defined and have descriptive names.

Dune types cannot be discriminated by the existing classifications. No difference is made between trochoidal dunes, barchans or linear dunes whereas they show distinctive morphologies and dynamics. The dune descriptors used (height, wavelength) are not sufficient for defining these classes, which will require the definition of more evolved descriptors and dynamical parameters. It will be interesting to see how the existing dune analysis techniques may be useful for the characterization of the dune types.

2.3 Dune morphology analysis

The monitoring and tracking of marine dunes, as they are subaqueous, is not as easy as for mountains or even eolian dunes. Dunes were discovered with the use of SingleBeam EchoSounder (SBES) sonars, and the understanding of dunes was strongly limited by these acquisition technologies, thus, before 1980, the interpretation of data was delicate. Now the advances in sonar and positioning technologies make possible the full description and analysis of dunes.

Since the middle of the 1990s and the appearance of MBES technology, a full 3D representation of the bathymetry is now accessible to scientists. In this regard, it is a major breakthrough for the study of dune morphology. In addition, the advents of Global Positioning System (GPS) (Differential GPS (DGPS) appearance, Real Time Kinematic (RTK) navigation, Precise Point Positioning (PPP) solution, *etc.*) enable high quality georeferencing indispensable for the analysis of dune migration.

SBES surveys generally consist in acquiring depth measurements along survey lines. Scientists then worked on these bathymetric profiles to quantify dune morphology and dynamics. It is essential to bear in mind that the study of dunes has long been related to these profiles and that most analysis methods and classifications were developed in this context. The visualization of dunes with bathymetric profiles is still very common despite the available 3D datasets.

With the new 3D acquisition systems, the richness of dune shape is steadily being exposed. Numerous publications aim to share new datasets of dunefields having remarkable characteristics with the scientific community. Dune diversity expresses itself in many ways. Dunes vary amazingly in terms of environment (depth, location, hydrodynamic forcings, sedimentary composition, dynamics, shape or size). As has already been said, dunes are seabed features regulated by complex, coupled mechanisms. Hence, this diversity could be expected. Dunes were discovered in rivers (Carling et al., 2000, Hardy et al., 2006, Lisimenka & Rudowski, 2013), nearshore (cf. Figures 2.8 and 1.3), by shelf breaks (Figure 2.5), and even in the deep oceans.

In order to quantify and understand this diversity, geoscientists have developed several dune morphology analysis approaches. These methods are presented in the next subsections.

2.3.1 Traditional dune descriptive analysis

Today, the analysis of dune morphology remains mainly manual. The extraction as well as the estimation of the descriptors are both made manually. Experts visualize the bathymetry of a dune area. Dune crests and feet are drawn on the computer screen. In many cases, it is not easy to determine where dune boundaries lie (Thibaud et al., 2013). In this case, the transitions between the dune flanks and the seabed are steady and gentle. The position of dune boundaries is easier to determine when dunes are parallel and close. The manual delineation of dunes is highly subjective. In cases like Figures 2.7, 2.9, 2.10 where dunes are entangled, it is not easy to determine where dunes start and end. The crest delineation may be stopped at each bifurcation and merging or a branch may be followed to extend the crest. Braid-like patterns are commonly found in field data. The manual digitization results depend on where the operator started his work.

MBES data acquisition brought 3D topography but the cost is the huge amount of data. The manual processing cannot keep up with the pace of collection and much data

remains to be analyzed. The estimation of the descriptors is made by human experts as well. This work is time consuming, tedious, subjective and not repeatable. It prevents scientists from spending more time on high added-value tasks such as the definition of new descriptors and classifications.

In this context, the need for the automation of dune delineation arises. An automatic algorithm would cope with the subjectivity and repeatability issues as well as save valuable human time.

The values of dune descriptors found in publications are estimated manually. Much works consist of presenting newly discovered and remarkable dunefields (Barnard et al., 2006, Franzetti et al., 2013, Garlan et al., 2013, Van Landeghem et al., 2013). The morphological descriptors are estimated and dune crests drawn to justify of the originality of the presented datasets. Classically, comparisons with datasets in the literature are also made, but dune characteristics (length, width, height, *etc.*) are manually estimated and the way they are calculated is often omitted, raising questions about the validity of the comparisons.

Even though bathymetric data is systematically recorded, other data sources bring complementary information. Collecting miscellaneous *in situ* measurements (bathymetry, currents, granulometry, *etc.*) appears useful to provide potential explanations to observed physical phenomena.

For instance, seismic data, Acoustic Doppler Current Profiler (ADCP) (current) measurements or grab samples are sometimes taken for explaining dune formation or migration (Ernstsen et al., 2004, Ferret et al., 2010, Mosher et al., 2000, Van Landeghem et al., 2013). In Ferret et al. (2010), the author thoroughly analyzes the different data to make assumptions about the dune formation, morphology and dynamics. ADCP and MBES are combined by Hardy et al. (2006), showing that dunes are 3D structures and that bathymetry and flow are too often considered from a 2D perspective. The impact of lateral flow and secondary circulation on the flow structure and thus dune morphology can be significant whereas it is generally neglected in the wider literature. ADCP and grain size measurements are used by Ernstsen et al. (2004) to explain how linear dunes turn into barchan dunes due to lateral grain size variability.

Other papers try to investigate hypothetical relationships between dune properties (Bartholdy et al., 2005, Flemming, 2000). The objective is to find laws between the morphological and migratory descriptors, hydrodynamics and granulometry. Flemming compiled height and spacing values from about 1500 subaqueous flow-transverse ripples and dunes Flemming (2000). The database is a mix of natural and laboratory dunes

bedforms. He attempted to prove the existence of an exponential relationship between these two descriptors. This law is deemed universal but not all site-specific datasets stick to it. When data do not follow the global trend, the explanation comes from the local conditions. In addition, Flemming points out the lack of real, scientific comparisons in the literature. Datasets differences are observed and put aside unexplained. The conclusion is that the study of specific cases is interesting but that the study of general trends is more important at first. Besides, data sharing should be a more common practice.

Accordingly, Bartholdy worked on common hypotheses such as the dependence of dune height and wavelength to flow depth or the influence of flow and grain size on dune dimensions (Bartholdy et al., 2005).

The descriptive analysis of dune morphology and dynamics is used for monitoring, economic and environmental purposes too. Marine dunes represent a major and easily accessible source of aggregate, which is a lucrative business. In Belgium, policies were adopted to control this activity. Its impact on dunes has been monitored for over thirty years, and many scientific publications have been written on the analysis of monitoring data (Degrendele et al., 2010, Roche et al., 2013, Van Lancker et al., 2010, Vera et al., 2010). These publications are very important as they assess the impact of the extraction on the sediment stocks but also on biodiversity and coastal protection. Based on this monitoring, extraction can be stopped in endangered areas.

Garlan (2009) shows that dune description should not be limited to the estimation of metrics. This information should be stored in GISs and used for other applications such as navigation safety, mine burial, installation of windfarms, pipelines or communication cables.

To conclude, these works highlight the fact that new dunefields are frequently discovered. They are exceptions in the sense that these new dunes differ from what is already known by their spatial organisation, morphology or dynamics.

Descriptive dune characterization is a key step towards a better understanding of dune mechanisms. Additionally, the descriptive analysis captures dune morphological and dynamical specificities in descriptors that can be integrated in models afterwards. In this respect, it has a role of support. The finer the dune description is, the more accurate models get. In return, modelling provides feedback on dune morphology and its relationship with the hydrodynamics. Then, dune parts impacting the hydrodynamics deserve being more thoroughly inspected, but it will require designing automated methods to take the analysis one step further.

2.3.2 Automatic morphological analysis methods

In order to remedy the shortcomings of manual and visual dune characterization, researchers have proposed automatic methods. The methods for analyzing dune morphology can be divided into three categories. The first attempts to mimic manual processing methods on bathymetric profiles, while the second fits models to the dunes and to tease out dune characteristics for the adjusted best fit. The third category pictures bathymetry as a 2D signal and evaluates its frequency content. A review of the main methods for the quantification of dune morphology is made in Van Dijk & Lindenbergh (2017).

2.3.2.1 Bathymetric profile analysis

The following methods rely on the analysis of bathymetric profiles. Generally the first step is to remove the main trend of the elevation profiles so that the elevation is centered on zero. Mohrig & Blom (2008) define a roughness function:

$$RF(\eta, L) = \sqrt{\frac{1}{N+1} \sum_{\phi=0}^N \sum_{x=\phi L}^{(\phi+1)L} (\eta(x) - \bar{\eta}(x))^2}.$$

This function is inspired by the usual standard deviation function where L is the window size at which the roughness is assessed and N the number of such windows in the profile. $\eta(x)$ is the elevation at position x and $\bar{\eta}(x)$ the mean elevation in the corresponding window. L is steadily increased until RF values no longer increase. It gives a roughness saturation RF_{sat} value and the associated saturation length L_{sat} . The characteristic height and spacing of dunes in the profile can be estimated from these saturation values:

$$H_c \simeq 2.8RF_{sat}$$

$$L_c \simeq 1.5L_{sat}$$

The author obtained these relationships after the analysis of 17 profiles.

The method presented in van der Mark & Blom (2007) takes a different approach. The algorithm imitates the steps of the manual processing. After the detrending stage, zero crossings are detected. Prior to this detection, the profile elevation has been smoothed to avoid spurious detections. The next step consists of detecting trough and crest

points. At this stage, dune boundaries are known and dune height, width, steepness as well as Lee and Stoss sides' metrics are calculated.

A plot of slope aspect against slope magnitude enables determining dune orientation (P.W. Cazenave & Dix, 2008). A 1D Fourier transform of bathymetric profiles gives information about dune wavelengths and amplitudes.

These algorithms are simple to implement and fast to run. Yet, the 2D analysis has major disadvantages as described previously. The relationship between the roughness function and the dune properties is also very empirical in the first algorithm. The relationship is certainly not valid in all cases and the values are averaged over the whole profile and not calculated for each dune in the profile. With the second algorithm, morphological descriptors are given for each dune. The filtering step is directly linked to the crests and trough detections. Henceforth, the filter tuning may modify the estimation of the descriptor values.

2.3.2.2 Model fitting techniques

Working on 2D bathymetric profiles is not the only potential way for estimating dune descriptors. Model fitting methods are directly applied on DTMs and not bathymetric profiles. Most of these algorithms have in common the definition of a window. Bathymetry is divided into rectangular windows of a given size. A chosen model is adjusted to best fit the bathymetry in the window, and the model parameters give an estimation of the dune descriptors. The main differences between methods are the choice of model and the way its parameters are calculated.

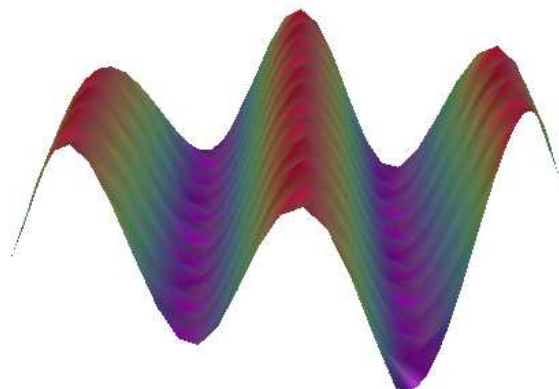


FIGURE 2.11: Base function of most fitting techniques.

Most of these techniques are based on a 3D sine wave function (cf. Figure 2.11). This function expression is:

$$d_p = \bar{d} + A \cos\left(\frac{2\pi}{\lambda}x_p + \phi\right),$$

where d_p is the depth at point P; \bar{d} is the average depth in the window; A the amplitude; λ the wavelength; x_p is the abscissa of point P in a rotated frame. This model requires knowing dune orientation to be fitted to raw data. In the end, A and λ are seen as measures of dune height and spacing in the window.

This model is adopted in Lindenbergh (2004). The model parameters are sequentially evaluated. Procedures are applied to estimate each parameter independently. The fact that parameters are not simultaneously estimated is regrettable and it appears as if data is tweaked to match a (unsuited ?) model.

Dorst extends the model by adding a slope term. The model expression becomes (Dorst, 2004):

$$d_p = \bar{d} + ax_p + by_p + A \cos\left(\frac{2\pi}{\lambda}x_p + \phi\right).$$

A window is tested against three base models: (1) a horizontal flat seabed; (2) a sloping seabed; (3) the addition of a wave pattern to the slope (cf. the above equation). A least square procedure is applied to adjust the models. Statistical tests (more details are given in Dorst et al. (2007)) provide insight into the validity/faithfulness of the models. This method distinguishes between a few seabed types and characterizes dunes where found. The addition of a slope term allows alleviating the hypothesis that dunes stand on a flat seafloor. This is not always true, especially so for dunes superimposed on banks.

The bathymetry is analysed at the window scale. The extracted information about dune absence or presence and their properties are valid at that scale. These algorithms assume: (1) dunes are parallel; (2) dunes are linear; (3) the bathymetry contains only one oscillatory pattern. The dunefields presented in the previous section showed that these hypotheses are not always valid. And, in these cases, the dune morphology and organization is special. Therefore, it is particularly important to accurately quantify the morphology of these dunes. Furthermore, the dune characteristics are average values over the window. The dunes are not individually described, and are not delineated. Consequently, the number of dunes or their spatial organization in the window remain unknown.

The afore-mentioned methods approximate bathymetry with one function. Other techniques decompose the bathymetry into a sum of elementary functions. The idea is to extract dunes, megaripples and ripples independently with reduced bias.

Diop et al. (2008) use an Empirical Mode Decomposition (EMD). The bathymetry is reduced to a set of oriented sand wave profiles. Then, each profile is decomposed into oscillations called Intrinsic Mode Functions (IMFs). Finally, Empirical Images (EIs) are constructed from IMFs. These EIs can be associated to bedforms such as ripples, sand waves or dunes (Megaripples).

The decomposition in components can also be realized by using an ordinary Kriging system (van Dijk et al., 2008). The sand wave orientation is assessed from the analysis of directional variograms (search for the orientation of maximum and minimum variability of the depth). A subset of the whole dataset is used so that the sampled subset still contains information about the sand waves while diluting the importance of smaller depth variations. The Kriging system enables reconstructing a bathymetry free from higher frequency components. By subtracting the smooth bathymetry from the original, one can get the residual signal and repeat the process to distinguish the components of the bathymetry: banks, dunes, ripples. The properties of each component are estimated from profiles as in van der Mark & Blom (2007) but crest and trough points are defined as curvature extrema along the profile.

The bathymetry could be divided into empirical orthogonal function (EOF) (Reeve et al., 2008). This technique is used to define the patterns of spatial and temporal behavior in the seabed elevations. It is very similar to Principal Component Analysis (PCA). Nevertheless, dunes or ripples are not clearly associated to a mode. Consequently, the modes are not exploitable to quantify dune morphology.

2.3.2.3 Frequency analysis

As with the model fitting techniques, the notion of window is essential with frequency methods. Bathymetry is seen as a 2D signal, and its frequential content is evaluated for each window. The main distinction between these methods is the choice of basic functions in which bathymetry is decomposed.

2D Fourier transforms are used in various works (Guala et al., 2014, Lisimenka & Rudowski, 2013, Lyons et al., 2002, P.W. Cazenave & Dix, 2008). Preprocessing is applied to deal with the spectral leakage. Then, lower frequencies corresponding to wavelengths less than half a window size are discarded as they mask the interesting higher

frequencies. The maximum energetic peak(s) are extracted from the power spectrum density graph. The analysis of these peaks gives the orientation and frequency of the sand waves. The standard deviation of the maximum peak provides information about the anisotropy of the seabed in the window (Lefebvre & Lyons, 2011, P.W. Cazenave & Dix, 2008); the presence/absence of dunes and dune height is estimated from the Root Mean square (RMS) of seabed amplitude (Lefebvre & Lyons, 2011). Differences between these techniques appear in the preprocessing stage and in the definition of the maximum peak (energy threshold).

In Lisimenka & Kubicki (2017), the height and wave length are estimated from the spectral moments. Spectral moments are metrics derived from the power spectrum.

An alternative to the 2D Fast Fourier Transform (FFT) is the Wavelet Transform (WT). Unlike Fourier analysis, the WT is spatially localized and gives spatial characteristics of the signals. A mother function (generally the Morlet) is chosen and scales corresponding to bedforms are defined. The main advantage of WT is that the amplitude of each bedform is known at any location. Furthermore, WTs can be extended to study time and spatial series. WTs have been applied to characterize seabed morphology (flume data (Cataño-Lopera et al., 2009), real data (Garcia & Best, 2012, Gutierrez et al., 2013)).

All the diversity and complexity of dune morphology and their environment show in the frequency analyses. The analysis of seabed frequency content appears useful to decide on the presence of dunes in the data and to characterize them. FFT techniques only give access to dune wavelength and orientation which are not the most relevant descriptors, and the information are regional (by window) and not for each dune. Wavelet analysis provides spatial information locally. Nevertheless, these methods aiming at decomposing the seabed into basic functions are dune detection and characterization algorithms more than extraction algorithms. These frequency methods allow for quantifying seabed roughness, discriminating the different bedform scales and estimating their respective characteristics. This information is precious especially for modelling purposes. Yet, our objective is to individually describe dunes. Thus, dune extraction is mandatory to know where dunes are, how many there are, analyze their morphology, their dynamics and their spatial organization. One of the goals of the thesis is to design an automated extraction algorithm meeting these specifications.

2.4 Dune dynamics and automatic algorithms

Similarly to dune morphology, the analysis of dune migration is still very visual. The migratory behavior was classically witnessed by surveying, with a SBES, the same line at different times (De Moor, 2002, Degrendele et al., 2010). Despite the development of MBES and 3D bathymetry, this procedure is still applied (Ernstsen et al., 2004, Mosher et al., 2000). But, the displacement direction being unknown, the estimation of the displacement is very uncertain.

Now that 3D maps are available, migration can be visualized by toggling back and forth between maps (Smith et al., 2007). DTM differences are also used to witness dune migration (Barnard et al., 2006, Franzetti et al., 2013). The problem with this technique is that dune location is unknown. Consequently, it is hard to estimate dune migration rate and direction. To drape the difference map onto the initial DTM is a way to determine the migration direction but not its rate (see Figure 2.12). On the figure, the dunes move, but it is not easy to see if they went to the left or the right and impossible to say how much they moved. The purple areas are areas where data were recorded only once so that the comparison cannot be made.

It must be noted that positioning accuracy directly impacts the quality of the migration rate estimation. Small bathymetric changes can now be observed thanks to Global Navigation Satellite System (GNSS) improvements. The depth differences in rocky areas are small in Figure 2.12, which proves the positioning consistency between the two surveys.

The most commonly used way to visualize and manually estimate dune migration is to draw dune crests and compare their positions at different times (Ernstsen et al., 2004).

Note that the dynamical behavior of dunes is often reduced to pure migration. The deformation of these structures is generally omitted as if dunes were rigid structures either staying still or migrating as a block.

Dynamics estimation algorithms

As for the dune morphology, automated methods have been designed to quantify dune migration. Some rely on the analysis of elevation profiles. The direction of migration is determined with asymmetry metrics in Xu et al. (2008). It is based on the observation that the Lee side is gently sloping and exposed to currents.

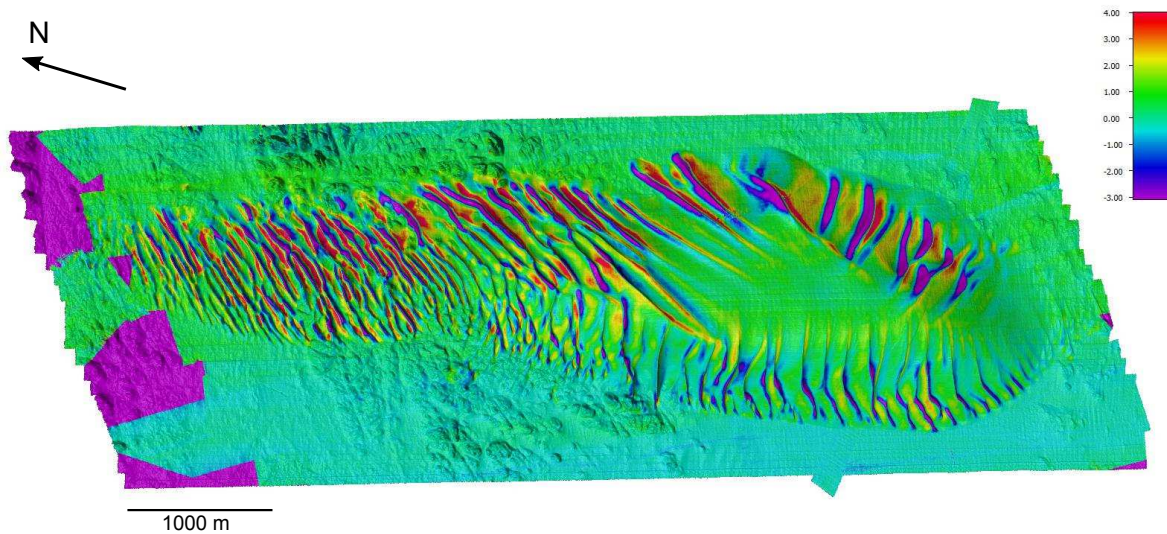


FIGURE 2.12: Seafloor variations on Ouessant bank between 2012 and 2016.

Therefore, the asymmetry indicates the migration direction. Another solution is to evaluate the correlation between elevation profiles and to determine the shift for which the profiles are best aligned (Mohrig & Blom, 2008).

A combination of 1D and 2D analysis is proposed in Knaapen (2004), Knaapen et al. (2005). Crest points are identified in bathymetric profiles. Next, a pattern recognition method is applied aiming at identifying corresponding crests. This technique makes the assumption that dune migration is smaller than a wavelength. A migration predictor was proposed by Knaapen (2005) after examination of real datasets with this technique.

2D methods for the estimation of the dune migration rate exist too. Most of them are based on a classic image processing technique, particularly spatial correlation (Franzetti et al., 2013, Zhang et al., 2016). The bathymetry is divided in rectangular boxes and compared to a later dataset by computing spatial correlation. The results are a migration vector for each box. An alternative is to estimate the correlation between slope maps (Duffy & Hughes-Clarke, 2005).

In Dorst et al. (2007), the authors reformulate their morphological model to integrate data from several surveys and estimate the migration rate in a selected direction.

Another way to study dune migration is to track dune crests, for which a graph-model approach is discussed in Thibaud et al. (2013). The graph is made of two types of relationships: spatial relationships and spatio-temporal relationships. Dunes are entities that have (close dune) neighbors (spatial relationships) and change over time (spatio-temporal relationships).

These migration estimation algorithms are implementations of visual analysis processes with the use of bathymetric profiles, crests and correlation. Their results are consistent with the manual estimations. However, dune dynamics are approximated by a vector (distance, angle) calculated over profiles or areas. We ought to analyze dune migration at an entity/dune scale. Furthermore, the distortion of dunes is often omitted and only the displacement part of dune dynamics is considered.

2.5 Dune numerical modelling

Modelers' goal is to reproduce hydrodynamic conditions, sediment transport and topography and to understand the functioning of this intricate system. Carling et al. (2000) is a perfect example. The author starts by making field measurements and then tries developing a model to find an explanation for observed local phenomena.

The first models used in this field were simple linear models, and complex interactions could not be taken into account. For instance, only unidirectional or spatially uniform tidal currents could be considered (Hulscher et al., 1993), and only large-scale dunes were generated by this model: smaller bedforms (small dunes, sand waves and ripples) could not be created. These models were 2D (Hulscher et al., 1993, Németh et al., 2002), but 3D modelling is possible (Besio et al., 2004, Blondeaux et al., 2001, Nabi, 2008, Németh et al., 2000).

Some models focus on one aspect of dunes: (1) dune generation (Besio et al., 2004, Blondeaux et al., 2001); (2) dune growth (Besio et al., 2004, Blondeaux et al., 2001); (3) dune migration (Blondeaux & Vittori, 2016, Dohmen-Janssen & Hulscher, 2008, Le Bot et al., 2000, Németh et al., 2000, 2002). Other models attempt to simulate all the dune development steps (Idier, 2002, Nabi, 2008). Idier (2002) simulated dunes having a behavior close to what is seen in the nature, but the model takes more time to run than real time. It is problematic for the prediction of dune evolution, but it is interesting to understand the functioning of dunes.

Models are developed to improve our knowledge of dunes. Thus, the principal mechanisms governing dune formation and growth were implemented in a basic model (Besio et al., 2004). Antidunes (Dunes migrating upstream) can be recreated in the model. The provided explanation is that it is caused with a particular phase difference between the M2⁴ and M4 tidal components and residual current strength.

4. M2 is the principal lunar semidiurnal constituent and M4 is a shallow water overtides of principal lunar constituent.

Thus, field observations may validate or not this theory. The model assumes the currents are unidirectional and it needs to be refined in order to estimate more accurately the migration speeds.

Physical phenomena can be studied separately to estimate their respective influence. The principal identified phenomena impacting the dune migration are the tidal currents, the specific circulation around banks, storms, and strong wind-induced currents that can reverse the migration speed or even direction (Le Bot et al., 2000).

Additional information (biology (Borsje et al., 2008) or field measurements (Le Bot et al., 2000)) can be integrated into models. The results show that the predicted wavelengths are closer to the observed values if biological activity is included in the model. Yet, improvements of the parameterization of biological activity would be necessary for long-term morphodynamic predictions.

As our understanding of dune-conducting mechanisms grows, more complex interactions can be added into the models. For instance, nonlinear models have been implemented to predict the influence of human activities such as sand dredging or the construction of pipelines on dunes. An overview of these models and their functioning is provided in Besio et al. (2008). Furthermore, three mine burial models are compared to field experiments in Guyonic et al. (2007).

Dune modelling is improving with realistic morphology and dynamics. However, models cannot explain all that is observed in the field. Knowledge needs to be input in the models to refine them, and the reliability of the simulations gets debatable for long-term analysis.

2.6 Conclusion

Dunes are the results of the interactions between sediment transport, currents and seabed morphology. The study of dunes relies on the analysis of field measurements or modelling. It is essential not to compare these approaches. Modelling is a scientific approach used for explaining observed, but not yet understood phenomena. Acquired data enables describing, quantifying and hypothesizing about dune morphology and dynamics. And, modelling helps in identifying the mechanisms under these phenomena, even evaluating their respective impacts and validating the hypotheses made from the field observations. Clearly, these works are complementary.

Although there is a true will to automate the analysis of dunes, the field still remains very empirical, visual, and descriptive. A lot of work needs to be done to cope with all the dune types. New dune types are being discovered and current classifications appear too simplistic. In addition, the common dune descriptors are directly related to these outdated classifications. Thus, many improvements can be brought to the descriptive analysis of dunes. And, as it complements the modelling approach, a more detailed description of dune morphology will help refining the models by making them more realistic. Furthermore, the rapid advances in calculation capacities enable the implementation of enriched models and reducing computational time.

The automation of dune morphological and dynamical analysis has started. Bathymetric data must be further exploited to improve quantitative dune analysis. The analysis of bathymetric profiles, or the regional approximations of the bathymetry, by sine wave functions do not allow analysis of the morphology of each dune and its changes.

Chapter 3

Database

Contents

3.1	Introduction	44
3.2	MBES Data and DTM construction	44
3.3	SHOM and Belgian Databases	48
3.3.1	Belgian data	48
3.3.2	SHOM data	51
3.4	Benchmark	53
3.5	Conclusion	58

3.1 Introduction

The main objective of this thesis is to design automatic algorithms for the study of dune morphology and dynamics. The primary step is to design an algorithm capable of automatically locating and, then, delineating dunes in the bathymetry. Once extracted, dune morphology and dynamics will be analyzed and quantitatively described using adapted descriptors. This procedure could be extensively applied to dunefields and the estimated metrics should be able to capture their observed, but as yet unquantified variability. Hopefully, this will lead to a better understanding of dune mechanisms and potentially to the development of a classification more representative of the terrain observations. There is a duality between morphology and dynamics and both aspects are to be considered equally. This chapter presents the database available to achieve our goal. A large amount of MBES data were made available to us by SHOM and the FPS Economy (Belgium Economy ministry) continental shelf service. These two offices respectively survey the French and Belgian continental shelves and so collect data over dunefields. First, MBES data properties and preprocessing steps are explained. Later, expected issues arising from data properties and processing for the extraction algorithm are discussed.

The SHOM and FPS Economy databases have distinctive objectives. The specificities shall permit studying thoroughly both aspects of dunes (morphology and dynamics). In this regard, the complementarity of FPS Economy and SHOM databases is examined. Instead of studying the entire databases, it was decided to focus on a restricted number of relevant datasets representative of dune diversity in shape and spatial organization. Thus, eleven benchmark regions were selected. These areas show a wide range of dune types and dunefield configurations, which allows for testing the robustness of the algorithm.

3.2 MBES Data and DTM construction

The 3D visualization of seafloor topography really began with the advent of MBES technology. But, to get this high resolution bathymetry, the acquisition of data other than MBES is mandatory. MBES data needs to be combined with multisensor data in order to get the final surface: a DTM. The merging of multisensors data and the following processing steps have potential issues that can lead to artifacts in the DTM and degrade its quality.

The construction of a DTM follows three steps. These processing stages are illustrated in Figure 3.1. The first step consists in creating "soundings" from raw data of several sensors. Soundings are georeferenced depth measurements. The second step aims at removing artifacts and outliers (spurious points). The third step is the generation of the DTM itself.

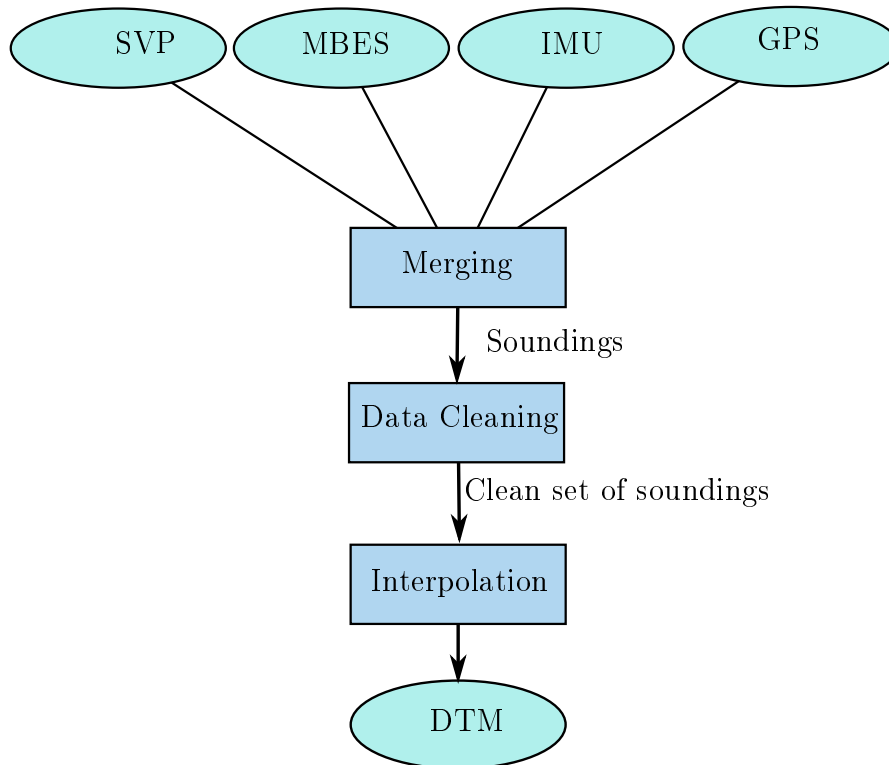


FIGURE 3.1: Diagram of the processing steps to transform raw data into a DTM.

In order to get soundings, four types of information are recorded and merged: Sound velocity profiles, MBES, Inertial Motion Unit (IMU) and GNSS¹ data. Sound velocity values merged with MBES raw data give range and bearing values corresponding to points on the seafloor in the MBES frame. The vessel attitude is monitored via the IMU. The depth measurements are corrected for the corresponding attitude values and then georeferenced using GPS data. Each sensor has its own frame, clock, and acquisition rate. Consequently, the merging of these data is not as simple and straightforward as it may seem. The rotation matrices between the frames, the lever arms between the origins of the frames and the eventual clock latencies must be estimated correctly. Calibration procedures are used to estimate these parameters prior to data merging. If the calibration is not conducted thoroughly, it might yield artifacts in the obtained sets of soundings. The presence of artifacts ought to be corrected in order to

1. The GNSS data used in this thesis are GPS data so that GNSS has been replaced by GPS in the following.

generate a faithful representation of the seafloor. However, the origins of artifacts are not always easily identified and corrected. These artifacts show in the final surface as vertical or horizontal shifts, oscillatory patterns or tilts visible where data overlap. At that stage, the seafloor topography is represented by a cloud of points: soundings.

Artifacts are not the only elements that can pollute the DTM. The next step is devoted to the removal of outliers. Outliers are spurious measurements that are inconsistent with the rest of the soundings. These outliers are caused by problems during the acquisition. Typically, they occur when the MBES algorithm fails in retrieving the depth measurement in the raw acoustic signal or when the GPS signal or corrections are lost. These erroneous data must be discarded. Traditionally, a human operator goes through all the soundings and cleans the dataset. Figure 3.2 is an example of a dune displayed as soundings after cleaning. The dune morphology is described by about fifteen thousand soundings. Over an entire survey, the number of soundings is generally of tens of millions or more, due to the increasing number of beams in MBES systems. This task is tedious, redundant and takes hours up to days but still requires great care to avoid deformations in the DTM. By consequently, automatic algorithms (Combined Uncertainty and Bathymetry Estimator (CUBE) Calder & Mayer (2003), Calder & Wells (2006), CUBE with Hierarchical Resolution Techniques (CHRT) Calder & Rice (2011), CHARM Debes et al. (2012)) have been proposed to at least help the human experts locating these inconsistent points and do the data cleaning if wanted. The first objective of CUBE and CHRT algorithms is to determine the depth value and the associated estimation uncertainty at any location for a noisy datasets. The obtained, faithful models can be used as reference surface and, thus erroneous soundings are detected.

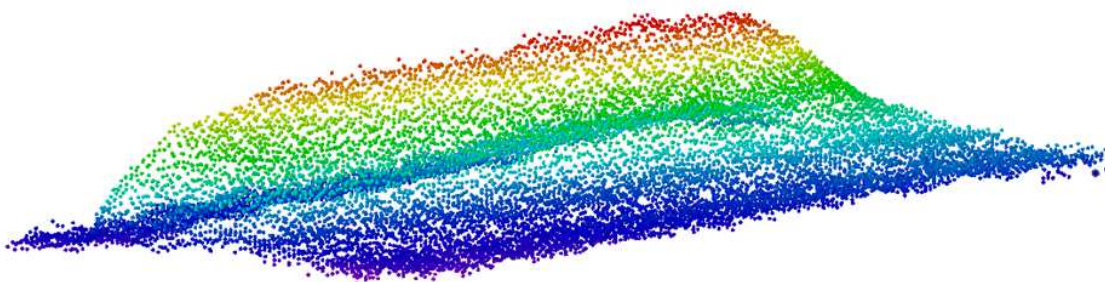


FIGURE 3.2: Representation of a dune ($750 \times 250 \times 4$ m) as a cloud of soundings. SHOM data acquired with a Reson Seabat 7111 - Western Brittany - October, 2012.

The third and final step is the sounding interpolation. A DTM is a grid covering the surveyed areas. A depth value is assigned to each cell of the grid. The estimation of these depth values is achieved by interpolating between the soundings. DTM interpolated depth values can be obtained by several ways. Kriging and its variations are a possibility. Another classic way is to define a search radius around the cell to gather the soundings close to each DTM cell. The gathered, measured depths are combined to determine the DTM cell depths. The afore-mentioned cleaning algorithms also reconstruct a DTM in similar ways.

The DTM resolution is directly linked to the cell size. A coarse resolution tends to smooth the bathymetry. Yet, the resolution cannot be arbitrarily selected. Each MBES beam corresponds to an insonified patch on the seafloor. This interaction between the acoustic signal and these patches leads to the estimation of the soundings. It was decided to define the DTM minimum resolution from the minimal size of these patches. This value will vary with the beam width (MBES resolution) and the depth. It would make no sense to lower the DTM resolution below this limit. Otherwise, the generated DTM would be finer than the data resolution it was made from. In other words, the DTM would not contain more valuable information and undesired noise that would make dune extraction more difficult. Once the resolution is fixed, the depths of the soundings within each cell are averaged to calculate the cell depth. In cases where the data density is too low, causing holes in the DTM, the DTM resolution was adjusted. Thus, a tradeoff is found to limit the impacts of acquisition noise, holes and smoothing in the process of dune extraction.

Figure 3.3 represents the 10m DTM of the dune shown in 3.2. This DTM is a representation of the dune with 1700 cells instead of fifteen thousand soundings with limited information loss and reduced noise. This dune lies at a depth of 140m and the sounding density is rather low. In shallow areas, the ratio between the number of soundings and the number of DTM cells can be much higher.

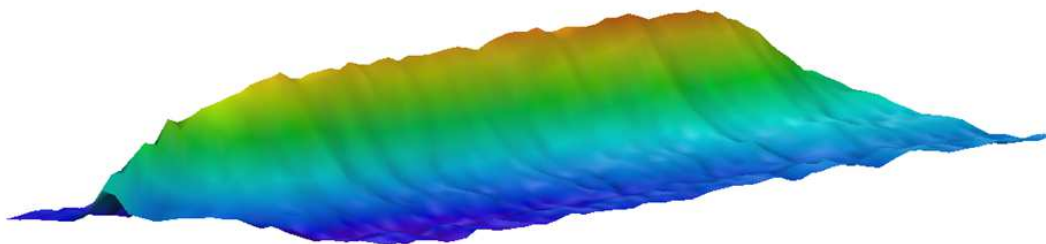


FIGURE 3.3: DTM of the dune created from the soundings.

3.3 SHOM and Belgian Databases

SHOM and FPS continental shelf service have acquired MBES data over sandy seafloors for over fifteen years. Both databases are unique in the nature of the dunes, the frequencies and purposes of the acquisition, the environmental conditions or the acquisition systems. These differences and their implications on the generated DTMs in the context of quantification of dune morphology and dynamics are presented in this section.

3.3.1 Belgian data

The Belgian continental shelf is not as extensive as the French one and has already been entirely surveyed. It is mostly shallow waters with depths up to 50 meters. Sand dunes and banks form a coastal protection and a large source of quality aggregate. In this context, FPS Economy continental shelf service is in charge of the sand and gravel extraction in the Belgian EEZ. Aggregate extraction is a major economic activity in Belgium so that it had to be framed in legislation. Each firm must be Belgian to be granted a concession from several authorities: the Minister competent for the economy, the Minister competent for the protection of the marine environment and an interministerial commission composed of governmental experts.

The conditions of extraction are described in a royal decree. It imposes the types of dredgers allowed, the minimal cruising speed when dredging. In addition, the extraction stops if the average depth in the area is 5m below the reference depth value. This reference value is the average depth of the area when it was first surveyed. Dredging is allowed in four control zones (cf. Figure 3.4).

In addition, eleven smaller boxes (see Figure 3.5) have been defined to monitor the impact of aggregate extraction on the sediment stocks. Some are within control zones in order to examine their health. Others are located in areas where extraction is prohibited to allow comparison with the exploited areas. When the dredging is considered too intensive, areas can be closed to extraction to protect the natural resources. The rule is to stop the dredging activity in an area when the area average depth is more than 5m lower than the first bathymetric data acquired on the area.

Continental shelf service makes one survey per year on control zones and several on monitoring areas. The objective is to estimate the global evolution of control zones and to make comparisons between extracted and non-extracted regions and a high resolution

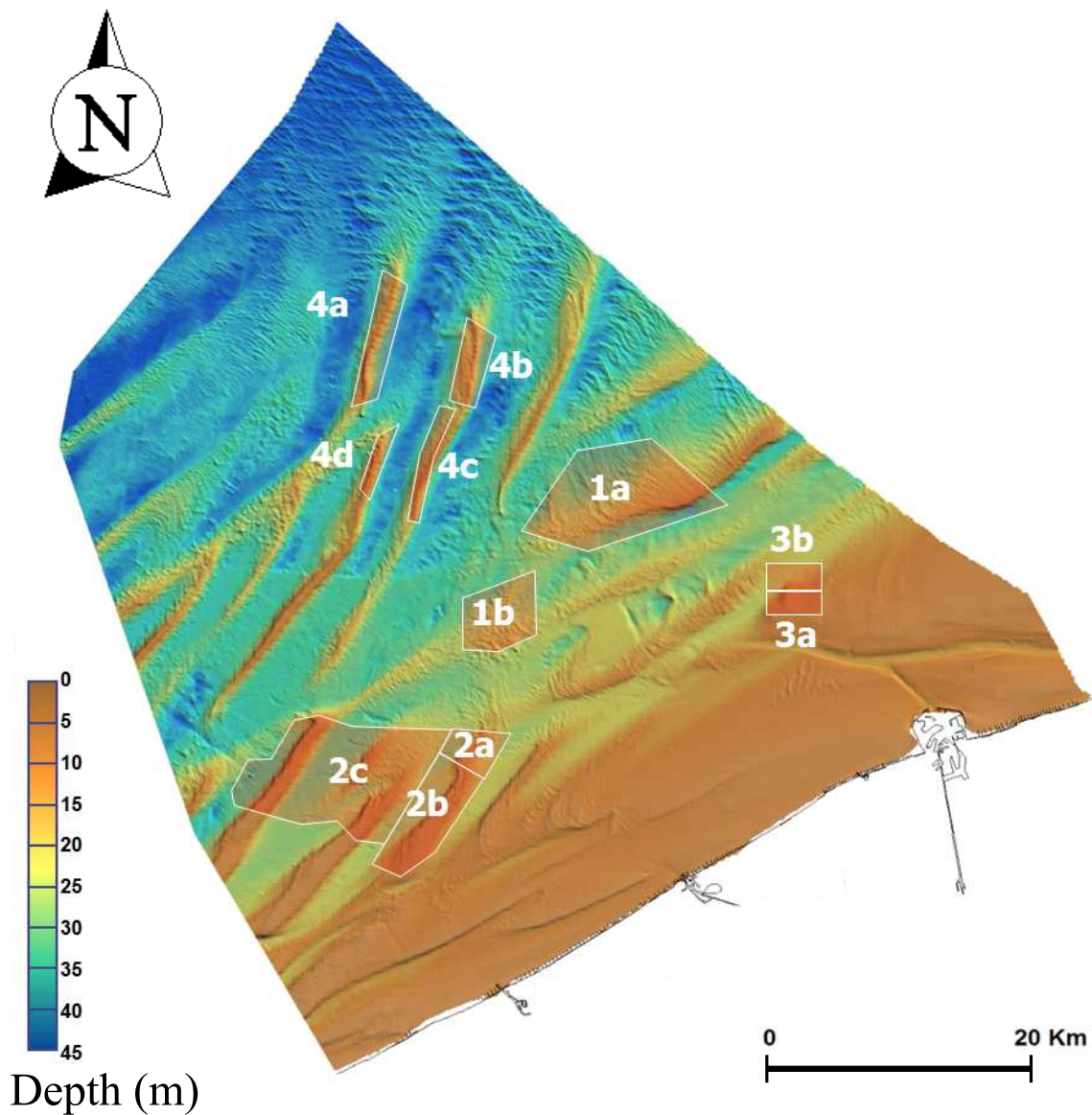


FIGURE 3.4: Locations of the 11 Belgian control zones

assessment of the extraction impact in the most intensively extracted areas, identified using ship tracking data. And, for some areas, MBES data have been recorded for about fifteen years. Most data were collected onboard R/V (Research Vessel) *Belgica* with little change in the acquisition systems except for the MBES, which was changed in 2008.

These regions of interest are located in shallow areas. The use of cutting-edge acquisition systems enables us to see great details of the complex seabed morphology. Three scales of sandy bedforms are present in the Belgian database: (1) sand banks; (2) dunes and (3) sand ripples. The order of magnitude of ripple height is 20/30 cm. Dune height is generally of two or three meters but can reach five meters or more. Banks

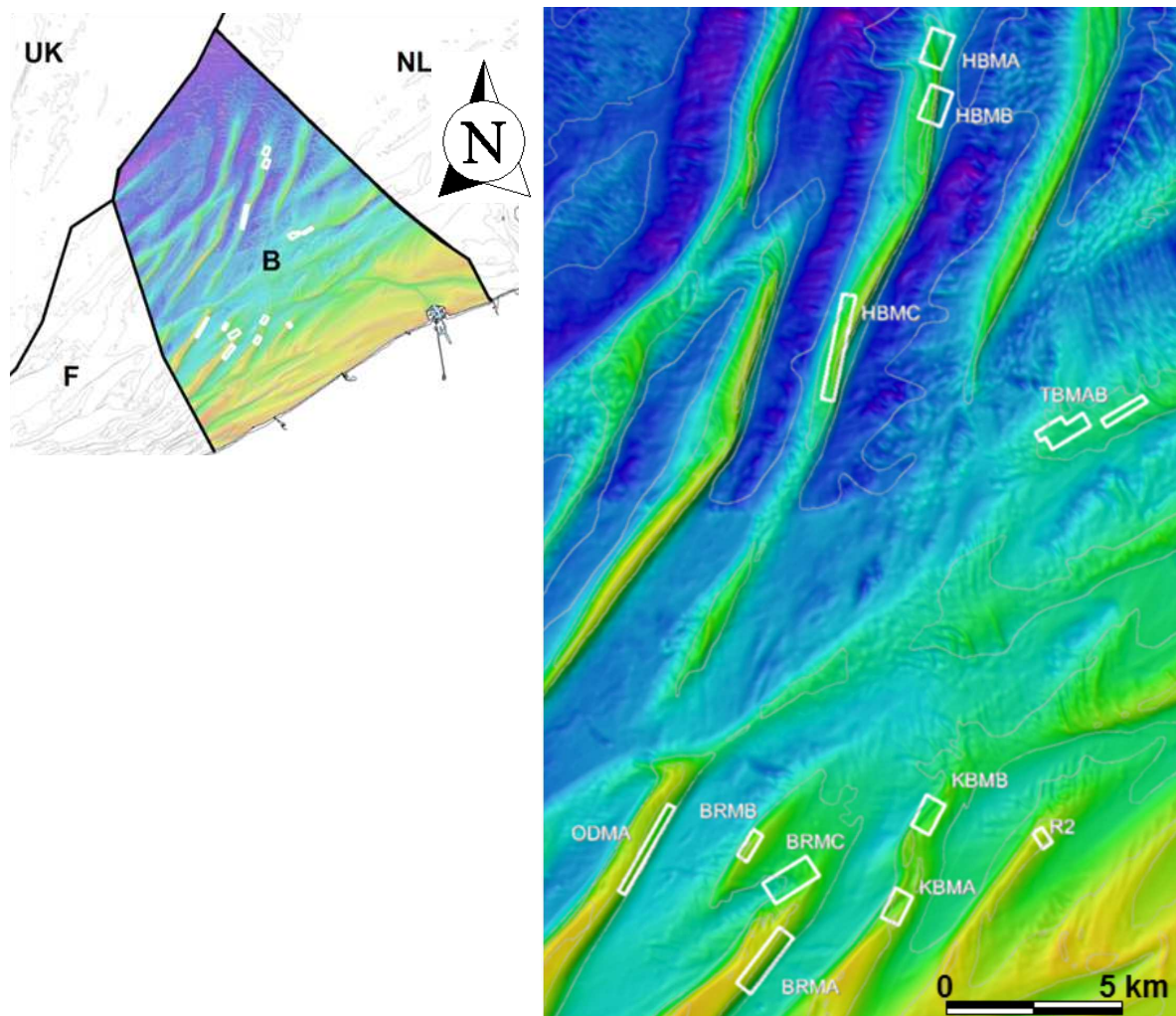


FIGURE 3.5: Locations and names of the monitoring areas

are more than fifteen meter high. These three levels of bedforms combine to create a complex topography. Note that ripples can be several hundred meters long, just like dunes, which will not help the dune extraction algorithm. The distinction between the two bedforms is not clear. For instance, dune height decreases at dune ends and sometimes split into ripples. But whether such a structure is several dunes or one is up to interpretation.

The Belgian database is ideal to study dune dynamics thanks to the consistency of the acquisition conditions and numerous surveys allowing the estimation of dynamics at different timescales. However, the complex spatial organization of dunes makes their extraction very challenging.

3.3.2 SHOM data

The French hydrographic office is interested in studying marine dunes too but for other reasons. The mobile nature of dunes makes them dangerous for human activities at sea and especially for navigation safety. Dunefields have to be regularly surveyed to ensure that navigation charts are up to date. The study of dynamics would enable optimizing survey planning. The sedimentology department is in charge of studying dunes. They store data DTMs in a Geographic Information System (GIS). These DTMs are used for digitizing dunes and estimating the values of dune descriptors. Most of the data I had access to were cleaned MBES datasets or DTMs. Artifacts were not all removed of these data and without raw data, no correction is possible. These artifacts are not a problem for visual analysis but might be for an automatic extraction. In addition, the acquisition date and system were not always available.

SHOM started recording data on dunes in the early 1990s, and annual campaigns are dedicated to dunes, although the French continental shelf is so large that it has not been fully surveyed at high resolution. The main objective of these campaigns is to explore what is unknown. Figure 3.6 shows a typical campaign dedicated to the study of dunes. It consists in running exploratory lines. These lines may be hundreds of kilometers long and aim to discover the extent of dunefields. These lines can only be used for identifying the dune regions. In fact, the dunes are partly surveyed so that the crest extraction is incomplete and the estimation of morphological descriptors is impossible. Nevertheless, the morphology is observable even with partial dunes. After the survey, boxes are delineated from the exploratory lines where new morphology and dune spatial organization are observed. These boxes are surveyed during the next campaigns. These campaigns revealed that dunes were present almost everywhere and particularly off the coast of Brittany (Celtic sea and Iroise sea) and in the northern part of the English Channel. Figure 3.7 illustrates examples of boxes that were surveyed by SHOM. The names of these boxes are given to correlate to the locations of the zones shown in Section 2.2.3. These interesting regions are surveyed less frequently than the Belgian boxes.

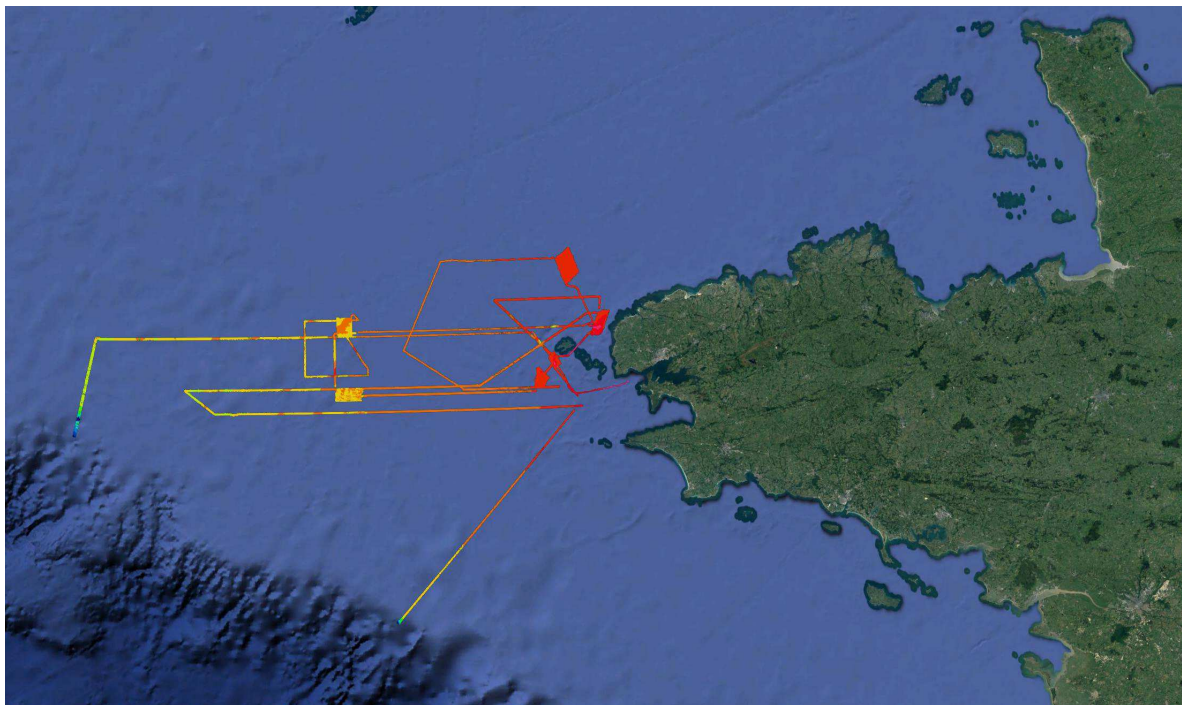


FIGURE 3.6: Bathymetric data recorded during the 2013 dune campaign.

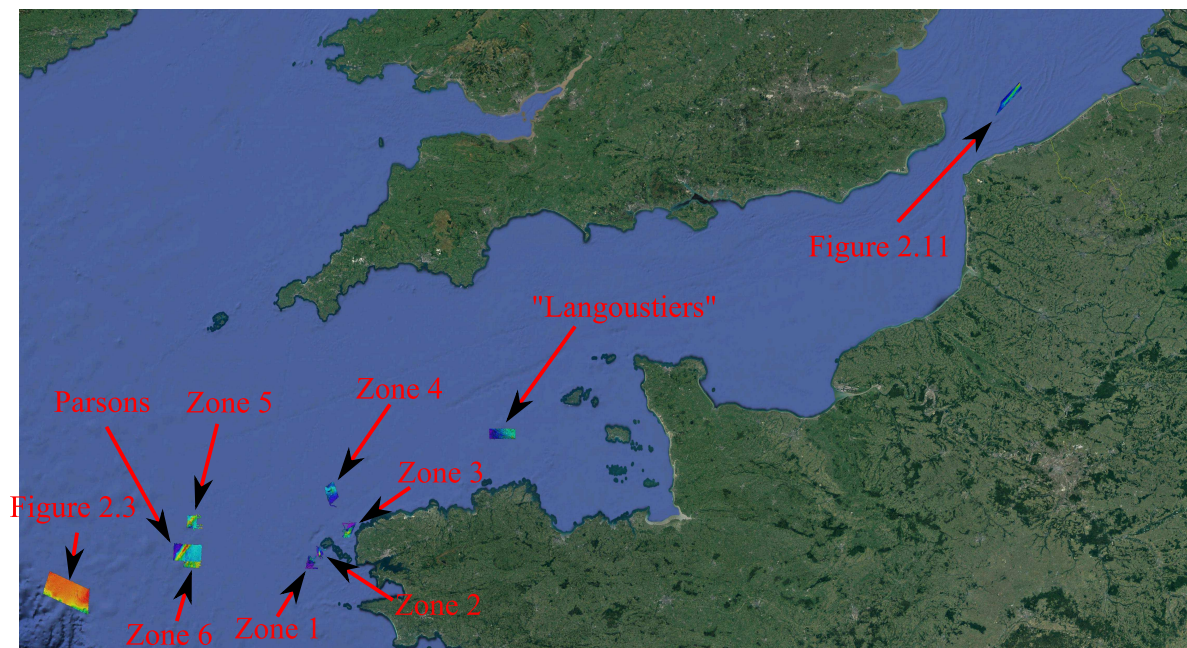


FIGURE 3.7: Locations of the available SHOM boxes.

Dunes are present almost everywhere across the French continental shelf. The environmental conditions (hydrodynamics, seafloor morphology, sediment type, depth) are not constant over such a large area and, consequently, the French database contains

a wide range of dune morphology. French data² were recorded onboard R/V La Pérouse, Beautemps-Beaupré, Borda, Laplace, Pourquoi Pas ? and seven smaller ships dedicated to nearshore surveys. Furthermore, the equipment were not the same from one survey to another. The depth ranges from a couple of meters to about two hundred meters deep. Thus, the data quality and accuracy are not consistent through the entire database. Hence, French data are less appropriate to estimate dune migration rates than Belgian. In this regard, the French and Belgian are complementary and allow exploring all aspects of dunes.

3.4 Benchmark

Although both databases are perfect to appreciate the wide variety of dunes in terms of morphology and dynamics, the volume of data is too large to be used entirely. The MBES data processing and the DTM constructions for both databases would have taken a huge amount of time. Therefore, benchmark zones were selected. The goal was to focus our interest on a limited number of regions. The eleven benchmark zones are presented in Figures 3.8 and 3.9.

These benchmark zones were defined to test the robustness of our dune extraction algorithm and, in this respect, they follow several specifications. The number of zones had to be kept low. This benchmark shall contain the widest range of dune types possible. The zones must not be too large, with a couple of dunes per area so that the analysis stays fast and simple. Each zone corresponds to one dune type in order to analyze the algorithm performances according to dune morphology. Reducing the spatial extents of the zones accelerates the computations and is useful to focus on potential extraction issues separately. It can be noticed that acquisition artifacts are visible in zone 2 and 6. Data with artifacts were purposely selected as they are part of the eventual problems with which the extraction algorithm has to cope.

The details about the acquisition of data over these benchmark zones are given in Table 3.1. Table 3.2 sums up the properties of the dunes in the benchmark zones. It explains and justifies the selection and use of each zone.

2. More information about the pieces of acquisition equipment and vessels characteristics may be found at <http://www.shom.fr/en/activities/activities-at-sea/ghoa/>.

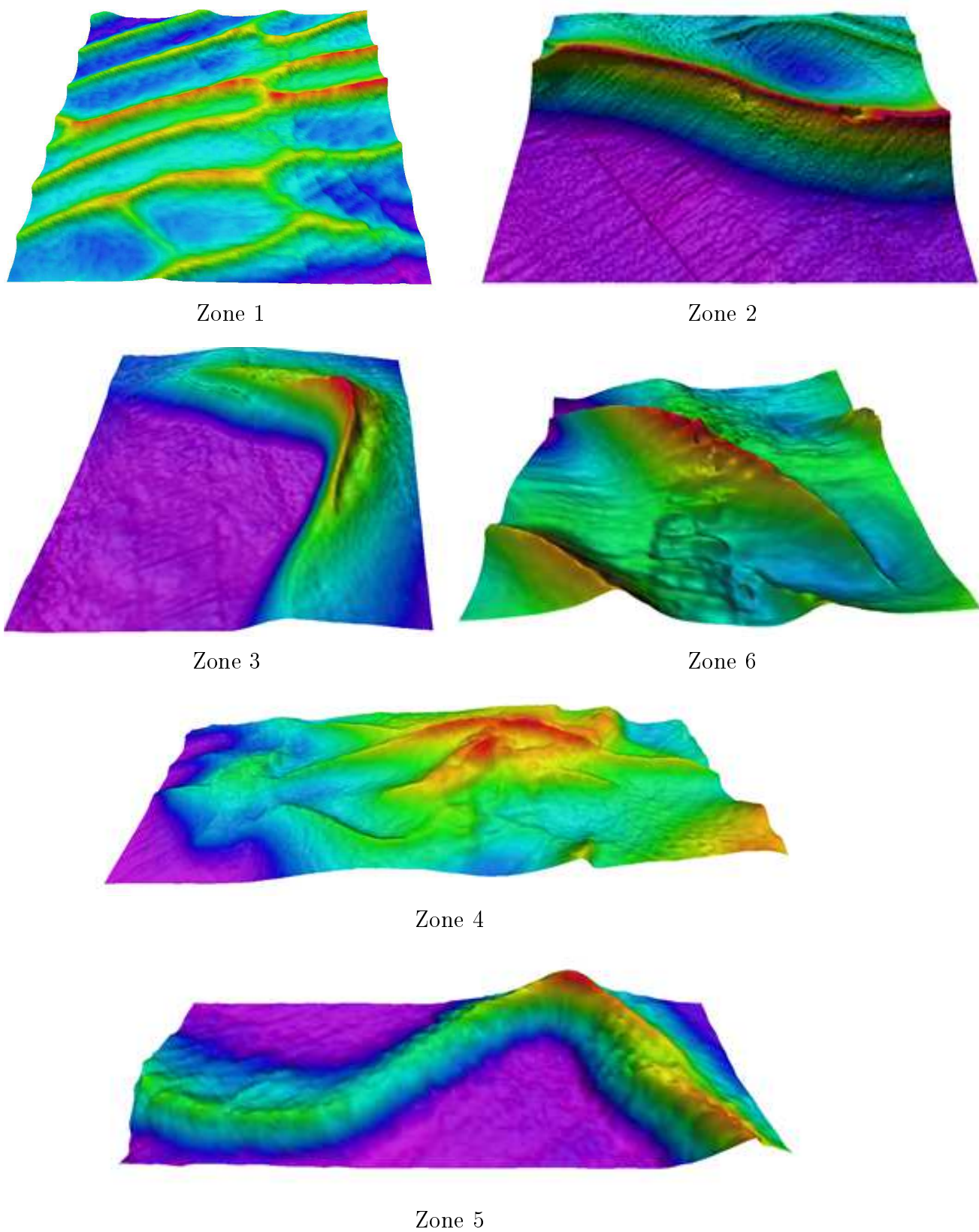
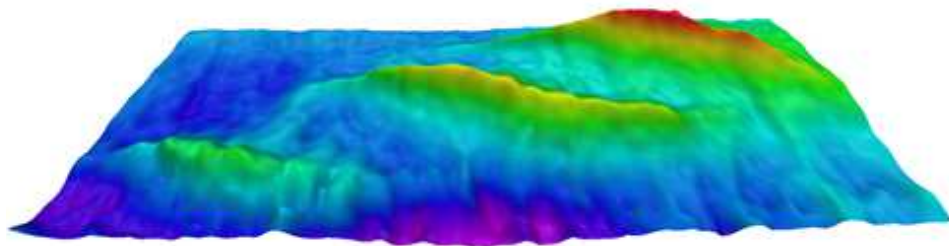
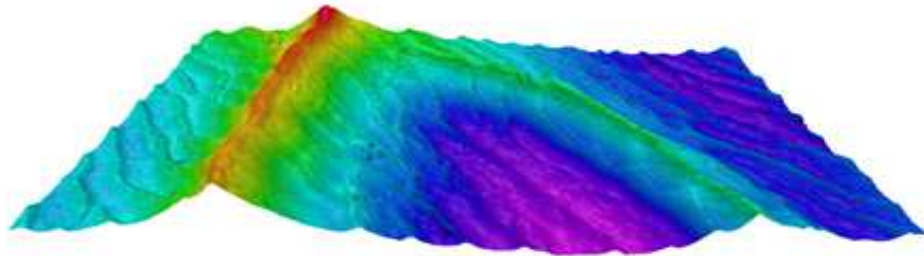


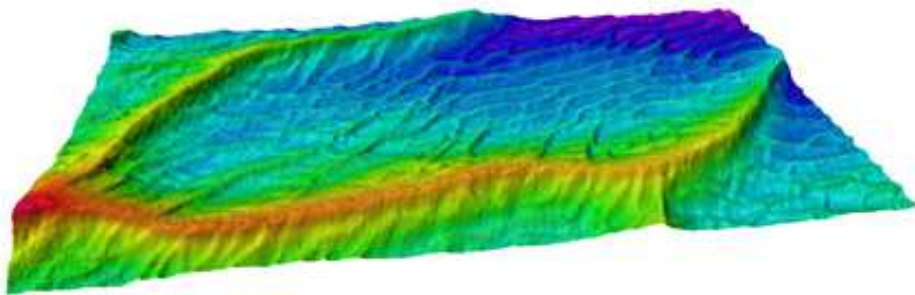
FIGURE 3.8: Bathymetry of the Benchmark zones 1 to 6.



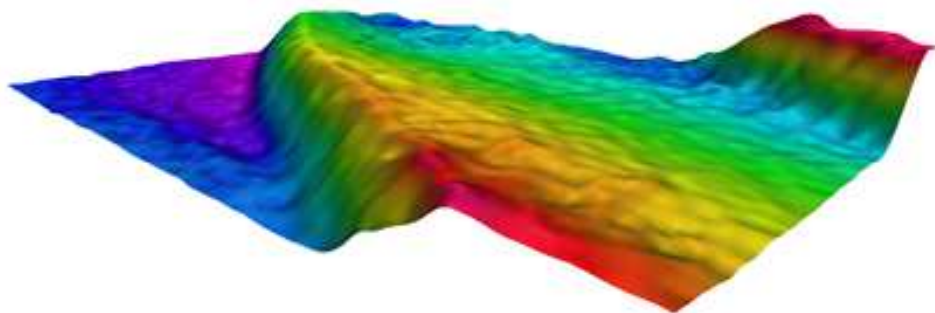
Zone 7



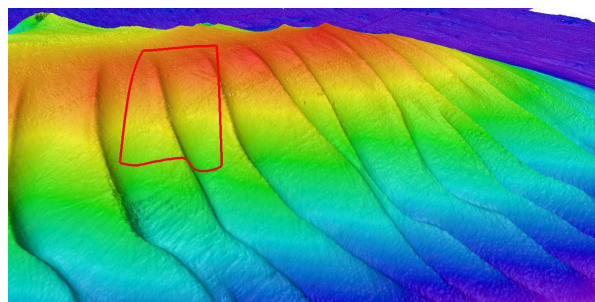
Zone 8



Zone 9



Zone 10



Zone 11

FIGURE 3.9: Bathymetry of the Benchmark zones 7 to 11.

Zone number	Source	Surveyed area	Acquisition date	DTM resolution (m)
1	SHOM	box 1	2012	3,10
2	SHOM	box 1	2012	3,10
3	SHOM	box 4		3,10
4	SHOM	box 1	2012	2
5	SHOM	box 1	2012	3
6	SHOM	box 5		4
7	SHOM	box 6		3,10
8	FPS Economy	R2	Sept,2012	1
10	FPS Economy	ODMA	Nov,2014	1
11	SHOM	box 6		4
12	SHOM	box 2	2013	2

Note: In the "surveyed area" column, the zone number for the SHOM boxes is the same as in figures of Chapter 2.

TABLE 3.1: Information about the data acquisition of the eleven benchmark zones.

Zone number	Projected coordinates (UTM30/31)(m)	Zone Dimensions (m)	Dune properties (m)		Description
			Length	Height	
1	330907; 5354297	400×400	400	3	Entangled dunes
2	333662; 5354000	800×600	900	15	High symmetric, isolated dune with a depression in the crest
3	348050; 5405100	600×600	800	12	Barkhan dune
4	334371; 5355512	850×300	300-800	3-5	Dunes split by rocks
5	329401; 5354117	450×150	400	2-7	Sinuous dune
6	241340; 5383284	500×500	600	>10	Trochoidal dune
7	240713; 5355154	550×250	150-300	1-2	Small fragmented dunes
8	483594; 5686171	200×110	100	1.5-3	Ripples on top of dunes
9	465546; 56859027	150×350	350	1.5-2.5	Splitting dune on a bank flank with ripples
10	236471; 5351599	500×350	400	4	Strongly asymmetrical dune
11	339214; 5360995	450×200	400	4	Part of a dune on a bank

Note: The coordinates correspond to the locations of the southwestern corners of the boxes.

TABLE 3.2: Locations and dune properties of the benchmark zones.

3.5 Conclusion

This chapter explains the processing steps from the recorded raw data to the DTM ready for dune extraction and how the MBES acquisition or the processing may influence the extraction. French and Belgian databases were presented to highlight their respective purposes, their differences and their complementary. It is important to recall that the accuracy of the morphometric and dynamic descriptors will be closely and directly related to the data accuracy and the derived DTMs. This is particularly true for dynamic descriptors. Their accuracy will depend on the two initial datasets. And all datasets do not have the same quality because of the acquisition sensors or even the depth. This accuracy matter is to be remembered when analyzing the derived descriptors. Some dunes were partly surveyed, so the algorithm should be able to deal with this case and to skip the estimation of their descriptors. For both databases, acquisition equipment could change from one survey to another. Therefore, the data quality varies according to the survey. This must be considered as it necessarily modifies the DTM and potentially skews the dune delineation. It is only problematic when comparing the detected dunes in the same area at two different times.

Although these databases are suited for the analysis of dune morphology and dynamics, the volume of data they represent is inconvenient. Thus, benchmark zones were selected to design an extraction algorithm robust to a large scope of dune types and capable of dealing with eventual issues arising from MBES data or processing.

Chapter 4

Geomorphometry

Contents

4.1	Introduction	60
4.2	Basic concepts of geomorphometry	60
4.3	Common metrics	64
4.3.1	Estimation techniques	66
4.3.2	Metrics estimation on dunefields	70
4.4	Classic terrain characterization algorithms	77
4.4.1	Pixel classification	78
4.4.1.1	Unsupervised classification	78
4.4.1.2	Supervised classification	79
4.4.1.3	Tests	80
4.4.2	Disparity line algorithms	83
4.4.3	Drainage algorithms	83
4.4.4	OBIA algorithms	85
4.4.5	Region growing algorithms	86
4.5	First dune extraction algorithm	87
4.5.1	Principles	87
4.5.2	Results and discussion	88
4.6	Surface Representation	93
4.7	Conclusion	96

4.1 Introduction

Geomorphometry is the science of digital terrain description. The terrain analysis is achieved by calculating numerous morphometric parameters derived from DTMs. Geomorphometry leads to terrain characterization, segmentation or classification at various scales. Geomorphometry¹ is a mix of Earth science, mathematics, engineering and computer science. Its wide scope of use keeps diversifying,: geohazards management (McAdoo et al., 2000, Rowbotham & Dudycha, 1998), generalisation (Jenny et al., 2011, Monier, 1997), ecology, Earth and environmental science (including oceanography and planetary exploration), civil engineering, military operations and video entertainment, *etc.* Lecours et al. (2015) gives an overview of these applications. This interdisciplinary field is expanding and specific tools are progressively integrated to GIS softwares.

Although the terrain descriptive parameters are locally estimated, the quantitative analysis of topography is not exclusively dedicated to pixel classification. The combination of local information proves useful for the identification of landforms, land elements, characteristic lines or areas, relief and even for the extraction of specific features. Geomorphometric algorithms already showed their utility for the delineation of volcanoes, drumlins, pockmarks or mountains. The purpose of this chapter is to investigate the applicability of geomorphometry-based methods to dunefield quantitative and qualitative characterization. It starts with the introduction of basic, but important, concepts. Next, the calculation methods of usual morphometric parameters are presented and illustrated on dune datasets. A list of most commonly used characterization algorithms is made and discussed in the context of dune extraction. A first extraction algorithm is designed based on the previous observations. Its results are shown and its limitations examined.

4.2 Basic concepts of geomorphometry

Geomorphometry has long been a quantitative tool at the service of geography, cartography, geomorphology, geology, *etc.* It has only been seen as an interdisciplinary field on its own since 1995 (Pike, 1995).

1. Information about geomorphometry and the latest innovations are referenced here: <http://www.geomorphometry.org/>.

Geomorphometric analysis focuses on the following aspects:

- Choice of relief attributes;
- Terrain numerical modelling;
- Error estimation and DTM preprocessings;
- Attributes formatting adapted to a specific application.

There are as many geomorphometric algorithms as there are of terrain types and applications. These algorithms keep diversifying and improving in several ways:

- Perpetual improvements of the existing metrics, parameters;
- Development of new parameters;
- New combinations of these parameters according to a specific context.

Specific applications, as it is the case in this thesis, are divided into five main steps:

1. Sample the surface (data acquisition);
2. Construct a model from the samples;
3. Correct the potential errors or artifacts;
4. Derive the parameters and objects;
5. Applications of the resulting parameter maps or objects (Initial objective of an analysis).

The first three steps have already been explained in Chapter 3. This chapter shall help in completing the last two. It is important to distinguish between two types of geomorphometric analyses: general and specific geomorphometry. The concept was first examined by Evans (1972). They correspond to different levels of specialization. Specific geomorphometry addresses discrete surface features whereas general is more focused on the continuous surface. There is a continuum between these two types. The more specific an object or analysis gets, the higher the number of attributes is. Height or slope are rather general attributes when catchment areas, crest lines or even dunes are much more specific.

The delineation of dunes in bathymetric data suggests a segmentation procedure. Segmentation is a major part of specific geomorphometry. The surface is composed of elements and forms. The definition of landforms and the problems arising from their extraction are a common topic. In Evans (2012), Evans makes an attempt to answer the question: “What is a landform?”. Geomorphology blends aspects of land surface form, materials, processes responsible for the shape and chronology.

In Pike et al. (2009), landforms and elements are defined as:

Discrete morphologic feature- such as watershed, mountain or drumlin - that is a functionally interrelated part of land surface formed by a specific geomorphological process or group of processes. Each landform may be composed of several land element, smaller divisions of the land surface that have relatively constant morphometric properties.

In other words, dunes are landforms and dune crests, sides or feet are the composing elements. A specific geomorphometric study such as landform delineation is not simple. Evans shows that, for drumlins, little variations in their form or their surroundings can complicate the delineation task. It happens when the drumlins contain bedrocks, when they merge into a hillside or when they are carved by streamlines. The impact of environment will certainly be an issue for the study of dunes. In specific geomorphometry, the 'leftover' region is never analyzed even if it could hugely help in understanding the characteristics of the landforms of interest and their development. To stand in the middle of a plain is not the same as standing on a hillside or at the bottom of a valley. One of the problems is still to find objective and repeatable definition of landforms even specific ones. Combining measurement of uniformity and the identification of boundaries is challenging. The clear boundaries never or rarely close perfectly but to extend them is not a simple exercise. Another notable idea is that one often forgets to think of a landform as a part of land systems. The relative positions of landforms can be the sign of a repeating pattern of the land surface. The contiguity of landforms witnesses some genetic processes and may provide valuable information in the prospect of extraction.

Another important notion in geomorphometry is the notion of signature. Pike introduces the notion of "geometric signature" (Pike, 1988). This is the set of indicators describing the topographic surface so that geomorphologically-different landforms may be distinguished. According to the delineated object, the choice of variables describing the topography shall be adapted. Thus, dune signature is to be identified to enable their extraction. A signature does not have to count many parameters to solve problems. Information redundancy in the attributes should be avoided as much as possible. The use of such a concept supposes believing that the perception of landforms is synthetic. This means that a landform can be reduced to a finite number of attributes. But, it is uncertain whether a finite number of parameters is enough to describe various topographic continua. Furthermore, one must be aware there is no "magic" parameter that can perfectly describe and make topographic landforms distinctive. Consequently,

a suite of parameters is used. In theory, one should be able to reconstruct the original topography from the parameters.

Terrain characterization is extremely linked to the concept of scale. The analysis scale may be defined as the characteristic spatial extent at which the surface is regarded. Figure 4.1 illustrates how scale can modify our perception of the Earth' surface. According to the chosen scale, the black point is located on a peak, in a bottom of a valley or is part of a more complex landscape and may be considered as a regional high point. If the scale influences human perception, it is also true for the numerical analysis. From a practical standpoint, it influences the estimation of the surface attributes and ultimately its characterization. Scale is closely linked to the DTM resolution and the neighborhood size at which morphometric parameters are estimated. Consequently, the resolution at which the surface is analysed has to be cleverly selected so that imprints left on the topography by the processes of interest are not partly lost. As already said, scale is what differentiates sand ripples from dunes or from banks. This concept is primordial and cannot be omitted for the study of dunes. In addition, these remarks raise questions: Is there a real interest in always wanting finer-scale DTMs? How to define the land surface since other structures are overlain on it, and should they be seen as parts of it? Particularities of the landscape such as boulders, caves or overhangs make difficult the definition of the land surface. For these reasons, simplifications need to be made and a scale selected in order to define a real land surface differing from the 'natural' land surface.

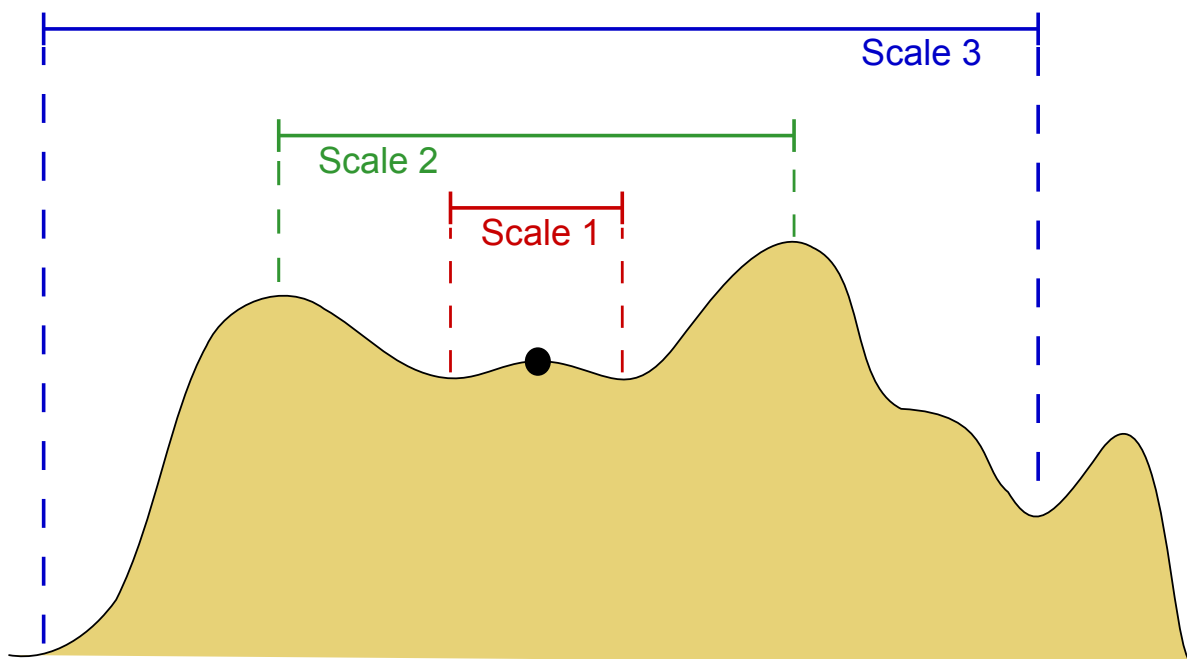


FIGURE 4.1: Notion of scale.

In this context, the importance of scale started drawing attention. Multi-scale classification has been designed in order to integrate all the properties of the surface in the classification process (Benz et al., 2004, Eisank et al., 2014, Fisher et al., 2004, Schmidt & Andrew, 2005)). Dragut & Eisank (2011) shows how object delineation is dependent of the scale and it can be optimized in this regard. And, a ESP (Estimation of Scale Parameter) method to estimate the most appropriate scale of analysis is presented in Drăguț et al. (2010).

The terrain characterization relies on a discrete model approximating the true surface and the estimation of local parameters. Through the steps of the analysis, errors appear and may skew the conclusions. DTM accuracy becomes a major concern (Wood, 1996). DTM error affects the evaluation of topographic parameters and, in the end, the characterization (Florinsky, 1998, Hunter & Goodchild, 1997, Oksanen, 2006, Oksanen & Sarjakoski, 2005, Zhou & Liu, 2004).

All the afore-mentioned concepts constitute the starting point of our dune analysis. Scientists working on dunes and eager to refine existing classifications shall find out whether or not each dune type has a signature, which makes it distinguishable from another. The human eye is capable of identifying this specificity to the point that we are able to differentiate two dunes of the same type. But this signature can only be captured through the estimation of descriptors. Therefore, these must be thoroughly selected and they must be kept simple and understandable. In this regard, much work needs to be done to get a classification matching the observations and it is not trivial.

Readers interested in geomorphometry should look at Pike et al. (2009). It sums up what is known about geomorphometry and the associated terminology. Furthermore, Wood's PhD thesis (Wood, 1996) addresses most of the issues inherent to DTM characterization and analysis.

4.3 Common metrics

Geomorphometry aims at providing quantitative information about the terrain topography. In order to do so, many parameters have been defined. They can be divided into five categories (Pike, 1988).

The first gathers the attributes directly derived from the altitude (e.g. mean, median, range, standard deviation, variance, skewness or kurtosis over regions). Parameters drawn from the power spectrum compose the second category. The basic principle is to

conduct a frequency analysis of the altitude along curves. In the third category, one can find the slope and its derivatives. This is probably the single most important parameter. Here is a short list of commonly calculated parameters: Slope between topographic reversals, frequency of slope reversal (an estimate of fine-scale texture), aspect (slope direction), length or height. The fourth category is about the slope at constant base length or multiples of this base length. The slope can be signed or not and computed in the four main directions. The analysis of histograms provides variables encompassing the slope properties. The base length should be modified to see how scale-dependent the slope values are. Finally, the fifth category deals with the second derivative of altitude: curvature. The curvature is approached like the slope in the fourth category with the same notion of slope length. Pike and more generally in geomorphometry this panel of parameters is assumed to be sufficient to make distinctions between various topographic units.

In Pike et al. (2009), morphometric parameters and objects are organized according to their purpose:

- Basic parameters and objects;
- Parameters and objects specific to hydrology;
- Parameters and objects specific to climate and meteorology.

The first-type metrics are the one of interest for the study of dunes. Basic metrics are surface derivatives (height, slopes or curvatures). Higher order metrics are rarely used since their values and variations are not easily interpretable in terms of morphological changes. An infinite list of parameters may be defined and obtained from these initial metrics. For instance, in Shary et al. (2002), twelve curvatures are used to classify terrain types. These metrics usually quantify the homogeneity, variations or the distributions of the basic parameters (*e.g.* mean, median standard deviation, kurtosis, skewness) in a fixed-size neighborhood. In Hammond (1964), slope (gentle or steep), local relief (lowlands or uplands) and profile type are combined to define a classification of a US map with five main landform types (plains, tablelands, plains with hills or mountains, open hills and mountains and hills and mountains). These main types are also divided into 21 classes and 45 subclasses according to the amount of gently sloping land in the area, local relief, and profile type (the amount of gentle slope on lowlands or uplands).

A type of metrics that is missing in the above list is the frequency parameters. Indeed, terrain roughness quantitative methods discrete Fourier transform, local Fourier histograms or wavelet transform have emerged (Berti et al., 2013, Cutter Jr et al., 2003, Lefebvre & Lyons, 2011). As explained previously, there is no point in considering many morphometric parameters to quantify dune signature as redundancy is not desirable. That is the reason why it was decided to concentrate on the most commonly used metrics.

Here is the list of metrics that were estimated on dunefield DTMs:

- Bathymetric Position Index (BPI);
- Slope;
- Aspect (slope direction);
- Profile curvature;
- Plan curvature;
- Minimal curvature;
- Maximal curvature;
- Gaussian curvature;
- Mean curvature.

This selection was also motivated by the fact that these metrics have already been used for the extraction of specific lanforms such as volcanoes, drumlins, mountains, pockmarks, *etc.*

4.3.1 Estimation techniques

The BPI is a mmeasure of the relative position of a point with respect to its neighborhood. It is only based on the depth values and, therefore, does not require the estimation of derivatives of the surface. It is calculated for each pixel P of a DTM as follows:

$$BPI(P) = Z(P) - \frac{1}{n} \sum_{Pi \in N} Z(Pi)$$

where $Z(P)$ is the depth value at the pixel P ; N is the neighborhood of pixel P and n is the number of pixels in the neighborhood N . The BPI values highly depends on the neighborhood properties. The neighborhood size (distance from the estimation pixel) and shape (square, rectangle, circle, ring, cone) may be changed to create new versions of this index.

Slope, aspects and the selected curvatures are respectively first order and second order derivatives of the height function. Slope and aspect are directly related to the gradient of elevation.

$$S = \sqrt{S_x^2 + S_y^2}$$

$$Aspect = \arctan\left(\frac{S_y}{S_x}\right)$$

Where S_x and S_y are the x and y components of the surface gradient. The slope is the magnitude of the gradient vector at a point and, the aspect, its direction. Curvatures are second order differential quantities. Each curvature is associated to a plane. The intersection of the plane and the elevation surface forms a curve and the second order derivative of this curve corresponds to the curvature. If the surface is approximated by a bivariate quadratic function:

$$Z = ax^2 + by^2 + cxy + dx + ey + f$$

the coefficients of the surface can be equated to the surface first and second order derivatives. This modelling of the surface by a polynomial function was first made in Evans (1980) and this expression has regularly been used since (e.g. Wood (1996)). Thus, in the previous expressions, S_x and S_y may respectively be replaced by d and e . These notations are used in the following to define the curvatures as it makes the formulas more readable than with partial derivative symbols.

Usually, curvatures are estimated by pairs corresponding to orthogonal directions. Profile curvature is the curvature of the surface in the plane defined by the gradient and the vertical. Plan curvature quantifies the changes in the XY plane. They can be calculated from the polynomial coefficients as follows (Evans, 1980):

$$ProfCurv = \frac{2(ad^2 + be^2 + cde)}{e^2 + d^2}$$

$$PlanCurv = \frac{2(bd^2 + ae^2 - cde)}{e^2 + d^2}$$

The minimal and maximal curvatures are the extremal normal curvatures. A curvature is called normal if the intersection plane contains the surface normal. It may be proven that they are estimated in perpendicular directions :

$$MinCurv = a + b - \sqrt{(a - b)^2 + c^2}$$

$$MaxCurv = a + b + \sqrt{(a - b)^2 + c^2}$$

The gaussian curvature is not a true curvature as it is the product of the minimal and maximal curvature. The mean curvature is the average of both extremal curvatures:

$$GaussCurv = MinCurv * MaxCurv$$

$$MeanCurv = \frac{MinCurv + MaxCurv}{2}$$

As can be seen in the above expressions, it is necessary to estimate the surface derivatives prior to the calculation of morphometric metrics. There are two main ways to determine the values of surface derivatives from a DTM: discrete approximation and function fitting.

The discrete approximation is similar to finite difference methods. The height field is the discrete function. Using Figure 4.2 notations, several discrete approximation schemes may be applied to determine the x component of the slope:

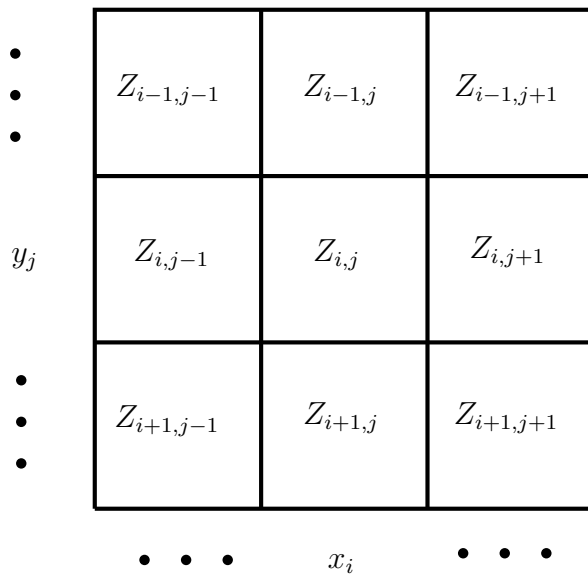


FIGURE 4.2: Notations used for the discrete estimations of morphometric parameters.

Definition 1:

$$S_x = \frac{Z_{i,j+1} - Z_{i,j}}{\delta x}$$

Definition 2:

$$S_x = \frac{Z_{i,j} - Z_{i,j-1}}{\delta x}$$

Definition 3:

$$S_x = \frac{Z_{i,j+1} - Z_{i,j-1}}{2\delta x}$$

where δx is the DTM resolution.

These definitions are examples among others. One could imagine to apply definition 3 to the previous and next rows as well and to average the obtained values. The principle is to approximate a differential quantity by a weighed sum of elevation values. The same procedure can be applied to obtain the y-component of the slope and, next, slope and aspect estimates via their expressions. Discrete schemes may be extended to estimate the second order derivatives of the surface and, then, the values of the curvatures.

The second possibility is to locally adjust a polynomial function to the surface (Horn, 1981). The local model is fitted to the surface on a small patch (neighborhood) around the estimation location. The polynomial coefficients may be determined by solving a least squares system. The least squares system to solve is:

$$\begin{bmatrix} z_1 \\ \vdots \\ z_n \end{bmatrix} = \begin{pmatrix} x_1^2 & y_1^2 & \dots & y_1 & 1 \\ \vdots & \vdots & \vdots & \vdots & \vdots \\ x_n^2 & y_n^2 & \dots & y_n & 1 \end{pmatrix} \times \begin{pmatrix} a \\ \vdots \\ f \end{pmatrix}$$

Where n is the number of points in the neighborhood and x_i, y_i and z_i the coordinates of these points.

The higher the polynomial degree is, the bigger the number of coefficients is. Therefore, the size of the fitting neighborhood is constrained by the polynomial order. Quadratic function is generally deemed to be an acceptable compromise since the expression is limited to nine coefficients as in Zevenbergen & Thorne (1987). It enables calculating the curvatures and a 3x3 neighborhood is sufficient to solve the system. The model with nine parameters fitted in Zevenbergen & Thorne (1987) is:

$$z = ax^2y^2 + bx^2y + cxy^2 + dx^2 + ey^2 + fxy + gx + hy + i.$$

With higher order polynomials, the neighborhood must be widened and, therefore, the model is not as local, nor are the derived morphometrical parameters. If the neighborhood is too small, there is not much redundancy and the estimation quality will depend on the DTM quality. On the other hand, a large neighborhood will no longer characterize the terrain locally around the estimation point but more regionally.

In addition, the neighborhoods of adjacent points will overlap and metrics disparities might be smoothed out in the resulting morphometrical maps.

Another alternative is a mix of both previous approaches (Zevenbergen & Thorne, 1987). It basically relies on the polynomial model as presented before except that the neighborhood size is set to 3×3 . Consequently, the least squares system reduces to a linear system with 9 equations and 9 unknowns. There is a unique solution that is exact which means that the model pass through all the neighboring points. The coefficients expressions can directly be derived from the point elevations.

4.3.2 Metrics estimation on dunefields

The utility of the most frequently used metrics for the extraction of dune needs to be examined. DTMs still contains errors such as the artifacts presented in Section 3.4. Discrete schemes are based on elevation values whilst fitting methods have a smoothing effect and are less sensitive to surface noise. Therefore, a quadratic function was chosen as fitting model for the estimation of the metrics on dune datasets.

BPI was selected to try out, at least, one metric directly based on the elevation. It quantifies the context of a DTM cell by comparing its vertical position with respect to its vicinity. It could have been replaced by any equivalent metrics such as the standard deviation of the elevation over the neighborhood or the number of neighbors above minus the number of lower neighbors. The BPI was estimated on 3×3 pixel neighborhoods. Figure 4.3 shows that most dune crests are characterized by "high" BPI values and part of the dune feet by "low" values. Nevertheless, the BPI is not necessarily constant from one crest to another and even throughout an entire dune. Moreover, DTM distortions (holes and bumps) are also highlighted by extreme BPI values. This type of metric is generally used alongside other metrics for general terrain analysis (Hammond, 1964). This metrics is rather simple and it may not be sufficient, on its own, for delineating dunes. This observation explains the use of evolved metrics capable of apprehending the specificity (signature) of a terrain objects for specific geomorphometry applications. The specificity of the terrain analysis requires the estimation of adapted and more sophisticated metrics.

In Figure 4.4, it can be noticed that slope reveals dune sides and drops to zero near the crest. The dune boundaries could simply be drawn based on this slope map. Yet, this is the same for rocks. In addition, these dunes are typical symmetric dunes forming a repetitive pattern which is a simple study case.

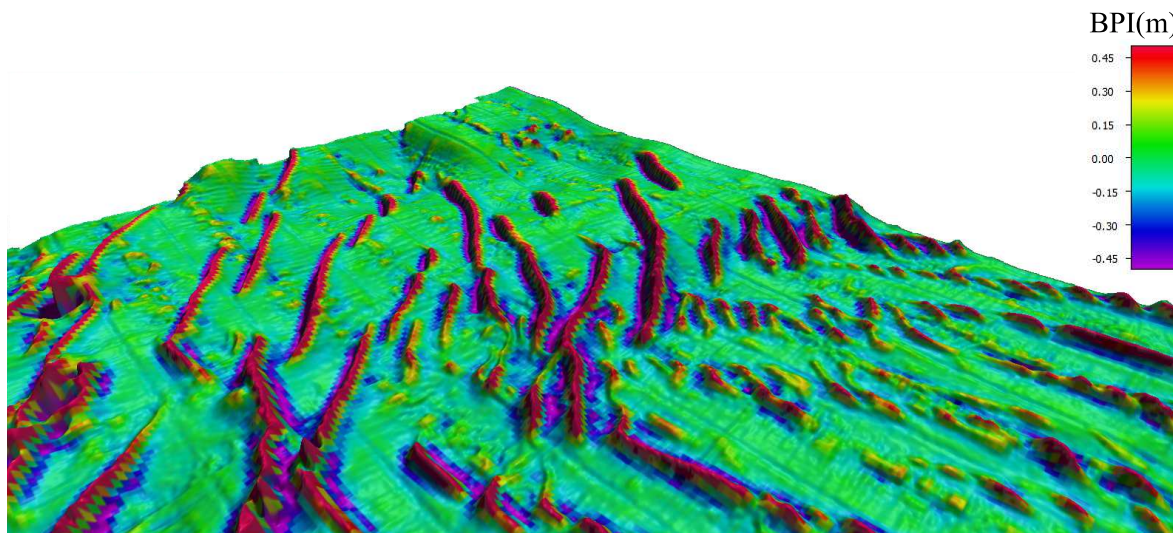


FIGURE 4.3: BPI estimation with a 3×3 neighborhood.

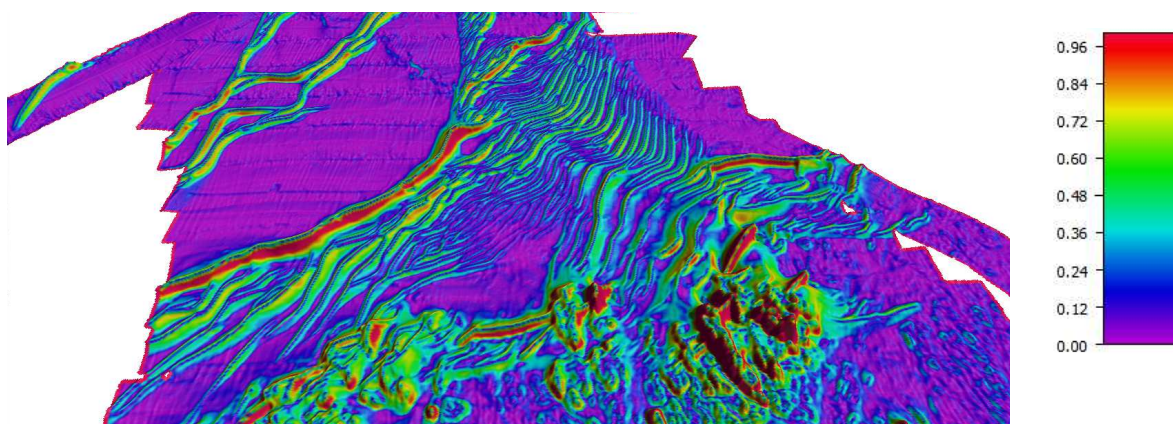


FIGURE 4.4: Slope map of SHOM zone 1 estimated with a 5×5 neighborhood.

This statement is qualified in Figure 4.5. In fact, on more original dune types, it may be noted that dune sides are not systematically outlined by a high slope. The tracing of the ends of dune flanks is uncertain on these dunes. In addition, the slope is not always the same of both sides and homogeneous across the entire side.

In Figure 4.6, the aspect varies between -90° and 90° . The slope aspect is hard to display because of its periodicity. Furthermore, it is not only difficult on a visualization level, it is also difficult to manipulate. Indeed, areas with similar aspect may be allocated extreme aspect values. For instance, a -93° aspect is equivalent to 87° but are at the extremities of the color map. Even with values ranging from 0° to 360° , the issue still rises as 0 and 360 are the same direction. This orientation issue is particularly visible in Figure 4.6 as the aspect shift appears at the crests. The slope aspect is not stable on flat areas and creates this noisy, speckle-like texture. It is also present on the sides of the dune which suggests dune sides are not as steep as their dimensions suggest.

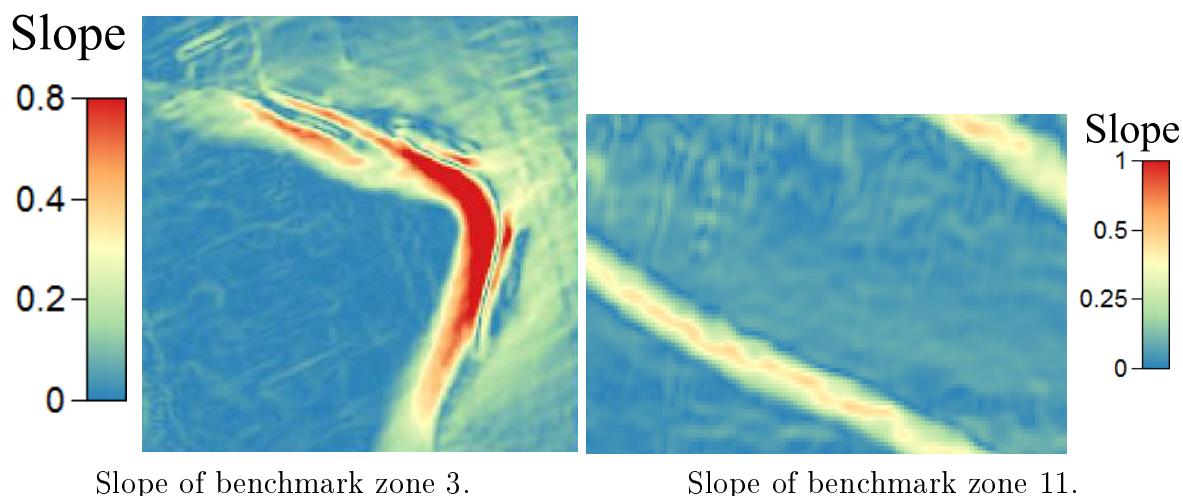


FIGURE 4.5: Slope estimation on two different dune types.

When the neighborhood is widened, this "noise" tends to be smoothed and the aspect is more homogeneous. But the presence of data artifacts is magnified and visible with the alternate red and blue stripes in the bottom-left corner of the figure. The figure emphasizes the importance of the neighborhood size. This issue is related to the DTM resolution and the notion of scale and how it helps highlighting some features more than others according to the scale. Therefore, it must not be neglected in our study. The problem of the sliding window size on the measured metrics is a current topic (Albani et al., 2004).

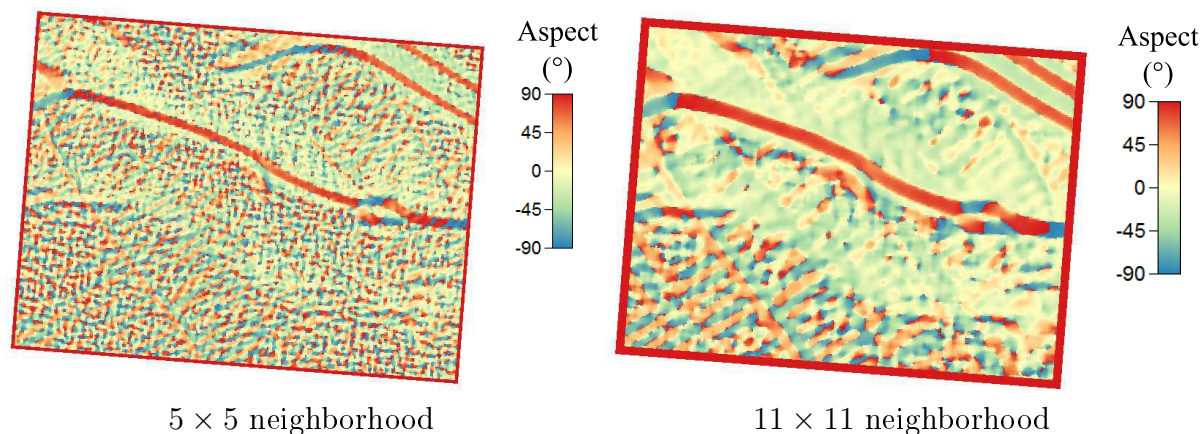


FIGURE 4.6: Comparison of aspect maps on benchmark zone 2 measured at two scales.

Profile curvature quantifies the concavity of the terrain in the slope direction. Observations of barchan dunes show that they have, unlike other dunes, a convex side and a concave side (Figure 4.7). The extreme values are located on both parts of the crest and the curvature is almost zero in the crest areas. This is due to the fact that its calculation depends on the x- and y- slope components. In the cases of Figure 4.7,

the slope is close to zero at the crests. But, the flat seabed is characterized with low slope values as well. Dunes are more distinguishable in the second zone. But this is mostly due to the difference between the color maps. On the small dunes, the curvature values are much smaller than for the barchan. For the example of Figure 4.7, the order of magnitude in the second case is 10 times smaller than in the first one.

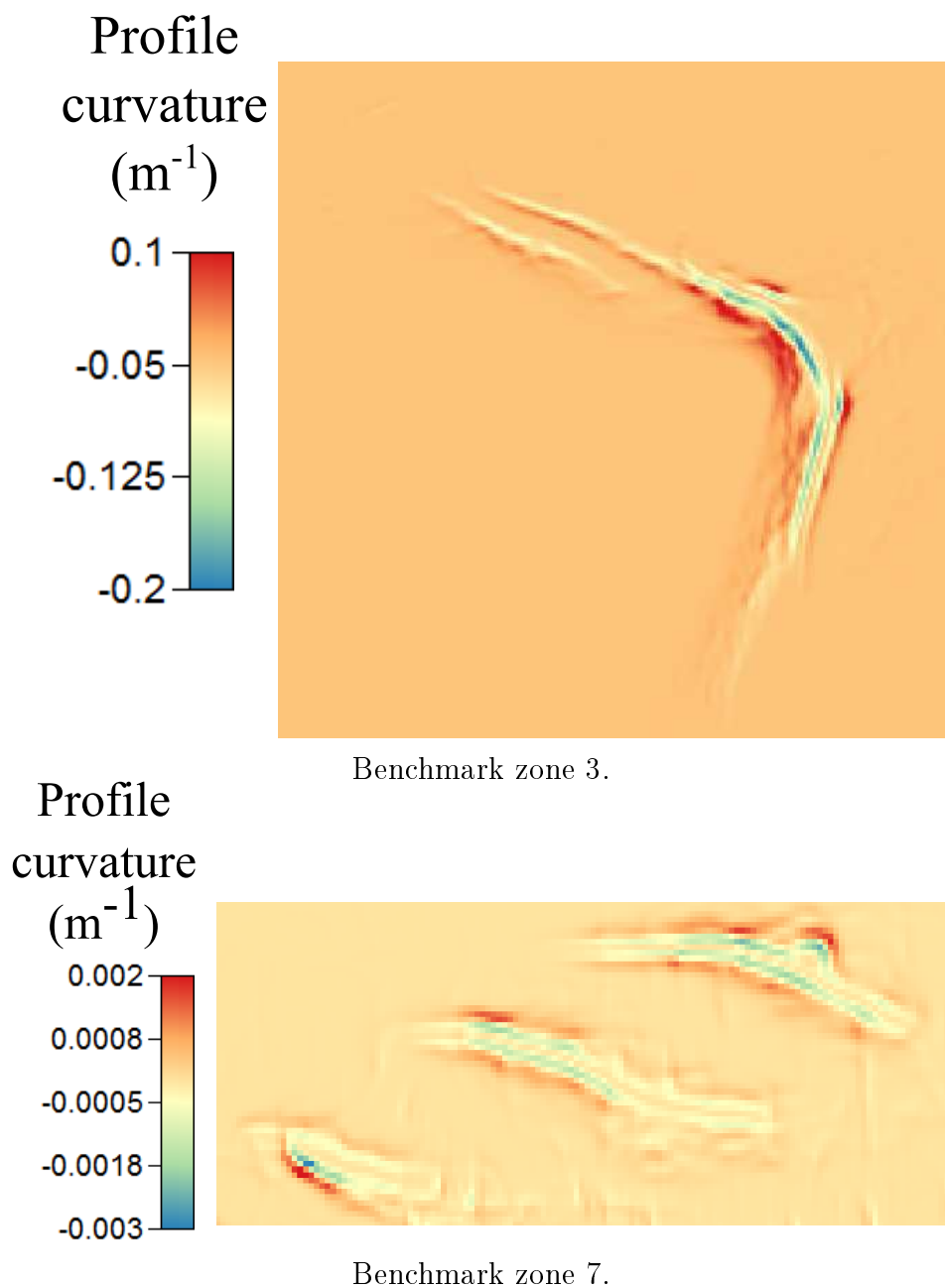


FIGURE 4.7: Profile curvature maps.

Similarly to profile curvature, plan curvature is null around crests (see Figure 4.8), which is evident from mathematical expression. The comments made on profile curvature still stand for plan curvature. The difference is that it brings out the longitudinal undulations of dune flanks. At first sight, it does not seem relevant for dune extraction.

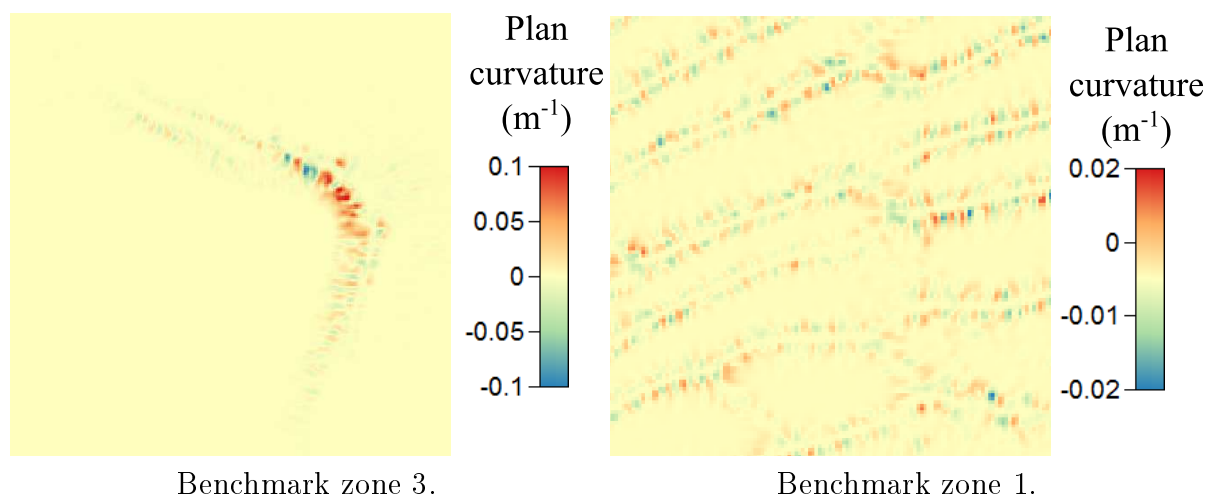


FIGURE 4.8: Plan curvature maps.

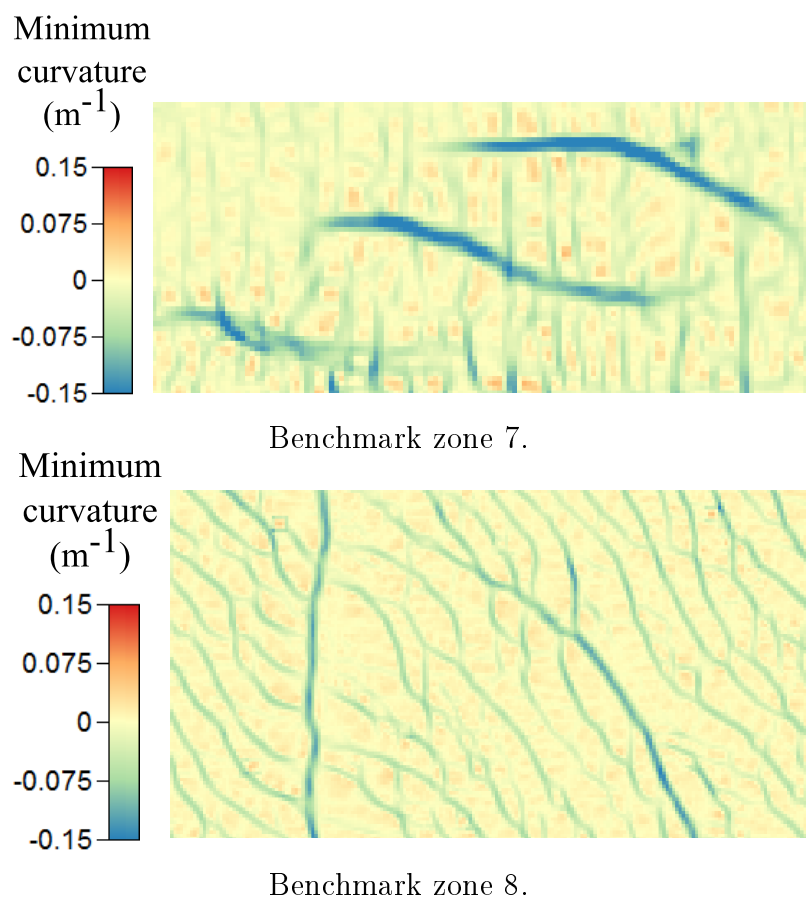


FIGURE 4.9: Minimal curvature maps.

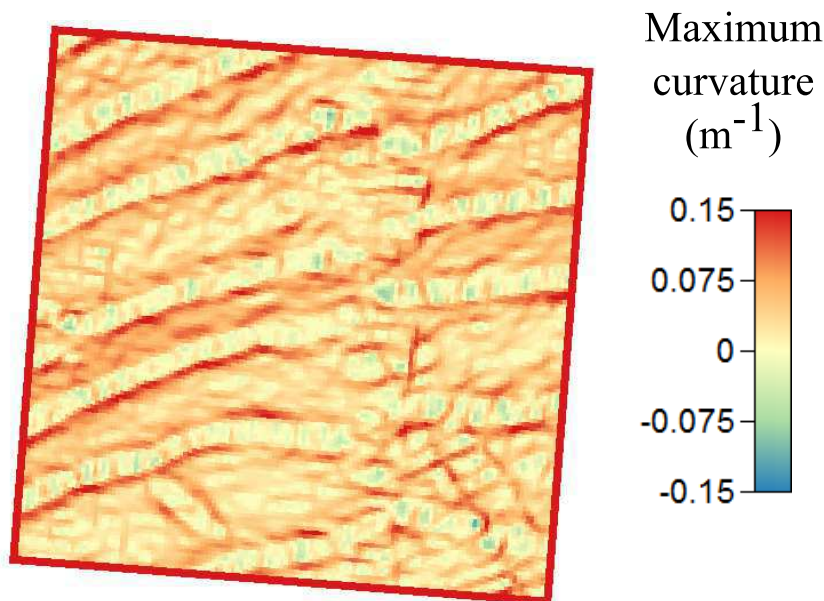


FIGURE 4.10: Maximal curvature estimation on benchmark zone 1.

Figure 4.9 demonstrates that crests are particularly visible on minimal curvature maps independent of the dune type. Minimal curvature may be used to emphasize convex parts of the terrain. Crests are identifiable with negative values. However, artifacts in the first case and ripples in the second case stand out too. The order of magnitude is higher than with the curvatures tested so far, and the estimation is totally independent from the slope.

Contrary to the minimal curvature, the maximal curvature is useful to highlight concave areas (positive values). If crests are very visible on minimal curvature maps, dune feet are not as easy to distinguish in the maximal curvature maps (Figure 4.10). The drawing of dune boundaries could only partly be done from these maps. This means that the feet of dunes are not as sharp as the crests. The transition between the dune sides and the seabed is too steady to be directly identifiable.

The gaussian curvature being the product of the extremal curvatures, high values are characteristic of a terrain curved in the corresponding direction. In Figure 4.11, it can be observed that, on dune data, this curvature highlights the height variations along the crests. Saddle points correspond to negative values and local peaks are associated to a positive curvature.

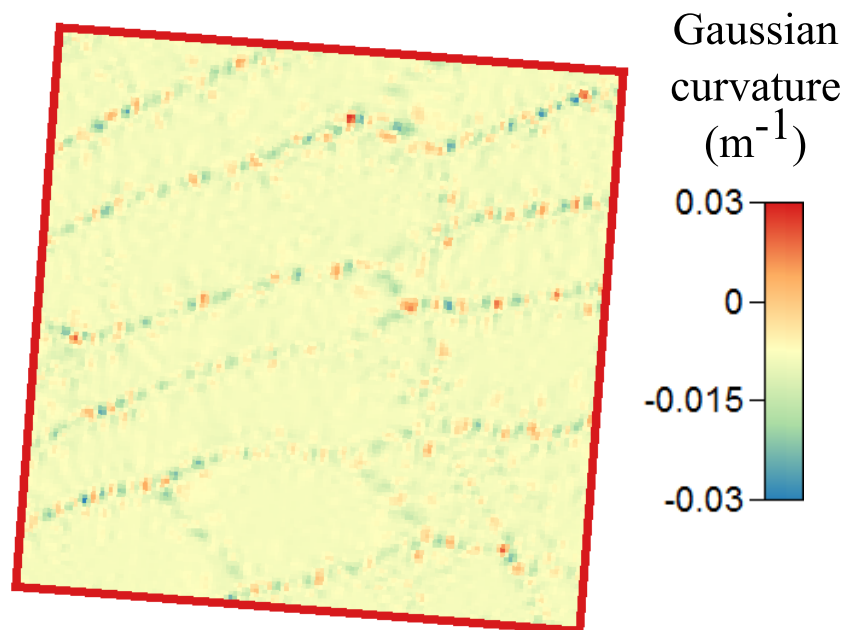


FIGURE 4.11: Gaussian curvature estimation on benchmark zone 1.

The mean curvature brings no additional information in the case of Figure 4.12. Negative values are still associated to crests and dune boundaries described by positive values. But, the information is diluted and, consequently, curvature changes are not as evident as in the original extremal curvature maps.

These metrics display different facets of dune or dune part morphologies. This will be useful for the purpose of delineation. The next section explains how these metrics are generally used for terrain analysis, presents the types of terrain classification algorithms and examines their applicability to dunes.

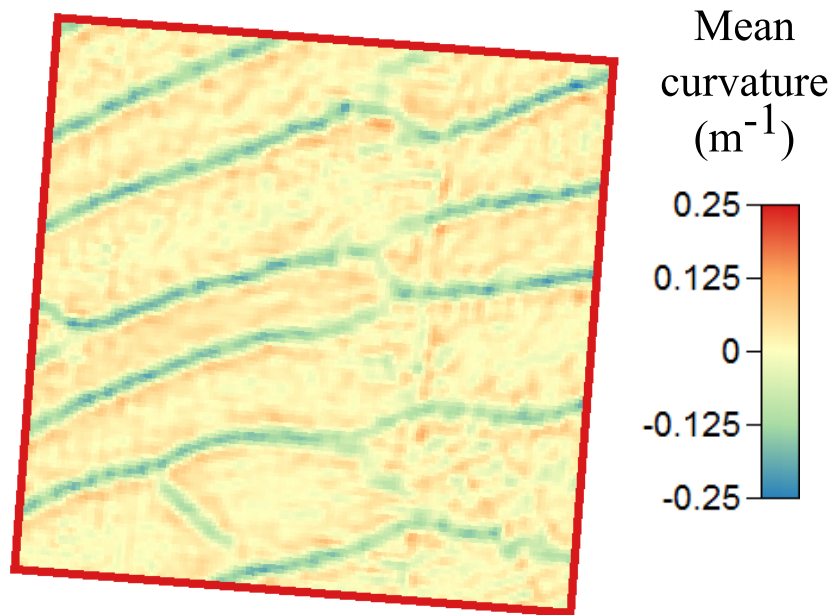


FIGURE 4.12: Mean curvature estimation on benchmark zone 1.

4.4 Classic terrain characterization algorithms

Our problem of dune extraction is a particular case of specific object delineation. This may be considered as a sort of landform classification where only one landform is regarded. In this section, the different categories of terrain classification are presented and analyzed in the context of dune extraction.

Landform mapping relies on four principles: morphologic, genetic, chronologic and dynamic (Minár & Evans, 2008). To minimize the share of subjectivity, a surface segmentation algorithm shall not rely on an endless list of criteria to define unit boundaries and stay as close as possible to natural geomorphic boundaries. The surface can be segmented at three different levels with relief unit arranged hierarchically according to their complexity. Elementary forms are the simplest and smallest segments than can be identified at a given resolution (crests, dune sides, *etc.*). Landforms are compound units (dunes). They are the gathering of several elementary forms. The last level of complexity is made of the characteristic pattern of the surface composed of associated forms (rocky areas, dunefield, *etc.*). They are referred to as land systems. The segmentation process should be aided by the specific structural elements of the surface (pit, peak, ridge, valley, inflections and discontinuities of the altitude and its derivatives). Therefore the detection of these structural elements represents an obvious and natural starting point for the segmentation (pixel classification).

The second major research axis is the classification approach. Unlike the first problem, the main focus is the understanding of the internal coherence of the elementary forms. A third approach is to directly focus on the delineation of the landforms.

Five principal groups of terrain analysis techniques can be identified:

1. Pixel classification;
2. Algorithms based on disparity lines;
3. Drainage basin –based algorithms;
4. Object-based algorithms;
5. Region growing algorithms.

4.4.1 Pixel classification

These algorithms are such named because of the parallel between a regular DTM (height grid) and an image. Each grid cell can be seen as a pixel. Therefore, pixel classification algorithms widely are widely inspired by algorithms commonly used in image processing.

The objective of pixel classification algorithms is to assign a class (label) to each pixel. Therefore, they can be qualified of general geomorphometry methods. Yet, they are considered here since pixels may be gathered into land elements. Gathering procedures aiming at reconstructing elementary forms can be found in the literature (Klingseisen et al., 2008, Romstad, 2001). A similar contextual merging technique to elementary forms can then be clustered to define land forms such as dunes. A good review of classification schemes is to be found in Iwahashi & Pike (2007). Prior to the classification, a set of features, a feature vector, is estimated at each pixel to describe the shape of the terrain at each location. According to the land elements of interest, the feature vector is adapted. These algorithms can be divided into two categories: unsupervised and supervised classifications.

4.4.1.1 Unsupervised classification

Unsupervised classification procedures consist in splitting pixels into clusters in the parameters space. The number of classes is often predefined and may be adjusted if the resulting classes are not satisfactory. The list of metrics can be very long and parameters may be redundant. It is the role of the clustering procedure to sort out which

are the discriminating parameters. K-means method is frequently adopted to achieve the clustering (Burrough et al., 2000, Trevisani et al., 2012), but alternate methods have also been used such as neural networks (Ehsani & Quiel, 2008). An original approach is to define the classes based on statistical thresholds that are dependent on the dataset. This is done in Iwahashi & Pike (2007) by comparing the pixel values of the parameters to the DTM mean values. Some classifications are based on a single morphometric parameter (Cutter Jr et al., 2003). Others determine the scales of interest before calculating the parameters values (Ismail et al., 2015). Another possibility is to introduce fuzziness to class boundaries (Burrough et al., 2000). Instead of having crisp classifications, each pixel is allocated its probability of belonging to each class. The methods are able to distinguish different classes as different from each other, but cannot determine what each class corresponds to. That is to say that it does not identify one class as ridge pixels and another as valleys. Consequently, it is difficult to create specific land elements (crests, dune sides, dune feet) from these classes. Thus, these methods are not adequate for the study of dunes.

4.4.1.2 Supervised classification

Supervised classifications suggest that the terrain composing classes are a priori known. It requires inserting the expertise into the classification. Thus, the classes are adjusted according to the applications. For dunes, classes containing ridges, valleys and flat steep areas can be imagined to detect dune crests, feet and sides. Unlike unsupervised algorithms, the choice of the metrics matters. All the selected metrics must help in the discrimination of the classes. In practice, classes are defined by heuristics, thresholds on the selected metrics. The number of classes is relative to the intended level of detail. For instance, 96 classes are proposed in Dikau et al. (1995). Multi-scale (Fisher et al., 2004, Schmidt & Andrew, 2005) and fuzzy (Schmidt & Hewitt, 2004, Wang et al., 2010) approaches has been proposed as well. These algorithms can consider geometric metrics (curvatures) (Raper, 1989), contextual information (relative position with respect to the vicinity) (Dikau et al., 1995) or combination of both (Schmidt & Hewitt, 2004). In addition, the classification reliability may be quantified using indices such as the entropy in Fisher et al. (2004). In Dymond et al. (1995), a method of regionalization is described to turn a pixel classification into a map of regions.

4.4.1.3 Tests

The Wood (1996) classification is a reference, and has been implemented in several GIS softwares such as GRASS (`r.param.scale` module). For this reason, we chose to try it out on dune datasets. It is also the first classification using minimal and maximal curvatures. The dictionary of forms (classes) is shown in Figure 4.13. The classes rely on two thresholds: one for the slope and one for the curvatures.

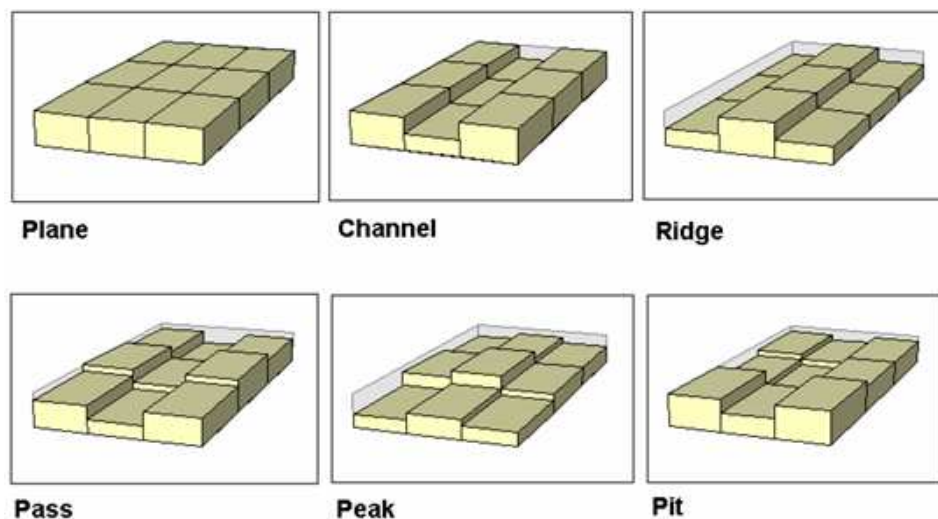


FIGURE 4.13: Wood's pixel classification. Illustration drawn from Wood (1996).

The classification was tested on SHOM zone 2. Results are shown in Figure 4.14. The color code is as follows: red = peak; orange = ridge; yellow = pass; light blue = channel; blue = pit; dark blue = plane. Table 4.1 summarises the adjustment of the algorithm parameters for the subfigures of Figure 4.14. The tested parameter values were empirically selected to highlight the respective impact of each parameter on the resulting classification.

In subfigure (A), the curvature threshold is so low that nothing is classified as plane. The dunes are not distinct except the dunes on the bank visible by the alternate pattern of channel and ridge. On the other hand, when the threshold is set too high (subfigure (C)), almost everything is tagged as plane. Only the few pixels corresponding to dune crests or rocks are seen as ridges. The results of subfigure (B) appear to be a better tradeoff concerning the curvature threshold. Yet, the part of the dunefield located at the foot of the bank is not clearly detectable. Subfigure (D) shows that the increase of the slope threshold yields better results. It can be seen that more peaks, passes or pits are detected and so the classification is more diversified. When the slope threshold is low, the classification principally relies on the two slope-dependent curvatures.

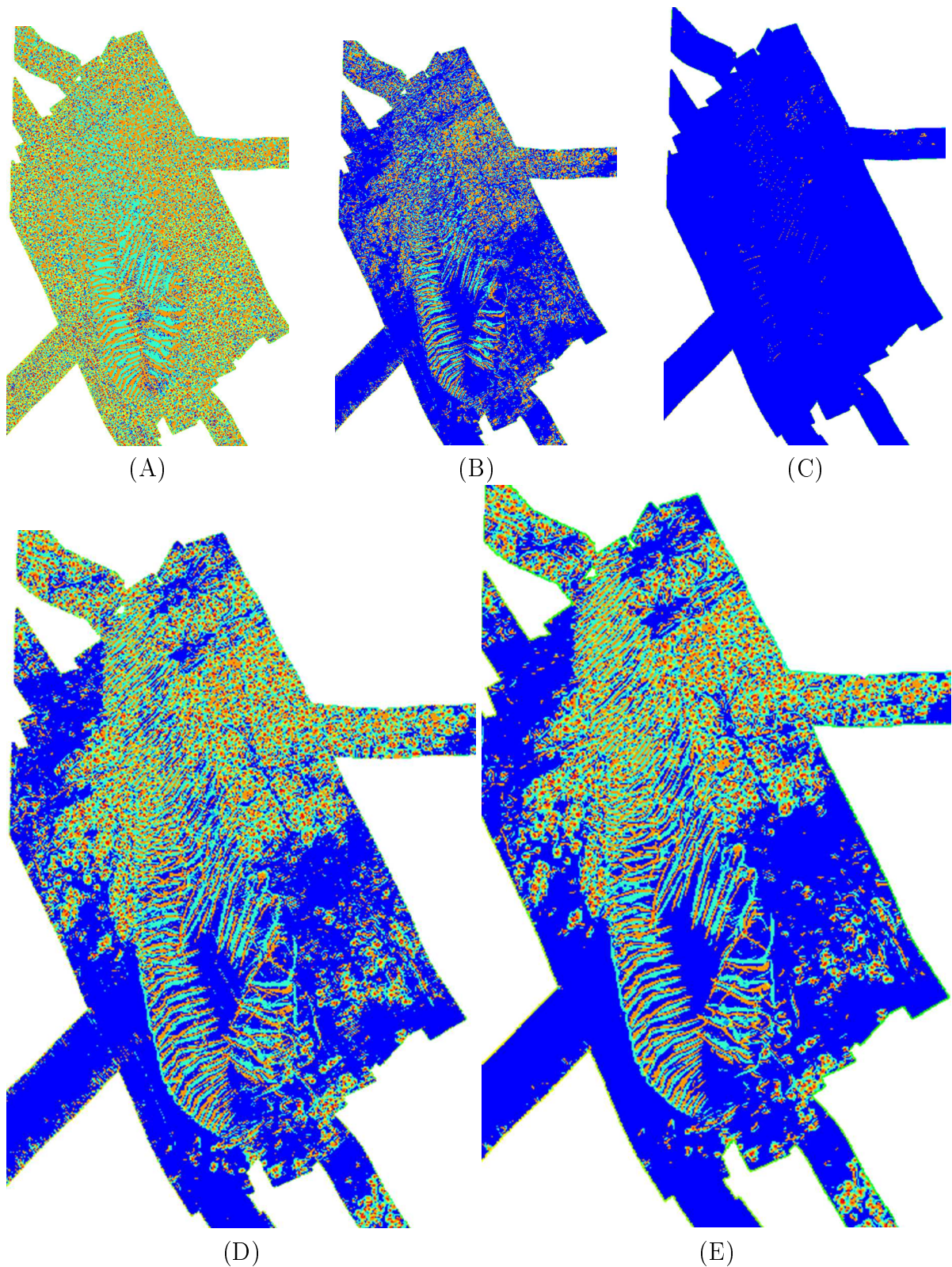


FIGURE 4.14: Application of Wood classification to SHOM zone 2.

As noted, these types of curvatures have lower values than the minimal and maximal curvatures and may more easily be below the curvature threshold. Consequently,

Subfigure	Slope threshold (°)	Curvature threshold	Neighborhood size
A	1	0.0001	3x3
B	1	0.001	3x3
C	1	0.01	3x3
D	5	0.001	3x3
E	5	0.001	7x7

TABLE 4.1: Thresholds setting of Figure 4.14.

classes associated to a flat terrain in at least one direction (ridge, channel or flat) benefit from a high slope threshold. The label of a pixel varies according to the scale of analysis (cf. subfigure (E)). The larger neighborhood tends to suppress small features, especially the terrain roughness in the flat areas. It corresponds to smaller scale terrain variations that get tagged as planes with a large neighborhood. Similarly, the flat parts of the seafloor between dunes are more often classified as channels.

Figure 4.15 shows that all the pixels near dune crests are not classified as being part of a ridge but also as pass or peak. Furthermore, the dune flanks or toes are a mix of channel, pass and plane pixels. This means that the clustering of pixels into homogeneous regions is not sufficient to build the elementary parts of a dune. Additionally, the classification results are highly variable according to the setting of the threshold values. And, the morphometric parameters are scale-dependent. All these elements combined make delicate matter the extraction of dunes from an algorithm with a general geomorphometry approach.

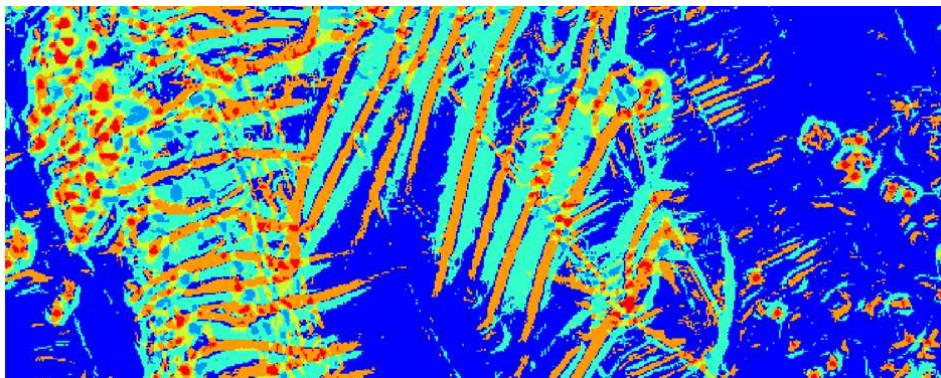


FIGURE 4.15: Zoom on dune classification of subfigure (E).

4.4.2 Disparity line algorithms

A classification alternative is to focus on disparity lines. This kind of approach is primarily used to identify terrain characteristic lines. But attempts to delineate landforms can be imagined. Indeed, landforms/objects are characterized by their interior homogeneity. Therefore, object boundaries are characterized by discontinuities, brisk variations of the descriptive metrics. This method has already been used for the extraction of faults (Schnur et al., 2011, Schnur, 2011) or the delineation of volcanoes by identifying the slope breaks (Grosse et al., 2012, Melis et al., 2014). The maps of metrics on dunes (cf. Section 4.3.2) do not reveal such discontinuities. It is true that slope decreases at dune toes but the value gently decreases. The lack of a significant slope break makes the application of a disparity line method impossible.

4.4.3 Drainage algorithms

Disparity line techniques are not the only algorithms based on the detection of object boundaries. Drainage network algorithms are a possible alternative (Jiang et al., 2013, O'Callaghan & Mark, 1984). They follow two basic approaches: the simulation of simultaneous flooding of the terrain from the regional minima or flow off regional maxima. These two approaches are equivalent. The surface is simply reversed to switch from one approach to the other.

The places where waters meet create lines called drainage divides. These drainage divides are the boundaries of areas named catchment areas or watersheds. Each catchment area is associated to one regional extremum. When flooding is simulated, the drainage divides are composed of crest lines or passes. The propagation of the downhill slope enables indicating for each pixel the number of pixels drained through it. Valley lines can be obtained by keeping pixels with high values. If the problem is reversed, drainage divides are valleys and the crests can be obtained from the uphill slope. Figure 4.16 illustrates the functioning of a drainage algorithm in a mountainous region. The red areas are regional maxima, yellow lines are crests and white lines are drainage divides.

The algorithm is divided into two steps: (1) the detection of the regional minima or maxima and (2) the delineation of catchment areas.

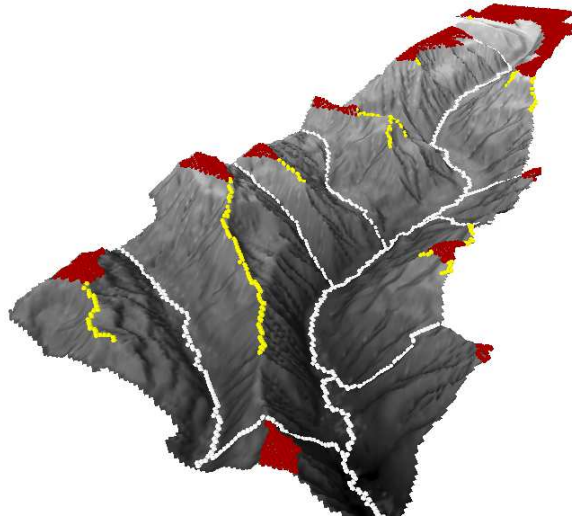


FIGURE 4.16: Example of drainage network algorithm.

At first sight, the algorithm might be well-suited for the extraction of dunes. Dune crests are regional maxima and each catchment, a dune. In practice, the algorithm has been used to study valleys (Tribe, 1992), canyons (Porter-Smith et al., 2012, Tubau et al., 2013), and drainage systems in steep areas (Pratson & Ryan, 1996).

Figure 4.17 illustrates the limitations of these algorithms when applied to dunes. Oversegmentation and undersegmentation are common issues. The segmentation success is determined by the definition of the regional maxima. In the case of this figure, the detection of the regional maxima is achieved using mathematical morphology tools. Subtracting the DTM after closing to the original DTM enables locating the terrain maxima. A height threshold can then be applied to only keep the regional maxima, clusters of pixels where the height difference is above the chosen threshold value. Note that the size of the structuring element (5x5 pixel window in the presented case) has also an impact on the results. In the figure, the number of segments varies from 14 to 187 when the threshold is decreased from 1 m to 50 cm and dune crests are not really visible. Dune crests are not the only regional maxima in the presented datasets, the bank or rocky peaks are too. In addition, catchment areas become extremely large where the terrain gets flat. Hence, the correct detection of dune crests would not be sufficient as drainage divides do not fall at dune toes. For these reasons, this type of techniques does not perform well on dune datasets.

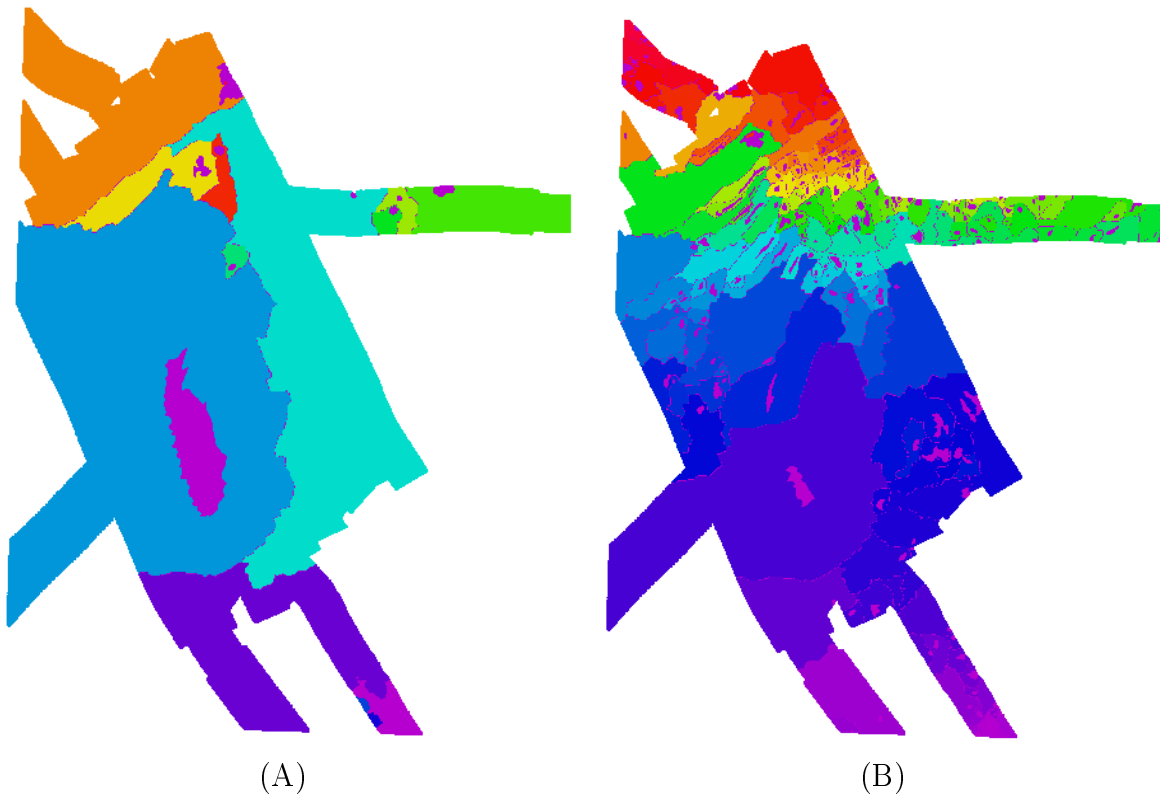


FIGURE 4.17: Catchment segmentations of SHOM zone 2.

4.4.4 OBIA algorithms

If line-based approaches failed at extracting dune boundaries, it might be judicious to detect objects from the inside. Based on the concept of geomorphometric signature, Object Based Image Analysis (OBIA) techniques assert that landforms are regions where a set of metrics is homogeneous. The choice of metrics is critical as it directly impacts the construction of the objects. Hence, the object signature must be well-identified *a priori*. Unlike unsupervised classification processes, OBIA method relies on the closeness of pixels in the spatial and parametric spaces. The algorithm starts with pixel-objects. Adjacent objects are sequentially merged if there are close enough in the attributes space. The aim is to preserve a high internal homogeneity.

Here is an example of formula to estimate the homogeneity difference between adjacent objects in a d -dimensional feature space:

$$h = \sqrt{\sum_d (f_{1d} - f_{2d})^2}$$

Homogeneity expressions generally look like distance functions. The homogeneity is not the only criterion constraining the merging of objects. Object size or form criteria can also be defined (Strobl, 1999).

OBIA algorithms have been developed to extract geomorphometric units (Drăguț & Blaschke, 2006, van Asselen & Seijmonsbergen, 2006), landforms such as gullies (dOleire Oltmanns et al., 2013) or drumlins (Eisank et al., 2014). Multiresolution analysis also exist for this type of method (Dragut & Eisank, 2011). Contrary to drumlins, no constant attributes at the scale of a dune were observed on maps of morphometric attributes. Dunes are complex landforms with concave, flat and convex areas. The slope is null at the top and bottom and higher on sides. The slope is no even constant across a dune side or from one side to another. This lack of homogeneous parameters makes OBIA techniques inappropriate for dune delineation.

4.4.5 Region growing algorithms

Another way to get a landform segmentation is the region growing approach. A region growing algorithm is composed of two phases: (1) the extraction of seed features; (2) the growing phase. Surfacially, they are similar to catchment-based segmentation algorithms. Indeed, seeds are first identified like regional extrema in the watershed approach. These seeds are remarkable terrain points, lines or regions. Local or regional extrema, discontinuity lines are examples of seeds. The principle is that the seed features are outstanding parts of the landforms of interest.

The second step is the growing of the seed regions. The regions are sequentially extended to the adjacent pixels and the operation is iterated as many times as needed. The growing can stop when every pixel of the DTM is assigned to a region (Mehnert & Jackway, 1997) or when there is no pixel complying with a growing criterion (Graff, 1992). In Graff (1992), a region growing technique is introduced to extract mountains. The mountain summits are selected to constitute the set of seed regions. They coincide with regional maxima of the mountainous terrain. The seeds are then extended to pixels of high slope. Observations on the slope values around the mountain feet help in determining an adequate slope threshold. A comparable method is implemented in Miliareisis & Argialas (1998) to segment the DTM into three classes: mountains, piedmont slopes and basins.

Region growing segmentation approaches were not only applied to land topography but also to the marine environment. For example, techniques were proposed for the

automation of seabed pockmarks extraction (Andrews et al., 2010, Gafeira et al., 2012). The final objective was the characterization of pockmarks.

When visualizing the DTM of a dunefield, the features that are particularly striking are the dune crests. On each side of the crest are the dune flanks. Although simple, this decomposition of dune morphology in elementary parts is well adapted to region growing segmentation and it avoids searching for boundary lines. Based on this observation, a first dune extraction algorithm was designed.

4.5 First dune extraction algorithm

4.5.1 Principles

Section 4.2 introduced fundamental notions of geomorphometry, some of which are crucial for the extraction of dunes in DTMs. The notions of scale, elementary forms and geometric signature must be taken into account by our dune extraction algorithm. Section 4.3 presents classical geomorphometric metrics and explains the terrain properties they highlight. In Section 4.4, different segmentation techniques have been studied for the purpose of automatic dune extraction. These techniques use the metrics presented in Section 4.3. They have already been applied in the literature for the extraction of landforms other than dunes.

Through these sections, it may be understood that the most remarkable part of a dune is its crest. It is often the only part that can be manually traced as the limits of the dune feet are sometimes hard to determine visually. Therefore, the dune extraction algorithm must focus on the crest and, then, consider the sides. In Section 4.3, it was observed that dune crests and sides are respectively characterized by extreme values of minimum curvature and slope. The identification of these metrics is important for dune extraction. The conclusions of Section 4.4 are that region growing methods might be suited for dune extraction as they decompose landforms into seed regions surrounding by regions where one or several metrics are homogeneous. This decomposition matches the definition of a dune as a crest surrounded by sloping sides.

Two things are critical for a region growing approach: (1) the choice of the seed regions and their extraction; (2) the growing criterion.

Crests are noticeable by their convexity and dimensions. As seen above, convexity is quantifiable with minimal curvature. Minimal curvature has also the advantage of

being slope independent unlike most of the other curvatures. This is a valuable property since slope values tend to zero near crests. The algorithm can define crest regions by applying a threshold on the minimal curvature map.

The second step is the growing of the seed regions. In the case of dunes, this consists of detecting the pixels belonging to dune flanks. What comes first to mind is to use the slope to identify the dune extent. Flanks are sloping areas in comparison with the base seafloor on which dunes stand. From a morphological signature standpoint, the algorithm summarizes a dune as a crest and steep sides that may be characterized with thresholds on the minimal curvature and slope. In practice, the seed regions are iteratively grown by adding the connected (adjacent) pixels where the slope is greater than a slope threshold visually adjusted.

4.5.2 Results and discussion

The algorithm was tested on several datasets in order to analyze its extraction capacity and its weaknesses. It was tested on various dune types, environments, DTM accuracies and resolutions. All these aspects are discussed in this subsection.

SHOM zone 6 is a perfect dataset to test the algorithm performance, since the dunes are not touching and so are easier to delineate. Furthermore, the manual dune tracing being relatively simple, it can be used as reference for comparisons with the automatic algorithm.

Figures 4.18 and 4.19 are respectively the minimum curvature and slope maps draped on the DTM of SHOM zone 6. The observation of these maps confirm that the two metrics are well-suited to highlight the dune crests and sides.

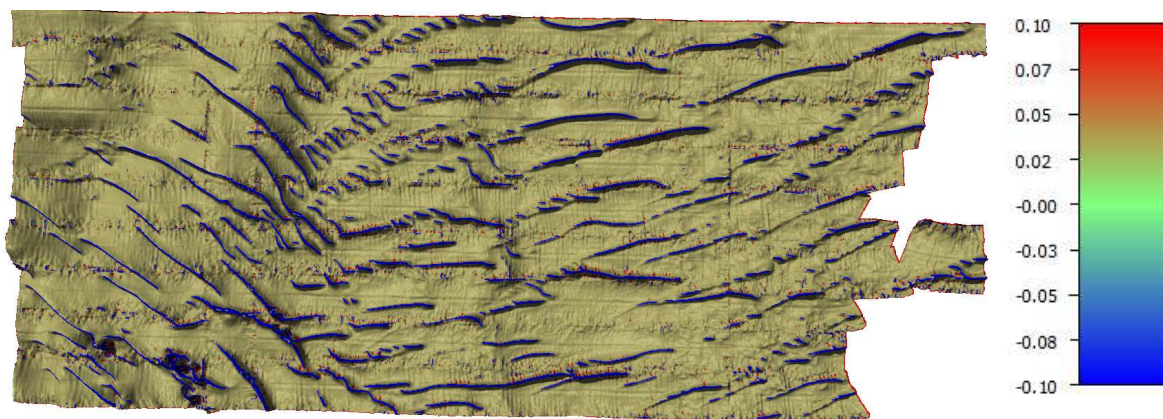


FIGURE 4.18: Minimum curvature (m^{-1}).

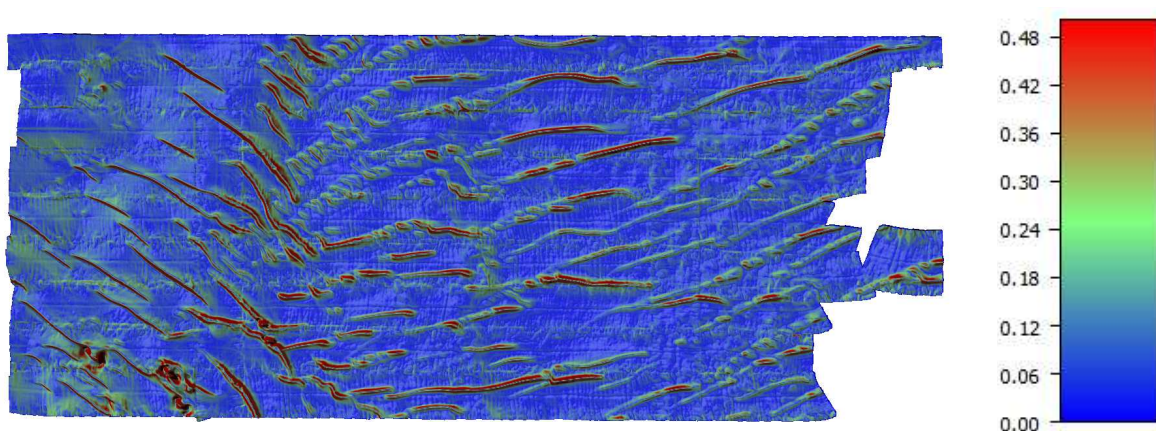
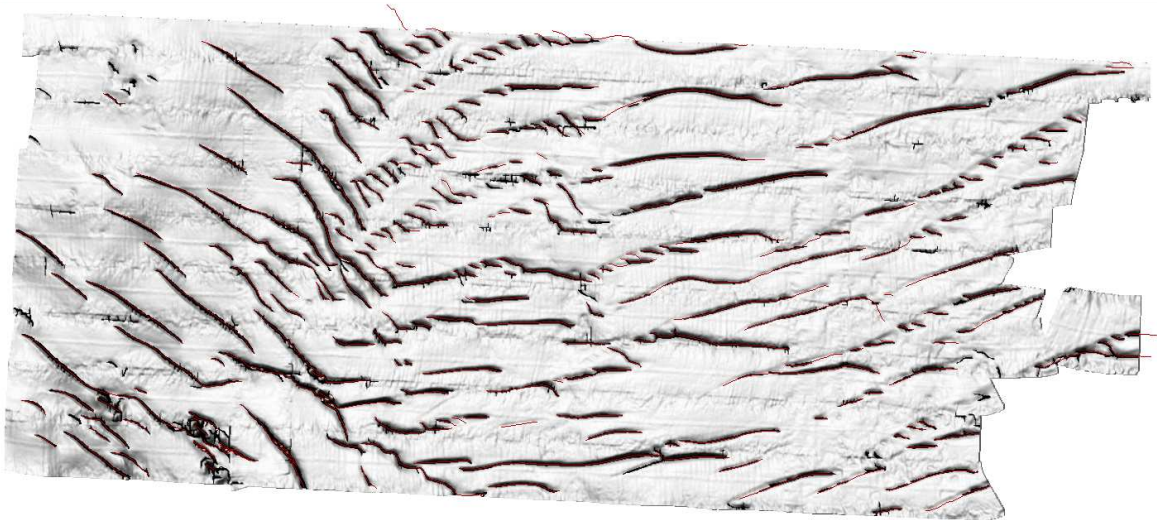


FIGURE 4.19: Slope estimation.

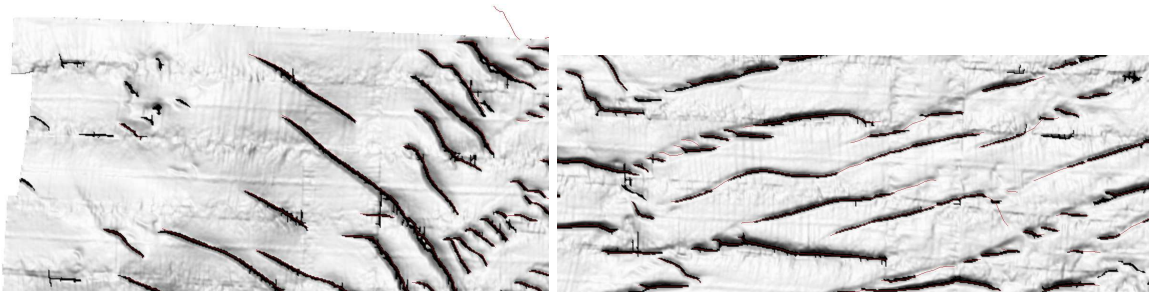
In order to extract the seed regions (crests) first and, then, to grow dunes, two thresholds must be adjusted. Their setting is empirical as it is only based on the visualization of the metrics maps.

If the curvature threshold is set to a very negative value, All dune crests may not be detected and some be divided into smaller crest clusters. If the threshold is set too loose (close to zero), other features not as sharp as dune crests can be detected when the objective is to focus on the extraction of dune crests. The acceptable trade-off for the SHOM zone 6 is to set the curvature threshold at -0.1 m^{-1} . The obtained seed regions with this threshold value are presented in Figure 4.20. 248 crests are detected by the algorithm against 252 by the human operator. Overall, the results are satisfying. Yet, the semi-automatic crest extraction is not perfect.

Subfigure (A) confirms that, in most cases, the manual and automatic detections are in accordance. Yet, differences exist. In the top left corner of subfigure (B), the inconsistency of MBES data generates rapid depth changes in the DTM that are wrongly detected as crests. A lower curvature threshold may have solved this issue, but it would cause others. Indeed, with the chosen value, the algorithm sometimes fails to recover the full extent of the crests (see Subfigure (C)). Some dune crests are even split into several seed regions. To prevent this, the curvature should be loosened. Subfigure (C) illustrates how a few dune crests may also be assembled into one big seed region. Additionally, spurious seed regions are detected due to the presence of artifacts in the data.

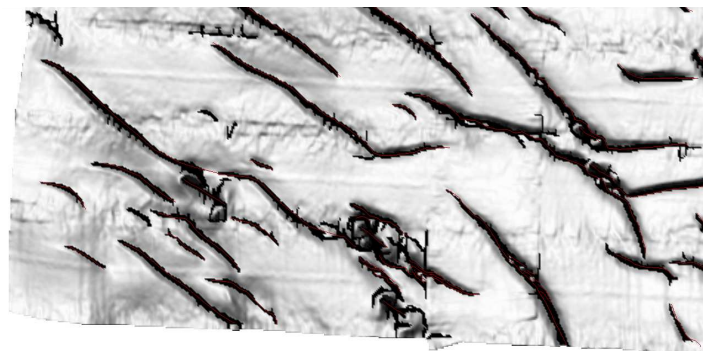


(A)



(B)

(C)



(D)

FIGURE 4.20: Comparison between the seed regions (black) and manually extracted (red lines) dune crests with zooms on failure cases.

The final segmentation is presented in Figure 4.21. The slope threshold was set to 0.2. The manual extraction is the final aim of the algorithm. Therefore, the overall results are satisfactory. Yet, the growing does not solve the problems identified during the seed construction phase. In addition, the slope threshold is as delicate to adjust as the curvature one. When it is set too high, dune sides are not fully recovered.

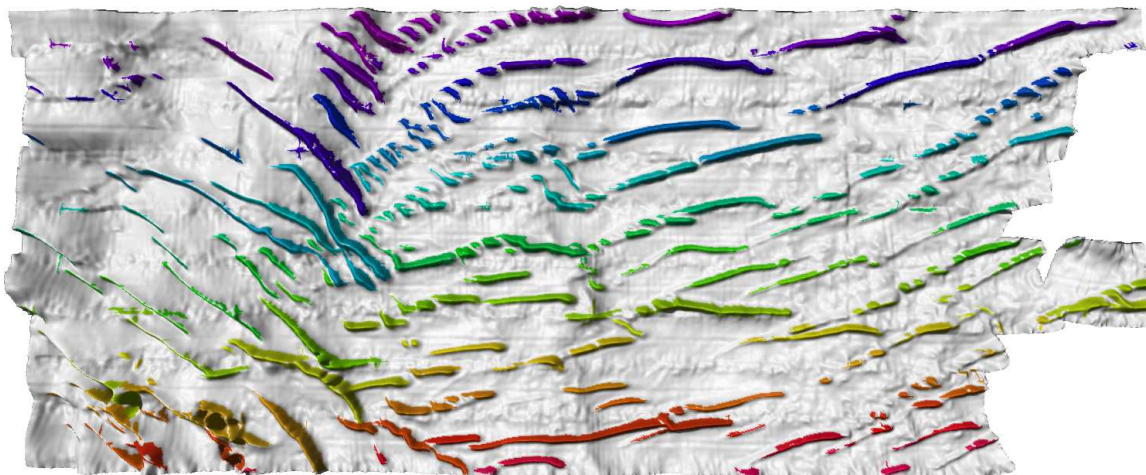


FIGURE 4.21: Results of the region growing algorithm in SHOM zone 6.

On the other hand, if it is set too low, small dunes and more gently sloping parts are well-extracted but this may lead to the overgrowing of other dunes.

In order to fix the shortcomings of the algorithm, additional parameters were added. The goal of the first parameter is to remove all the spurious seed detections. In practice, it is a threshold on the minimal number of pixels required to be a dune crest. In the case of Figure 4.21, seeds corresponding to artifacts were discarded. This parameter is referred to as region size parameter in the following.

Figures 4.22 and 4.23 explain how this parameter is not sufficient to remove all the undesired seed regions. On these figures, the curvature threshold was set to -0.3 m^{-1} . The use of the region size parameter enables solving part of the problem. In fact, seed regions are detected in the rocky areas. Although rocks do not have the same spatial extent as dunes, they are clustered in large seed regions. To split the rocks into small seeds would require lowering the curvature threshold and, consequently, losing seeds corresponding to dunes.

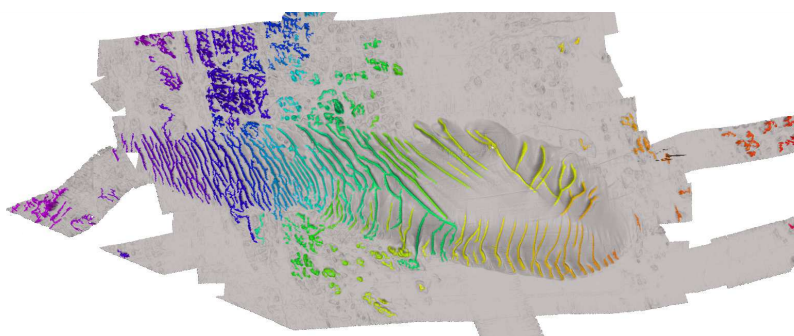


FIGURE 4.22: Seed regions with the initial algorithm.

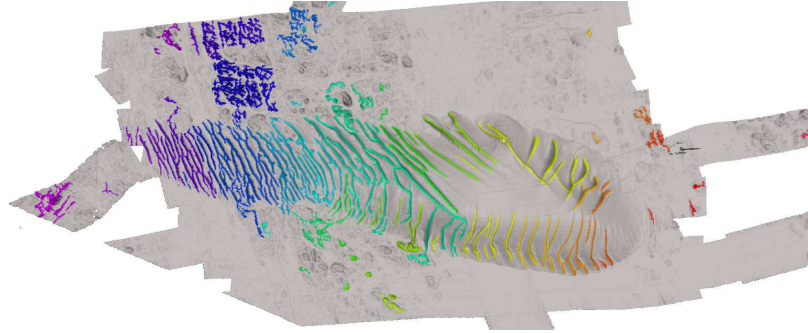


FIGURE 4.23: Seed regions using the region size parameter.

SHOM zone 2 shows dunes on the flank of a bank. This study case is interesting to observe the impact of the slope threshold on the dune growing. It may be inferred from Figures 4.24 and 4.25 that, in this case, the adjustment of the slope parameter is delicate. To lower the threshold causes the overgrowing of bank dunes. But dunes are unexpectedly shrunk in the opposite case. Therefore, a maximum distance parameter was defined to prevent the regions growing too far from the initial seeds. This parameter enables lowering the slope threshold with no risk of overgrowing (cf Figure 4.26). It works as expected, but it bypasses the slope threshold: the distance parameter becomes the only parameter constraining the growth. This parameter is empirical and is not suited for all dunes. Indeed, some dunes are wider than others.

The explained improvements provide more knowledge about dune morphology in the algorithm but require the definition of additional empirical parameters. The modifications of the algorithm finally yield little benefit for the derived segmentation.

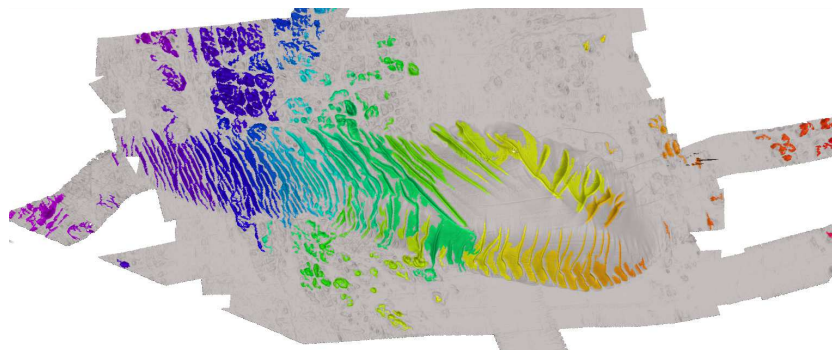


FIGURE 4.24: Extraction results with a 0.8 slope threshold.

To summarize, our semi-automatic algorithm is based on two heuristics: slope and minimal curvature thresholds. These two heuristics are too dependent on the dataset (dunefield characteristics). The curvature and slope values change according to the calculation neighborhood, the DTM resolution, the dune type, the locations of the dunes (on banks or not). Therefore, it is hard to correctly tune the thresholds in order

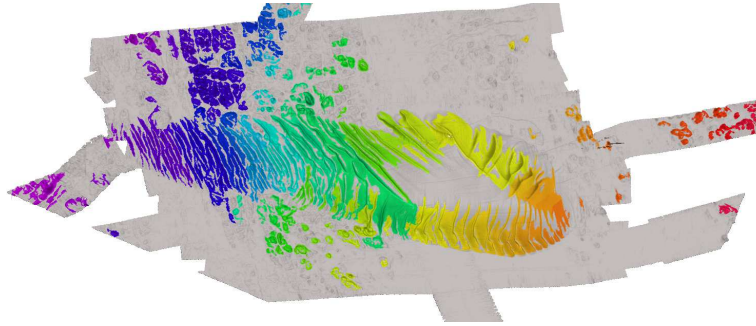


FIGURE 4.25: Extraction results with a 0.5 slope threshold.

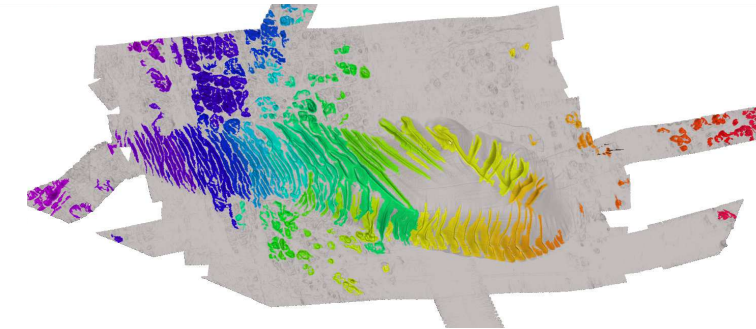


FIGURE 4.26: Extraction results with a 0.5 slope threshold and a maximum distance of 70 m.

to extract dunes satisfactorily. Moreover, curvature is not a metric that is easy to appreciate for a human being. Improvements were made to cope with data specificities, but, this demands setting additional heuristics for a limited impact on the quality of the extraction. Despite all these limitations, the approach is interesting. The crest recovery is the key step. Therefore, great care must be taken to faithfully detect realistic dune crests. Their definition as regions of extreme convexity remains valid but should rely on a less empirical parameter than the curvature threshold.

4.6 Surface Representation

Geomorphometry is devoted to the quantitative study of the Earth's surface. In this context, the terrain is almost always represented by a DTM. DTMs are 2.5D representations of a 3D surface. DTMs are particular images (2D representations) since the intensity level represents elevation values. That is, they are height maps (2.5D representations) rather than strict 3D representations. For each (x,y) , there is only one depth value. This representation of the terrain does not allow for "overhangs" and concavities. DTMs can be based on a grid (gridded DTM) or on a triangulation (Triangulated Irregular Network (TIN)).

In this chapter, it was seen that the existing techniques for terrain analysis on gridded DTMs proved unsatisfactory for extracting dunes. The question of the surface representation and the associated processing algorithms must be discussed. Other potential representations exist and can be used for the extraction of dunes as illustrated in Figure 4.27.

Initially, the seafloor is approximated by a cloud of soundings. This approximation takes into account the 3D geometry of the seafloor surface. The main issue comes from the fact that point clouds are not easy to manipulate due to the acquisition noise and the number of points. Therefore, they are badly suited for visualization or surface analysis purposes. However, a DTM is not the only alternative to point clouds.

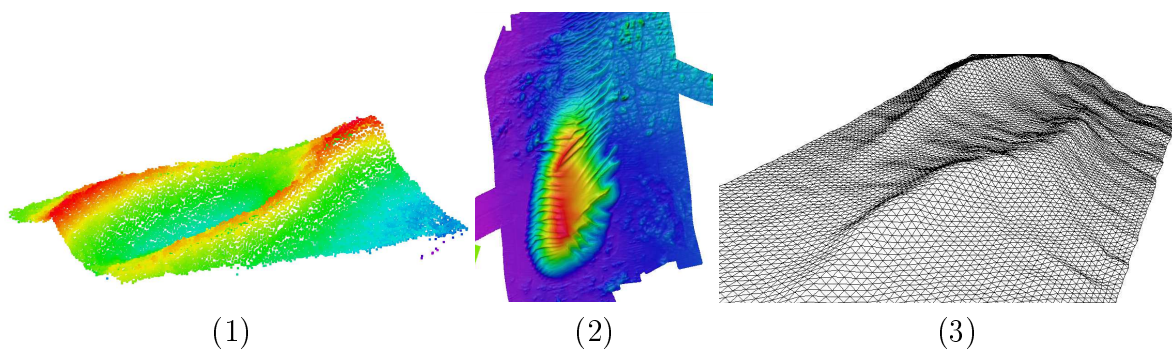


FIGURE 4.27: Three types of surface approximations: (1): Cloud of soundings; (2): gridded DTM; (3): Triangular mesh.

Another possible approximation is the 3D mesh, where the surface is tiled by triangles, quadrangles or polygons. In this model, the surface geometry is described by vertices connected by edges. The edges delimit elementary surface areas called faces (see Figure 4.28). 3D meshes are extensively used in many scientific domains such as medical visualization, computer aided design, 3D object visualization, video games, *etc.* The types of segmentation algorithms used on 3D meshes are equivalent to these presented in this chapter. A wide range of solutions for extracting dune crests might be accessed by adopting this surface representation.

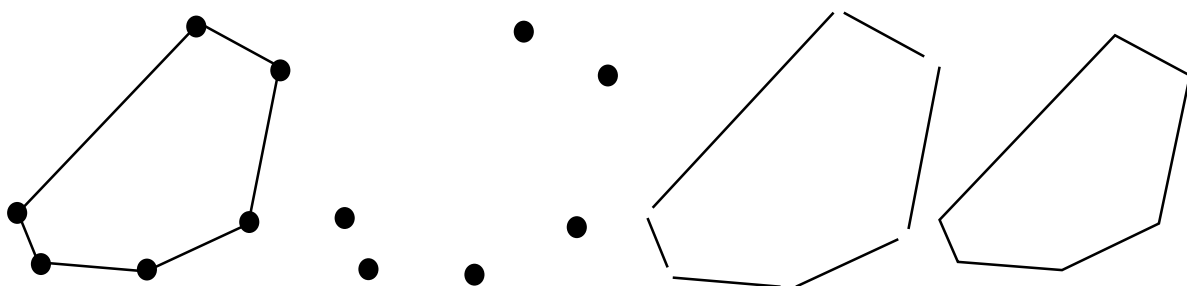


FIGURE 4.28: Decomposition of the mesh into three types of elements.

It can be seen that triangular meshes are a simple generalization of a TIN as they allow having more than one depth at a point (x,y) . But, the surface is still approximated by triangular facets.

Choosing this representation over gridded DTMs has a number of advantages. Unlike DTMs, a triangular mesh is a representation that does not make the distinction between x,y and z coordinates. All three coordinates are considered equally as spatial information. It does not make assumptions on the surface geometry. All 3D objects or surfaces can be modelled by a triangular mesh. A gridded DTM has a fixed resolution or, at least, imposes a regular sampling of the terrain. With a triangular mesh, more vertices may be added in the regions where the terrain variations are significant. Therefore, feature lines such as dune crests can be described at high resolution. Flat areas can be modelled by a limited number of vertices and facets. In other words, the sampling of the surface can be adapted to model the regions of interest only and, therefore, reduce the size of the representation (number of vertices). The sampling can also be adjusted according to the data density. More vertices can be used to model a region with a high sounding density. Gridded DTMs usually do not account for the density leading to holes in the surface or noise in the DTM for the cells where the data density is low compared to the cell size. A gridded DTM has a certain rigidity that does not allow adjusting to the terrain or data properties.

To conclude, the irregularity of triangular meshes make it more flexible than gridded DTMs. With DTMs, the crest extraction consists of finding a group of pixels that are close to the real crests. With a triangular mesh, real lines could be extracted. These lines could pass through the mesh vertices or even cross freely the mesh faces. The tracing of crests would not be as much limited by the geometry of the seafloor representation if they were extracted on triangular meshes. These reasons made us change the representation of the seafloor from gridded DTM to triangular mesh.

The construction of a discrete surface from point sets is not a trivial problem and deserves great care. But, for simplicity reasons, the triangular faces of the mesh were created by connecting the DTM elevation values as shown in Figure 4.29).

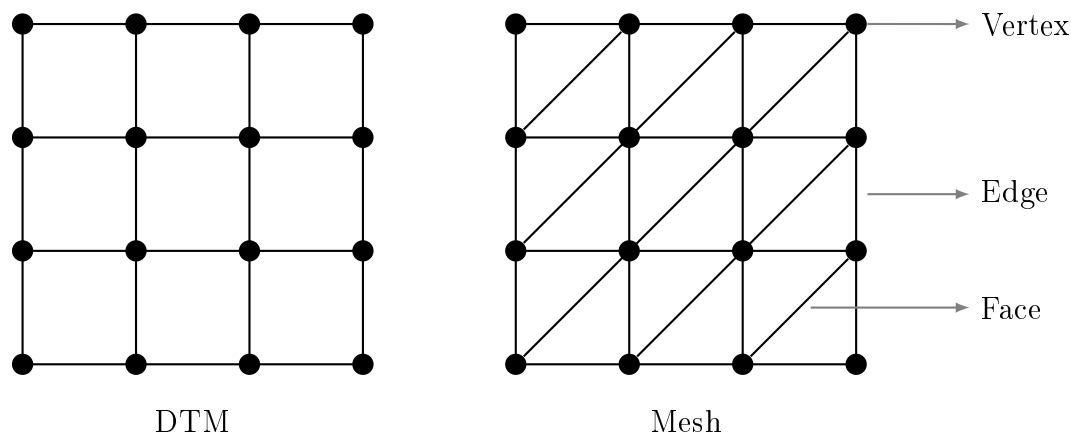


FIGURE 4.29: Mesh construction from a DTM.

All the algorithms presented in the remainder of this thesis rely on a mesh approximation of the seafloor. The use of Computational Geometry Algorithms Library (CGAL)² was motivated by the fact that it provides C++ libraries for most applications related to geometric computation. Consequently, it already contains the classes describing the geometry of meshes (vertex, edge, face) as well as basic functions to explore the surface.

4.7 Conclusion

In this chapter, the problem of dune delineation was considered from a "geomorphometry" point of view. The geomorphometric analysis introduces notions that appeared relevant for the study of dunes: specific geomorphometry, scale, landforms and signature.

Common topographic descriptors were presented, calculated on dunes to better appreciate dune morphology and select those which might be useful. Morphometric parameters help characterizing the terrain nature.

A catalog of segmentation methods relying of these attributes was examined and tested on dunefields. It was observed that the proposed segmentation processes have little theoretical foundation and stand on rules of thumb and intuition. In addition, the DTM resolution and the neighborhood size are very influential.

2. <https://www.cgal.org/>

Pixel classification techniques are based on the thresholding of metrics to set a label on a pixel (peak, ridge, valley, *etc.*). It is very delicate to associate classes to dune parts. For instance, ridge, saddle or peak pixels might all belong to a dune crest. In addition, the classification results are highly variable according to the tuning of parameters. No metrics show discontinuities at the dune boundaries so that disparity line methods were discarded. Drainage algorithms generate drainage divides that can partly match with dune crests or boundaries, but the problem is that there is no way of knowing which parts. Furthermore, the catchment areas rarely (never) corresponded to dunes. Each catchment area is associated to a regional maxima. Their definition/parametrization is very sensitive which can generate under or oversegmentations of the seafloor. OBIA algorithms aim to extracting objects from an image by gathering pixels in regions based on a homogeneity criterion. While this was successfully adapted for drumlin extraction, no metrics was constant over an entire dune. Consequently, these techniques cannot be applied for dune extraction.

The first algorithm gives results similar to the manual reference. Nevertheless, a number of limitations have been pointed out. If the idea of designing a region growing algorithm for dune extraction is interesting, the use of minimum curvature and slope thresholds is a problem. Their setting is manual and highly empirical. These metrics are also not intuitive so that it is impossible to know which threshold values are optimal without visualizing the metrics maps. The ideal threshold values are not the same for two datasets or even two dunes. When some crests are extracted well, others are only partly extracted or not seen at all. Dune crests might be fragmented or merged with neighbors. The setting of the slope threshold is also difficult and can cause overgrown or shrunk dunes. Additional parameters were developed to correct these issues, but they had a limited impact on the extraction quality and make the algorithm even more empirical. The tuning of the thresholds is simply achieved by determining tradeoff values reducing these undesired effects.

More sophisticated techniques relying on 3D models need to be explored to go beyond these limitations. The conceptual geomorphometry approach is crucial and shall be kept. Much effort must be devoted to the construction of quality dune crests. The fact that the human eye is able to trace dune crests better than dune boundaries enhances this assumption. Crests are the key part of dunes. The use of triangular mesh may improve the quality of the extracted dune crests. Their geometry will no longer be restricted to a pixel representation as they will be seen as true 3D lines.

The extraction of the crest lines requires the estimation of curvatures. Curvature estimation techniques on meshes are presented in the next chapter. These techniques are compared to determine the one that is the most appropriate for dune crest extraction. The curvature values can, next, be used to trace dune crests. Crest line extraction algorithms are analyzed in Chapter 6. The objective of the chapter is to choose among these techniques the one that is the most suited for the processing of dune datasets. As discussed in this chapter, the notion of scale is fundamental in geomorphometry. The scale at which the terrain is analyzed changes our perception. Our first algorithm had problems with the detection of dunes and rocks or data artifacts. To avoid these issues, mesh simplification algorithms are presented in Chapter 7. A mesh simplification procedure is proposed to adapt the mesh resolution for the purpose of crest extraction. These improvements are combined to propose a new region growing algorithm for dune extraction (Chapter 8).

Chapter 5

Differential Geometry and triangular mesh

Contents

5.1	Introduction	100
5.2	Useful notions of differential geometry	100
5.3	Curvature estimation on meshes	107
5.3.1	Discrete methods	108
5.3.1.1	Angular deficit	108
5.3.1.2	Angle excess	109
5.3.1.3	Spherical image	109
5.3.1.4	Integral absolute mean curvature	109
5.3.1.5	Mean curvature normal vector/operator	110
5.3.1.6	Normal curvature vector	110
5.3.2	Fitting methods	111
5.3.3	Tensor estimation methods	112
5.4	Comparison of curvature estimation	113
5.4.1	Comparisons on benchmark zone 2	116
5.4.2	Comparisons on benchmark zone 7	121
5.5	Conclusions	124

5.1 Introduction

Differential geometry is basically dedicated to the study of the local properties of curves, surfaces and equivalents in higher order spaces. Most geomorphometrical metrics introduced in the previous chapter were initially defined in the context of differential geometry. Differential geometry relies on notions of linear algebra and differential calculus. The studied curves and surfaces are defined by differentiable functions. Surfaces of \mathbb{R}^3 are a classical models that are used to model 3D objects surrounding us. Therefore differential geometry became useful for many applications: Computer aided geometric design (CAGD), solid modeling computational geometry, computer graphics, computer gaming, medical imaging, computer visualization, *etc.* Farin (2001) outlines the methods and algorithms designed in the field of CAGD.

In this chapter, only the theorems and definitions that proved useful for the estimation of curvatures and the construction of crest lines are presented. More information about the theory of curves in \mathbb{R}^2 , surfaces in \mathbb{R}^3 , their geometry and mathematical demonstrations may be found in Do Carmo (1976). Parts of these fundamental notions are summarized in Berger & Gostiaux (1987) for French-speaking readers. The various methods inspired from these mathematical definitions for the estimation of curvatures on 3D tessellations are then explained and compared. The comparisons will lead to conclusions on which technique is the best suited for the later dune crest reconstruction.

5.2 Useful notions of differential geometry

Definition 1. At each point of a \mathbb{R}^3 surface, an infinity of curvatures may be defined. The intersection of the surface with another surface forms a curve. A special local coordinate frame can be associated to the curve, the Frenet frame $(\mathbf{P}, \mathbf{t}, \mathbf{n})$ (see Figure 5.1). In this frame, the circle that has a second-order contact¹ with the curve at point P is called the *osculating circle*. This yields the definition of the surface curvature associated to this curve at point P:

$$k = \frac{1}{R}$$

Where k is the curvature and R is the radius of the osculating circle. Figure 5.1 illustrates the particular case of the osculating circle of a planar curve.

1. Two functions have a contact of order k , at a point P, if their values and their first k derivatives are equal at this point.

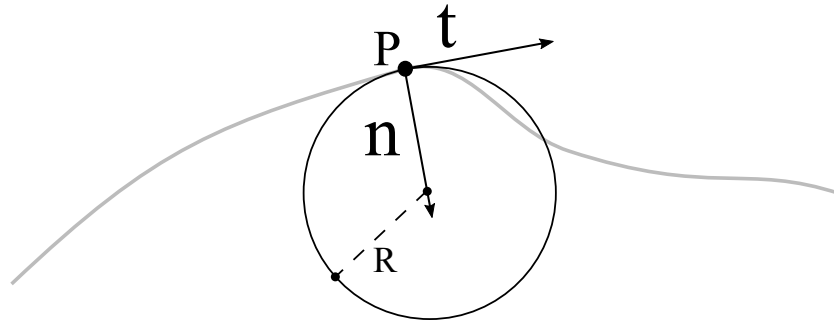


FIGURE 5.1: Osculating circle and definition of the curvature at a point of a at least C^2 curve.

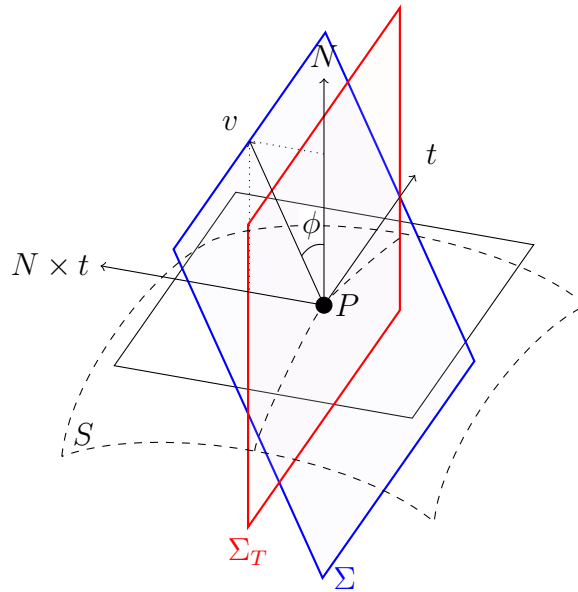


FIGURE 5.2: Link between a curvature and the corresponding normal curvature.

Definition 2. Normal curvature

A normal curvature K_T at a point P of a 3D surface S is defined by a direction, a vector tangent \mathbf{t} to S in P and a vector n_T normal to S at P . By definition, the normal curvature at P in the direction of \mathbf{t} is the curvature of the curve formed by the intersection of the surface and the normal section Σ_T . At each point of the surface, there is an infinity of normal curvatures, each being associated to a direction. If the curvature \mathbf{K} of the curve formed by the intersection of the surface and the section $\Sigma(P, \mathbf{t}, \mathbf{n})$ at P is known, the normal curvature k_n associated to \mathbf{t} may be obtained as follows:

$$k_n = \mathbf{K} \cdot \cos \phi \text{ with } \cos \phi = \langle \mathbf{n}, \mathbf{n}_T \rangle \text{ and } \langle \cdot, \cdot \rangle, \text{ the Euclidian inner product on } \mathbb{R}^3.$$

Figure 5.2 explains the notions and notations used in the previous definition.

Definition 3. First Fundamental Form

The inner product of the Euclidian space \mathbb{R}^3 restricted to any tangent plane $T_p(S)$ ² to the regular surface S is also an inner product $\langle \cdot | \cdot \rangle_p$. This restricted inner product is a bilinear form and so has an associated quadratic form $I_p: T_p(S) \rightarrow \mathbb{R}$

$$I_p(w) = \langle w, w \rangle_p = |w|^2 > 0$$

If we consider the surface S in a parametric form:

$$\mathbf{X} = \mathbf{X}(u, v) = \begin{bmatrix} x(u, v) \\ y(u, v) \\ z(u, v) \end{bmatrix}; \text{ with } (u, v) \in \mathbb{R}^2 \text{ } X_u \text{ and } X_v \text{ are tangent vectors to}$$

the surface S at point P . These vectors form a base in which the matrix of the first fundamental form, \mathbf{I}_p , can be expressed:

$$\mathbf{I}_p = \begin{pmatrix} E & F \\ F & G \end{pmatrix} = \begin{pmatrix} \langle X_u, X_u \rangle & \langle X_u, X_v \rangle \\ \langle X_u, X_v \rangle & \langle X_v, X_v \rangle \end{pmatrix}$$

This yields the equation of the first fundamental form:

$$I_p(w) = w^T \mathbf{I}_p w = Ew_1^2 + 2Fw_1w_2 + Gw_2^2;$$

with $w = (w_1, w_2)$ in (X_u, X_v) basis.

Definition 4. Gauss map

The Gauss map of a surface S is the morphism $N: S \rightarrow s$, the unit sphere in \mathbb{R}^3 , such that $N(P)$ is the unit vector normal to S at point P .

Definition 5. Second Fundamental Form

The second fundamental form is a quadratic form defined on the tangent plane $T_p(S)$ by:

$$II_p(v) = -\langle dN_p(v), v \rangle$$

2. The tangent plane to a surface S at point P is noted $T_p(S)$.

It is usually expressed as following:

$$II_p = Ldu^2 + 2Mdudv + Ndv^2$$

where $L = \langle X_{uu}, N(P) \rangle$, $M = \langle X_{uv}, N(P) \rangle$, $N = \langle X_{vv}, N(P) \rangle$. X_{uu} , X_{uv} and X_{vv} are the second-order partial derivatives of surface X with respect to u and v .

By identification, the matrix of the second fundamental form in the basis (X_u, X_v) is:

$$\mathbf{II}_p = \begin{pmatrix} L & M \\ M & N \end{pmatrix} \quad (5.1)$$

Definition 6. Shape operator

The shape operator is also called Weingarten map or endomorphism. The shape operator is the differential dN of Gauss map N . The shape operator is linked to the first and second fundamental forms by the relation:

$$II_p(v, w) = \langle d_p N(v), w \rangle$$

where $v, w \in T_p(S)$.

As a reminder, the first fundamental form is the inner product restricted to $T_p(S)$. Hence the matrix \mathbf{W} of the Weingarten map may be obtained by:

$$\mathbf{W} = \mathbf{I}_p^{-1} \mathbf{II}_p$$

Note that the normal curvature $k_T(P)$ in the t direction can be calculated as follows:

$$k_T(P) = t^T \mathbf{W} t$$

Definition 7. Principal curvatures

The principal curvatures are the eigenvalues of the shape operator. They are generally denoted by k_1 , k_2 or k_{max} and k_{min} . The curvatures are the extreme values of the normal curvatures at a point P . The associated eigenvectors t_{max} (t_1) and t_{min} (t_2) are called principal directions. These directions are orthogonal.

Definition 8. Gaussian and mean curvatures

k_1 and k_2 are eigenvalues of the Weingarten map which means:

$$\det \begin{pmatrix} k_1 - k & 0 \\ 0 & k_2 - k \end{pmatrix} = k^2 - (k_1 + k_2)k + k_1k_2 = 0$$

The term $K = k_1k_2$ is called the Gaussian curvature and the term $H = \frac{k_1+k_2}{2}$ is called the mean curvature. These two parameters locally describes the surface geometry. A point P of surface S is said:

- elliptic if $K > 0$
- hyperbolic if $K < 0$
- parabolic if $k_1 = 0$ or $k_2 = 0$
- planar if $k_1 = k_2 = 0$

The principal curvatures can also be derived from H and K by:

$$k_i = H \pm \sqrt{(H^2 - K)}$$

Definition 9. Umbilic

An umbilical point is a point where both principal curvatures are equal ($k_{max} = k_{min} \neq 0$). That is to say that the surface is locally spherical.

Definition 10. Darboux frame

A Darboux frame is a moving frame similar to the Frenet frame for curve of \mathbb{R}^2 . It is made of two unit, non colinear tangent (randomly selected) vectors and one normal vector to S at a point P (cf. Figure 5.3). The Darboux frame shown in this figure is particular as the two chosen tangent vectors correspond to the principal directions t_{min} and t_{max} at point P. This frame is called the Monge frame.

Definition 11. Extremality

Extremality is a notion associated to a direction and a curvature. It is defined as the directional derivative of a curvature k in the associated direction t . The extremality formula is:

$$e = \nabla k \cdot \vec{t}$$

In the literature, extremality is usually denoted by e or b .

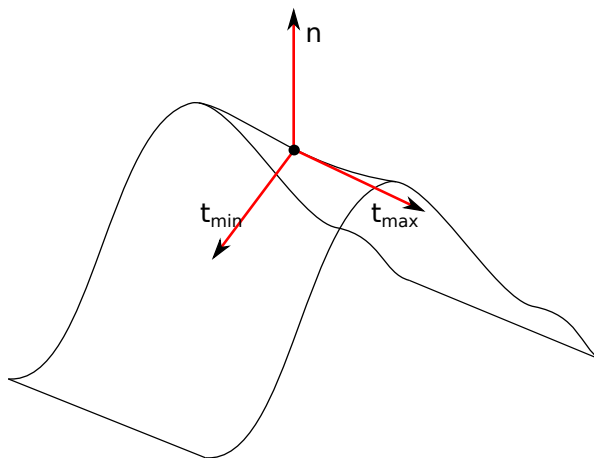


FIGURE 5.3: Example of a Darboux frame at a crest point.

Theorem 1. Meusnier's theorem

All curves C of a surface S passing through point P having the same tangent vector have the same normal curvature. With the notation of Figure 5.2, this yields the relation:

$$k_n(P) = k \cos \phi$$

Theorem 2. Euler's theorem:

Normal curvatures in different directions t are not independent of each other. The consequence is that any normal curvature k_n may be expressed as a function of the invariant principal curvatures:

$$k_T = k_1 \cos^2 \phi + k_2 \sin^2 \phi$$

with ϕ the angle between the principal direction t_1 and t .

Definition 12. Dupin's indicatrix

If we select the Monge frame (P, t_1, t_2, n) , the second order Taylor approximation of the surface gives:

$$z = k_1 u^2 + k_2 v^2$$

The intersection of the surface with a plane parallel to the tangent plane yields the conic equation:

$$k_1 u^2 + k_2 v^2 = \text{constante}$$

This is named Dupin's indicatrix. Analyses of the signs of H and K determines the nature of this conic and, then, the nature of the point of the surface considered. Dupin's indicatrix provides a geometric interpretation of the point nature.

The link between Euler's theorem and Dupin's indicatrix is straightforwardly obtained by setting $u = \frac{\cos \phi}{|k_T|^{\frac{1}{2}}}$ and $v = \frac{\sin \phi}{|k_T|^{\frac{1}{2}}}$.

Definition 13. Geodesic

Geodesics are the locally shortest paths between points of a surface. The shape of the geodesics dependent on the distance function used. From this definition comes the notion of geodesic distance that is the length of the shortest path on the surface between two points.

Theorem 3. Local Gauss-Bonnet theorem

The excess over π of the sum of the angles φ_i of a geodesic triangle T is equal to the integral of the Gaussian curvature K over T . Figure 5.4 gives an example of such a geodesic triangle. Mathematically, the theorem yields the formula

$$\iint_T K dT = \sum_{i=1}^3 \varphi_i - \pi$$

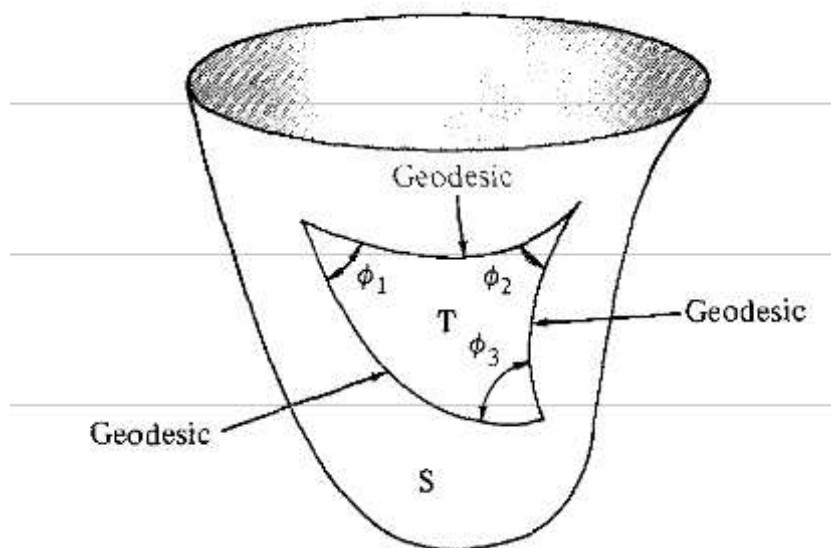


FIGURE 5.4: Link between a curvature and the corresponding normal curvature. Drawn from Do Carmo (1976).

Definition 14. Lines of curvature

A line of curvature is a curve of the surface that, at each point, is tangent to one of the principal directions.

Definition 15. Focal surface

The two focal surfaces F_i are particular surfaces defined for each principal curvature by:

$$F_i(P) = S(P) + \frac{N(P)}{k_i(P)}$$

with $F_i(P)$, the point of the focal surface F_i corresponding to the point P on surface S; $N(P)$, the vector normal to the surface S at point P and k_i one of the principal curvatures. For instance, the maximal focal surface is the surface of centers of circles tangent to the maximal curvature lines. And, a "crest" point of a surface corresponds to a cusp point in the related focal surface.

Theorem 4. The Gaussian curvature may be expressed as a limit:

$$K_p = \lim_{A \rightarrow 0} \frac{A'}{A}$$

This formula translates the fact that the Gaussian curvature at point P may be calculated from the area of a neighborhood of P denoted A and the area of the image of this neighborhood by the Gauss map, A' . Proof can be found in Do Carmo (1976) p.167. Similarly, the mean curvature H can be defined as the following limit:

$$2HN(P) = \lim_{A \rightarrow 0} \frac{\nabla A}{A}$$

Where $N(P)$ is the normal vector in point P; A an infinitesimal area around P and ∇ the gradient with respect to P.

5.3 Curvature estimation on meshes

The purpose of this section is to make a quick presentation of methods of curvature estimation on 3D meshes. These techniques are based on the definitions and theorems presented in the previous section. They make the transition between the differential properties of the 3D regular surface and its discrete approximation, the mesh. There are three main types of curvature estimation techniques. Similarly to the estimation on DTMs, the estimation on triangular meshes may be done through discrete schemes or local fitting of polynomial functions. The third and new approach aims at estimating the tensor of curvature.

One of our final objectives is the tracing of dune crests that are specific lines of curvature. Therefore, the calculation of the principal curvatures alone is not sufficient and the estimation of the principal directions is also required.

5.3.1 Discrete methods

Discrete methods make discrete approximations to the definition of the curvature. They generally approximate the integral of a curvature by a sum of attributes at neighboring vertices, edges or faces. The main advantage of these techniques is their low computational cost. One of their peculiarities is that they often calculate one curvature (Gaussian, mean, principal) so that the methods must be combined to calculate principal curvatures directly or via the formulas relating it to Gaussian and mean curvatures. Furthermore, these techniques do not necessarily calculate the principal curvatures that are essential to us.

For a better understanding of these methods, vocabulary terms related to tessellations must first be explained. The valence of a vertex is the number of edges connecting this vertex with its neighbors. The vertices sharing an edge with a vertex form its 1-ring neighborhood. This notion of order of a neighborhood may be generalized. Thus, the n -ring neighborhood of a vertex is the set of vertices for which the shortest path to the vertex contains n or fewer edges. The dihedral angle of an edge is the angle made by the normal vectors to the faces meeting at the edge.

The most commonly-used discrete techniques for estimating mean and Gaussian curvatures or directly principal curvatures are presented in the next sections.

5.3.1.1 Angular deficit

This technique is inspired by the Gauss-Bonnet theorem for calculating the Gaussian curvature Dyn et al. (2001), Meek & Walton (2000), Stokely & Wu (1992), estimating

$$\mathbf{K}(\mathbf{P}) = \frac{1}{A} (2\pi - \sum_{i \in F} \alpha_i)$$

where A is the area of a bounded part of the surface around point P (generally the 1-ring neighborhood); F the set of faces of the 1-ring neighborhood of P ; α_i the face angle for face F at point P . Modifications and improvements were brought to this method by Cohen-steiner & Morvan (2003).

5.3.1.2 Angle excess

This method, also called turtle-walking Stokely & Wu (1992), is much like the previous one. A closed path L is defined around point P . This path is generally the 1-ring neighborhood. The points composing this path are denoted by V_i . The Gaussian curvature is estimated via the formula:

$$\mathbf{K}(\mathbf{P}) = \frac{1}{A} (2\pi - \sum_{i \in L} \beta_i)$$

With β_i , the angle at neighbor V_i made by the projection of the segments $V_{i-1}V_i$ and V_iV_{i+1} onto the tangent plane at V_i .

5.3.1.3 Spherical image

This method relies on the limit theorem presented in the previous section, linking the area of the surface with the associated area of the unit sphere (Gauss map). In practice, the unit normal vectors to the faces over the 1-ring neighborhood are translated to the estimation point. The ratio between the area of the polygon formed by the normal vectors ends and the 1-ring neighborhood area gives an estimate of the Gaussian curvature Meek & Walton (2000).

5.3.1.4 Integral absolute mean curvature

In Dyn et al. (2001), the integral of the absolute mean curvature is expressed as a linear combination of the dihedral angles of the edges of the 1-ring neighborhood:

$$H = \frac{1}{A} \sum_{e_i \in E} \alpha_i L_i$$

With: E , the set of edges connecting the estimation vertex to its 1-ring neighbors; α_i , the dihedral of the edge e_i ; L_i , the length of edge e_i and A , the area of the associated neighborhood.

5.3.1.5 Mean curvature normal vector/operator

The mean curvature vector can be estimated using a cotangent formula,

$$2H_p N(P) = \frac{1}{2A} \sum_{j=1}^N (\cot \alpha_j + \cot \beta_j) (P_j - P)$$

Where P is the vertex of computation; \cot is the cotangent function; P_j , the j -th 1-ring neighbor of P ; α_j and β_j the angles opposite to the edge PP_j and A an estimate area of the vertex neighborhood. This expression is applied in Desbrun et al. (2002, 2000), Hildebrandt & Polthier (2004). A justification of the formula is provided in the appendix A of Desbrun et al. (2000).

5.3.1.6 Normal curvature vector

This method is not a totally discrete curvature estimation method. In fact, a discrete approximation scheme is used to obtain normal curvature values but a linear system is solved to calculate the principal curvatures and directions. This method is applied in Flynn & Jain (1989), Goldfeather & Interrante (2004). Considering a point P and its close by neighbor P_i , the surface can be locally approximated by its unique osculating circle passing through P and P_i with normal $N(P)$ at P . The normal curvature in the d_i direction (direction of the vector PP_i) is the inverse of the radius of the osculating circle and follows the formula:

$$k_{d_i} = 2 \frac{\langle (P - P_i), N(P) \rangle}{\langle (P - P_i), (P - P_i) \rangle}$$

Thus, for each pair (P, P_i) , the normal curvature in the direction d_i is related to the curvature tensor by:

$$k_{d_i}^N = d_i^T \mathbf{W} d_i$$

This equation may be reformulated as a linear system that, once solved, gives an estimate of the three tensor coefficients. At least three neighbors are required to solve the system.

This method can directly be used to estimate the principal curvatures and directions or simply used to compute the principal directions as in Desbrun et al. (2000).

Discrete methods generally enable computing mean and Gaussian curvatures then yielding to principal curvatures. The methods only focus on the estimation of one curvature at a time which means that they have to be combined to calculate the principal

curvatures. Therefore, there are many papers in the literature explaining these methods, possible modifications and combinations. The last method is only "semi-discrete" and is the only one providing principal directions.

5.3.2 Fitting methods

Contrary to discrete methods, fitting methods approximate the surface at a point by a model function. The main changes from one method to another are principally the type of adjusted model, the surface parametrization and the size of the fitting neighborhood. The coefficients of the analytic function yield the estimation of the principal curvatures and directions.

In this regard, the last presented method in the previous section is also a fitting method where the function model is the osculating circle.

A very similar approach has been presented by Chen & Schmitt (1992). Instead of a pair of vertices, triplets are considered in this technique. There is only one circle passing through all three points. Considering a vertex V and two neighbors, the curvature at V in the direction tangent to the circle is obtained from the circle radius. Meusnier's theorem gives the corresponding normal curvature. Euler's formula links the normal curvatures to the principal curvatures. Thus, using at least three triplets of vertices, the principal curvatures and directions can be calculated. In practice, close neighbors (1-ring neighbors) are preferred so that the circle approximation remains valid and only the triplets close to a normal section are used.

The second main type of model is approximations by a polynomial.

In Douros & Buxton (2002), the authors chose to fit an implicit ($f(x, y, z)$) quadric. Unlike the use of a parametric model, for an implicit formulation, the projection of the vertex onto the model function is not as simple and requires heavy computations. Furthermore, the equations of the principal directions are not given in the paper.

In general, the local surface patch is approximated by a parametric polynomial. The polynomial may be adjusted in a general frame or in a local Darboux frame. The local parametrization is often preferred. Indeed, it simplifies the polynomial expression through suppression of the first-order coefficients. This supposes that the local surface normal is already known. In most cases, the surface normal at a vertex is expressed as a linear combination of the normals of the faces around this vertex Max (1999). Hamann et al. Hamann (1993) locally fit a quadric. In Goldfeather & Interrante (2004), the order of the chosen model is increased to a cubic function. The classic linear system is

also modified in order to account for the surface normals at vertices. Thus, equations linking the model coefficients to the surface normals are added to the linear system.

Cazals & Pouget (2005a) formalizes and generalizes the polynomial approximations to higher order functions. It introduces the notion of osculating jet that is the truncated Taylor expansion of the surface to a given order. Here, the local frame is defined using a PCA of the fitted vertices. The eigenvector corresponding to the smallest eigenvalue gives the z-axis. In this frame, the problem is equivalent to a linear system $MA=Z$ with A the polynomial coefficients vector; M , a Vandermonde matrix $(1 \ x_i \ y_i \ x_i y_i \ \dots)_{i=1\dots N}$; Z the vector containing the third coordinates of the neighborhood points to the estimation point. Cazals & Pouget (2005a) add a preconditioning step aiming at improving the conditioning of matrix M . In fact, the solution might be biased because of the difference between the values of the columns corresponding to the first order coefficients and to high order coefficients. A modification is proposed in Cazals & Pouget (2005a) to solve the problem. Instead of a classic least-squares solution or weighted least squares solution Goldfeather & Interrante (2004), a Singular Value Decomposition (SVD) is selected to solve the problem. In fact, a SVD provides conditioning estimates in order to assess the quality of the adjustment.

Dune datasets and, more generally, bathymetric datasets often require the use of a vertical exaggeration parameter. In fact, the vertical excursion of the seafloor features is rather short compared to its horizontal extent. Hence, the vertical exaggeration is necessary for visualizing the data. According to the exaggeration value, the PCA surface normal definition may no longer be true. Therefore, the method was modified to use normals derived from faces normal vectors.

5.3.3 Tensor estimation methods

These methods are also discrete but slightly differ from the above-mentioned discrete approximations. Instead of directly estimating the curvature values, the objective is to approximate the curvature tensor but still using discrete approximations schemes.

These techniques tend to calculate the curvature tensor for each face or edge of the mesh and then obtain the values at vertices by averaging face/edge curvature tensors.

For instance, in Taubin (1995), the curvature tensor is approximated by the formula:

$$M_{v_i} = \sum_{v_j \in V^i} w_{ij} K_{ij} T_{ij} T_{ij}^t$$

With v_i : the vertex of interest; v_j : the $j - th$ vertex in the 1-ring neighborhood V^i of vertex v_i ; T_{ij} : the unit direction vector of the edge $v_i v_j$; w_{ij} , a chosen weight and K_{ij} : the normal curvature in the T_{ij} direction.

This algorithm approximates the curvature tensor based on an estimation of the normal curvatures in the directions of the 1-ring edges. The normal curvatures K_{ij} are obtained via the osculating circle discrete scheme.

In Rusinkiewicz (2004), the author chose a *per face* approximation method. Consequently, it makes the assumption that the tensor is constant on each face of the mesh.

5.4 Comparison of curvature estimation

A wide range of curvature estimation methods on meshes is available. This is a topic that has been intensively searched as it plays a role in many other applications. Other methods, similar to (or inspired from) the above methods, exist or could be imagined Abdelmalek (1990), Petitjean (2002). Yet, the above sample is a good overview of the existing possibilities. And, it is sufficient to make comparisons and conclusions on the type of techniques that is the most suited for our data.

The methods that are compared in this section are a sample of all presented methods:

- Discrete approximations:
 - Meek & Walton (2000);
 - Desbrun et al. (2000);
 - Dyn et al. (2001);
- Fitting approximations:
 - Hamann (1993);
 - Goldfeather & Interrante (2004);
 - Cazals & Pouget (2005a);
 - Modified Cazals;
 - Chen & Schmitt (1992);
- Curvature tensor approximations:
 - Taubin (1995);
 - Rusinkiewicz (2004).

Meek's and Dyn's algorithms only estimate principal curvatures, thus, if these discrete methods proved efficient for highlighting dune crests, the principal directions would be calculated from the osculating circles method (Desbrun et al., 2000).

Several papers deal with the topic of comparison of curvature estimation techniques Csákány & Wallace (2000), Goldfeather & Interrante (2004), McIvor & Valkenburg (1997).

Gatzke & Grimm (2006) is a reference paper as it thoroughly summarizes the characteristics of these methods and when one should be chosen over another according to the mesh properties and the objectives. In order to assess the performance of the estimation methods, a test procedure is presented in the paper. To make these comparisons, 2D triangulations were generated and then elevated to the surface to produce a 3D mesh. A variety of surfaces were considered among which were a sphere, a monkey saddle, a cubic polynomial, a trigonometric function and an exponential function. These surfaces have known mathematical expressions so that the expected "ground truth" values of the curvatures are known at each vertex. Thus, the calculation error may be estimated and error statistics computed for each surface.

The 2D triangulations are also modified to analyze the impact of the noise (perturbations in the normal direction at each vertex), the mesh regularity (valence and face shape) and the mesh resolution (size of the faces).

The impacts of these parameters were evaluated separately for each type of curvature calculation method. The accuracy of each method depends on its capacity to give the right estimation when the length of the edges tends towards zero. The principal conclusions of the tests are:

- Fitting methods are not sensitive to the valence as long as the fitting patch contains enough neighbors. Moreover, the mesh regularity has no visible impact on the estimated curvatures.
- Fitting methods converge faster towards the true value for small ring neighborhood. This may be explained by the fact that a function better fits the surface at a vertex when the neighborhood is not too large. Note that the cubic method does not necessarily converge if the true normal vectors are replaced by estimated vectors.
- Quadric and conic fitting methods are very sensitive to surface noise when the adjustment is made on a 1-ring neighborhood. In these conditions, the cubic approximation performs best.

- Fitting methods are equivalent for 2-ring neighborhood and larger. The calculation error is not much reduced using the larger neighborhood, but it slows down the calculations. Therefore, the 2-ring neighborhood appears as a good tradeoff between accuracy, robustness to noise and computational time.
- Discrete methods are dependent on the mesh regularity (valence and shape of the faces). This comes from the fact that most of these methods approximate the curvature by an integral curvature. In other words, if the curvature is constant over the integration area, the calculation is satisfactory. If this assumption is not valid, an exact discrete method should be preferred.
- Discrete methods are very sensitive to noise and the relative position of vertices. These estimations are based on face angles, normals and dihedral angles so that any changing of vertex position modifies the calculated curvature.
- Discrete methods are fast.
- The comments made on discrete methods are also true for tensor estimation methods.

The comparisons are made on analytic surfaces. In other words, the ground truth is known so that a statistical analysis can be conducted. In our case, the surface is totally unknown. The surface resolution is fixed and cannot be changed to estimate the convergence of the estimation algorithms. The only possible comparisons are visual. It is important to bear in mind that the objective is to extract crest lines. As the readers will see in the next chapter, the crests are characterized by extreme values of curvature and the principal directions must indicate the directions tangent and perpendicular to the crest lines. Therefore, the visual analysis shall address both aspects (curvatures and directions) equally. In addition, the estimated curvature values need only be accurate in relative terms and not in absolute terms. Indeed, the crest extraction requires determining where the curvature extrema are regardless of the curvature values. Only the estimations of the minimum curvature and its direction are analyzed since, we are interested in crests and not valleys.

5.4.1 Comparisons on benchmark zone 2

Zone 2 is appropriate to make the first comparisons since it is a simple case with a rather high isolated dune with a straight "sharp" crest.

Figure 5.5 shows the minimum curvature maps obtained with the Desbrun's (subfigure (A)) (Desbrun et al., 2000), Meek's (subfigure (C)) (Meek & Walton, 2000) and Dyn's (subfigure (D))(Dyn et al., 2001) methods. Subfigure (B) depicts the field of minimum directions from Desbrun's method. The discrete methods base the curvature calculation on the 1-ring neighborhood that is not symmetric and has a reduced size at the edges of the zone. Therefore, extreme spurious values (below -1 m^{-1}) are obtained there. Crests are visible with negative curvature values, but the curvature values are not constant along the crests, although, the crest seems globally similar. The Dyn's method is particularly affected by localized extreme values. It can be seen with a more pronounced sandpaper effect in the background compared to the other two methods. Dyn's method is more sensitive to the surface roughness, as also confirmed by the fact that artifacts are seen in the minimum curvature map: the survey lines can be guessed from the maps. Surface roughness and artifacts are also presented in the two other methods' maps but are less visible. All the observations show that the construction of the crest lines would be challenging due to some of these unwanted minima of minimum curvature. The minimum direction is supposed to be perpendicular to the crest lines at crest vertices. Desbrun's direction estimation method relies on a finite number of directions. If the number of directions is high and the 1-ring neighbors are homogeneously distributed around the vertex of interest, then the estimation is reliable. In the case of subfigure (B), the 1-ring neighborhood contains at best six vertices and only three directions. Therefore, the estimated directions often point northward and have difficulties in depicting the changes of direction of the crest.

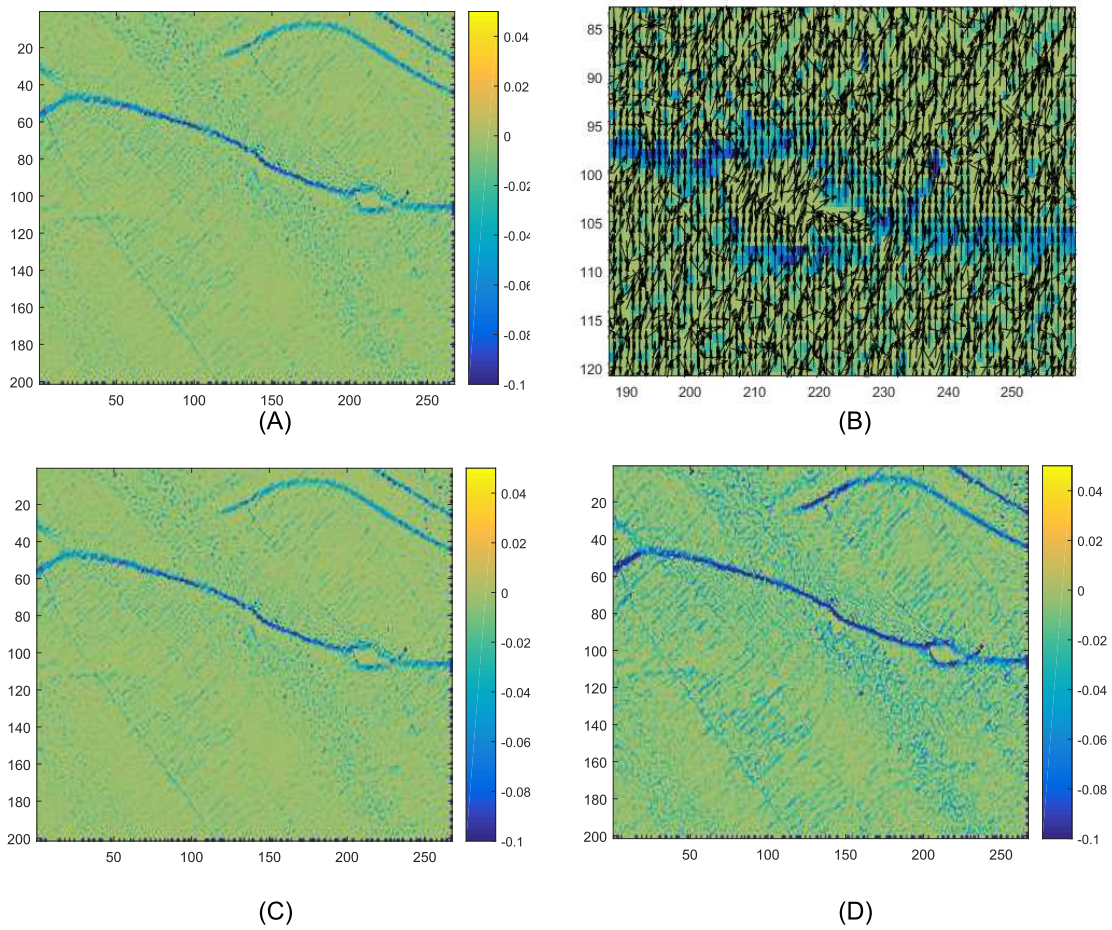


FIGURE 5.5: Discrete methods applied to benchmark zone 2.

Figure 5.6 illustrates the estimations of the method that is halfway between the discrete and fitting methods: Chen & Schmitt (1992) algorithm. The dynamics of the curvature map is preserved (range: $[-0.1; 0.05]$) and the extremely low curvature values disappeared. However, the directions are still mainly northward due to the limited number of directions of the fitting neighborhood.

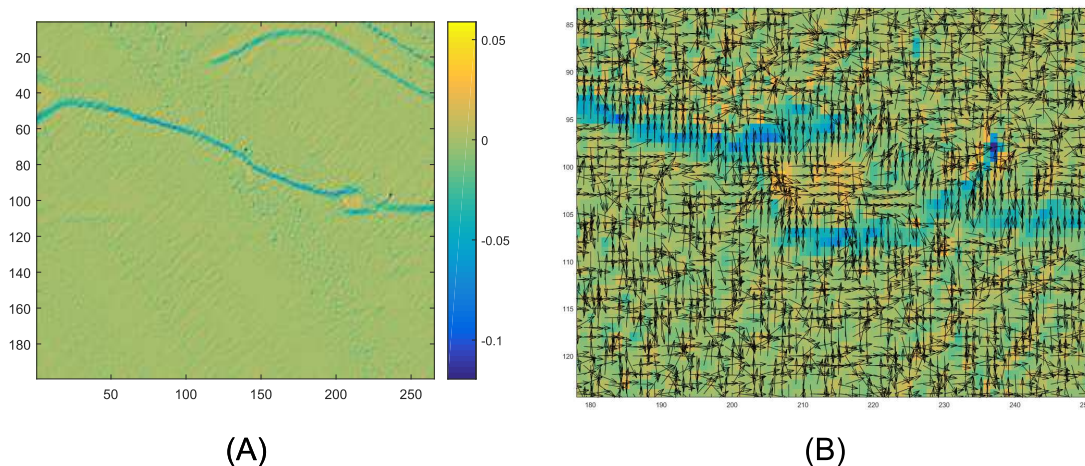


FIGURE 5.6: Minimum curvature and associated direction by Chen's algorithm.

Figure 5.7 reveals how the neighborhood size impacts the results of Hamann (1993) fitting algorithm (1-ring: subfigures (A), (B); 2-ring: subfigures (C), (D); 3-ring: subfigures (E), (F)). This method has been chosen as it was one of the first fitting methods presented in the literature and that it uses a quadric model, which is the minimum polynomial order required to estimate the principal curvatures.

The results of subfigures (A) and (B) may be compared to previous results as the estimation neighborhood is the same (1-ring). Observe that the curvature range is unchanged but the curvature map is much like Chen's (Figure 5.6). That is to say, the fitting approach is less sensitive to the surface noise than discrete schemes. But, unlike Chen's algorithm, the directions change along the crest. The directions seem correct where the crest is straight, but the curvature directions no longer match crest directions where the crest has a "0" shape (right part of the crest). There, the direction estimates are less stable.

The increase of the neighborhood size causes a loss of information in the curvature map. In fact, the curvature range also decreases. However, the surface noise and roughness are smoothed out. And, the principal direction vectorfield becomes more stable around the whole crest. It can be noticed that the use of a 3-ring neighborhood over a 2-ring neighborhood does not bring a significant improvement while the running time is increased.

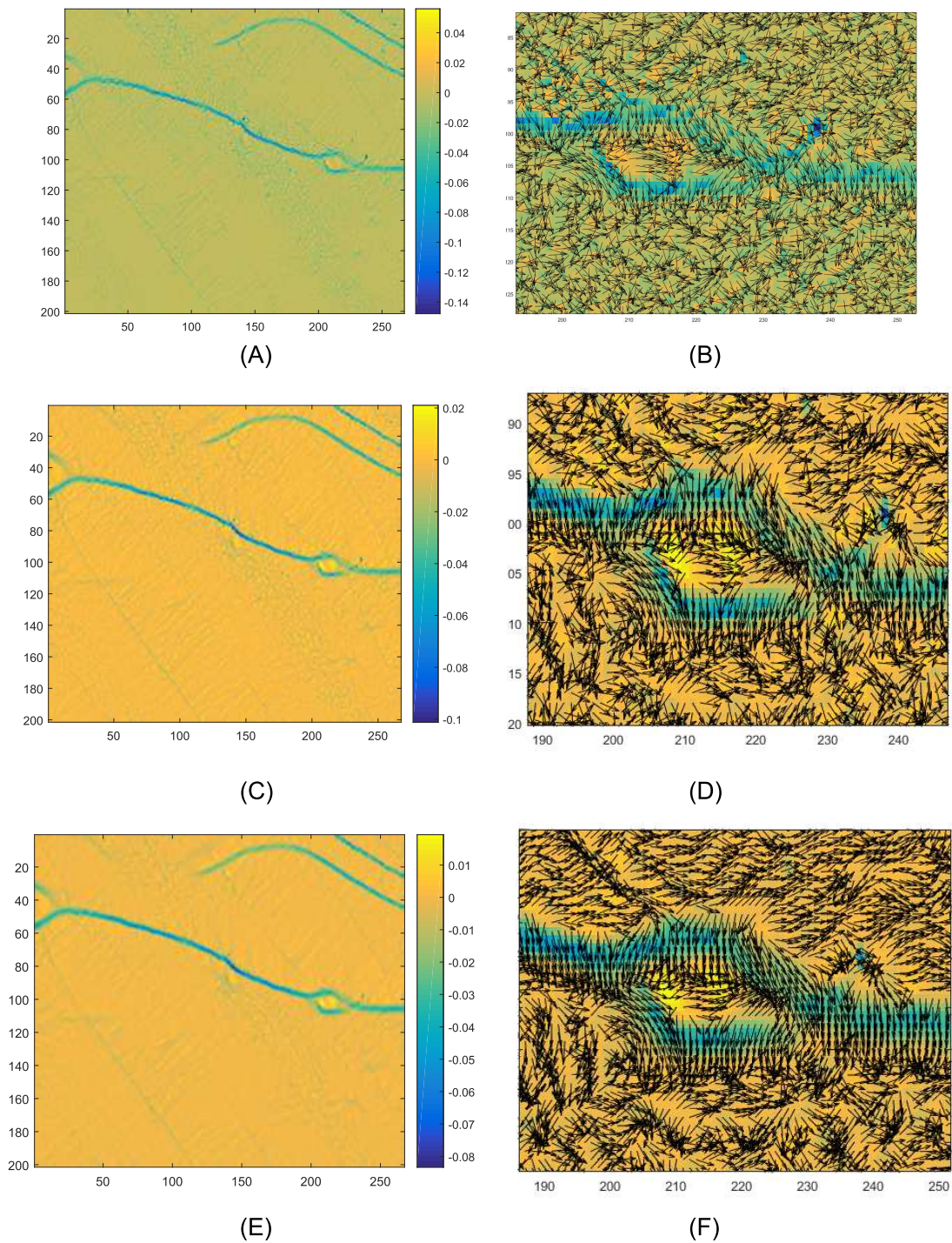


FIGURE 5.7: Influence of the neighborhood size on the Hamann curvature and direction.

The results of curvature tensor techniques are presented in Figure 5.8. These algorithms are impacted by the surface roughness like discrete methods. Yet, the curvature range is not as wide as fewer extreme values are obtained, especially with Rusinkiewicz's method (Rusinkiewicz, 2004). Furthermore, the directions are better estimated in the

sense that the curvature directions indicate correctly the direction perpendicular to the crest. Taubin's directions seem slightly better. Although the results are more satisfying than with discrete methods, it is not as good as fitting method. This is due to the fact that they remain specific discrete methods with more than a sum of surface normals and angles on the 1-ring neighborhood. Therefore, they are more robust to surface roughness.

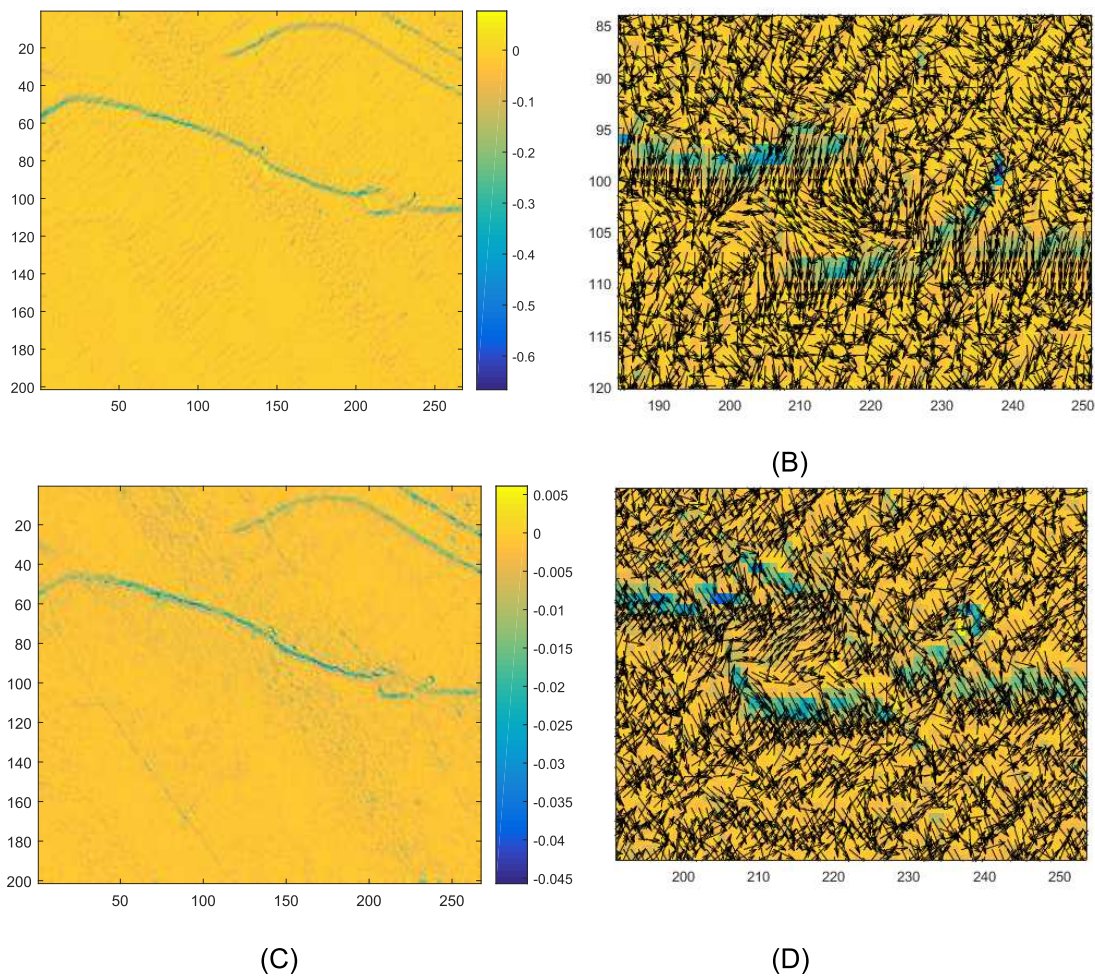


FIGURE 5.8: Principal curvatures and directions in benchmark zone 2 with discrete tensor estimation methods. Taubin: (A), (B); Rusinkiewicz: (C),(D).

Discrete methods are disturbed by the presence of artifacts in the surface and by the surface roughness. Thus, a filtering or smoothing step is generally added, when a discrete technique is selected, to reduce these problems. But, these methods remain more efficient in terms of computational cost. Fitting algorithms already integrate a sort of smoothing. In this regard, they are the most appropriate for the analysis of dune datasets. The smoothing effect is controlled by the neighborhood size. A too large neighborhood also smooths out the crests and affects the computational time.

The curvature estimations shall remain local, at the dune scale. In order to detect the vertices close to dune crests more accurately, the study neighborhood must only encompass information about the shape of the crest.

5.4.2 Comparisons on benchmark zone 7

The small dunes of benchmark zone 7 support analyzing the capacity of the different fitting methods to recover dune crests with a common 3-ring neighborhood. These methods essentially differ by the degree of the fitted polynomial function.

Figures 5.9 and 5.10 respectively show the estimation results for Hamann (1993), Goldfeather & Interrante (2004), Cazals & Pouget (2005a) and modified Cazals's algorithms. In Figure 5.9, it can be noticed that both curvatures and directions are little influenced by the degree of the polynomial. Indeed, the results are globally similar when one uses a quadric model and the other a cubic one. Hence, for the purpose of curvature estimation, a quadric function is recommended as fewer coefficients have to be determined and thus the linear system redundancy is improved.

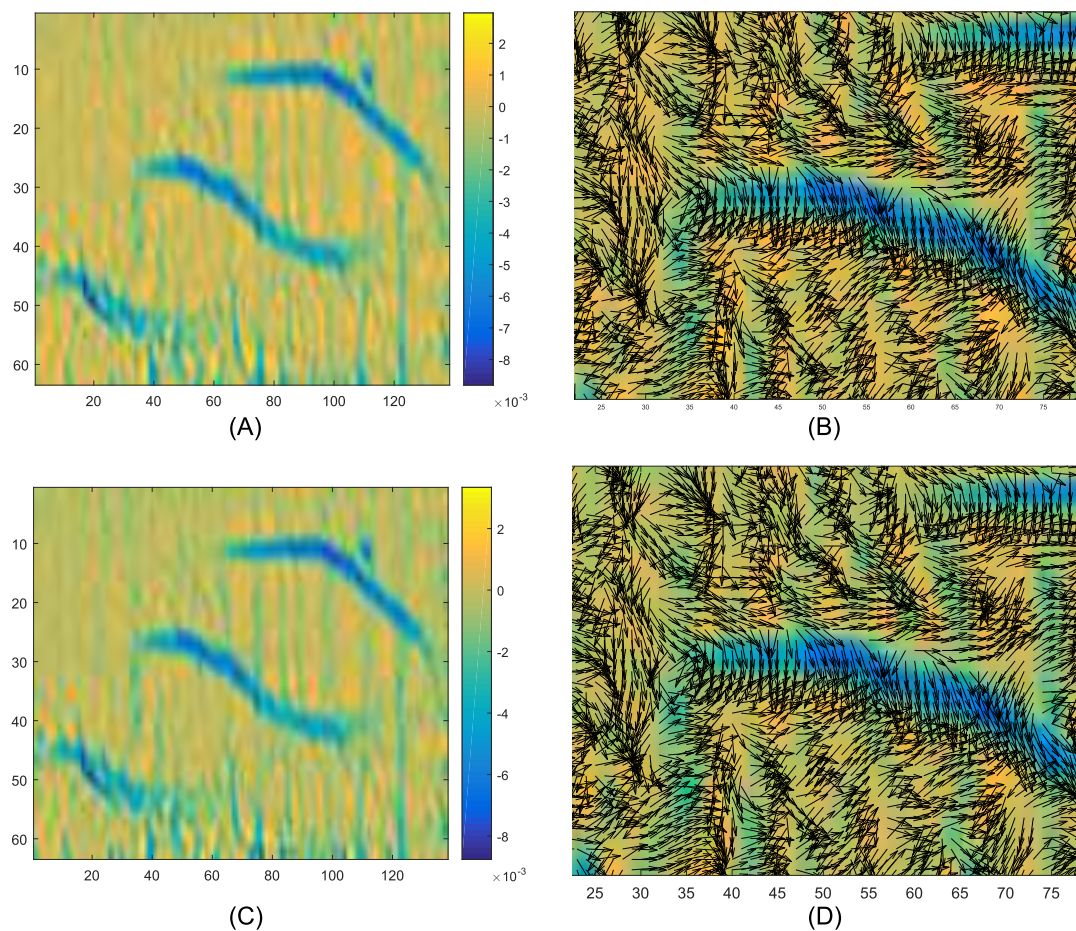


FIGURE 5.9: Principal curvatures and directions of benchmark zone 7 with fitting methods. Hamann: (A),(B); Goldfeather:(C),(D).

Figure 5.10 shows that the modification of the surface normal used in Cazals method does not dramatically change the results. The main difference is that, with the modified version, there are fewer direction reversals at the crests. These reversals are due to the Cazals's adjustment frame that is based on the PCA eigenvectors and is therefore less stable. Since the modification is useful for vertically exaggerated meshes and gives equivalent results otherwise, this new version is interesting for surfaces on which the assumption of good sampling is not verified.

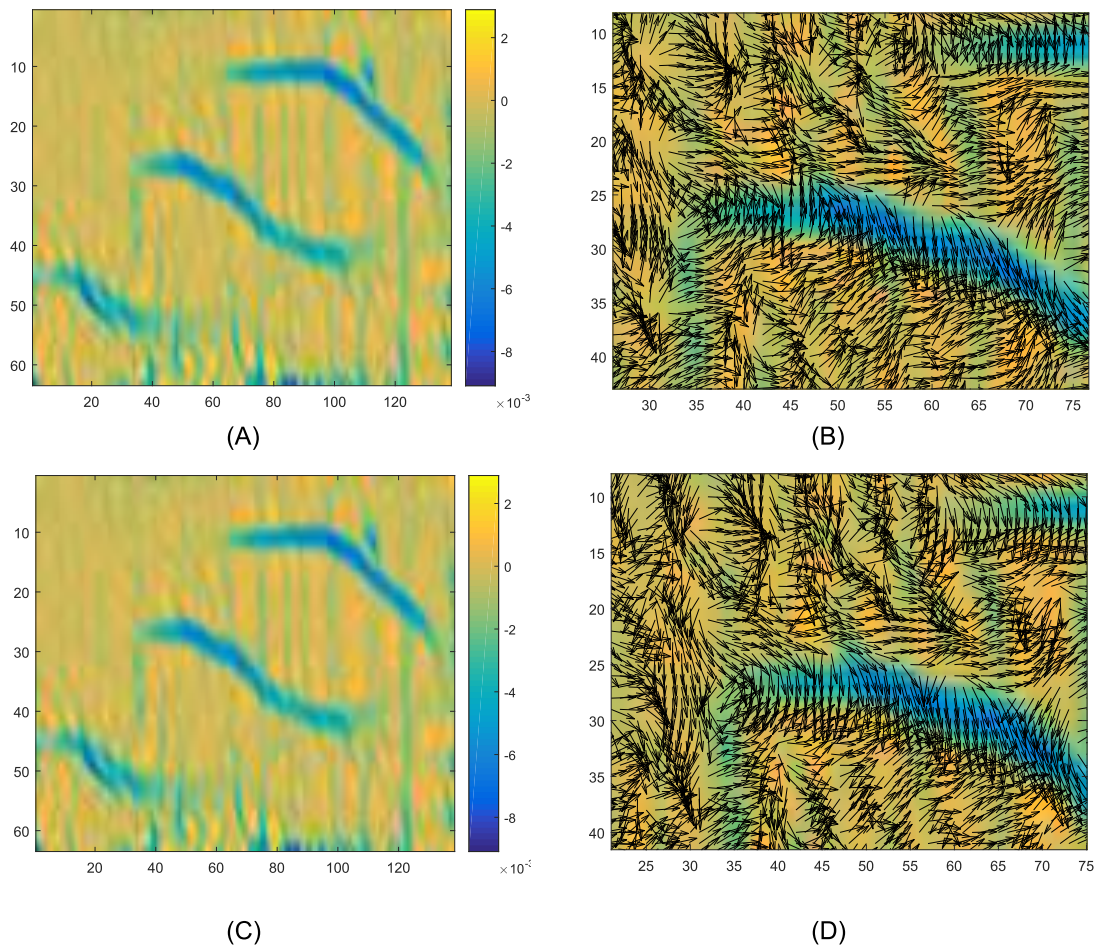


FIGURE 5.10: Principal curvatures and directions of benchmark zone 7 with fitting methods. Cazals: (A), (B); modified Cazals:(C),(D).

These comparisons, although purely visual, were necessary to understand the behavior of the estimation techniques on bathymetric data. The objective is to estimate the curvature magnitude and the associated direction for the purpose of dune crests tracing. The observations confirm the tests made in Gatzke & Grimm (2006). That is to say, discrete methods are more suited on smooth, dense meshes and, thus, are not appropriate to our case without a smoothing processing step. The neighborhood size must be adjusted to smooth surface roughness without losing information at crests. In addition, a second-order approximation of the surface is sufficient to estimate the principal curvatures and directions.

5.5 Conclusions

To summarize, three principal categories of curvature estimation methods may be distinguished: discrete, fitting and tensor based algorithms. The last type is a particular type of discrete approximation. The results of tests conducted in Gatzke & Grimm (2006) are confirmed by our tests on dune datasets. Discrete algorithms are sensitive to noise and the triangulation regularity, but they have the advantage of being fast to compute. Fitting techniques are robust to noise, but with a higher computational cost. It is preferable to keep the fitted polynomial degree low as much as possible. In fact, increasing the order does not necessarily bring additional information, as high order coefficients capture mostly surface noise. Furthermore, more coefficients to estimate is synonymous with an increase of the computational time. The neighborhood size modifies the resulting values. If it is set too small, the estimated values quantify the noise and, if it is too large, valuable information of the terrain morphology is lost. A tradeoff needs to be found.

In the end, the choice between the types of estimation methods depends on the application. A balance between noise robustness and running time is required to lead a decision in accordance with data and application requirements. Regarding the data properties and the application, the estimation of principal curvatures based on a local fitting approximation is more judicious and relevant in the context of the thesis. Cazals's method has the advantage of being general in the sense that the degree of the osculating jet may be changed according to the order of the surface properties required by a later application. The next chapter will explain how the estimation of these local differential quantities can be used for extracting surface features: crest lines.

Chapter 6

Crest line extraction

Contents

6.1	Introduction	126
6.2	Surface characteristic lines	126
6.3	Crest line extraction methods	128
6.4	A new quantitative comparison procedure	134
6.4.1	Comparisons on benchmark zone 1	135
6.4.2	Comparisons on benchmark zone 2	143
6.4.3	Analysis of the dune crest descriptors	144
6.5	Crests and mesh resolution	154
6.6	Conclusion	156

6.1 Introduction

This chapter is devoted to the extraction of crest lines from 3D tessellations and, more specifically, to their adaptation for the tracing of dune crests. Crest lines are useful for numerous applications such as visual enhancement (Interrante et al., 1995) and rendering (DeCarlo et al., 2003, Lesage & Visvalingam, 2002), shape matching, object registration Pennec et al. (2000), Thirion (1996), remeshing, face recognition, segmentation (Guo et al., 2005, Lévy et al., 2002, Stylianou & Farin, 2004), quality mesh construction (Kalogerakis et al., 2009), *etc.* Therefore, many algorithms have been developed to locate these remarkable feature lines. Crest lines are one type of specific lines of curvature that are mathematically defined using the notions of differential geometry explained in the previous chapter. The extraction algorithms follow more or less thoroughly their theoretical definition. Such algorithms have already been applied to terrain datasets (Kudelski, 2011, Little & Shi, 2014) or even dunes (Debese et al., 2016).

When the crest lines of the surface are extracted, the issue that arises is that dune crests are often a subset of the detected lines. The set of interesting lines has to be filtered so that only dune crests remain in the final set. The feasibility of this filtering by thresholding existing and new quantitative metrics describing the crests is examined and a promising solution is presented.

6.2 Surface characteristic lines

If Chapters 4 and 5 showed that dune crests are characterized by high values of minimal curvature, the use of thresholds to define these special features of the seafloor is limited. No clear definition of these lines has yet been provided in this thesis.

Eight types of characteristic surface lines of curvature can be distinguished. These eight types of lines of curvature are generally called ridge lines or simply ridges¹. Crest lines are one of them. These ridges are lines of extremal curvature. In fact, they correspond to extrema (either maxima or minima) of one type of principal curvatures in the associated principal direction. Two main classes are thus defined: maximum and minimum ridges also respectively called blue and red ridges in Cazals et al. (2008, 2006).

1. For more information about ridge types, their classifications and applications, the reader is referred to (W. Hallinan et al., 1999).

Mathematically, this means that, at any point of a characteristic line, either the minimal extremality e_{min} or the maximal extremality e_{max} is null. And, the sign of the second-order derivative of the principal curvature determines whether it is an elliptic or hyperbolic line of curvature. Crest lines are defined as elliptic ridges with a maximum of $\max(|k_{min}|, |k_{max}|)$.

Figure 6.1 illustrates the classification of ridges with the notations of Cazals et al. (2008, 2006). It supposes that $k_1 > k_2$. b_0, b_3, P_1 and P_2 are notations defined following The Taylor expansion of the surface in the local Monge coordinate system is:

$$z(x, y) = \frac{1}{2}(k_1^2x^2 + k_2^2y^2) + \frac{1}{6}(b_0x^3 + 3b_1x^2y + 3b_2xy^2 + b_3y^3) + \frac{1}{24}(c_0x^4 + 4c_1x^3y + 6c_2x^2y^2 + 4c_3xy^3 + c_4y^4) + h.o.t$$

h.o.t is an abbreviation for higher order terms.

The Taylor expansions of k_1 and k_2 along their respective curvature lines are:

$$k_1(x) = k_1 + b_0x + \frac{P_1}{2(k_1 - k_2)}x^2 + h.o.t, \text{ with } P_1 = 3b_1^2 + (k_1 - k_2)(c_0 - 3k_1^3).$$

$$k_2(y) = k_2 + b_3y + \frac{P_2}{2(k_2 - k_1)}y^2 + h.o.t, \text{ with } P_2 = 3b_2^2 + (k_2 - k_1)(c_4 - 3k_2^3).$$

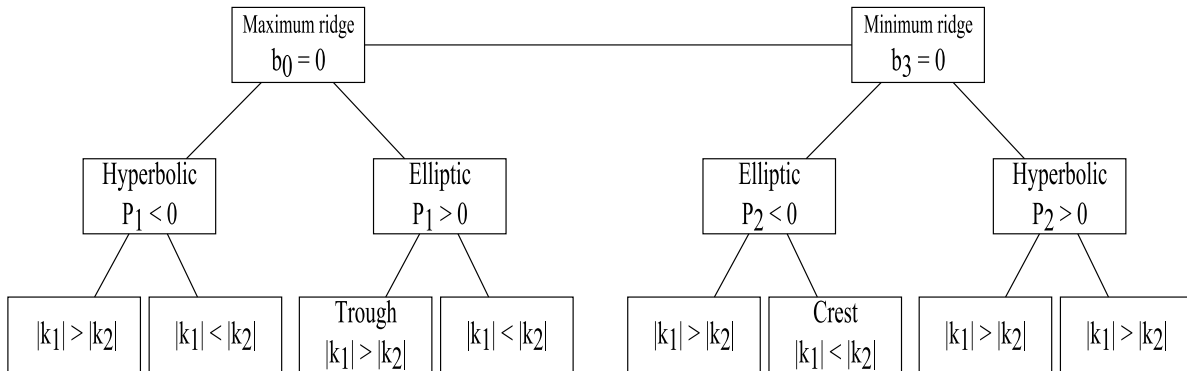


FIGURE 6.1: Classification of ridge lines.

Note that the ridge classification depends on the sign of metrics that are calculated in a local coordinate system. If the system is reversed, k_1 and k_2 are switched and a minimum ridge point becomes a maximum point. In order to reconstruct ridge lines, it is essential that these local coordinate systems have a consistent orientation.

In this thesis, the surface normals are systematically pointing upward so that the crest lines we are interested in satisfy the following conditions:

$$e_{min} = \nabla k_{min} \cdot t_{min} = 0$$

$$P_{min} = \nabla e_{min} \cdot t_{min} > 0$$

$$|k_{min}| > |k_{max}|$$

The construction of ridges is also made difficult by the presence of umbilical points. Procedures to deal with the local orientation of the principal directions and identification of ridges and umbilics types near umbilic are explained in Cazals et al. (2006). Although dune crests normally meet the above specifications, it might not be the only features to do so. Consequently, a difficulty in sorting between dunes and these features (rocks, artifacts, *etc.*) may occur as seen in the results of the first region growing algorithm.

6.3 Crest line extraction methods

If crest lines are theoretically defined characteristic lines, all crest tracing algorithms do not intend to strictly apply the definition. That is to say, the mathematical criteria are verified with several degrees of compliance. Indeed, checking all the conditions might be costly and avoidable according to the application.

Crest extraction is often tightly linked to curvature estimation but not always. Thus curvature estimation is generally a full part of crest extraction algorithms. But, this is not the part we want to study: the focus here is on crest line reconstruction, as the issue of curvature estimation was already discussed in the previous chapter.

An example of a feature extraction method not based on curvatures is Weber's method (Weber et al., 2010). It was developed to identify sharp features in point clouds but could also be applied to vertices of a triangle mesh. Here, the feature detection does not even require the estimation of curvatures. For each point, the angle between the normals of planes defined using pairs of its k -closest neighbors is analyzed. If the standard deviation of this angle is less than 13° ², the point is in a flat area of the surface. Otherwise, a clustering algorithm further analyses the normals to determine if the point stands by a sharp feature.

2. This threshold value was empirically determined and is valid on a particular dataset for a specific application

Metrics other than the curvatures may also be found to quantify the surface variation and detect features. For instance, the surface variation metric is introduced in Pauly et al. (2003). It is based on the eigenvalues of the surface covariance matrix computed for a range of neighborhood sizes. The persistence of a feature is estimated as the number of times the surface variation exceeds a threshold across the scales.

In Vidal et al. (2011), an original approach is explained. First, the objective is to detect edges near crest lines and not the vertices. The classification of the mesh edges in normal or crest edges is achieved via a supervised learning method: Support Vector Machines. A feature vector is estimated for each edge (normals, dihedral angles and other parameters estimated at a few scales). Although interesting, this technique relies on several heuristics and do not use the mathematical properties of crest ridges.

Dihedral angles and extended descriptors are used in Hubeli & Gross (2001) to assign a weight to the mesh edges. The weight is proportional to the probability that the edge belongs to a mesh feature.

This type of algorithms does not require the expensive calculations of the curvatures and their derivatives, which makes them faster and perfectly suited for applications where no precise reconstruction of crest lines is needed. This is generally the case for visualization purposes such as visual enhancement or non-photorealistic rendering. But, it also necessitates the definitions of several empirical parameters making the methods highly heuristic. Since crests contain precious information about the dune geometry and, therefore, dunetype, the estimation of curvature seems unavoidable for our purpose.

Although the previous algorithms replace curvature by other metrics to quantify the surface variations, most algorithms are based on the estimation of the curvature. These algorithms comply with the mathematical definition of crest lines to a certain extent.

To the best of our knowledge, the only algorithm of the literature tackling the problem of dune crests and valley extraction is Debese et al. (2016). Extraction is achieved using curvature values after an anisotropic filtering. The filtering step generates a smooth (free of ripples) surface for simpler extraction of lines. The objectives are to provide an automatic method that may provide an enhanced visualization of dunefields by displaying interactively modifiable crests and toes of dunes on top of the bathymetry. The paper shows that the valley lines do not match entirely the dune toes, which validates the conclusions that a disparity line approach is effectively inappropriate for dune extraction. The use of region growing or watershed approaches are also mentioned and briefly tested.

The method proposed in Rossl et al. (2000) extracts crest regions of the mesh using thresholds of principal curvatures primarily filtered by a median filter. Morphologic operators are applied to discard spurious crest areas and merge others. A skeletonization step enables reconstruction of crest lines. This method is similar to the algorithm explained in Section 4.5 and, therefore, have the same limitations.

Another original way to extract crest lines is to focus on the shape of the focal surfaces in crest areas. Watanabe's algorithm (Watanabe & Belyaev, 2001) aims to detect crest lines based on the properties of the focal surfaces. The detection is done by computing the ratio between the area of a surface face and the corresponding face of the focal surface. Crest areas are depicted by high ratio values. Erroneous face detections corresponding to noise in flat areas are suppressed with a threshold on the curvature. A skeletonization procedure gives the crest lines.

A procedure for the extraction of remarkable lines of a surface based on a sharpness indicator is examined in Di Angelo & Di Stefano (2010). The calculation of the indicator is based on the principal curvatures and the surface normals, and can be computed for a range of neighborhood size. The threshold value is determined by comparing thresholding procedures found in the literature and picking the best.

Stylianou & Farin (2004) proposed an automatic method for extracting crests for medical applications (brain imagery analysis). Hamann's method is applied to compute the principal curvatures and directions. In practice, the curvature value is compared to the 1-ring neighborhood to determine whether a vertex is a minimum of curvature in the principal direction. Here, crest lines are obtained by region growth around the initial crest vertices followed by a skeletonization to recover lines. This procedure avoids having split lines due to the mesh noise.

In Monga et al. (1992), the crest lines are identified as the zero-crossings of the minimum curvature derivative where the curvature is relatively negative.

Similarly, Zheng's method (Zheng et al., 2011) checks the sign of the curvature derivative to trace crest lines. Three original discrete schemes are analyzed to estimate the gradient of the minimum curvature. False detections are found in flat areas so a statistical curvature threshold is set to remedy the issue. Crests are assumed to be in the 5 to 10 percent most convex parts of the surface.

In Kim & Kim (2005), the presence of a crest line is indicated by the extremality sign changes on the mesh edges. For each edge having higher curvature values, the end vertex with the minimal curvature is a ridge vertex. The final stage aims at connecting

these ridge vertices in order to get ridge lines, which is done by exploring the 1-ring neighborhoods of the crest vertices and connecting them. This method respects all of the definition criteria except for the sign of the surface fourth-order derivative. Nevertheless, one of its limitations, like the afore-mentioned techniques, is the fact that the crest lines pass through the mesh vertices. This means that the quality of the tracing depends on the triangulated surface representation. Since crest reconstruction is a key step towards dune extraction. Moreover, parameters such as its length must be accurately estimated. And, the fact that this method only provides crests following the mesh edges is problematic.

Other algorithms allow a more flexible reconstruction of the crests, for example with Hildebrandt's algorithm (Hildebrandt et al., 2005). This method only requires knowledge of k_{min} at each vertex of the mesh. To evaluate e_{min} at a vertex V , e_{min} is calculated for each face containing V . Since e_{min} is supposed constant on a face, an average of the e_{min} values on the face containing vertex V gives an estimate of e_{min} at V . On edges where there is a e_{min} sign change, a possible crest segment is drawn. It corresponds to the segment of zero level of e_{min} . Finally, the following conditions are tested on face T to validate the previously detected segment:

$$|\sum_{v_i \in T} k_{min}(v_i)| > |\sum_{v_i \in T} k_{max}(v_i)|$$

$$\nabla e_{min} \cdot \sum_{v_i \in T} t_{min}(v_i) > 0$$

Unlike Hildebrandt's algorithm, Ohtake's requires input of e_{min} values, but avoids making the assumption that the extremality is constant on a face. This time the tests below are made on each edge $[v_1 v_2]$:

$$k_{min}(v_i) < -|k_{max}(v_i)| \text{ with } i=1,2 \text{ and } e_{min}(v_1)e_{min}(v_2) < 0$$

$$e_{min}(v_i) * [(v_{3-i} - v_i) \cdot t_{min}] < 0 \text{ with } i=1,2.$$

If the edge satisfies the above conditions, a crest point is defined where e_{min} is equal to zero. e_{min} is assessed to change linearly along the edge so that the crest point location can be estimated. When two edges of a face are crossed by a crest, a segment is drawn between the corresponding crest points. The idea behind the last condition is to check whether the curvature value decreases when moving towards the crest point.

Yoshizawa et al. (2008) noticed that the previous algorithm sometimes creates small fragmented crests. A small modification is made to avoid the overfragmentation of the crest lines by connecting close crest lines with a criterion on the angles at the end-points.

In Kudelski (2011), a similar reconnecting approach is explained. The extraction method is applied to meshes of rocky outcrops in order to automatically trace the faults and the boundaries between sediment layers.

Cazals's work is not limited to the estimation of local differential quantities. He also proposed two algorithms for extracting surface ridge lines³ (Cazals & Pouget, 2005b). The first is very similar to Ohtake's as it is based on the third order differential properties of the surface. The second alternative uses P_{min} values (4th order quantities). We will respectively call them Cazals1 and Cazals2 algorithms in the remainder of the document.

The only distinction between Ohtake's and Cazals1 algorithms is on the last condition. Instead of making a test on the edges, a test on the face is proposed. On a triangle, if moving towards the crest segment in the t_{min} direction k_{min} increases for at least two vertices of the face, the tested segment is effectively a minimum of k_{min} . The second alternative validates all the criteria of the theoretical definition of crest lines by checking the sign of P_{min} at the ends of the crest segment $[r_1r_2]$:

$$P_{min}(r_i) > 0 \text{ with } i=1,2$$

An osculating jet must include fourth-order coefficients in order to calculate the values of P_1 for the last algorithm.

Figure 6.3 depicts the bathymetry along the profile defined on zone R2 (see Figure 6.2). These figures explain how the vertical exaggeration coefficient used to visualize bathymetric data actually skews our perception of the seafloor. Without exaggeration, the dunes are seen as small depth variations. The aim of this chapter is to determine how to accurately locate these variations. As dunes are, in fact, low amplitude variations of the seafloor, their detection using techniques based on the estimation of higher order derivatives of the surface is difficult.

3. Remark: the work of Pouget and Cazals is complete as it addresses all the aspects from the estimation of local differential quantities to the extraction of characteristic lines. All the information about the developed algorithms and the encountered issues are provided in Pouget's PhD thesis (Pouget, 2005).

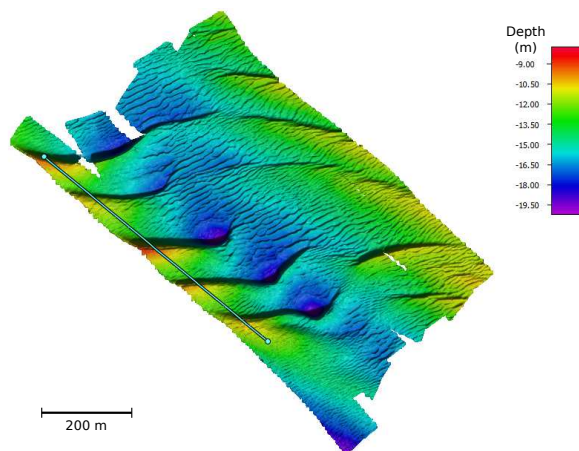


FIGURE 6.2: Bathymetry of Belgian zone R2.

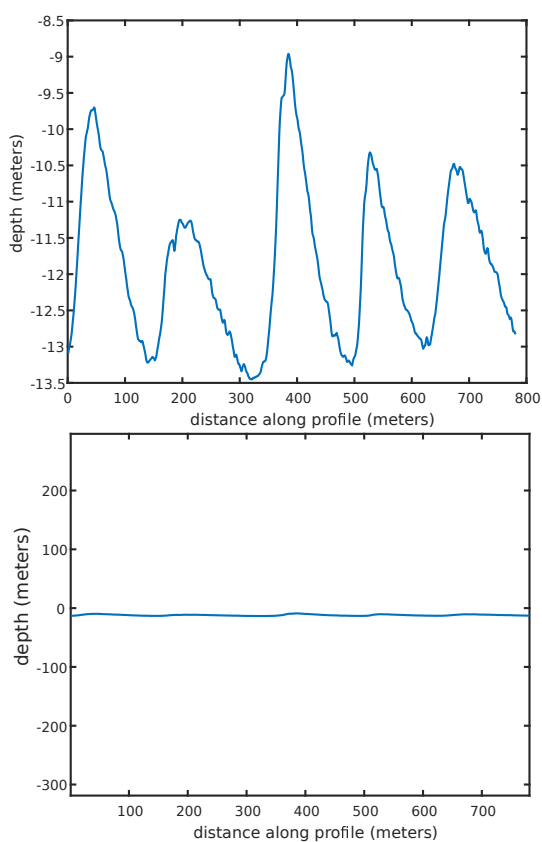


FIGURE 6.3: Influence of the vertical exaggeration on our perception of dunes.

The extraction algorithms make sign tests on low magnitude coefficients (derivatives of the height). Their estimations should be accurate to prevent for extraction issues.

For Cazals1 or Ohtake's algorithms, the adjustment of a cubic polynomial is sufficient. A quadric function model is appropriate for Hildebrandt's method.

Hildebrandt's, Ohtake's and Cazals's algorithms provide crest lines independent of the mesh structure and following the mathematical definitions. The other methods output lines running through the mesh vertices (Stylianou & Farin, 2004) or even simply detect the faces crossed by crest lines (Watanabe & Belyaev, 2001) making them less appropriate for the detection of crests. An accurate extraction of the crests is essential as many dune descriptors depend on the crest (e.g., height, length, asymmetry, etc.). Consequently, the first four algorithms might help us achieving our objective and will be compared in the next section.

6.4 A new quantitative comparison procedure

The goal of this section is to provide a procedure to quantitatively compare the performances of crest extraction algorithms. When a new method is designed, it is usually compared to the literature. These comparisons remain visual. A limited set of surfaces is systematically used to highlight the difference and the added value of the new algorithm. This set is a sort of benchmark set. Examples of these surfaces are presented in Figure 6.4.

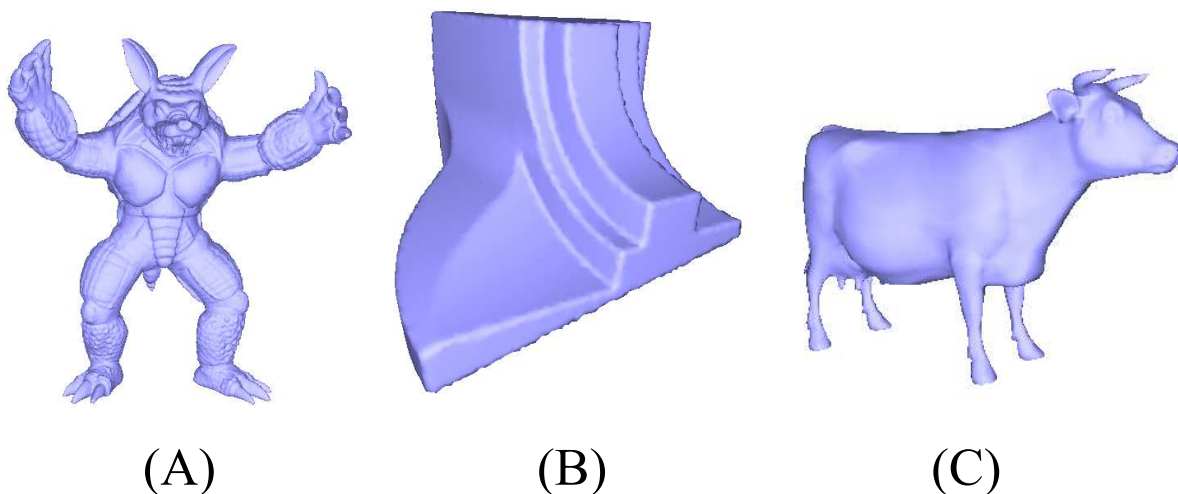


FIGURE 6.4: Examples of usual test surfaces. (A): Armadillo; (B): Fandisk; (C): cow.

In general, these meshes represent real objects such as statues (Buddha, Michelangelo, dragon, etc.), animals (cow, bunny, etc.) or mechanical parts. They are perfect to test the robustness of algorithms thanks to their complex and sharp edges and various texture types. However, these surfaces are very different from bathymetric data. Therefore, comparisons will be made on our own benchmark. A qualitative analysis of the algorithm performance might be satisfying for other applications. For dunes, the

crest detection is important so that a quantitative comparison frame was developed. The comparisons will only consider the reconstruction of the crest lines by the four selected algorithms. Thus, the differential quantities (curvatures and derivatives) are all estimated using the modified osculating jet method presented in the previous chapter. The degree of the jet is set to 4 since Cazals2 method requires fourth-order derivatives and a 3-ring neighborhood is selected to have enough vertices and redundancy for the fitting.

6.4.1 Comparisons on benchmark zone 1

Figure 6.5 shows that the crest lines resulting from the four algorithms look like each other. The extraction algorithms are meant for detecting features locally resembling to crests. So dune crests are not the only extracted lines, although they are the most remarkable features to the bare eye.

Lines are detected in the flat areas between dunes. These features are real and are due to smaller sand structures or acquisition artifacts. In the southwestern part of zone 1, the surface is rough because of consistency problems. This occurs where data from two survey lines overlap and that appear to be two different surfaces due to calibration issues. This leads to the detection of NW-SE oriented crest lines in this part of the seafloor (especially visible in Figure 6.5(b-d)). These artifacts have an influence on the curvature and its derivatives (see Figure 6.6) and this translates to detections by the four algorithms.

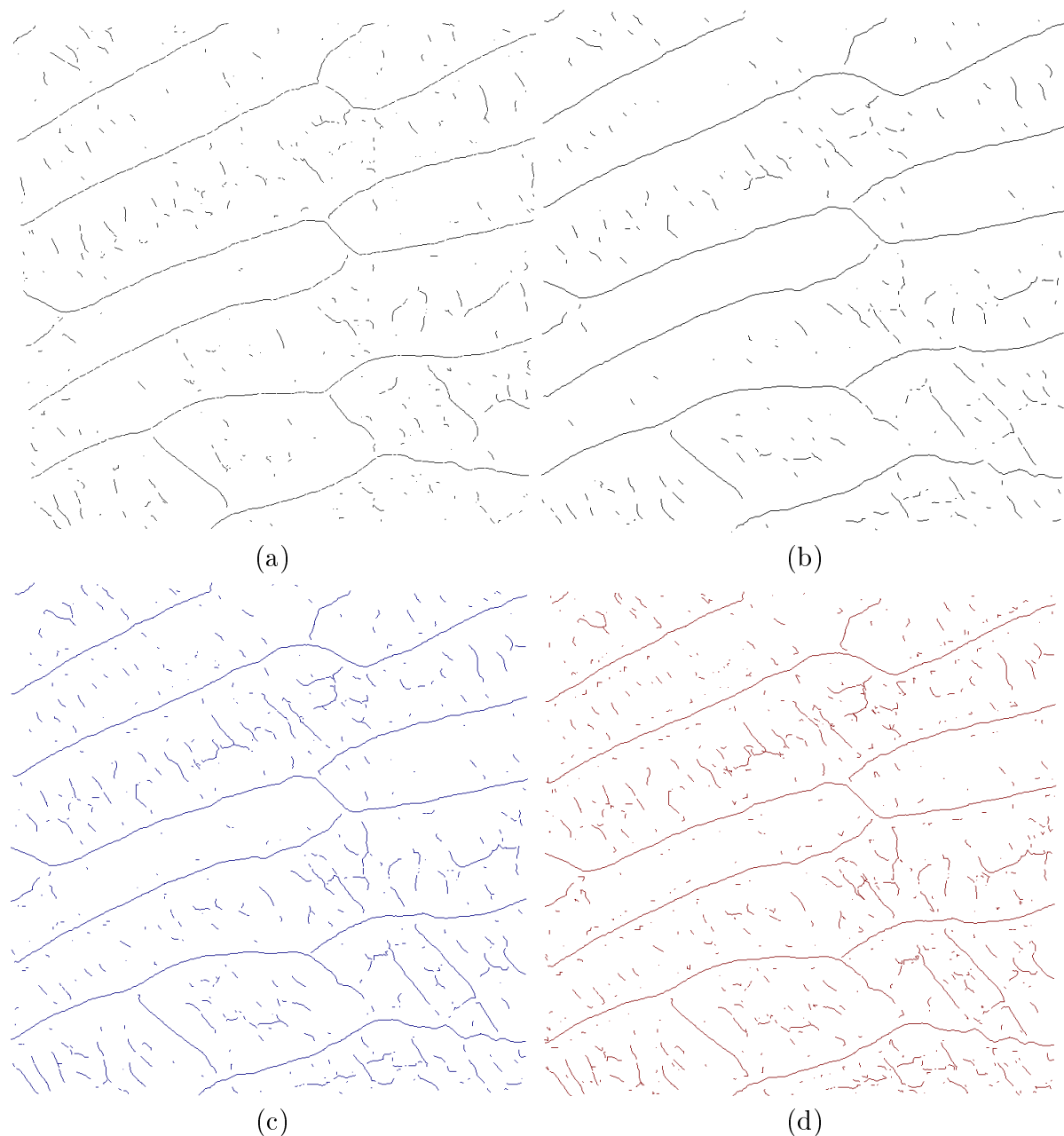


FIGURE 6.5: Crest lines detected by the four algorithms: (a) Hildebrandt; (b) Ohtake; (c) Cazals1; (d) Cazals2.

Subfigure (d) of Figure 6.6 explains why the neighborhood should not be extended if not necessary. Here, the neighborhood size can not be decreased as it is imposed by the polynomial order. But, when possible, it is better to lower the neighborhood size so that the height difference between the polynomial and the fitted surface are not too high over the neighborhood. In fact, here, the standard deviation of the distances between the mesh and the fitted model is extremely high around crests. The differences are up to 1m when the dunes are only a few meters high. This relates to the difficulty of the model in following the terrain morphology at this scale in the regions of interest.

Therefore, a 3-ring and larger neighborhoods should only be used if imposed by the order of the model.

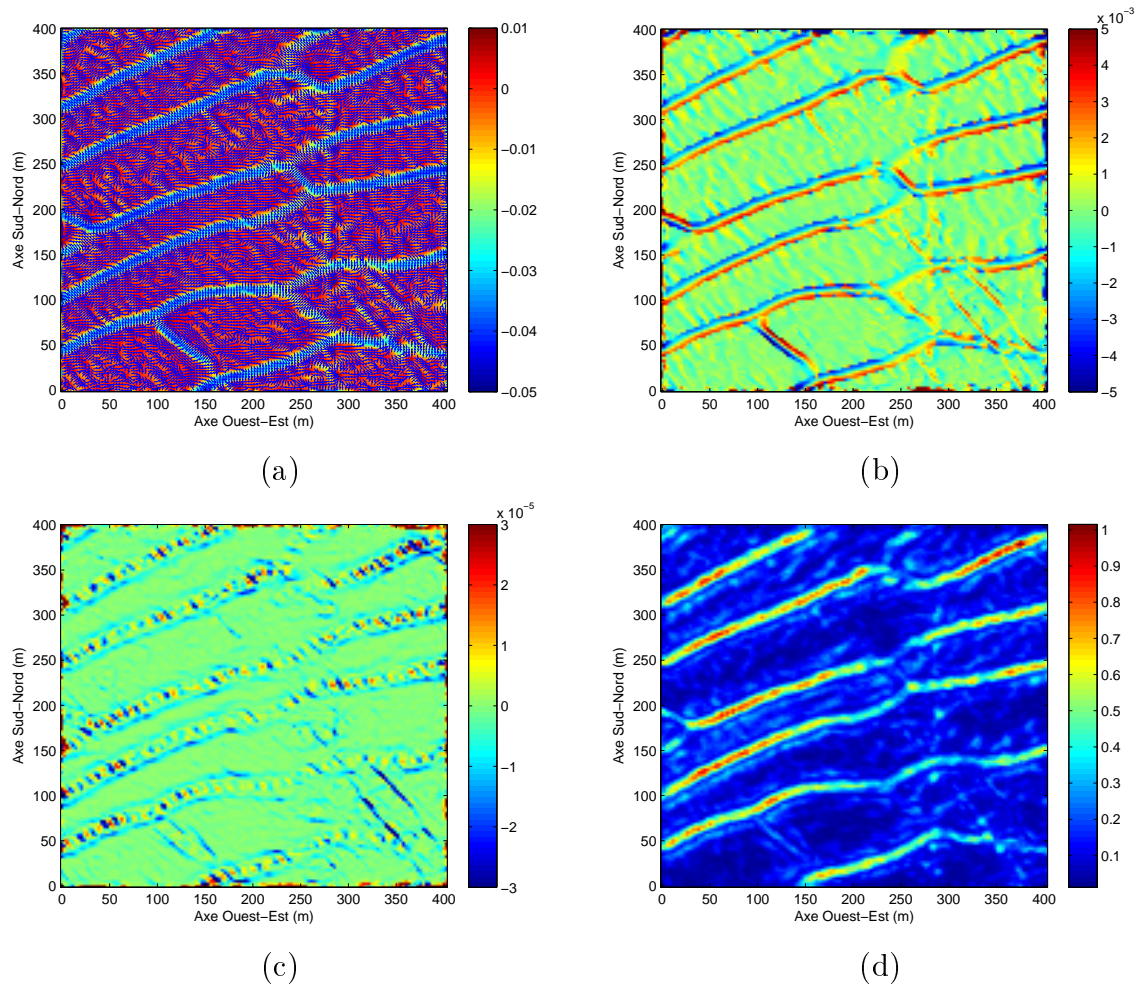


FIGURE 6.6: Differential quantities deriving from the osculating jet method (degree:4; neighborhood size:3): (a) k_{min} (m^{-1}) and t_{min} ; (b) e_{min} (m^{-2}); (c) P_{min} (m^{-3}); (d) fitting error (m).

Despite the visual similarities, the four sets of crest lines are different. Metrics have been selected to quantify these differences that are not so obvious with visual comparisons. The first metric is the number of extracted crests. Ideally, this should correspond to the true number of dunes in the studied area. The second are the quartiles of the crest length, which shows if an algorithm extracts short or long crest lines that may be crests due to artifacts in the surface or even because the algorithm extracts segmented crests. The third indicator is the quartiles of sinuosity that provide information complementary to the length indicator. In fact, the sinuosity tells whether a crest is straight or not. For a dune, the value is generally around 0.9-0.95 as they are relatively straight features. Crests with a higher sinuosity value may correspond to long artifact crests that are not straight and short crest tend to have a high sinuosity values. The last metrics are the length of the five longest crests. Five is an arbitrary choice that was selected as the number of dune crests in the benchmark zones never exceeds five. Therefore, this indicates if the algorithm is capable of detect the full-extended dune crests.

Table 6.1 gathers these quantitative metrics for zone 1. First, Hildebrandt's algorithm has a tendency to extract intermittent dune crests. The number of detected crests confirms this observation. In addition, the constructed lines are smaller with this method (five longest crest lines and length quartiles). Since the lines are split, they are straighter (sinuosity). The three other algorithms, despite unwanted lines, are capable of reconstructed entire dune crests as shown in the five longest crest lines column.

TABLE 6.1: Comparisons of the crests detected by the four algorithms on zone 1.

Algorithm	Number of crests	Length (m) (quartiles)	Sinuosity (quartiles)	Five longest crests (m)
Hildebrandt	874	1.6 3.2 6.1	0.98 1 1	43 41 37 36 30
Ohtake	254	2.9 5.4 9.7	0.97 0.99 1	440 428 277 265 205
Cazals1	515	1.9 3.6 9	0.95 0.99 1	442 433 306 281 278
Cazals2	696	1.5 3.6 7.9	0.83 0.98 1	447 433 282 278 270

In order to further compare the set of crest lines, the resemblance between lines detected was quantified. The number of mesh edges commonly crossed by two sets gives an indication about their similarity. The results for zone 1 are given in Table 6.2. Thus, it can be seen that even if Hildebrandt's lines look like the others they are quite different. In fact, more than half of the edges crossed by Hildebrandt's crest lines are not crossed by the other lines. On the contrary, more than 2700 edges crossed by Ohtake's lines (out

of 3000) are also crossed by Cazals's. In addition, Cazals's sets of lines are very similar (4100 common edges out of 4300). What can also be noted is that Ohtake's method detects fewer lines than Cazals1 that also detects fewer lines than Cazals2.

	Hildebrandt	Ohtake	Cazals1	Cazals2
Hildebrandt	3524			
Ohtake	1432	3089		
Cazals1	1649	2783	4383	
Cazals2	1759	2763	4123	5253

TABLE 6.2: Closeness of the detected crests on zone 2.

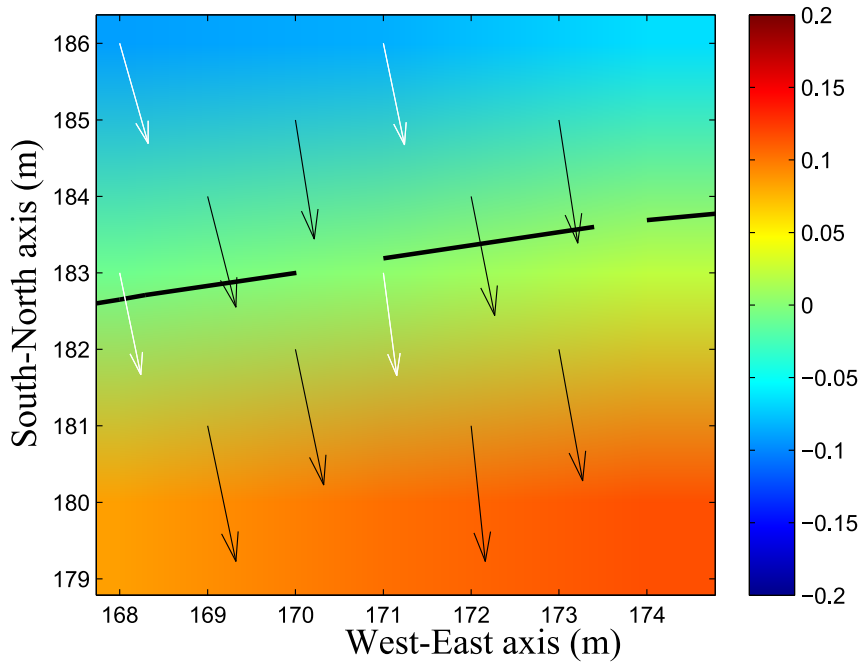


FIGURE 6.7: Failure case of Hildebrandt's algorithm. This is a zoom on a part of zone 1 where Hildebrandt's algorithm creates two separated crest lines instead of one. The white arrows indicate the t_{min} direction at mesh vertices and black arrows the e_{min} gradient estimates per face located at the center of the faces. The background colours correspond to the Hildebrandt's e_{min} values.

Figure 6.7 illustrates that Hildebrandt's algorithm fails in detecting some crest segments due to the sign condition on the projection of the e_{min} gradient onto the t_{min} vector. In the figure, the condition seems to be met (positivity of the inner product).

As seen before, the seafloor is almost flat despite the presence of dunes. The values of e_{min} being all near zero, the gradient is almost vertical. Indeed, its vertical component is about 30 times bigger than the horizontal. In addition, the seafloor surface itself is nearly flat. Therefore, the surface normals are almost vertical too and, thus, the t_{min} vectors are almost horizontal.

The test made by the algorithm relies on the inner product of almost orthogonal vectors. Knowing that t_{min} can slightly point upward or downward, this small change can change the sign of the inner product and disturb the crest reconstruction.

The algorithm is not suited for dune data and was originally designed for applications on very different surfaces (cf. Figure 6.4). In order to validate our explanation, it was decided to modify the algorithm. The vertical components of e_{min} gradient and t_{min} vectors are discarded when doing the inner product test.

Figure 6.8 shows that the modification allows the dune crests to be extracted without undesired splits. Yet, the modification cannot be mathematically justified, being essentially empirical. The results with the modified algorithms are however much better, closer to what one could expect for dune crests (cf. Table 6.3) and also a bit closer to the other extracted line sets (see Table 6.4). Yet, the set of lines still remains different from the others with, at best, 2100 common crossed edges with Cazals's sets.

Algorithm	Number of crests	Length (m) (quartiles)	Sinuosity (quartiles)	5 longest crests (m)
Hildebrandt	355	1.8 3.4 7.7	0.96 0.99 1	434 428 328 289 278

TABLE 6.3: Characteristics of the set of crest lines obtained with the modified Hildebrandt's algorithm.

	Modified Hildebrandt	Ohtake	Cazals1	Cazals2
Modified Hildebrandt	3498	1771	2116	2136

TABLE 6.4: Tracing similarities between modified Hildebrandt's crests and the others.

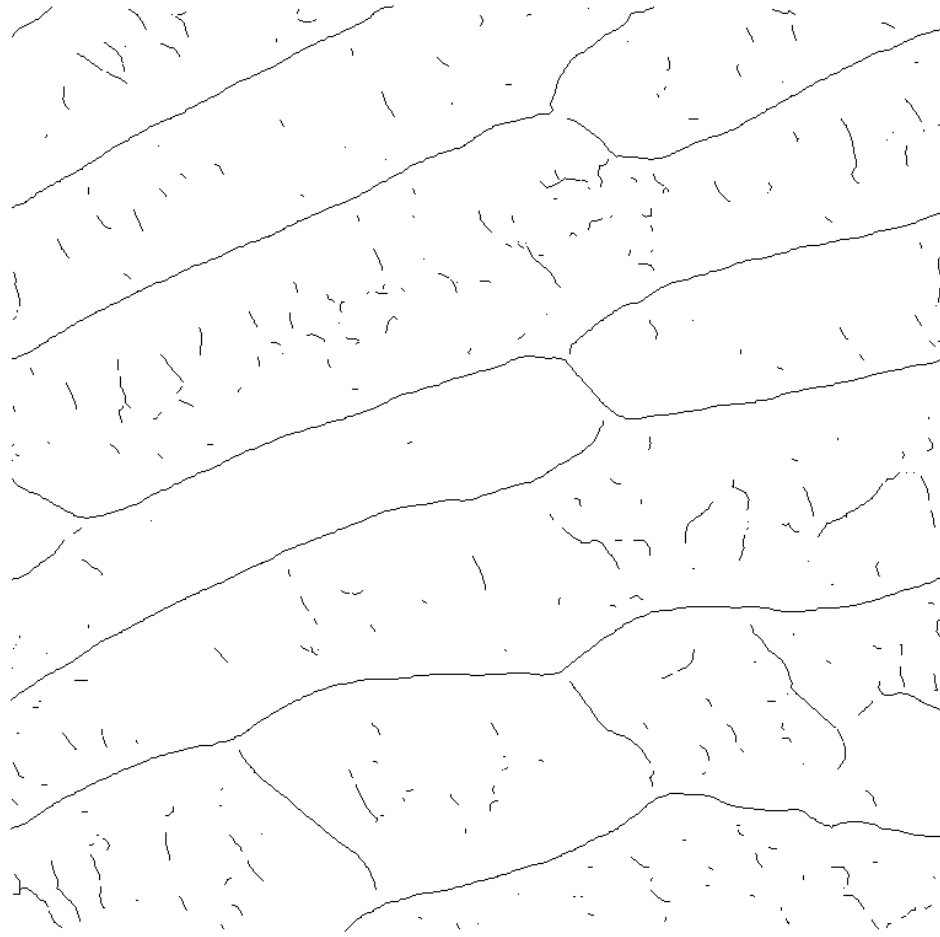


FIGURE 6.8: Set of crest lines detected by Hildebrandt's algorithm after modification.

Ohtake's method extracts fewer lines than the others and especially than Hildebrandt's. There are fewer crests due to the surface roughness and fewer dune crest splits. The first observation is confirmed by the first two quartiles of the crest length, which are almost twice Hildebrandt's (Table 6.1). Longest crests pass from 40 to 200 m. Sinuosity is lower but is still high (>0.9) which corresponds to linear dunes or smaller seafloor features (artifacts, roughness or small sand structures).

Cazals's algorithms best reconstruct dune crests (longest crest lines). But, they also detect other features more "easily" (number of crests). Therefore, they produce fewer crest lines than Hildebrandt's algorithm but more than Ohtake's (less sensitive to small features). Both variants of the algorithm extract dune crests similarly but Cazals1 generates fewer undesired lines (cf. Table 6.1). These differences probably come from the fact that Cazals2 tests the sign of a fourth-order quantity with magnitude of order 10^{-5} (cf. Figure 6.6). This requires great accuracy in the estimation, and the fitting on a 3-ring neighborhood is not optimal as previously mentioned.

It is also important to note that Ohtake's algorithm sometimes has problems in building the continuous dune crests, for example for the two large dunes in the southeastern part of zone 1 (see Figure 6.5 (b)). The reason for this lower extraction capacity of Ohtake's algorithm is explained in Cazals & Pouget (2005b). It is said that errors might be made by the algorithm nearby umbilical points.

Figure 6.9 shows, for each vertex, the t_{min} direction (vectors in the figure) and the extremality value (background), e_{min} . These are the two elements used by the algorithm to decide whether or not an edge is crossed by a crest line. In the displayed case, the tested edge is almost parallel to the crest line (black line). Once more, it is a case where vectors are almost perpendicular: the tested edge and the principal directions. The test success or failure only depends on the orientation of the principal direction vectors.

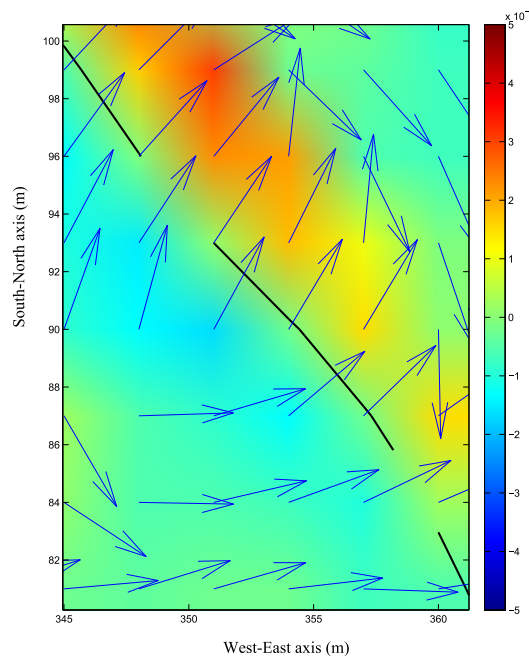


FIGURE 6.9: Failure case of Ohtake's algorithm.

As remarked by Cazals, the principal directions at the edge extremities might be followed to get closer to the crest line, but, it does not necessarily make you closer to the edge point where e_{min} is null. For this reason, Cazals1 algorithm tests whether a segment is part of crest rather than a point.

As the segment is supposed to be part of a crest line, following the principal directions at the face vertices must lead to the supposed crest. This also explains why Cazals1 algorithm detects more crests than Ohtake's.

All these comments lead to the conclusion that Cazals1 method is more suited for a correct extraction of crest lines with a limited number of undesired lines. In fact, it is preferable to have nice dune crests with spurious lines that fewer undesired detections and dune crests that need merging. Furthermore, the degree of the osculating jet may be set to 3 instead of 4 for Cazals2 and, then, the neighborhood size decreased to 2. Then, the estimation of the curvature and extremality would be more local and the jet adjusted to the surface with smaller errors.

6.4.2 Comparisons on benchmark zone 2

The conclusions made on zone 1 are not sufficient to definitively conclude as to the applicability of these algorithms for the extraction of dune crests. The methods have been compared on other benchmark zones to analyze the results for other dune types and configurations.

Figure 6.10 shows the results of the algorithms on benchmark zone 2. At first glance, the results confirm the observations made on zone 1. Even more crests are detected than on zone 1. The presence of artifacts pollutes the extraction of many crest lines and some of them can be even longer than dune crests.

The figures gathered in Table 6.5 quantify the observations from Figure 6.10. In this area, there are only three partial dunes: one long dune crossing the area and two smaller in the top-right corner of the area. Instead of three dune crests, at least 1600 crest lines are obtained. Furthermore, the five longest crests show that some crests are due to the acquisition artifacts or rugosity might be several hundred meters long. And, the smallest dune crest is not as long as these artifacts. The capacity of Cazals1 algorithm to reconstruct good dune crests is validated. But, if this confirms the choice of an algorithm for dune extraction, another issue appears: the number of lines corresponding to other features is huge and a way to filter out these lines must be determined.

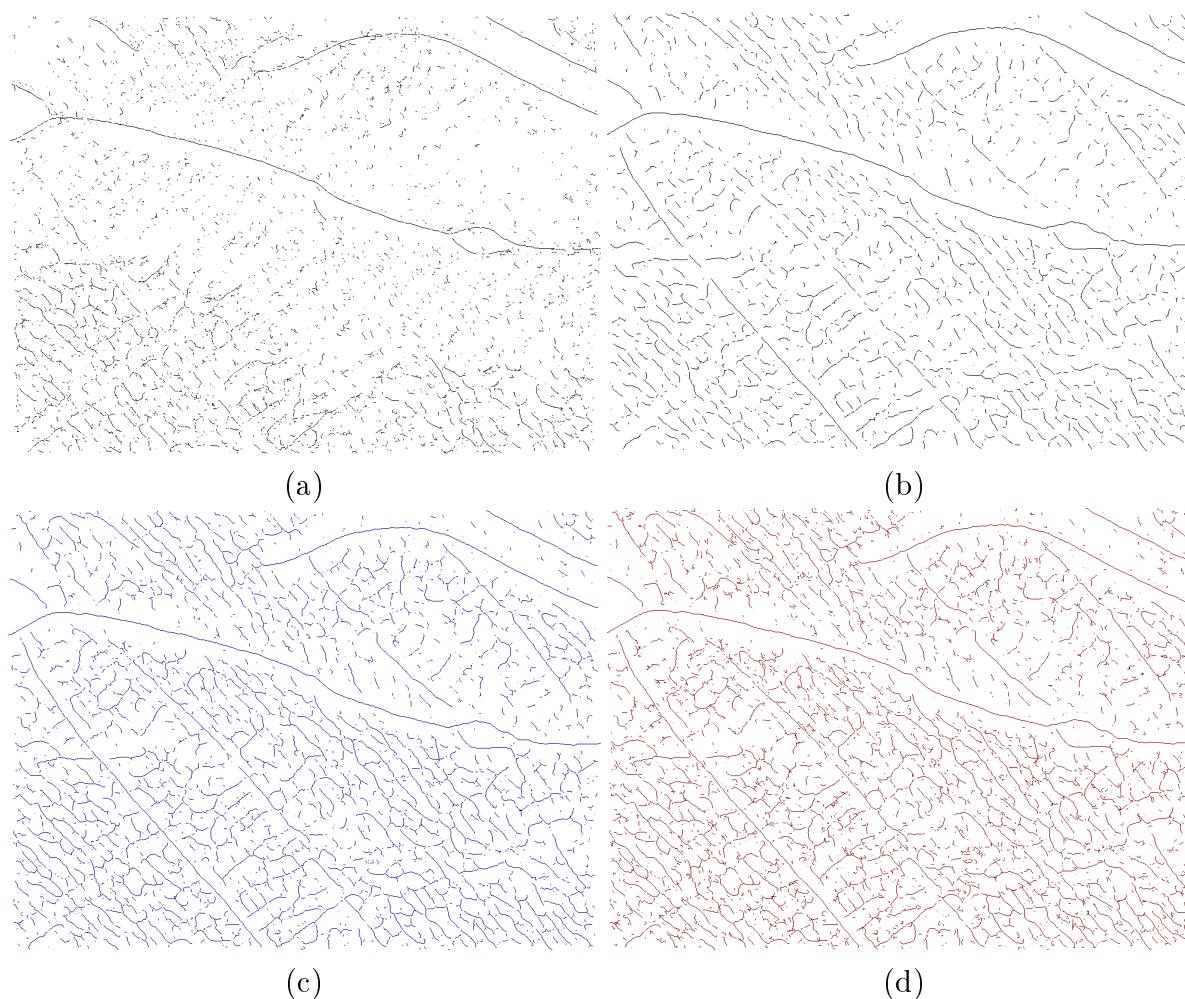


FIGURE 6.10: Detected lines by the four algorithms on benchmark zone 2: (a) Hildebrandt; (b) Ohtake; (c) Cazals1; (d) Cazals2.

Algorithm	Number of crests	Length (m) (quartiles)	Sinuosity (quartiles)	5 longest crests (m)
Hildebrandt	4239	1.6 2.5 4	0.98 1 1	111 108 49 42 39
Ohtake	1643	2.6 5.6 12	0.95 0.98 1	737 302 203 163 163
Cazals1	2615	1.9 4 11.1	0.92 0.98 1	845 496 322 170 150
Cazals2	3267	2.1 4.5 9.8	0.79 0.95 1	845 495 323 170 151

TABLE 6.5: Quantitative comparisons on zone 2.

6.4.3 Analysis of the dune crest descriptors

The most direct way to filter the set of crest lines is to sort dune crests from other crests based on the analysis of crest descriptors. These descriptors may be classified in two categories: common dune crest descriptors and mathematical descriptors.

The objective is to determine whether one or a set of these descriptors can help discriminating dune crests from the rest. Specific dune descriptors have already been presented in Subsection 2.2.2. The list of dune crest descriptors that were considered is:

- Length;
- Sinuosity;
- Height.

The height was defined as the maximum distance between the points of the crest line and the straight line linking the crest extremities. If the crest of the dune is correctly extracted and the dune is totally included in the area, the height value will be higher than 1m. If a crest ends at the area boundaries, its value is set to -1 to avoid suppressing not entirely described dunes.

The mathematical descriptors are generally applied to results of characteristic line extraction algorithms to keep the most distinctive (sharpest) lines (Kim & Kim, 2005). The strength descriptor is defined as the integral of the minimum curvature along the crest. The sharpness descriptor is defined as the integral of the second order derivative of this curvature in the associated direction. More details about these metrics are given in Cazals & Pouget (2004). In the context of this thesis, a third mathematical descriptor was defined as the integral of the ratio between the two principal curvatures along the crest line. Unlike the first two metrics, the third accounts for the shape of the surface at crests in both transversal and longitudinal directions.

These descriptors were estimated on benchmark zones 2,4,6 and 9. These zones were selected to study the discriminating capacity of the descriptors. The results of the extraction on these areas are presented on Figure 6.11. In fact, these zones gathered rocks, ripples or remarkable artifacts, but even though crest dunes are well-reconstructed, these features are also detected. However, the human eye is able to make the distinction between dune crest lines and the others. The crest lines of zone 9 show that this final comment is not true for ripples that have crests much like dunes. In addition, ripples are superimposed on top of the dunes and, at places, their crests cross. There, the reconstruction is delicate and it may happen that the algorithm starts following a ripple crest. Thus, some crest lines are a mix of dune and ripple crests. And, the full length of the dunes is not always recovered.

Sinuosity

In Figure 6.12, the sinuosity of dune crests is generally around 1.05 to 1.1. However, other features might have crests with similar sinuosity values. In subfigure 6.12(d), it can be observed that the length is not sufficient to distinguish between sand dunes and ripples. Actually, ripples can be as long as or even longer than dunes.

Height

The dunes we aim at detecting are more than 1m high. In Figure 6.13, it may be noticed that, on zones 2,6 and 9, this threshold enables filtering most of the undesired crests and, especially ripples on zone 9. On zone 2, the threshold is enough to remove artifact lines. Yet, for zone 4, rocks are detected and correspond to lines with a height above the threshold.

Strength

One of the main issues with this descriptor is that, for two dunes with the same length, the strength value can be double for one of them as seen on Figure 6.14. Furthermore, it can be concluded from subfigure 6.14(d) that dunes and ripples have similar strength values. The setting of a strength threshold would be very empirical as there is no proof that there is one value appropriate to every dataset. Hence, the quality of the set of lines after filtering would be uncertain. In addition, the descriptors based on the derivatives of the surface have values depending on the mesh resolution. They are estimated by fitting polynomials to approximate the surface. When the mesh resolution is changed, the area on which the fitting is made also changes leading to different curvature estimations. Table 6.6 illustrates the impact of the mesh resolution on the strength values (see Figure 6.17 for the visualization of the crest lines). Strength depends on the curvature values, which are lower as the mesh is coarsened. Again, this is due to the fact that the curvature is estimated at a larger scale and that the osculating jet does not locally describe the surface variations. There is a ratio of five in the strength values between the 1m and 8m meshes. This confirms the difficulty in using a strength threshold. It can be remarked that the dune crests are still detected on the 8m mesh and that the number of undesired crests dramatically drops to 110 against 2231 on the full resolution terrain. Therefore, there is a balance problem: lower resolution implies fewer false positives but more approximation. For this reason, a tradeoff must be found in order to obtain only dune crests with a "good" resolution.

Mesh resolution (m)	Crest number	Strength quartiles
1	2231	4.8 12.5 22.8
4	204	2.8 6 12.3
8	110	1 2.3 4.3

TABLE 6.6: Comparisons of the strength values according to the mesh resolution on benchmark zone 8.

Sharpness

Although it is supposed to be scale-independent, the sharpness is a highly fluctuant descriptor (see Figure 6.15). Dune crests are not characterized by a particular value of sharpness. Therefore, the automatic setting of a threshold to prune the set of crest lines may lead to the removal of dune crests.

Third mathematical descriptor

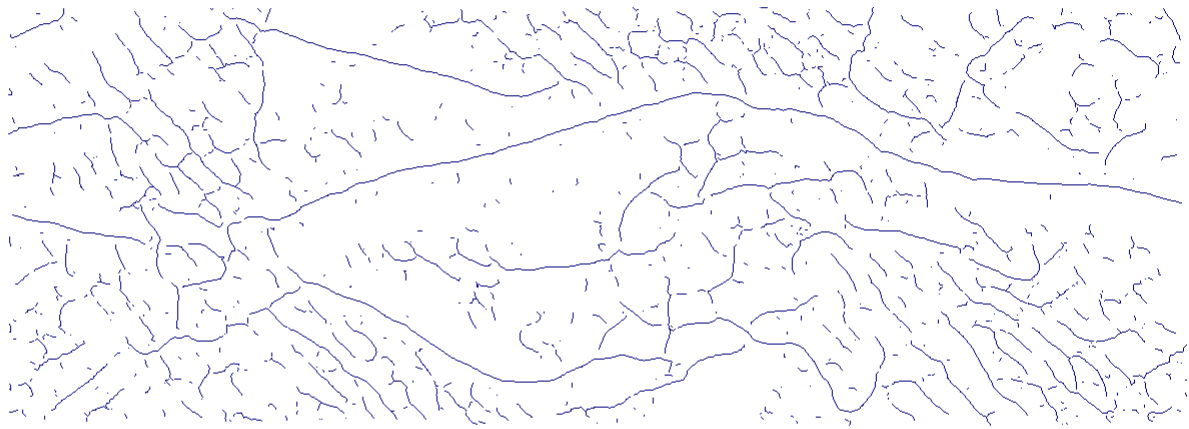
For this descriptor, dune crests exhibit values around 0.03/0.04 (cf. Figure 6.16). But, it is less discriminatory than the length. It is less intuitive than the length too. Hence, length is more adapted for the sorting of crest lines.

No descriptor on its own can filter the sets of crest lines. Most crest lines can be suppressed using the length. But, artifacts and ripples lines still remain. The height discriminates ripples from dunes but not from rocks. Mathematical descriptors are derived from surface derivatives so the adjustment of a threshold is very delicate, and depends on the fitting neighborhood. These descriptors can be relatively non-discriminatory in the context of the study. In other words, feature types may not be differentiated in all cases with certainty.

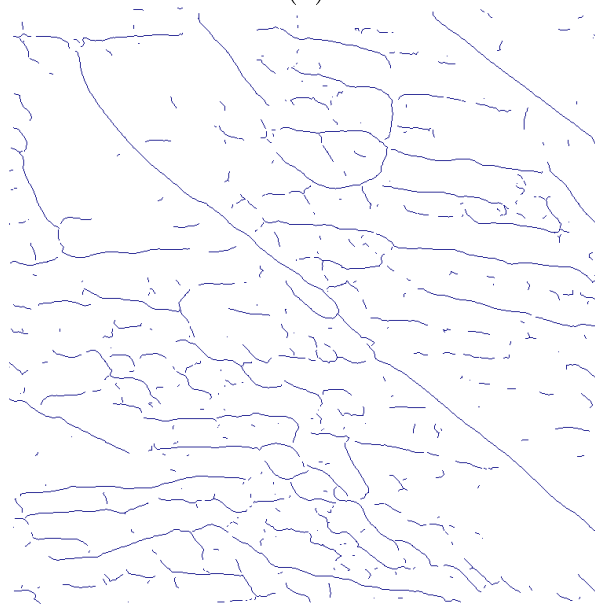
Height and length have the advantage of being intuitive so that an operator might easily set their values. It is not true for the other descriptors (sharpness, sinuosity, *etc.*).

Ripples are hard to distinguish from dunes. The difference can only be made by the height. But, features ending at the boundaries of the analyzed area are not discarded by the height descriptor (height=-1m) and many ripples are in this situation.

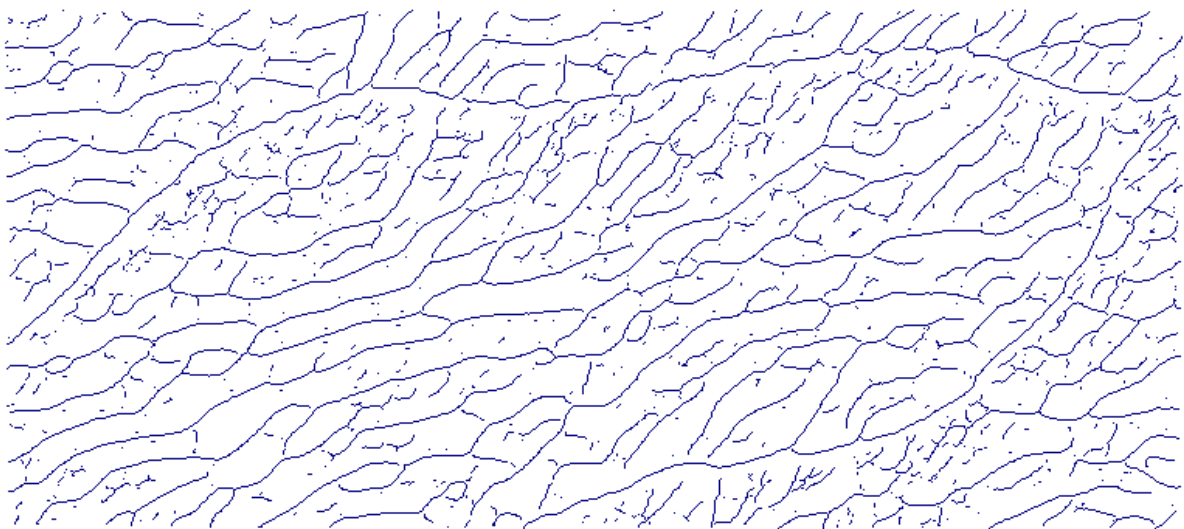
In conclusion, even if descriptors are useful for pruning line sets for other applications, the removal of undesired lines is nearly impossible or, at least, would be empirical with heuristics established through a trial and error process for each mesh.



(a)



(b)



(c)

FIGURE 6.11: Cazals1 extracted crests on benchmark zones.(a): Zone 4; (b): Zone 6; (c): Zone 9.

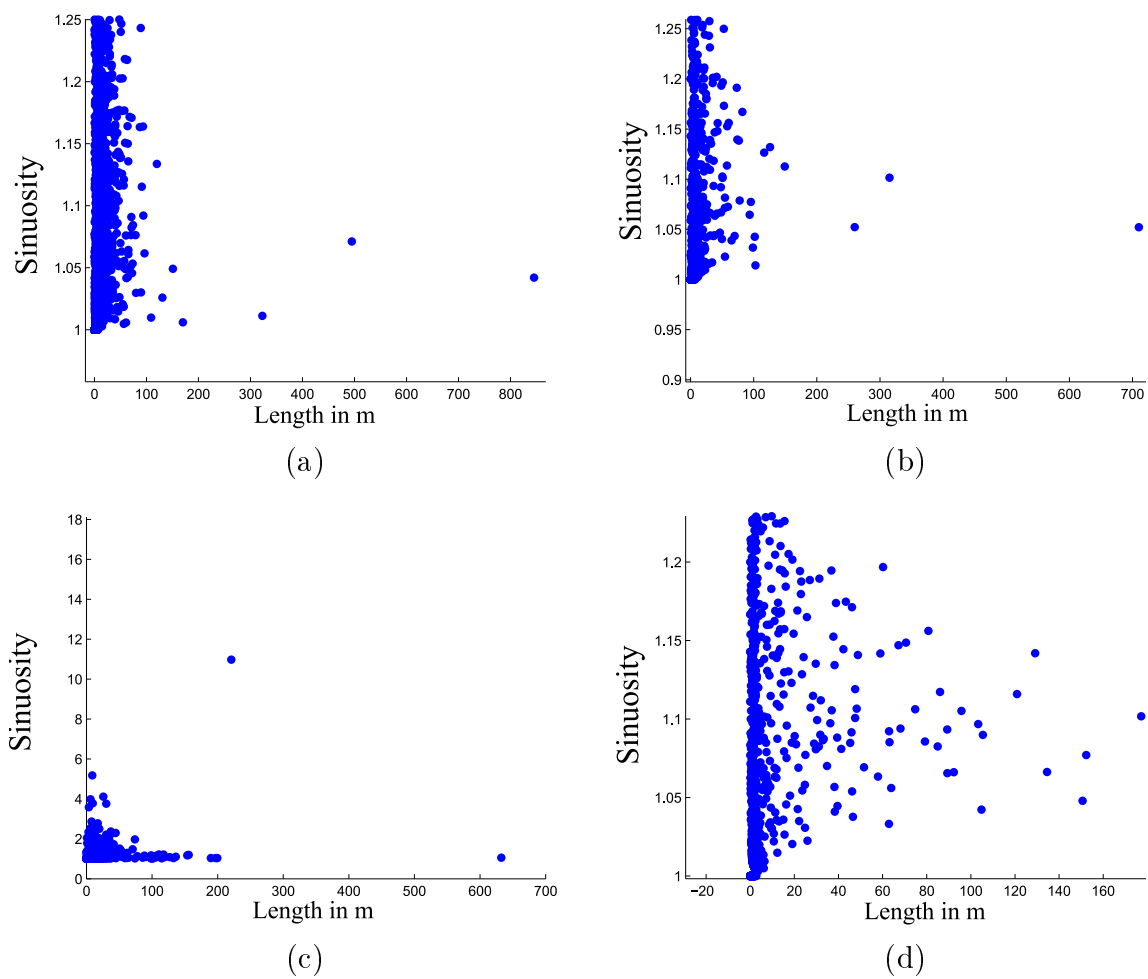


FIGURE 6.12: Sinuosity of the crests on benchmark zones: (a) zone 2; (b) zone 4 ; (c) zone 6 ; (d) zone 9.

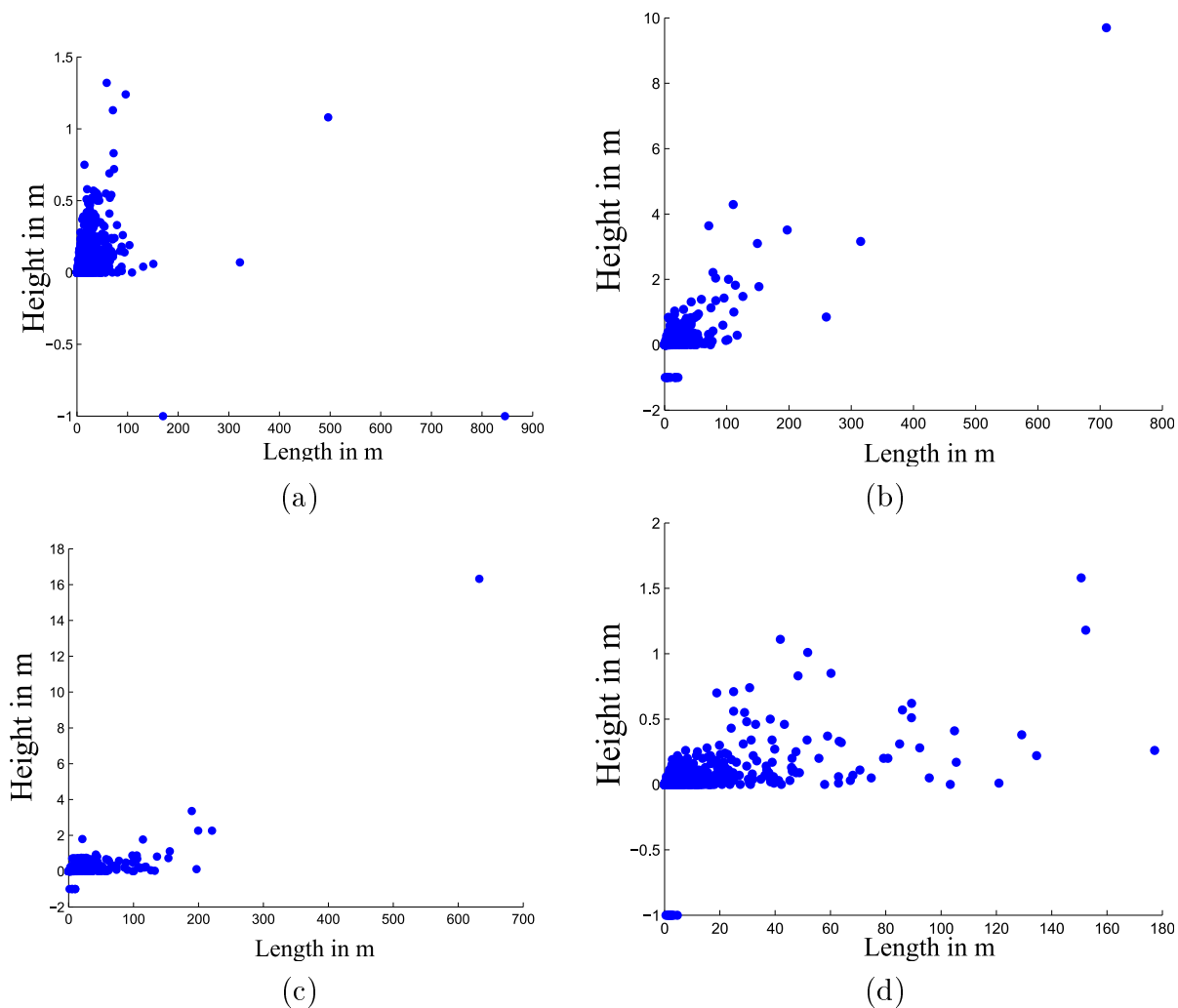


FIGURE 6.13: Height of the crests on benchmark zones: (a) zone 2; (b) zone 4 ; (c) zone 6 ; (d) zone 9.

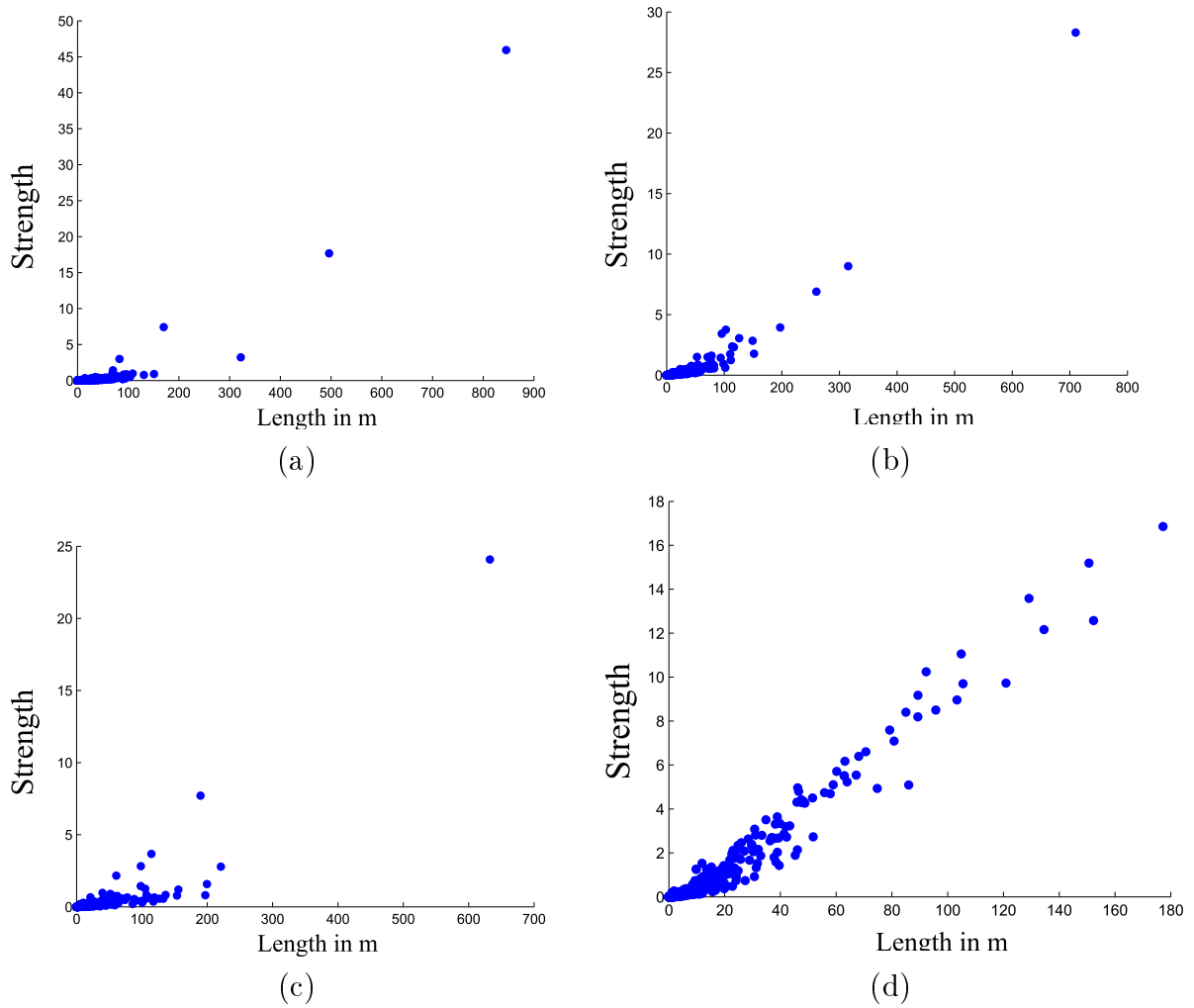


FIGURE 6.14: Strength of the crests on benchmark zones: (a) zone 2; (b) zone 4 ; (c) zone 6 ; (d) zone 9.

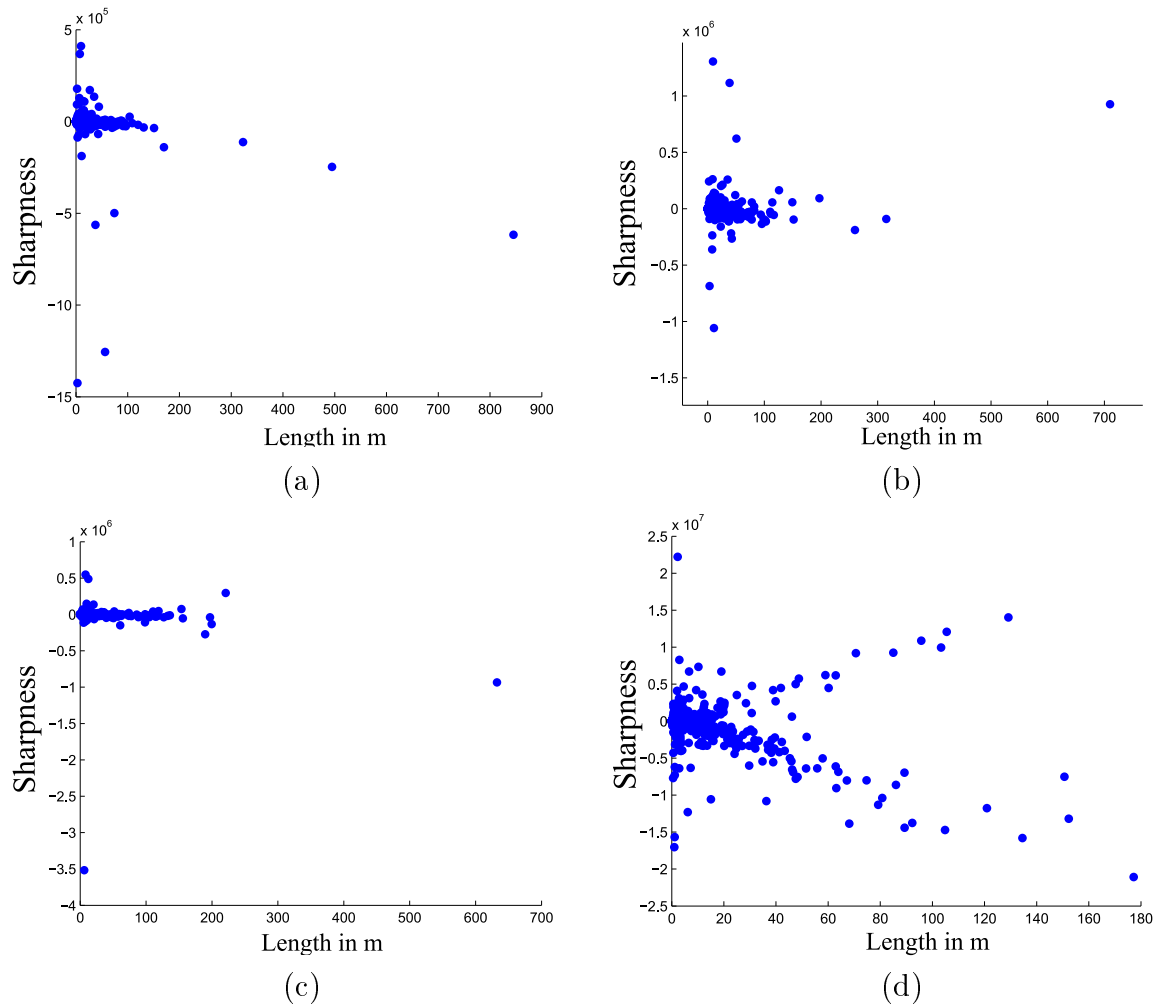


FIGURE 6.15: Sharpness of the crests on benchmark zones: (a) zone 2; (b) zone 4; (c) zone 6 ; (d) zone 9.

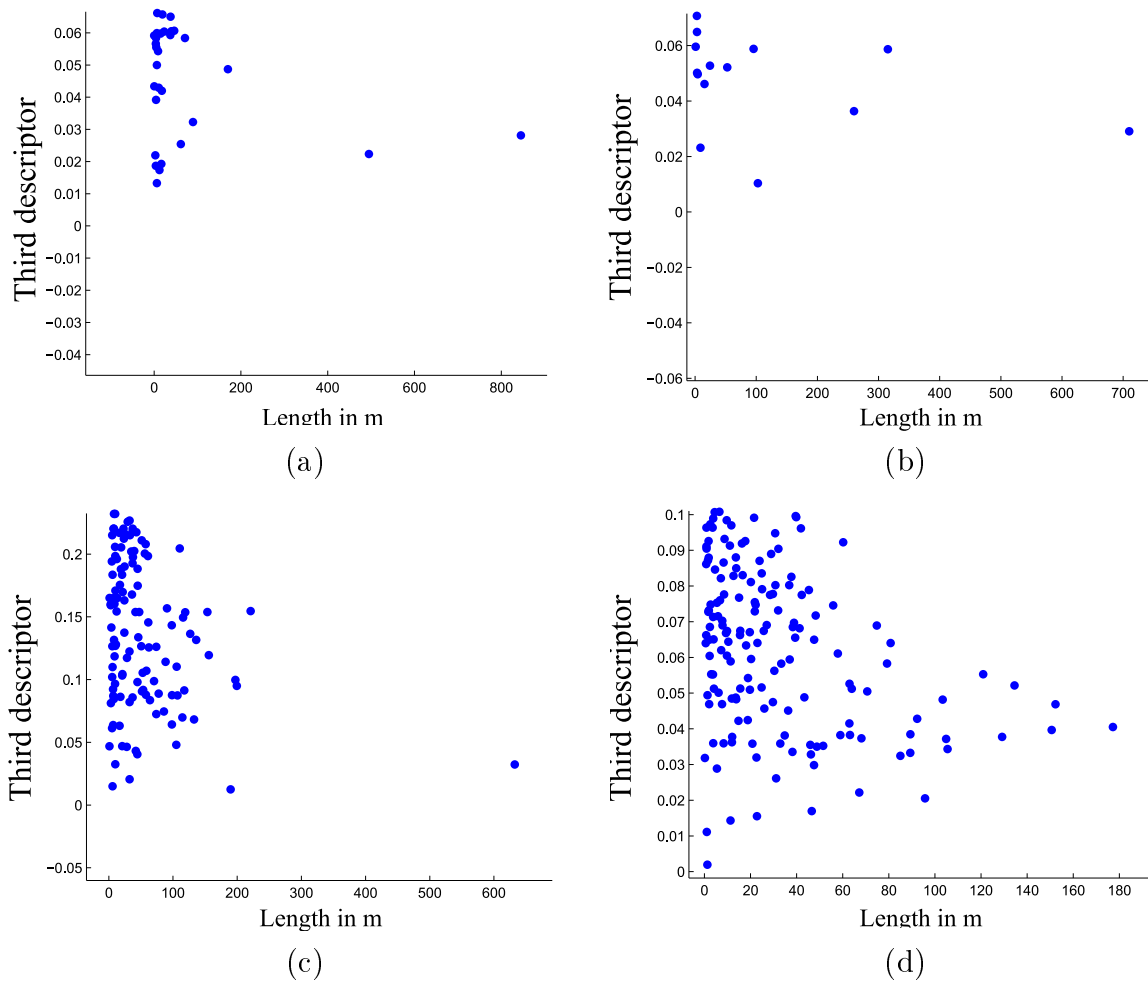


FIGURE 6.16: Third mathematical descriptor values of the crests on benchmark zones: (a) zone 2; (b) zone 4 ; (c) zone 6 ; (d) zone 9.

6.5 Crests and mesh resolution

When analyzing the strength, it was noticed that changing the mesh resolution modifies the extraction results. It is important to observe the impact of the resolution as it is a parameter that can be optimized in order to better extracted dune crests. Figure 6.17 outlines the impact of the surface resolution on the extraction of crest lines. When the mesh resolution is coarsened, the resulting lines correspond to more global features. This illustrates the notion of scale of a seafloor (terrain) feature already mentioned in Chapter 4. If, at a fine scale, a crest of a ripple might be similar to a dune crest in terms of descriptors, an adapted scale helps distinguishing between the two.

The mesh resolution can be adjusted so that the fitting neighborhood is adapted to dune detection. This modification enhances detection of features existing at this scale (and larger scale) and to suppress the others such as lines caused by ripples, rocks or artifacts. But, dune crests can also be discarded if the scale is not carefully selected. In addition, crests detected on a coarse mesh are roughly delineated and it would be preferable that they are obtained at the finest resolution possible.

The mesh resolution is not the only parameter controlling the scale of the extraction algorithm. The neighborhood has an equivalent influence. Table 6.7 depicts the influences of neighborhood size and jet degree on the extraction with a fixed mesh resolution (Zone 8). As for the curvature estimation, adding coefficients to the jet only degrades the quality of the set of lines and it might also require the growing of the neighborhood. Thus, the jets used here shall be limited to third order coefficients. In addition, the growth of the neighborhood has a beneficial impact similar to the mesh resolution. The issue is that it significantly slows down the algorithm. There is a tradeoff between running time and the number of crest lines. There is therefore real value in taking a 3-ring neighborhood over a 2-ring as the crest number is nearly divided by three. For n -neighborhood ($n > 3$), the bargain is reduced with the number of crests "only" dropping by 100 and neighborhoods composed of more than 61 vertices instead of 37 with a 2-ring neighborhood.

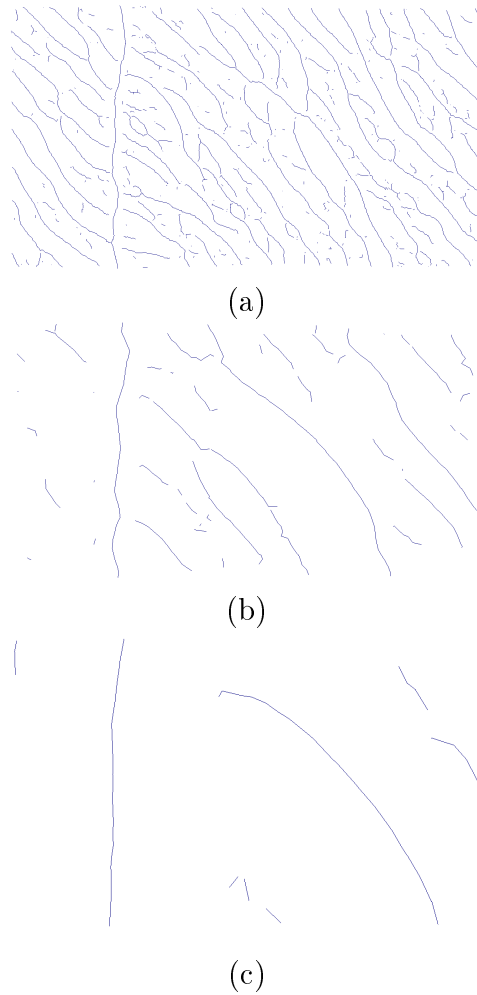


FIGURE 6.17: Crest lines extracted with Cazals1 algorithm on meshes of benchmark zone 8 with various resolutions: (a) 1m; (b) 4m; (c) 8m.

Neighborhood size	Jet degree		
	3	4	5
2	918	2124	-
3	350	906	1187
4	211	417	558

TABLE 6.7: Number of extracted lines according to the degree of the fitted jet and the neighborhood size.

6.6 Conclusion

The problem of surface characteristic lines extraction has been extensively researched. These lines may be mathematically determined from the local surface properties (curvatures and derivatives).

Numerous extraction algorithms were proposed to extract the feature lines of a surface. They more or less thoroughly follows the theoretic definition. Indeed, not all applications demand a rigorous construction of crest lines. For dunes, the crest is a crucial part so a theoretic approach is preferred.

In order to make a choice between these algorithms, a quantitative comparison procedure was designed, which avoids making usual visual comparisons. It was concluded that Cazals1 algorithm performs best on dune datasets.

Yet, another problem remained. The set of extracted dunes contained dune crests of other features. Crest descriptors were compared. The objective was to determine whether one or a set of them could be used to prune the set of crests. It appears that filtering through descriptor thresholding is delicate and highly empirical.

Another way to remove the undesired crest lines is to adapt the scale of the extraction of the algorithm to match dune scale. It was observed that the best tradeoff is to fit a 3-order jet on a 3-ring neighborhood. Most crest lines are no longer extracted and the rest can easily be filtered out with the intuitive height and length descriptors.

Mesh resolution has to be adapted to the extracted features: dunes. Therefore, the next chapter will present algorithms for simplifying meshes. Simplification consists in obtaining a compact surface representation by optimizing the number of vertices, edges and faces of a surface mesh.

Chapter 7

Mesh simplification

Contents

7.1	Introduction	158
7.2	Requirements for the extraction of dune crests	158
7.3	State of the art	159
7.4	Proposed mesh simplification algorithm	165
	7.4.1 Description	165
	7.4.2 Results	168
7.5	Conclusion	172

7.1 Introduction

Mesh simplification is the process that consists of progressively modifying a surface mesh in order to get an optimal 3D triangulated surface. One of the first applications was the design of multiresolution algorithms (Iuricich et al., 2015, Johnson & Hebert, 1998, Lee et al., 1998, Maximo et al., 2014, Reinhard, 1998) for analyzing the characteristics and geometry of 3D objects at several scales. A simplified mesh has many advantages. It is faster to explore, describe or analyze. Its storage is less demanding and it is easier to share. Moreover, for visualization purposes, a simplified mesh facilitates the displaying of the surface. Simplification algorithms find applications in computer-aided design, architectural walkthroughs, finite element methods, scientific visualization, shape acquisition, web graphics, movie special effects, virtual reality or video games.

Most algorithms were designed for a precise application. They are generally empirical and, thus, can rarely be applied in another context. Furthermore, the quality of the output mesh is not always controlled.

The goal of the chapter is: (1) to define the list of specifications a mesh simplification algorithm must satisfy for extracting dune crests, (2) to understand how these algorithms are classified and how they meet our conditions and (3) to design an algorithm meeting the specifications.

7.2 Requirements for the extraction of dune crests

Although simplification methods have been applied to terrain data, the seafloor is very different from the surfaces that are usually simplified. Terrain simplification is generally used in GIS or cartography, and the scientific research is focused on the visualization. Usually, terrain meshes are used to approximate the land topography rather than bathymetry. In addition, our problem is a decimation (size reduction) problem and not a visualization one.

Marine dunes are very specific objects that have no land equivalent. They can be differentiated from land dunes especially by their smaller dimensions. Their extraction will be done via Cazals¹ method. But, first, the mesh resolution must be adapted so

that the extraction step is made at the proper scale: a dune specific scale. In this particular context, the mesh simplification must therefore be subject to rules.

It must:

- Be simple. Mesh simplification is only one step towards the extraction of dune objects. Therefore, the addition of an endless list of simplification criteria would be synonymous with plenty of additional parameters. The algorithm would be complicated and this would probably slow down the extraction process.
- Be led by the mesh resolution and stop when it is appropriate for the extraction of dune crests. If the mesh is too simplified, dune crests might be missed and, in the opposite case, the filtering of crest lines might be insufficient.
- Not insert new vertices. In the previous chapter, it was shown that, on a coarse mesh, the quality of the retrieved crest lines is affected. In order to get fine crest lines, the final extraction must be made on the initial mesh. If the vertices of the simplified mesh are vertices of the initial mesh, the locations of the coarse crest lines in the initial mesh may be inferred. This would enable reconstructing fine dune crests. No new vertex should be inserted during the simplification.
- Preserve the crests. Simplification involves a loss of information about the surface morphology. The details of surface features are smoothed, complicating their extraction. The algorithm should curb this loss at crests as much as possible.

7.3 State of the art

The need for simplification methods has not stopped growing in the last decades. Scanning instruments (LIDAR, laser scanner, sonars, MRI, volumetric imaging followed by an isosurface extraction) provide increasingly dense point clouds describing the geometry of 3D objects. Consequently, new solutions had to be developed in order to display increasingly complex, dense 3D meshes.

The concept of ROAM (Real-time Optimally Adapting Mesh) was invented for the interactive visualization of 3D data, especially of terrain in GIS. A solution for a dynamic display of the surface is to adopt a representation with several Levels Of Details (LOD) (de Berg & Dobrindt, 1995, Hesse & Gavrilova, 2003). A view-dependent refinement scheme of the mesh may be adopted, particularly for large terrain (Lindstrom & Pascucci, 2002).

However, visualization is not the only reason for which simplification algorithms were developed. The construction of an optimal mesh describing a scanned surface/object facilitates its storage and transmission too.

A mesh is said to be optimal with respect to a given error metric if, for a given number of faces, the triangulated model minimizes the error metric. The error metric indicates the closeness of the simplified version of the mesh to the original surface or mesh. In Heckbert & Garland (1999), a theoretical analysis of the output mesh of simplification methods is explained. The L_2 -norm is selected as the error metric. The quality of the approximating mesh is regulated by the L_1 -norm in Agarwal & Desikany (1997) and the Hausdorff distance in Reinhard (1998). The error metric was generalized to a quadric expression called Quadric error metric (QEM) in Garland (1999).

This search for an optimal mesh has long been ignored. The first algorithms are generally heuristic and do not take into account the faithfulness of the output mesh.

The survey by Heckbert & Garland (1997) summarizes the knowledge on simplification algorithms and particularly on terrain mesh simplification algorithms. Particular care is paid to the simplification and representation of height fields.

Six classes of methods for the simplification of height field surfaces may be identified:

- Regular grid. These methods generate a regularly distributed 3D representation of the height field. This is typically the type of algorithms applied to construct a DTM from clouds of bathymetric soundings.
- Triangulation (de Berg & Dobrindt, 1995). Instead of an equally-spaced sampling of the surface, these techniques output a 3D triangular representation of the surface.
- Hierarchical subdivision (Maximo et al., 2014). This is the favorite category for algorithms for the editing and rendering of complex, dense meshes. Hierarchical subdivision methods are fast, simple and facilitate multiresolution modeling and rendering at adaptive levels of details. They are top-down algorithms generally based on a tree architecture. These methods start with a coarse triangulation that is refined by recursively subdividing the faces (Hagbi & El-Sana, 2010). Two of the most famous hierarchical subdivision methods are the Progressive Meshes (PM) approach (Hoppe, 1996) and Multiresolution Adaptive Parametrization of

Surfaces (MAPS) approach (Lee et al., 2005). The first consists of storing the simplification sequence where the second incrementally induces local parametrizations of the surface on each simplification step.

- Feature. These techniques are surface reconstruction methods that adapt the locations of the vertices to better describe the surface features. It is preferred when the subsequent objective is to detect the features of the constructed mesh.
- Decimation. These are bottom-up techniques aiming at reducing the size of the surface representation (mesh). This is done by iteratively removing, collapsing or clustering vertices (Reinhard, 1998, Schroeder et al., 1992), edges (Kim et al., 2002), or faces (Hamann, 1994).
- Refinement. The objective is the opposite of decimation methods.

Although all six classes are applied to height field meshes, refinement and decimation are the only classes commonly applied to the more general surface representations: manifold and non-manifold surfaces. A manifold surface is a representation where an edge cannot be the intersection of more than two facets. Non-manifold surfaces are the most general surface representation.

Because of the wide range of simplification methods, Cignoni et al. (1998) decided to introduce another interesting taxonomy. Unlike the Heckbert & Garland (1997)'s survey, mesh simplification algorithms are not classified according to the type of input surfaces. The goal of the paper is to briefly introduce the six identified classes of algorithms and mainly to compare the faithfulness of the results. Six representative algorithms (one for each class) were implemented to make empirical performance comparisons. The paper focuses on algorithms measuring the approximation error. The proposed classification is:

- Coplanar facets merging. The basic idea is to merge small, almost coplanar triangles and to replace them by fewer facets.
- Vertex/edge/face decimation with error estimations with respect to the step $n - 1$ (local estimation) or initial (global estimation) meshes.
- Re-tiling. Vertices are randomly added to the initial surface and moved to high curvature regions. The initial vertices are progressively removed to get an optimal retiled mesh.

- Energy function optimization (Hoppe, 1996). The cost of each modification is evaluated. The move causing the lowest increase of the energy function is chosen.
- Vertex clustering (Garland, 1999). Close vertices are clustered and replaced by a single representative vertex.
- Wavelet-based approaches. A wavelet representation of the surface is created after a resampling of the mesh. The wavelet decomposition can easily be extended for multiresolution analysis.
- Hierarchical representation: a coarse-to-fine approach (Kobbelt et al., 1999).

Cignoni explains that other classifications may be imagined based on the approximation quality evaluation (local or global, preservation of features), incremental or not, the type of removed entities, the insertion of new entities into the mesh or not, constraints on the computational burden (Boubekeur & Alexa, 2009), the prior objective of the approaches: preserve the mesh topology or select mesh elements for removal; build a minimal error mesh for a given mesh size; or build the minimal mesh for a given error bound. All these aspects are considered in the paper and gathered in a recapitulative table.

Note that the simplification algorithms preserving the surface shapes and features are mostly based on curvature estimation (Boubekeur & Alexa, 2009) or even ridge extraction algorithms (Ma et al., 2015, Meng & He, 2016) as presented in the previous chapter.

Other surveys of simplification methods for specific applications have been proposed (Thakur et al. (2009) for physics-based simulation applications, Pajarola & Gobbetti (2007) for terrain rendering or Payan et al. (2015) for remeshing algorithms improving the regularity of the facets).

With regard to these analyses, it appeared essential to establish a list of criteria that a mesh simplification shall meet for our application (cf. Section 7.2). And, then, the existing approaches are compared to these specific needs to design a customized simplification method.

Although Heckbert & Garland (1997) makes the comment that: "the decimation approach is not so common for height field simplification.", decimation is the only simplification approach that can support with our mesh reduction requirement. Decimation algorithms also have the advantage of being simple. The elements of the mesh that are removed are the main variable in the decimation procedure. One has to choose between

the vertices, edges and faces. Usually, it relies on a priority queue. The removed elements are sorted based on various metrics such as moment-based metrics (Tang et al., 2007), global curvature (Kim et al., 2002), error/distance metrics (Agarwal & Desikany, 1997, Garland, 1999, Heckbert & Garland, 1999, Reinhard, 1998). The first element in the queue is removed and, the queue is updated. The operation is repeated as long as necessary.

The vertex removal procedure (Lee et al., 1998, Reinhard, 1998) is divided into several steps. First, the vertex to be removed is selected; then, the vertex and the connected faces and edges are removed too. It creates a hole in the surface that is filled via retriangulation step. The retriangulation scheme generally emphasises equilateral triangles over elongated ones, the objective being to preserve the regularity of the faces as much as possible. The retriangulation might be done via a Constrained Delaunay Triangulation (CDT) (Reinhard, 1998) or by maximizing a metric such as the aspect ratio (length/width) (Heckbert & Garland, 1999, Schroeder et al., 1992). Figure 7.1 represents the results of a vertex removal on a mesh.

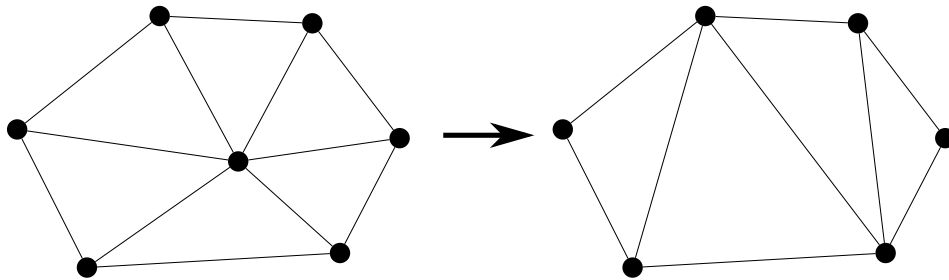


FIGURE 7.1: Simplification by vertex removal.

Edge collapse (Kobbelt et al., 1998) is an alternative to vertex decimation methods. The concept is to move one edge ending vertex towards the other so that an edge disappears and that the mesh size is reduced. Figure 7.2 illustrates three edge collapse types.

The first and third cases differ in the choice of the moved vertex. In the second case of Figure 7.2, both vertices are moved along the former edge. They are classically moved to the middle of the edge. But, other positions can be chosen, for instance, to minimize the cost of the simplification step in terms of distance between the former and updated meshes. Moving both vertices tends to generate more regular facets, which is preferable for later visualization or computations (e.g., feature line extraction). This procedure is similar in a way to vertex clustering where a set of vertices are replaced by a single vertex whose location is carefully selected. Furthermore, it is important

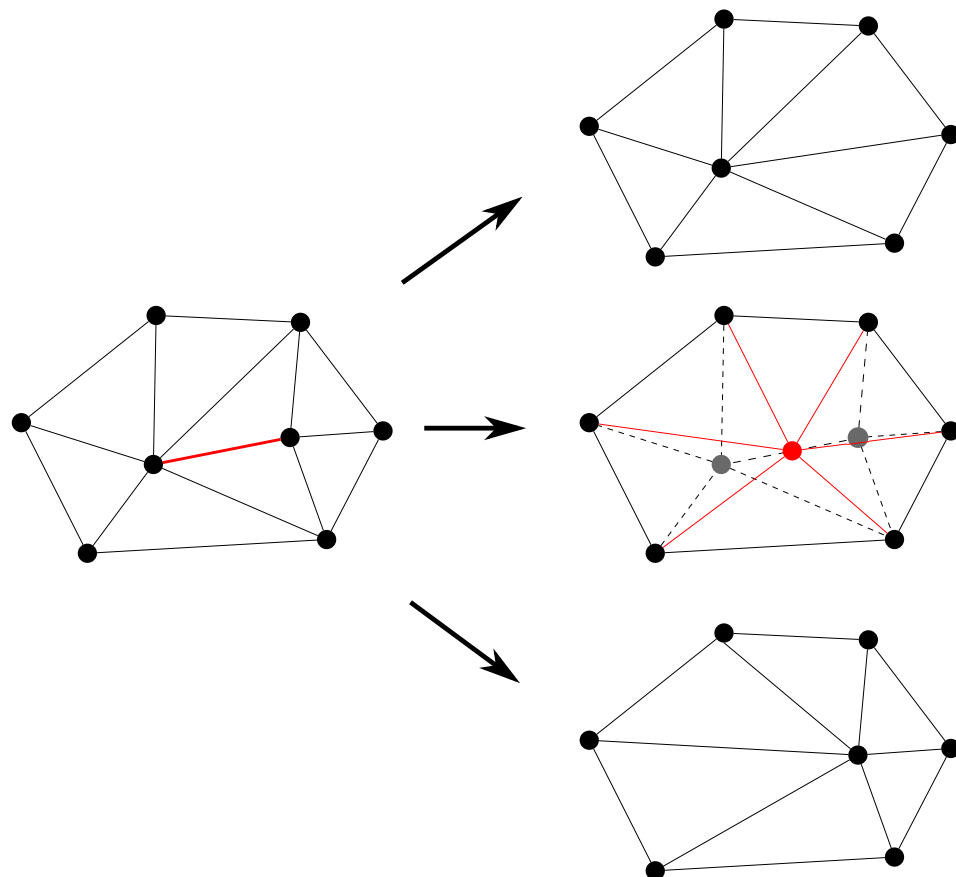


FIGURE 7.2: Three types of edge collapse procedures.

to notice that, unlike vertex decimation or vertex clustering, edge collapse includes no retriangulation step. So the procedure is very fast and simple.

The last possibility to reduce the mesh size is to adopt a face decimation approach. The coplanar facet merging mentioned in Cignoni et al. (1998) may be included in this category. The purpose is to modify the mesh to reduce the number of faces. Hamann presented a different procedure in Hamann (1994) (see Figure 7.3).

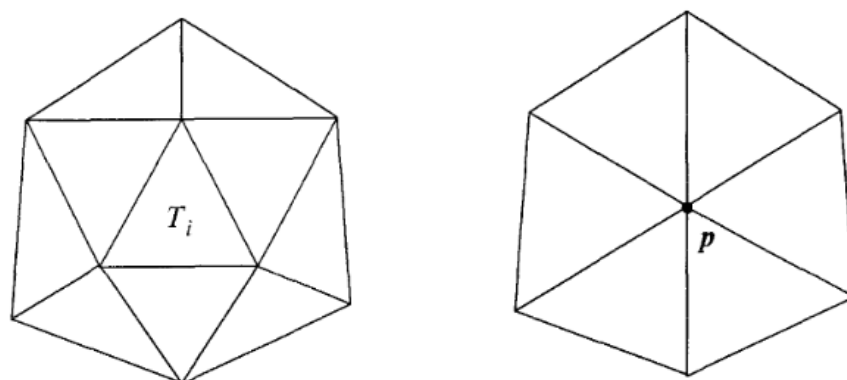


FIGURE 7.3: Principle of a triangle removal algorithm. Drawn from Hamann (1994).

A triangle and its neighbors are removed. A new vertex is inserted and the mesh hole is retriangulated. Finally, an edge swapping step is used to get the hole triangulation to maximise a metric: in this case, the angle weight. This metric is maximal for equilateral triangles.

Another recently presented decimation approach is the tree collapsing (Lee & Kyung, 2016). The concept is to collapse connected acyclic edges. It is very similar to vertex clustering without the complex retriangulation step.

Decimation methods perfectly comply with our simplicity criterion. Although the preservation of the crests would be beneficial, the use of a topology-preserving algorithm would computationally complexify the process. Indeed it requires the computation of faithfulness metrics (curvatures, distances and derivatives). Since no new vertices should be added to the surface, the only remaining possibilities are the vertex removal and edge collapse approaches. If the vertices are not moved, the edge collapse methods tend to create elongated triangles. The underlying problem is that the vertex neighborhood might not be regular, which can skew the curvature values and then the crest extraction. Therefore, vertex decimation is the most indicated algorithm for our application.

Usually, the decimation process stops when the mesh size has reached the objective or when no simplification operation may be made without violating the error bound. Here, the mesh resolution is not an aspect of the mesh that is often considered. The resolution of a mesh is measured by the average edge length. Johnson & Hebert (1998) noticed that the resolution has no real meaning as the length of the edges is not constant due to the uneven distribution of the mesh vertices. The presented algorithm transforms the mesh so that the resulting mesh is a more even representation of the modelled surface. Yet, in our context, the decimation scheme should be controlled by a resolution parameter. Since the average length is not representative of the surface resolution, it must be replaced by a more relevant alternative.

7.4 Proposed mesh simplification algorithm

7.4.1 Description

A vertex removal procedure necessitates the construction of a priority queue. As mentioned in the previous section, the length of the edges is what will define the scale at which the bathymetry is described and the crest lines will be extracted. A naturally inferred sorting parameter is therefore the minimum edge length. The simplification

stops when all edges are longer than a user-defined limit. This criterion enables sorting edges whereas the objective is to design a vertex decimation procedure. The vertex has to be chosen from the two extremities of the shortest mesh edge. In order to maintain as many vertices near the crests as possible, the removed vertex is the deepest. It is most likely that shallow vertices are close to dune crests, so its tends to preserve crests.

Figure 7.4 explains the stages of our decimation algorithm. First, the shortest edge of the mesh is identified (subfigure (b)). Next, the deepest of the two edge vertices is determined (subfigure (c)). The connected edges and faces are removed too (subfigure (d)). Finally, the hole is retriangulated (subfigure (e)).

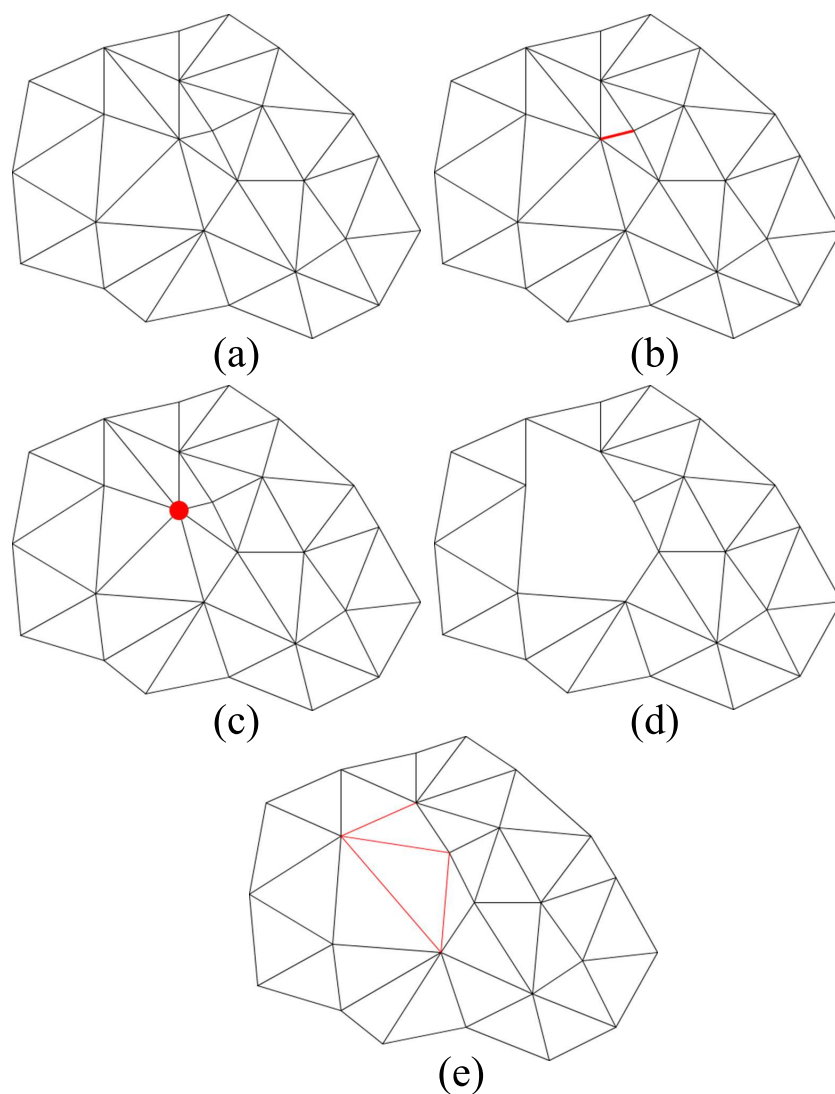


FIGURE 7.4: Five main steps of the mesh simplification algorithm.(a): initial mesh; (b): shortest edge detection; (c): Deepest vertex is picked; (d): removal of the vertex and its connected edges and faces; (e): retriangulation of the hole.

The removal makes a hole in the surface, where the hole boundary is a polygon that has to be retriangulated. The proposed retriangulation process starts by dividing this polygon into two subpolygons. The operation is repeated on the subpolygons until all subpolygons are triangles. Each pair of non-adjacent vertices of a polygon defines a potential subdivision. The quality and regularity of the final mesh depends on this subdivision process. Therefore, the chosen pair is the one that leads to the subpolygons with the maximum aspect ratios. This minimises the distortion of the triangles. The aspect ratio is the ratio between the height and the width of a triangle or more generally of a polygon. The width is the longest edge of the triangle and the height is the distance of the opposed point of the triangle to the longest edge.

An issue that may occur is that the chosen pair of vertices generates a folding of the surface as illustrated in Figure 7.5. Modifications have been brought to cope with these folding cases.

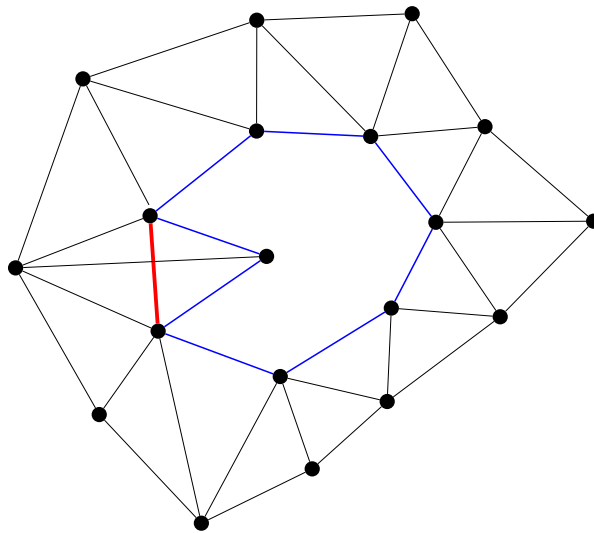


FIGURE 7.5: Forbidden retriangulation.

Besides, our mesh is a bonded surface representation. This means that our surfaces have boundaries and are not closed. Another problem appeared at the borders of the surface. Figure 7.6 shows a case where the selected vertex is on the mesh border. In this case, its removal would reduce the spatial extent of the mesh. If similar removals are undertaken, the mesh might be considerably shrunk. Boundaries preservation is a topic that is rarely examined in the literature (González et al., 2009), but the risk of shrinkage may be problematic in many specific domains. It is the case for us, as a shrunk mesh may cause shortened dune crests or totally remove the closest to the borders of the initial mesh. Corrections were also made to preserve the initial mesh extent and prevent undesired shrinkage.

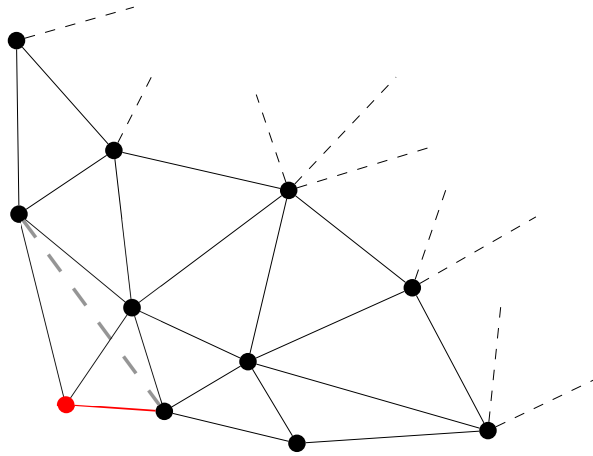


FIGURE 7.6: Particular case at the border of the surface.

7.4.2 Results

Figure 7.7 represents the simplified mesh of benchmark zone 8 with a minimum edge length of 4m. It may be observed that the output tessellation is satisfactory in terms of regularity. Except from some triangles along the mesh boundaries, the triangles are regular.

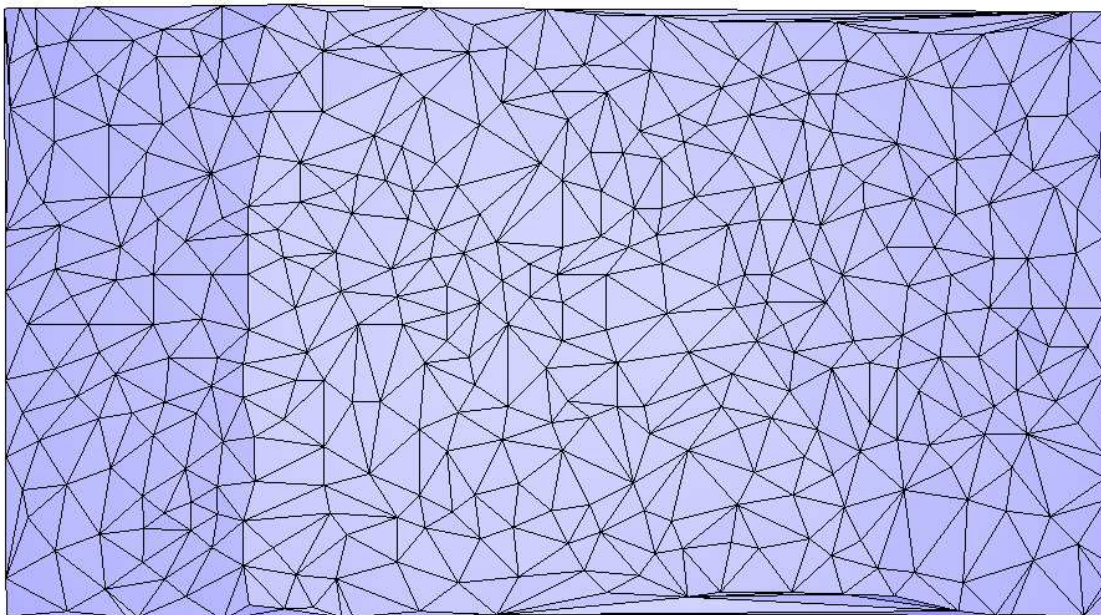


FIGURE 7.7: Simplification output mesh of zone 8 with a 4m resolution threshold.

The coarsened mesh is composed of 396 vertices, 1146 edges and 751 faces against 22311 vertices, 66310 edges and 44000 faces for the initial mesh. Therefore, the time lost to simplify the mesh is, at least, partly compensated by the reduced number of vertices where the curvatures and its derivatives are computed.

Figure 7.8 shows that the ripples present in the initial mesh are no longer visible after simplification. However, the vertices near crests are well-preserved so that the dune crests may still be easily distinguished in the simplified mesh. The choice of removing the lowest vertices has the expected impact.

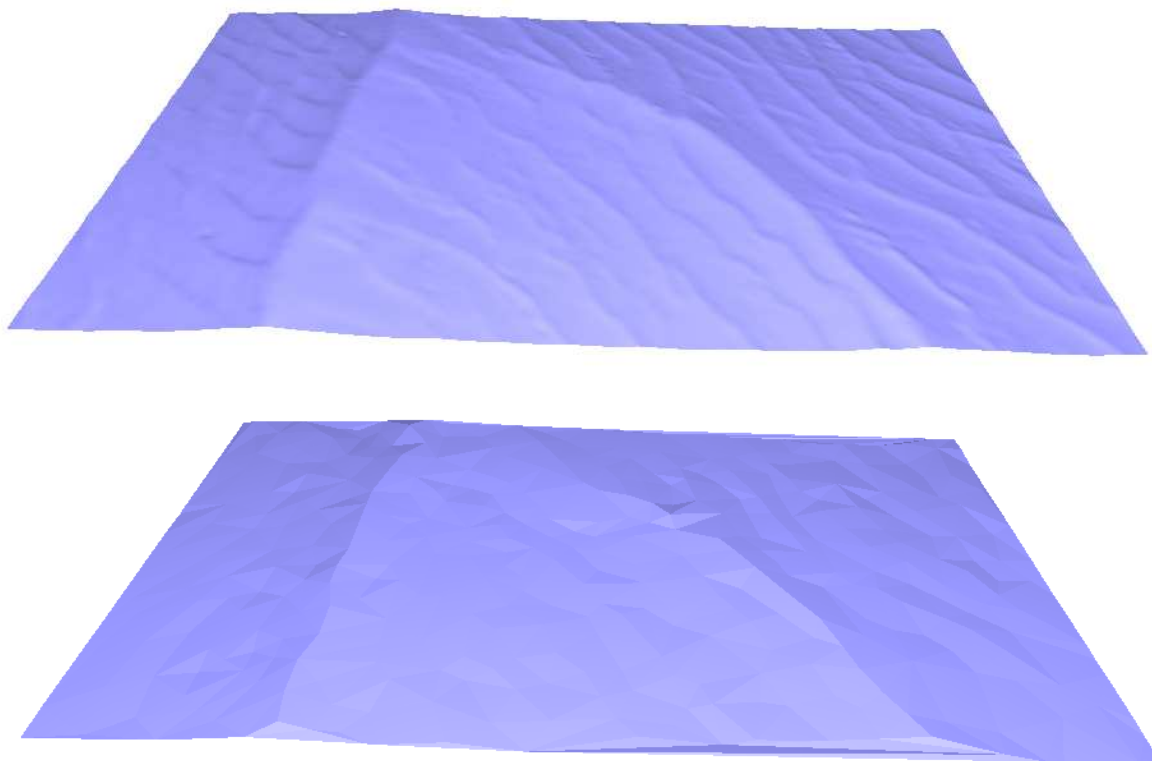


FIGURE 7.8: Comparison between the input and output meshes.

If the simplification did not change the overall running time of our algorithm, the primary objective is to reduce the number of extracted crests by adapting the mesh resolution. The sets of extracted crests on the initial and simplified meshes are shown in Figure 7.9. The number of crests drops from 350 to 34 crests. Although there are only two dunes in this area, their crests are still detected on the new mesh. These dunes, and especially the one to the right of the image (only 1.5m high), are difficult to extract due to their small heights and the presence of ripples. Despite that, they are well-reconstructed. The crest lines corresponding to ripples are only partly reconstructed. The length and height criteria analyzed for the filtering of the set of crests would now be sufficient to discriminate the dune crests from the rest.

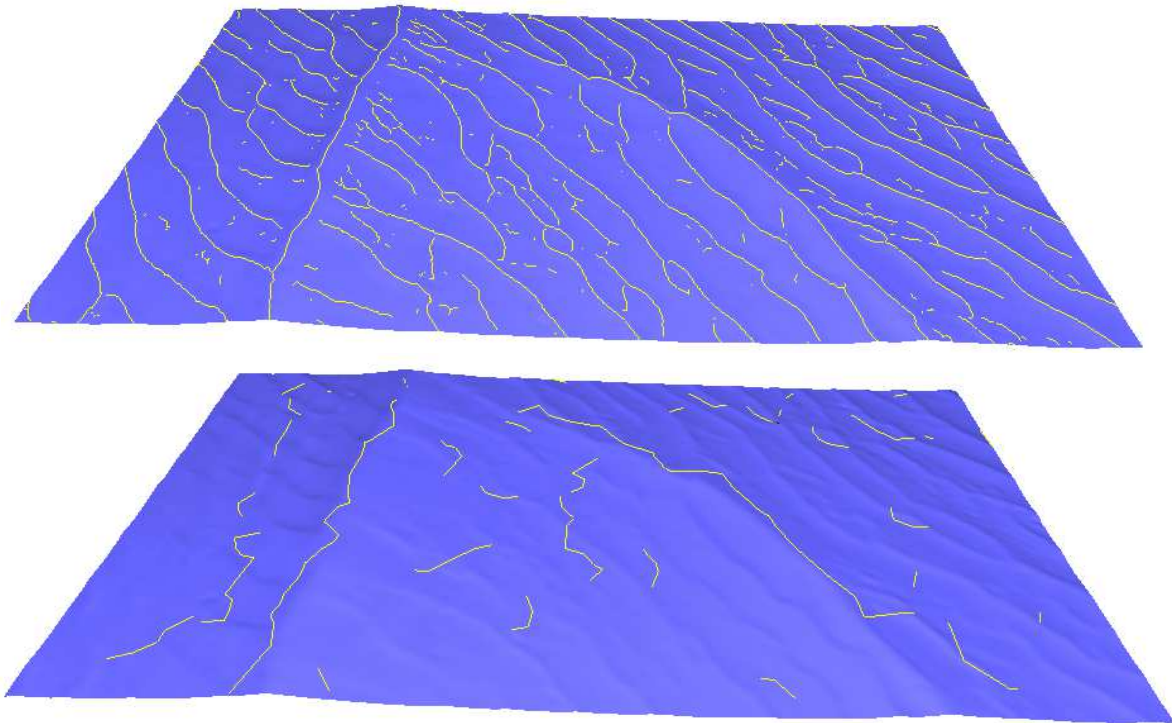


FIGURE 7.9: Sets of extracted lines before and after simplification on zone 1.

Although the filtering through adaptative mesh simplification works for ripples of zone 8, it has to be tested on other areas. The results of the extraction on zone 1 after simplification (Figure 7.10) demonstrates that the simplification dramatically reduces the impact of the artifacts and surface roughness on the crest extraction. Eighteen crest lines are detected on the coarser mesh instead of 515 on the initial surface. In addition, almost all the lines are dune crests and the others are shorter and so may be quickly discarded. The resolution threshold was set to 4m.

The algorithm has been applied to benchmark zone 4 to see how, in a very delicate case due to rocks, the extraction is improved by the simplification of the mesh. The mesh resolution threshold was fixed at 6m. The results of Figure 7.11 shows that the number of crest is trimmed to 22 lines, and most of them are actual dunes or dune parts disrupted by rocks. Other lines still remain but the number of spurious lines is being reduced.

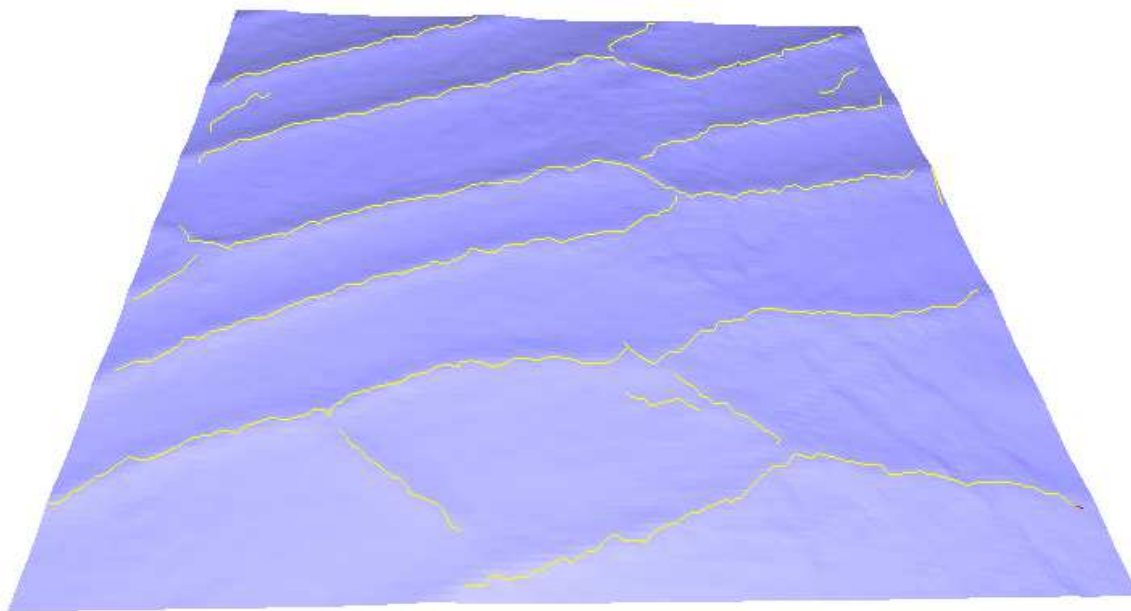


FIGURE 7.10: Set of lines extracted on the simplified representation of zone 1.

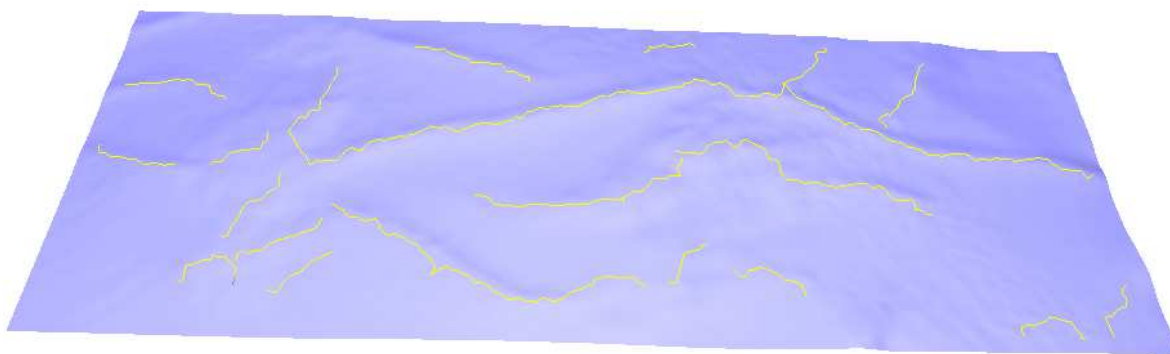


FIGURE 7.11: Set of lines extracted on the simplified representation of zone 4.

The mesh resolution thresholds were selected to smooth out the undesired features and have crest extraction at a scale more representative of the actual dune scale. The presented results are encouraging and confirm that the design of a simplification algorithm in order to filter the set of extracted lines was a better approach than an immediate filtering via crest line descriptors. The algorithm for dune extraction presented in the next chapter integrates the mesh simplification algorithm in order to adjust the resolution and thus facilitate the detection of dune crests.

7.5 Conclusion

Simplification of 3D meshes has been a recurrent problem in many scientific domains and for many applications. Most of them are linked to the multiresolution representation of a surface, its visualization and network transmission. The algorithms dedicated to the reduction of the mesh size are called decimation algorithms. They seek for the optimal mesh, which is related to the notions of mesh size and error metrics. A mesh may be optimal in the number of vertices or edges or faces for a given error bound or in the total approximation error for a fixed mesh size.

However, our main objective was not to build an optimal mesh preserving the surface topology and geometry. Our main objectives were to design a simple algorithm driven by the mesh resolution (unlike most algorithms). No new vertices must be inserted to the simplified mesh in order to easily locate coarse crest lines in the initial surface and the crests should be correctly reconstructed.

In this context, the analysis of the literature led to the development of a vertex decimation algorithm. The results show that the simplification has a real interest. The dune crests are well reconstructed despite the ripples, surface roughness or rocks. The extracted set of lines are reduced and the remaining undesired lines are smaller than the dune crests. The next step is to reconstruct detailed dune crests and to finally extract dunes in the bathymetry.

Chapter 8

Dune extraction algorithm

Contents

8.1	Introduction	174
8.2	Description	174
8.2.1	Mesh simplification	175
8.2.2	Crest extraction	178
8.2.2.1	Approximate crest extraction	178
8.2.2.2	Crest refinement	180
8.2.3	Dune extraction	181
8.2.3.1	Dune selection	181
8.2.3.2	Dune growing	182
8.2.4	Assessment of the dune descriptive parameters	191
8.3	Results	192
8.3.1	Benchmark zone 8	192
8.3.2	Part of SHOM zone 1	193
8.3.3	Periodic dunes	195
8.3.4	Dunes on Ouessant bank	197
8.4	Conclusion	198

8.1 Introduction

One of the principal goals of this thesis is to propose an automatic procedure for the extraction of dunes in bathymetric data. Such an algorithm is necessary to thoroughly analyze dune morphology and dynamics. It would provide an objective framework for the estimation of morphological and dynamical descriptors. Currently, dune extraction and descriptor estimation remain manual. With the automation of this processing, dune specialists could spend more time on valuable work such as the definition of new morphological and dynamical descriptors or even the elaboration of a new classification of dunes more in line with the observed dune diversity.

Our algorithm must be as user-friendly as possible. That is to say that the set of parameters of the algorithm should be small and their tuning must be simple and intuitive. In Chapters 4,5, 6 and 7, the prerequisites for the automatic extraction of dunes have been outlined. The proposed algorithm takes into account the conclusions and findings of these chapters: dune scale, signature, region growing algorithm, crest extraction on seafloor meshes, and resolution adaptation via mesh simplification.

First, the functioning of the algorithm is presented. Then, the results on benchmark and larger areas are shown and discussed.

8.2 Description

The algorithm consists of five main steps that are summarized in the flowchart presented in Figure 8.1. The dune extraction starts with the creation of a triangular mesh. Next, the mesh is simplified in order to adjust the mesh resolution to the dune characteristic scale and, therefore, get a reduced set of crest lines. The aim of the third step is to reconstruct high resolution crest lines that will serve as seed regions for the algorithm. Then comes the growing step. The seeds (crest lines) are grown based on a slope criterion. At this stage, the set of extracted features might still contain features other than dunes. Therefore, a second filtering stage is applied to discard the last undesired features. The last step consists of estimating the morphological descriptors for each dune that could be stored in a database.

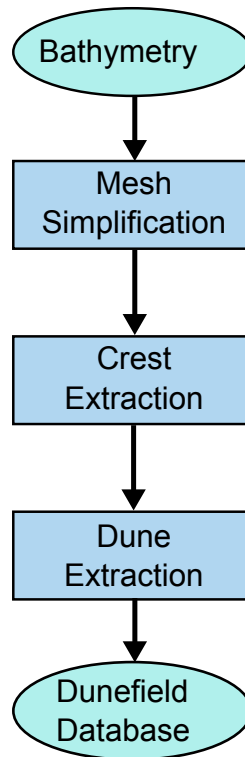


FIGURE 8.1: Main steps of the dune extraction algorithm.

The mesh creation is the first step of the algorithm. The problems related to the processing of bathymetric data (calibration of the acquisition system, issues of artifacts, outliers) and the generation of DTMs with an appropriate resolution were discussed in Section 3.2. The way the triangulated surfaces are derived from these DTMs is presented in Section 4.6. The other steps are described in more detail in the following subsections.

8.2.1 Mesh simplification

The mesh simplification algorithm was introduced and tested in Chapter 7. Here, the objective is to adjust the resolution of the mesh so that it is well-suited for the later crest extraction. Indeed, in Chapter 4, we have learned that the extraction of terrain elements is linked to the notion of scale. Terrain elements exist for a range of scales. If the extraction is directly made on the initial fine-resolution mesh, it is highly probable that seafloor features other than dunes will be extracted. Changing the resolution is an effective way to limit the number of these undesired extractions, particularly of sand ripples and sand waves. These sedimentary structures, though smaller than dunes, have crests geometrically very similar to dunes' (cf. subsection 6.4.3).

Our mesh simplification algorithm is controlled by the length of the mesh edges. Although this is correctly adapted to guarantee a good, later crest extraction, it might not be very convenient for users. One of our objectives is to design an algorithm driven by intuitive parameters, and this resolution parameter requires knowledge of the algorithm to correctly set its value. Consequently, it was decided to replace it by a more intuitive parameter. A way to achieve it is to link the resolution parameter to dune properties. Figure 8.2 explains how this new parameter was conceived.

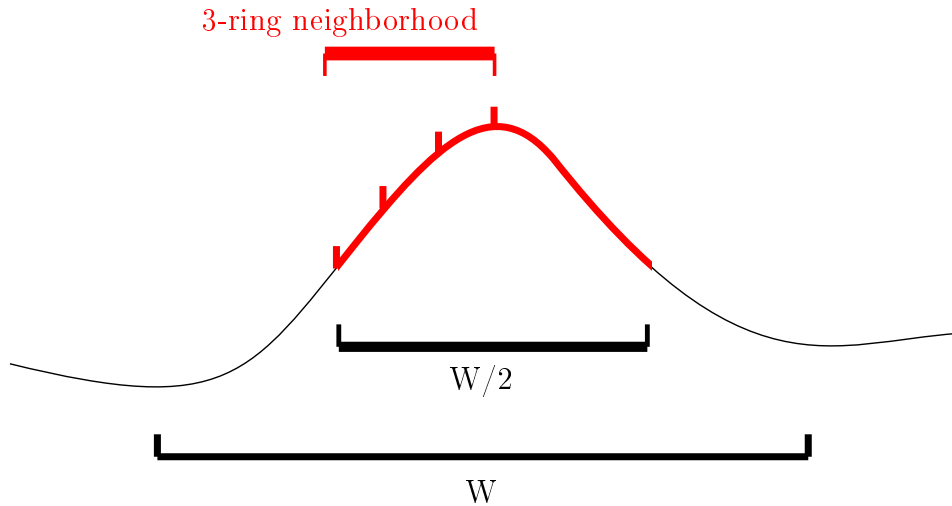


FIGURE 8.2: End condition of the mesh simplification algorithm.

The construction of Figure 8.2 comes from several specifications that appeared essential throughout the thesis. Based on our observations and on the existing dune (sand waves) classifications (cf. Section 2.2.4), the width of the marine sand dunes (height > 1m) is, at least, several tens of meters whereas the wavelength of smaller features is less than 10 meters. A correctly selected neighborhood should be large enough to prevent the detection of sand waves and ripples, but small enough for the fitted osculating jets to recover the morphology of dune crests and therefore facilitate their extraction. Ideally, the neighborhood of a vertex near the crest of a ripple contains vertices belonging to other ripples. Hence, the jet is not adjusted to a terrain that locally looks like a crest as it contains several crests (those of the neighboring ripples). On the other hand, the neighborhood must be local with respect to the dune characteristic scale. That is to say, the jets must be able to faithfully capture the shape of the seafloor near dune crests in order to extract crests as a whole instead of in segments. In addition, an unnecessary large mesh resolution would result in an increase in the running time. In fact, it would take time for the mesh simplification algorithm to generate a coarser mesh.

In order to answer these specifications, the minimum dune width is a parameter that is preferred over the mesh resolution. It is a more suited parameter as a simple visualisation of the dataset is sufficient, even for a non-expert, to set it correctly. In practice, the mesh resolution parameter is used to define when the simplification stops and is connected to the minimum dune width by the following expression:

$$\text{MinimalEdgeLength} = \frac{W}{6} = \frac{\frac{W}{2}}{3}$$

with W is the minimum dune width.

This relationship assumes that the jets should not be fitted on neighborhoods wider than half a dune width. Considering the orders of magnitude of the wavelengths of sandwaves, dune width and the previous comments, this expression seemed to be a good compromise. It will be confirmed in the next section where the resulting sets of crest lines are shown.

Figure 8.3 depicts the simplified mesh of benchmark zone 7 with a minimum dune width set to 60 m.

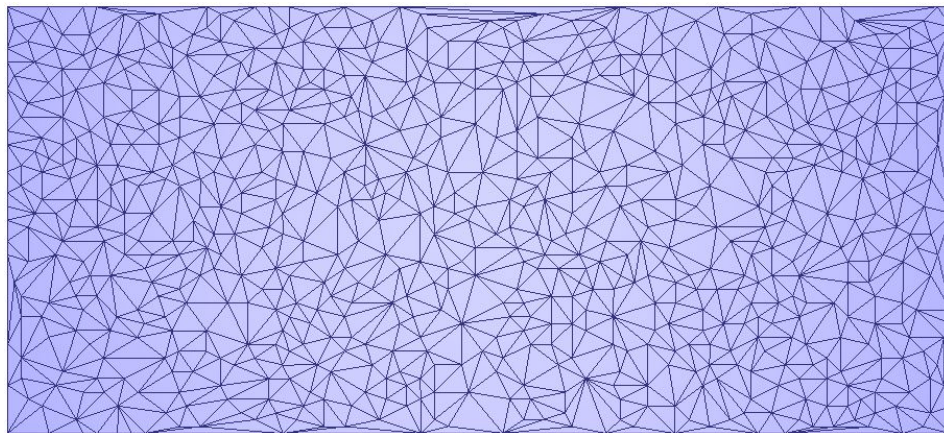


FIGURE 8.3: Output mesh of the simplification algorithm of benchmark zone 7. Minimum dune width = 60 m.

8.2.2 Crest extraction

8.2.2.1 Approximate crest extraction

The results of the crest extraction step on the coarse mesh of Figure 8.3 are shown in Figure 8.4. Note that the crests of the two dunes are identified and approximately constructed, and that the relatively long crest detected in the bottom-left corner of Figure 8.4 corresponds to a structure that could be described as a dune except that it does not satisfy our height criterion. The other crests are also much shorter than those of the dunes. These crests will be easy to discard later using a basic length threshold. Additionally, there are 15 crests that are detected which is low compared to the number of crests generally extracted on fine meshes (cf. Sections 6.4 and 6.5). Without the mesh simplification step, hundreds of "dunes" are commonly obtained (cf. results of Chapter 7 (subsection 7.4.2)).



FIGURE 8.4: Coarse crests detected in benchmark zone 7.

The crest is the most remarkable part of a dune. It is an important indicator of the dune morphology and dynamics. As visible in Figure 8.4, the crests recovered from the simplified surface are rough approximations of the real dune crests. The tracing of the extracted crests is still to be refined.

For this purpose, the mesh simplification algorithm had to comply with a particular specification: the vertices of the simplified mesh are a subset of the vertices of the initial mesh.

This property of our simplification process is illustrated in Figure 8.5. An initial mesh and its simplified version are simultaneously displayed to confirm that no new vertex is inserted in the mesh during the simplification.

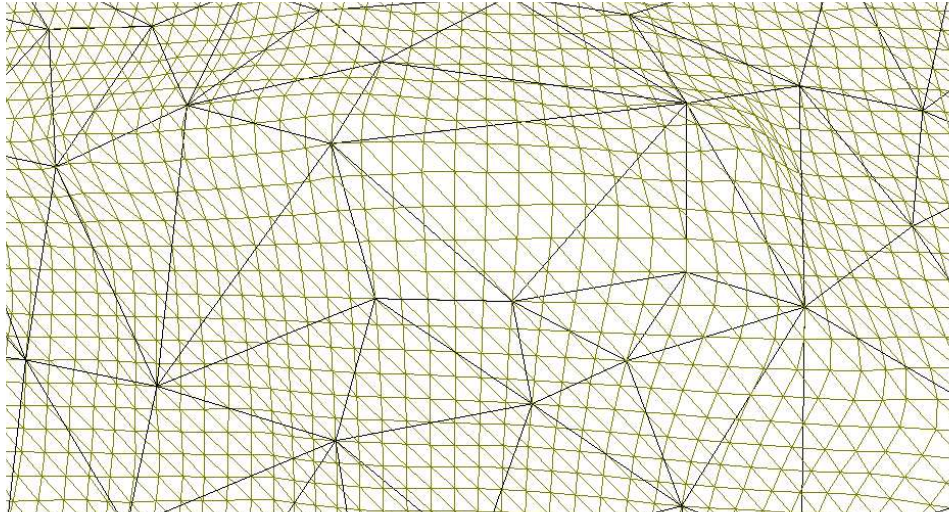


FIGURE 8.5: Link between the vertices of the fine and coarse meshes.

The rough crests are primary approximations of the real crests. They can be used to concentrate the search for fine-traced crests on small areas of the initial mesh. Figure 8.6 illustrates how these regions of interest are defined. The rough crests (green line) cross edges of the coarse mesh. The end vertices of the crossed edges (red dots) are thus close to the crests. Since the ID number of a vertex is the same in the fine and coarse meshes, these particular vertices can be located in the initial mesh. A search radius can be associated to each of these vertices, so that the union of these circles form regions in which dune crests might be found.

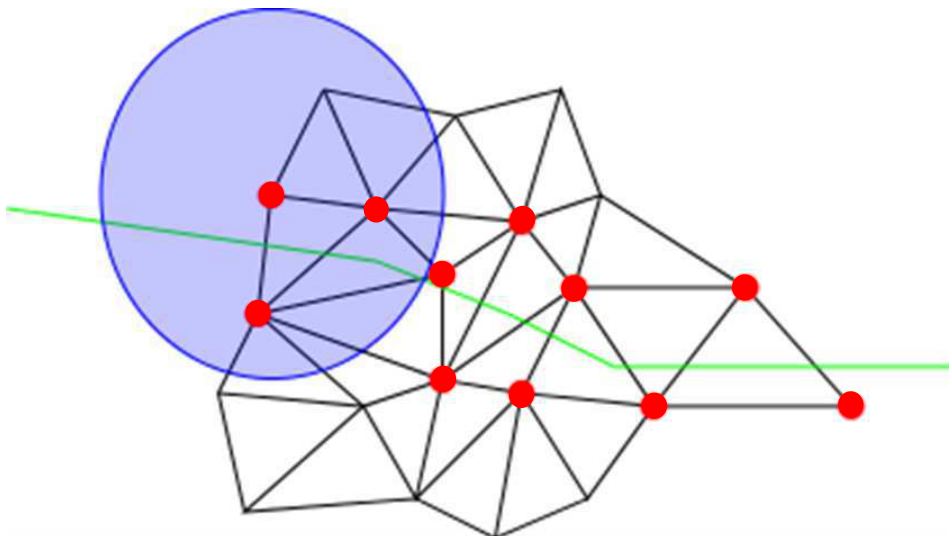


FIGURE 8.6: Definition of the areas of interest for reconstructing fine crests.

The search radius is related to the dune extraction scale. If the minimum dune width is set to 200 m, the vertices within a 100 m distance to the vertices close to crests are gathered to create the potential crest regions. These regions of interest for zone 7 (vertices colored in red) are shown on Figure 8.7. The minimum dune width is set to 60 m again.



FIGURE 8.7: Regions of interest around rough crests on the fine mesh of zone 7.

8.2.2.2 Crest refinement

Once the regions where dune crests are potentially located are identified, new fine crests have to be extracted. This is done using the fitting of osculating jets on 3-ring neighborhoods and the application of the version 1 of Cazals' algorithm in these regions of interest (directly on the fine mesh this time). Figure 8.8 shows the fine resolution crests drawn on top of zone 7 bathymetry. A total of 212 crest lines are obtained in the regions of interest, but the two true dune crests are noticeable for their length. With this crest extraction method, full length dune crests are traced regardless of the steadily decreasing height of the dunes at the extremities; previously the curvature thresholding approach proposed in Chapter 4 failed in recovering the dune tails where the curvature values drop with the height decrease.

The crest regions contain 6000 out of the 8700 vertices of the fine mesh (cf. Figure 8.8). The presence of artifacts in the initial mesh, that are still visible after simplification, explains this relatively high number. On datasets with ripples that disappear in the simplified mesh, the filtering effect of the simplification is more convincing (see case of benchmark zone 8 (Figure 7.9)).

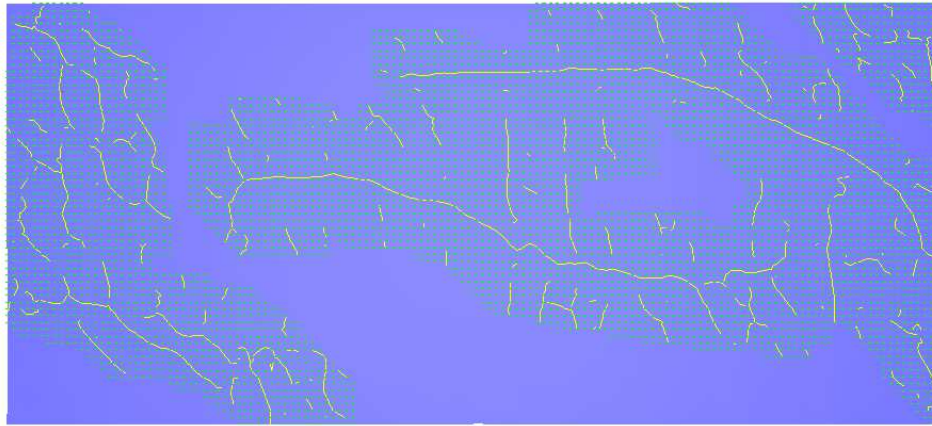


FIGURE 8.8: The set of fine crests included in the crest regions of zone 7. The green dots are the vertices belonging to the crest regions. The yellow lines are the final reconstructed crest lines in these regions of interest.

8.2.3 Dune extraction

8.2.3.1 Dune selection

At this stage, the extracted set of crests describes the seafloor features that have crests persistent at the same scale as dunes. Prior to the feature growing, the features that are too small are discarded. The user is requested to input a value for the minimum dune length. Once more, this parameter is easy to determine if the user has examined the bathymetry before using the algorithm. Crests with a height below 1m are removed too. The filtered sets of crests should now contain dunes exclusively.

This is the case on zone 7 (cf. Figure 8.9). The minimum dune length was set to 150 m and the only two remaining crests effectively correspond to the crests of the two dunes. The other "dune" is removed as its height does not comply with the 1 m (height) criterion. The crests of dunes are detected even though the dunes are small, where the first region growing algorithm based on a curvature threshold presented in Section 4.5 required fine tuning to detecting these dunes. This confirms idea that the transition from DTMs to triangular meshes was a good decision.

It may also be noted that the crests are well and fully reconstructed which was not always the case with the first presented algorithm (Figure 4.20). If features other than dunes were kept, they could disturb the dune growing. In fact, the growth of the seed regions is classically controlled by two mechanisms. The first is that it stops when the boundaries of two features meet. The second stopping condition is usually set via

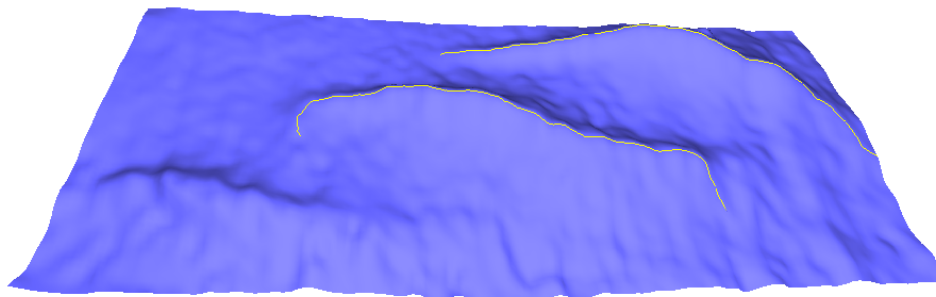


FIGURE 8.9: Final set of dune crests on benchmark zone 7 with a $VE = 20$.

the thresholding of one (or more) chosen geomorphometric parameter. As said before, a slope threshold was assessed adequate for dune growth.

8.2.3.2 Dune growing

Now that the dune crests are extracted, the crests are used as seed regions for the dune growth. The Lee and Stoss sides of a dune may have very different properties. For instance, this is the case for asymmetric dunes or barchan dunes for which both dunes sides are not alike (slope, volume, width, *etc.*). In order to make the distinction between the two sides, different labels are allocated to vertices according to the side they belong to. Once the vertices on both sides of the dune crests have been labeled, the upstream and downstream boundaries of the dunes are initialized. The initialization in the case of zone 7 is illustrated in Figure 8.10. In this figure, the yellow and red lines are the upstream and downstream borders of the dunes. They surround the (black) crest lines. These boundary lines are the initial regions input in the growing algorithm. The growth will make them move until they match with realistic dune boundaries.

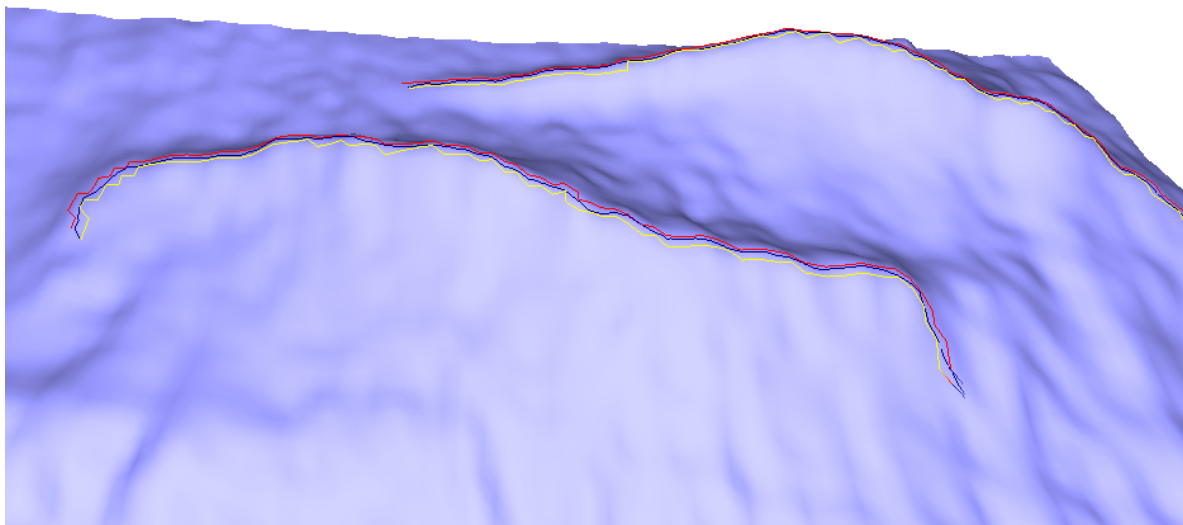


FIGURE 8.10: Initialisation of the Lee and Stoss face boundaries for zone 7.

In Chapter 4, it was noted that the dune sides are characterized by their slope, but the tuning of such a slope threshold turned out to be very empirical. It was also impossible to perfectly recover all the dunes using a single, global slope threshold. In particular, problems have been identified for asymmetric dunes or dunes standing on banks. This was predictable considering dune diversity of shape.

Therefore, a new way to grow the dunes has to be developed. It will still be based on the measure of slope but it is adapted for each dune and even for each dune side. To only consider the component of slope in the direction of the dune sides seems judicious to prevent overgrowing of the dunes due to other terrain variations.

Figure 8.11 confirms that even when the base terrain, on top of which the dunes lie, appears flat (benchmark zone 11), it is not the case. Our vision of the terrain is often biased because of the VE (VE=1 on Figure 8.11). The comparison between the total slope vectors (yellow segments) and the vectors¹ (blue segments) pointed towards the extracted dune crest (green line) shows that using the total slope is not relevant as it does not indicate that you are on a dune side. Therefore, applying a threshold on the total slope is inappropriate. In the end, it was decided to base the growth only on the slope component induced by the presence of a dune and nothing else.

1. determined using the method explained in the following

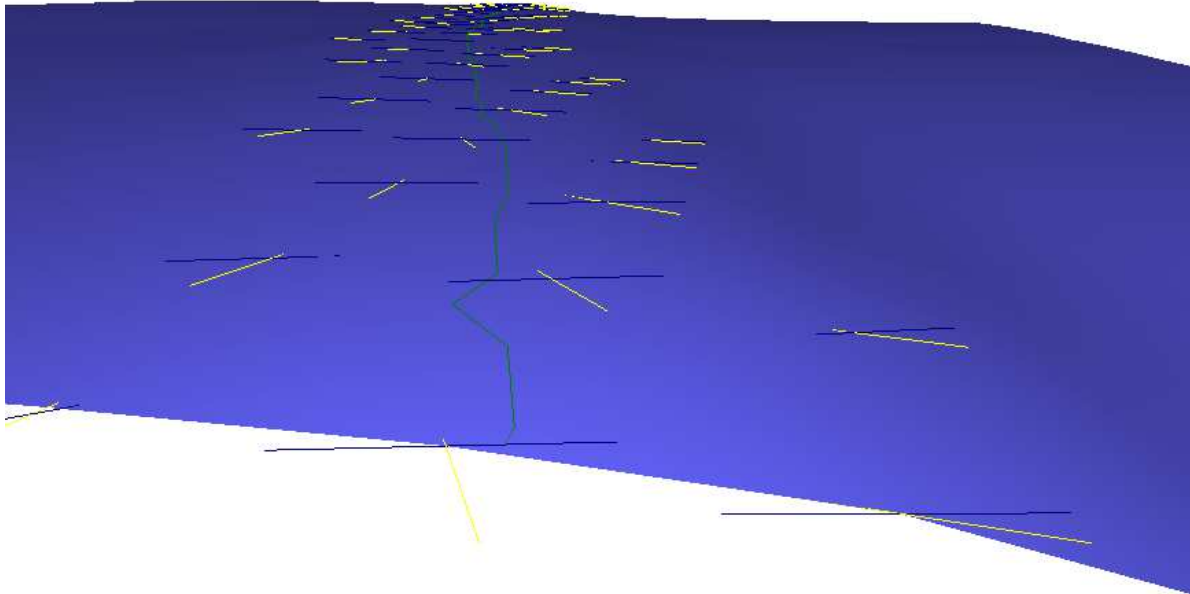


FIGURE 8.11: Comparisons between the direction of the slope vector and dune side direction for a dune on a bank.

Only keeping a specific component of the slope vector requires knowing the direction (of the dune sides, here) at every vertex tested during the growth process. The procedure developed to estimate this direction is depicted on Figure 8.12.

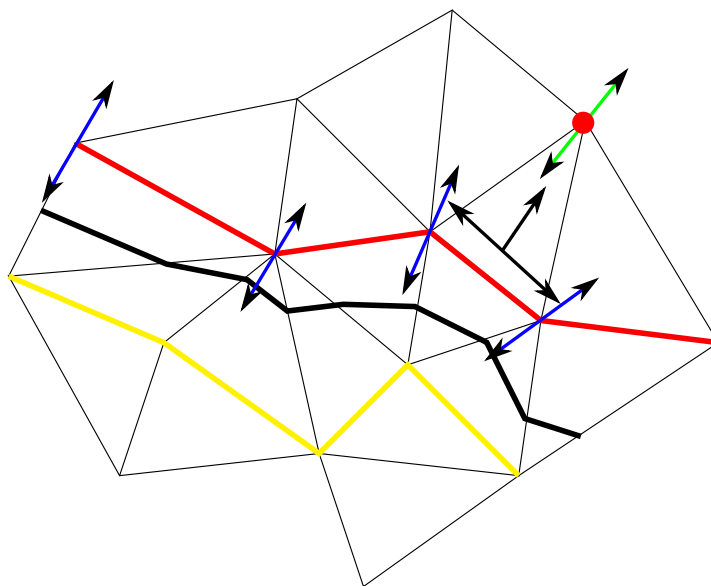


FIGURE 8.12: Propagation of the information about the local orientation of the dune sides.

When a vertex (red dot) is tested for growing, the direction of the dune side (green vector) at this vertex is estimated from the directions at the neighboring vertices. It is calculated by taking the average of the directions (blue vectors) of the neighbors that already belong to the dunes.

At each vertex of the initial dune boundaries (red and yellow lines in Figure 8.12), the minimum principal direction (t_{min}) is supposed to indicate the direction to follow in order to get closer to the crest. However, this principal direction and the direction towards the crest become uncorrelated when a vertex is far from the crest. The minimum direction is a good proxy of the dune side direction but its validity is related to the size of the jet fitting neighborhood. The neighborhood should be wide enough to contain vertices on both sides of the crest, but, if set too large, the neighborhood includes information other than just the local direction of the crest. Hence, problems occurred where the dune crests flattens, in particular at the extremities of the crests. This appears logical as the crests, there, are not as sharp feature lines and the orientation estimation is, therefore, not as reliable¹.

Instead of deriving the dune side orientation for the vertices of the initial boundary lines (blue vectors in Figure 8.12) from the minimum direction around crests, it was directly estimated from the direction of the segments of the crests. The calculation is explained in Figure 8.13. The values of dune side direction are first computed at the vertices of the dune boundaries (red vertex in Figure 8.13). For all of these vertices, the directions perpendicular to the immediate crest segments (blue vectors) are computed. The average of these vectors (green vector) is taken as approximation of the local dune side direction. Then, the dune side direction is propagated to the surrounding vertices during the growing process as described previously (cf. Figure 8.12). The resulting crest directions obtained for one of the dunes of benchmark zone 7 are visible in Figure 8.14. It can be seen that the determined directions (yellow segments) are coherent with what could be expected. The dune crest is represented by the red line. The directions follow the crest orientation changes, in particular, at the dune extremities.

1. The extreme case occurs at umbilics where no principal direction may be defined (cf. definition in Section 5.2).

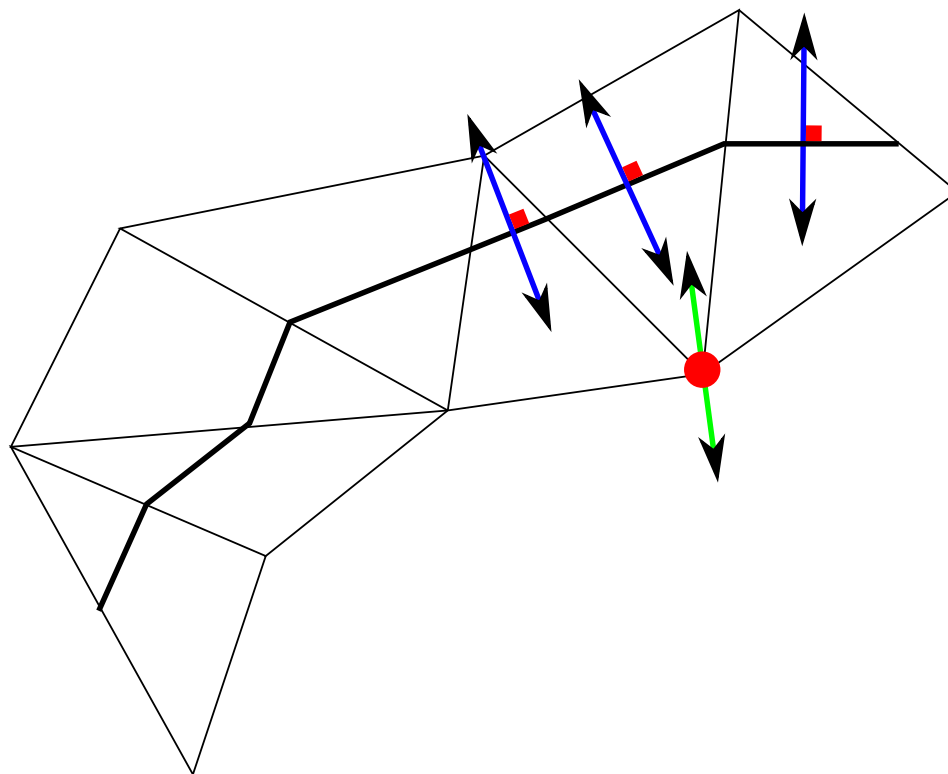


FIGURE 8.13: Initialisation of the direction of the dune sides from crest segments.

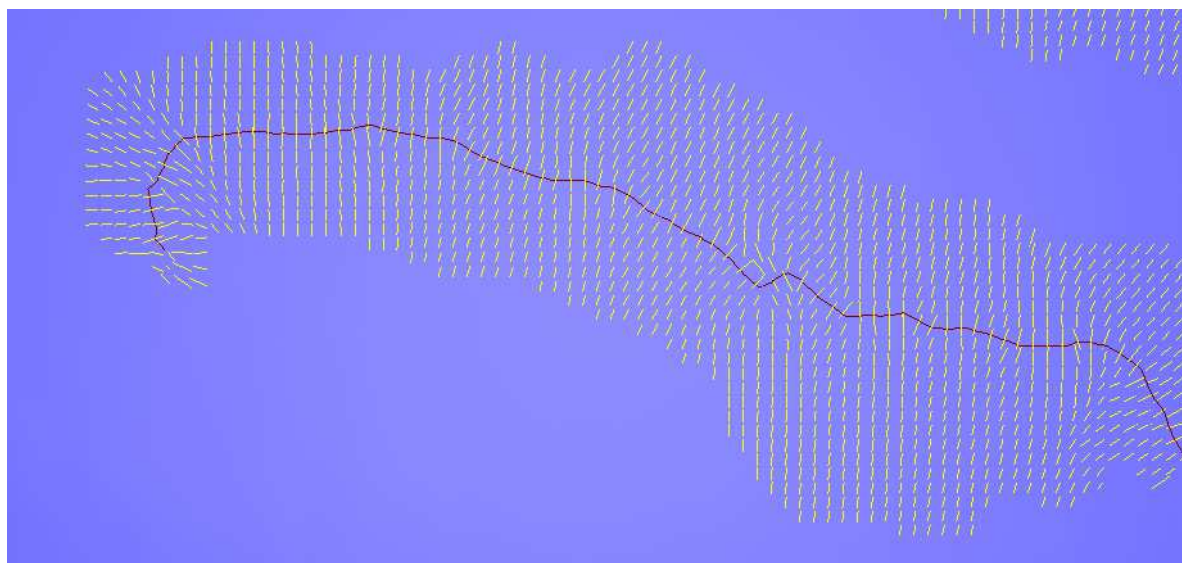


FIGURE 8.14: Results of the propagation of the directions of the dune sides.

The estimation of the direction towards the crest is useless on its own to define a stopping condition of the growing process. Indeed, a slope threshold must be determined. As described before, it is recommended that this parameter is data-driven so that the growing process is adjusted differently for each dune side.

In order to judiciously determined a slope threshold, it is essential to closely observe dunes. A compilation of dune profiles is provided in Figure 8.15. The bathymetric profiles (perpendicular to the crest of dunes) show how the bathymetry changes along the flanks of dunes. A panel of dune types was selected in order to determine a way to set a slope threshold adapted to most cases.

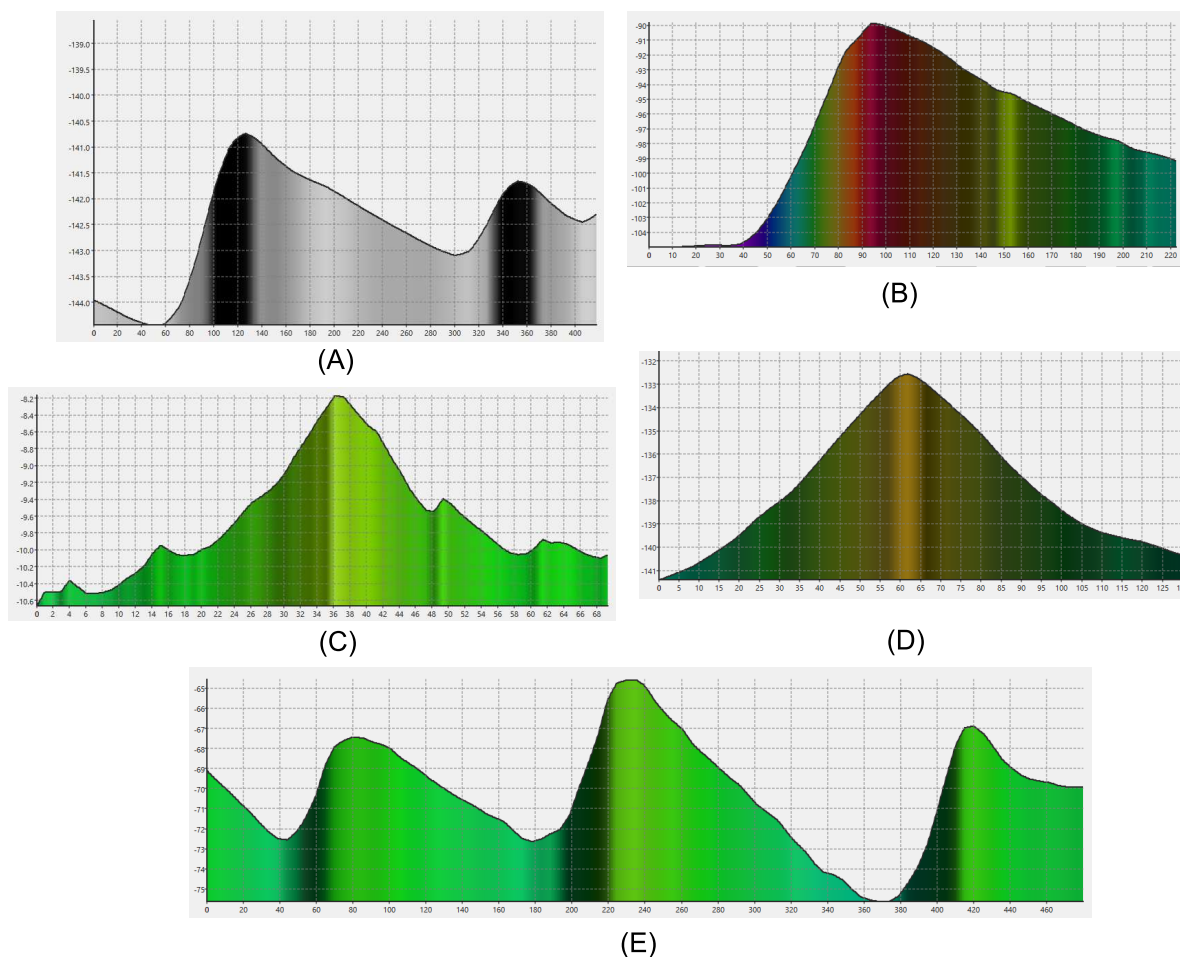


FIGURE 8.15: Observations on the slope of the dune sides. Subfigures (A) to (E) respectively represent the bathymetric profiles of asymmetric dunes, a barchan dune, a dune with superimposed ripples, a trochoidal dune and asymmetric dunes on the flank of a sandbank. The vertical axis corresponds to the depth in meters and the x-axis to the distance along the profile.

In the examples of Figure 8.15, it can be seen that, when dunes are close and parallel (sawtooth-like profiles: subfigures (A) and (E)), the delineation of the boundaries of the dunes seems obvious. The fact that the growing process stops when two dunes meet is sufficient to deal with these cases. But, for the others, the question of where to put the boundaries is not as clear. This is why the manual processing is often limited to the tracing of the crests.

In all cases, it appears that the seafloor is less sloping at the crests. The slope increases and varies along the sides and gently decreases near the toes. Therefore, the slope threshold was firstly initialized at the vertices surrounding the dune crest (vertices on the yellow and red lines of Figure 8.12). In each of these vertices, the threshold is equal to the the slope in the previously-defined direction towards the crest. Similarly to the direction propagation, the slope threshold is calculated as the average of the values of the threshold of the neighboring vertices already belonging to the dune. This method for setting the threshold was inspired by the fact that the slope in the direction of the crest is gentler at the dune crests and toes.

The results on benchmark zone 7 using this method are shown in Figure 8.16. It can be observed that the two dunes are overgrown. This is due to the fact that the initial slope threshold values (at the seed vertices) are nearly null. If the mesh resolution was coarser, the initial vertices would be further from the crest (flat seafloor) and more on the flank (higher slope). Hence, the overgrowing effect would be curbed.

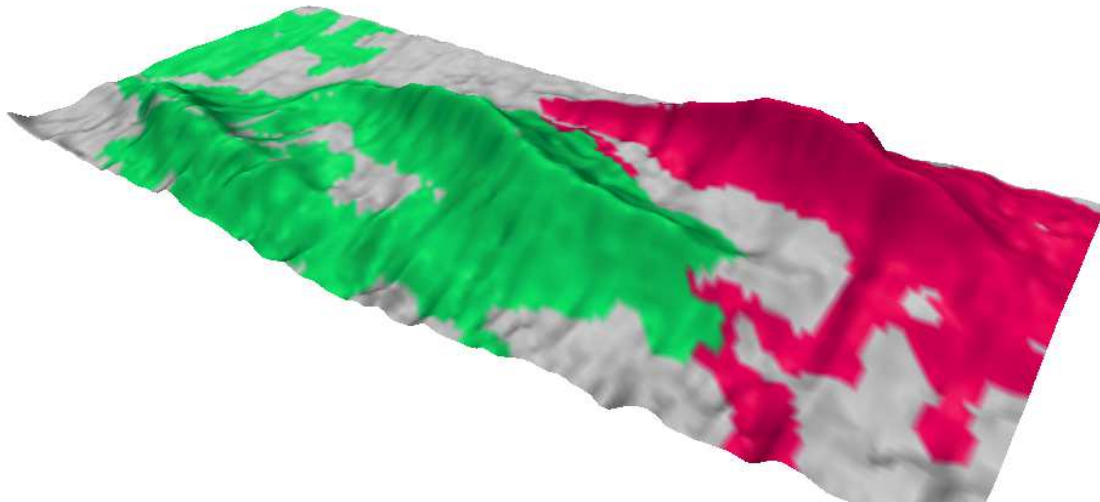


FIGURE 8.16: Extracted dunes when setting the threshold from slope near the crest for benchmark zone 7. $VE = 20$.

In order to avoid this overgrowth, the values of the slope threshold should be higher. The chosen solution was to initialize it at vertices further from the crest than the initial boundary lines (yellow and red lines in Figure 8.10). To do so, the dunes are grown until all the vertices of the boundaries of the dunes have a slope higher than a given value:

$$MinSlope = \frac{1}{Width}$$

The users are already asked to set a minimum dune width and the minimum dune height is arbitrarily set to 1m. This yields a minimum slope value of the dune sides, *MinSlope*. This value is smaller than the slope on most parts of the dunes except from the crest and toes. After the pregrowing step, the slope threshold is determined at the dune boundaries and propagated as described before.

This modification is sufficient to prevent the overgrowth of the dunes regardless of the dune type and mesh resolution. The new results obtained with the modified growing process for benchmark zone 7 are shown in Figure 8.17. This time the extracted dunes are not overgrown and meet the expectations.

As already said, the manual extraction of dunes is generally limited to the crest delineation as the delineation of the toes is very uncertain in many cases. Consequently, there is no manual reference of entirely-extracted dunes and no comparison between the manual and automatic extraction processes can really be made (except for crests). In this context, it is important to note that the automatic extraction and the tuning of the slope threshold are empirical and their validity cannot be checked. It is only possible to visually qualify the resulting extractions.

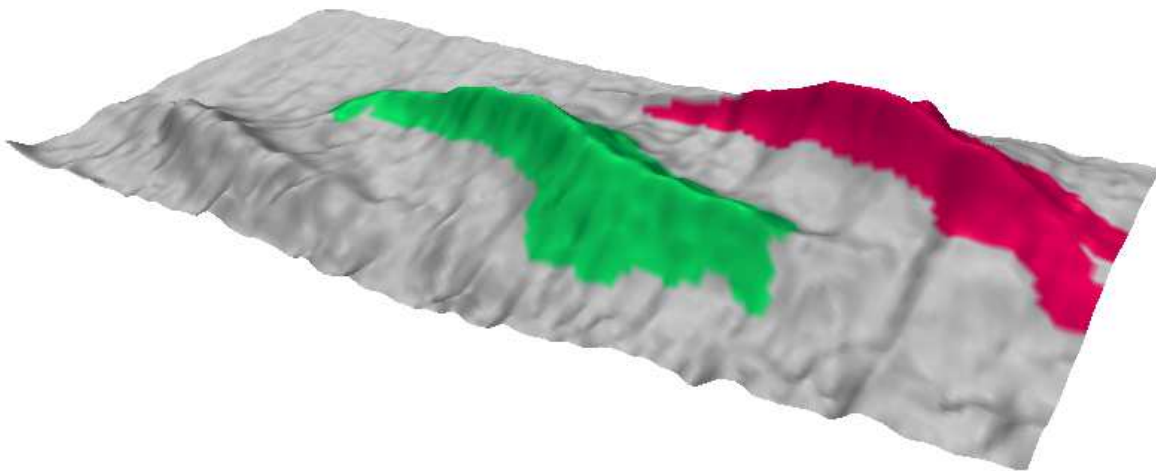


FIGURE 8.17: Results of the dune extraction algorithm on benchmark zone 7.

A final modification was implemented to cope with the potential seafloor variations along the dune sides. For instance, in the case of a mesh with a 1m resolution, small variations of the seafloor (*e.g.*, in Figure 8.15, sand ripples or waves (subfigure (C)) or other variations (subfigure (B),(E))) may be present in the mesh and cause the growth to stop. In order to prevent this undergrowth, a smoothed slope is estimated prior to the growing process.

At each vertex, the smoothed surface normal is determined as the average of the face normals within a 5 meter radius from the vertex. The size of the radius was defined from the maximum wavelength of the sand waves of 10 m. Figure 8.18 illustrates how the smoothed normals are calculated.

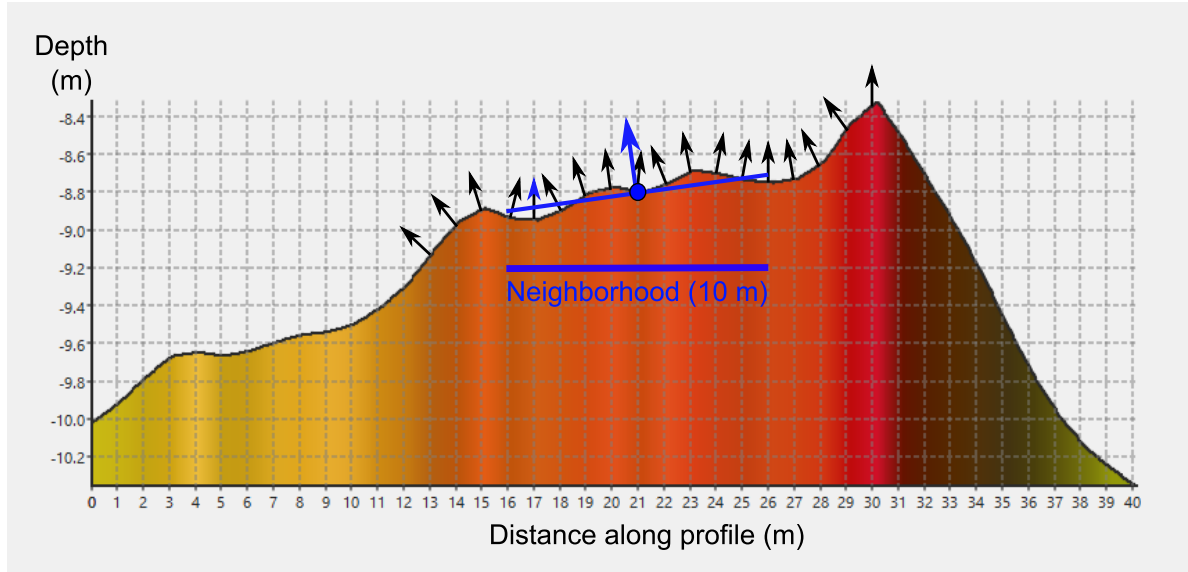


FIGURE 8.18: Estimation of smoothed surface normals for an improved growth.

Although the use of a smoothed slope was not necessary for dunes of benchmark zone 7, its importance is illustrated in subsection 8.3.1.

To sum up, the growing process is controlled by two stopping conditions. A new vertex $V \in \bigcup_{V_i \in d} 1\text{-ring}(V_i)$ (belonging to the 1-ring neighborhood of a vertex already belonging to a dune d) is added to this dune if:

- This vertex V does not already belong to any dune.
- $\langle \overrightarrow{S_{smooth}}(V), \overrightarrow{DirC}(V) \rangle > T_s(V)$,
with $\overrightarrow{S_{smooth}}(V)$, the smoothed slope at vertex V ; $\overrightarrow{DirC}(V)$, the unit vector indicating the direction towards the dune crest and T_s , the propagated slope threshold. \langle, \rangle is the inner product on \mathbb{R}^3 .

The algorithm stops when there is no vertex meeting these two criteria left.

Even though the growing process is empirical, it has the advantage of taking into account the specifics of each dune (e.g., differences between the Stoss and Lee sides), the situation of a dune (e.g., located on a flat seafloor, on a sloping seafloor, on a bank, *etc.*) and the mesh resolution. Two similar dunes will be extracted in a similar way which is not the case with the manual extraction. This relative objectivity will prove

essential to study the dynamics of dunes. The automation is also repeatable so that a same dune will also result in the same extraction.

8.2.4 Assessment of the dune descriptive parameters

Once dunes have been extracted, their morphology can be quantified. The estimation of the morphological descriptors is straightforward. Actually, it is more difficult to clearly define the descriptors than to calculate their values. The morphological descriptors currently estimated by the algorithm are:

- the length;
- the widths of the Lee and Stoss sides;
- the height;
- the volume;
- the asymmetry.

More attributes could be added to this list. But, at first, the values of the basic attributes should be calculated on many datasets in order to determine whether or not they are sufficient to distinguish the dune types and propose a new classification. Additional attributes, then, may be considered if needed.

The estimated values of the selected morphological descriptors for the extracted dunes of benchmark zone 7 are given in Table 8.1. The extraction of these dunes is particularly difficult because of their dimensions (the two dunes are small). This is confirmed from the height values as they are close to the minimum 1m height. In addition, the extraction is made difficult by the presence of artifacts in the bathymetry. Yet, the algorithm is capable of extracting the dunes correctly and to estimate values of the morphological descriptors coherent with those that can be estimated manually.

	Length (m)	Lee side width (m)	Stoss side width (m)	Height (m)	Volume (m ³)	Asymmetry
Dune 1	353	17	30	1.1	4140	0.99
Dune 2	249	40	72	1.4	4144	0.97

TABLE 8.1: Estimated morphological descriptors for the two dunes of zone 7.

8.3 Results

The goal of this section is to confirm the behaviour of the algorithm not only for benchmark zone 7, but also on larger areas, other dune types and different dunefields. It is important to mention that the minimum width and length values required by the algorithm were determined by examining the bathymetry, and the setting of these parameters is rather flexible. That is to say that the results are little influenced by their values as long as they are representative of the dimensions of the dunes to extract.

8.3.1 Benchmark zone 8

One of the main concerns when designing this new algorithm was to account for the potential presence of ripples in the dataset. This case is typical since, in shallow areas², sand ripples are often superimposed on dunes. In the algorithm, the impact of the sand ripples on the crest extraction is limited by adapting the mesh resolution and the proposed solution to minimize their impact on the growth consists in using smoothed slope values.

In order to ensure that these modifications had the expected influence, the algorithm was tested on benchmark zone 8. The results of the extraction algorithm on this zone are represented in Figure 8.19.

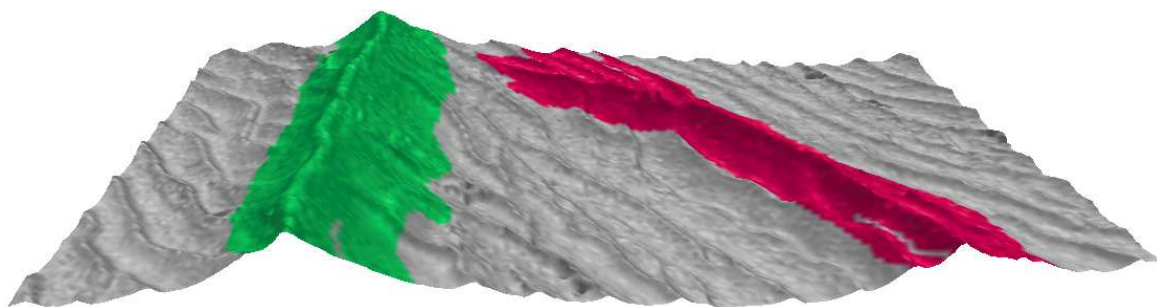


FIGURE 8.19: Dunes extracted in benchmark zone 8.

It can be observed that the algorithm detects only two dunes despite the presence of numerous ripples. The extremity of the fuchsia dune closer to the green dune is a delicate case to handle. Indeed, at this end, the dune splits into several smaller branches

2. This is particularly true for the Belgian data where the seafloor is generally a mix between sand banks, dunes and ripples.

(ripples). The algorithm adds these branches to the dune but not the neighboring ripples. There is not a unique way to delineate the dunes in such cases. What can be said is that the results of the algorithm for this dune and this area is not absurd. To conclude, these observations indicate that the algorithm is capable of dealing with ripples and that its results are reliable in the case of ripples.

8.3.2 Part of SHOM zone 1

The algorithm presented in Section 4.5 gave satisfactory results on SHOM zone 1; this zone was interesting, as manually drawn crests are available for this dataset. The original algorithm had difficulties to correctly recover the full extent of the small dunes in this area (~ 1 m high and ~ 150 m long), but the extraction of this type of dunes is "closer" to what is expected with the new algorithm than with the original one (cf. Figure 8.17). Overall, the first algorithm worked well³ on zone 1 so that another part of the area was selected to compare the new algorithm with the original, and the manual processing.

This area is shown on Figure 8.20 (white rectangle in subfigure (a)). Note that this area is much wider than the benchmark zones (Spatial extent: 2500×1200 m). The red and white crest lines in subfigures (b) and (c) are respectively the crest lines obtained manually and by the new algorithm.

In subfigure (b), the results of the original algorithm are illustrated. Each color corresponds to a dune. It may be noticed that the extracted dunes are rather good except for extremities. The dunes are not as high at the extremities so that the curvature and slope values are lower there. The result is that the dunes are not fully grown at the extremities.

Subfigure (c) displays the extracted dunes with the new algorithm. It can be noticed that the extraction of the long dune at the bottom of the figure is better with the new algorithm. In fact, the dune is further grown at the extremities so that the dune is entirely extracted.

Furthermore, note that the crests drawn by the new algorithm and manually are almost identical in most places. The extraction of the dune at the top of the image is not as good. At the left extremity, the algorithm creates two small crests when the manual extraction says there is one long dune (not three).

3. see subsection 4.5.2 for the comparisons with the manually-traced crests.

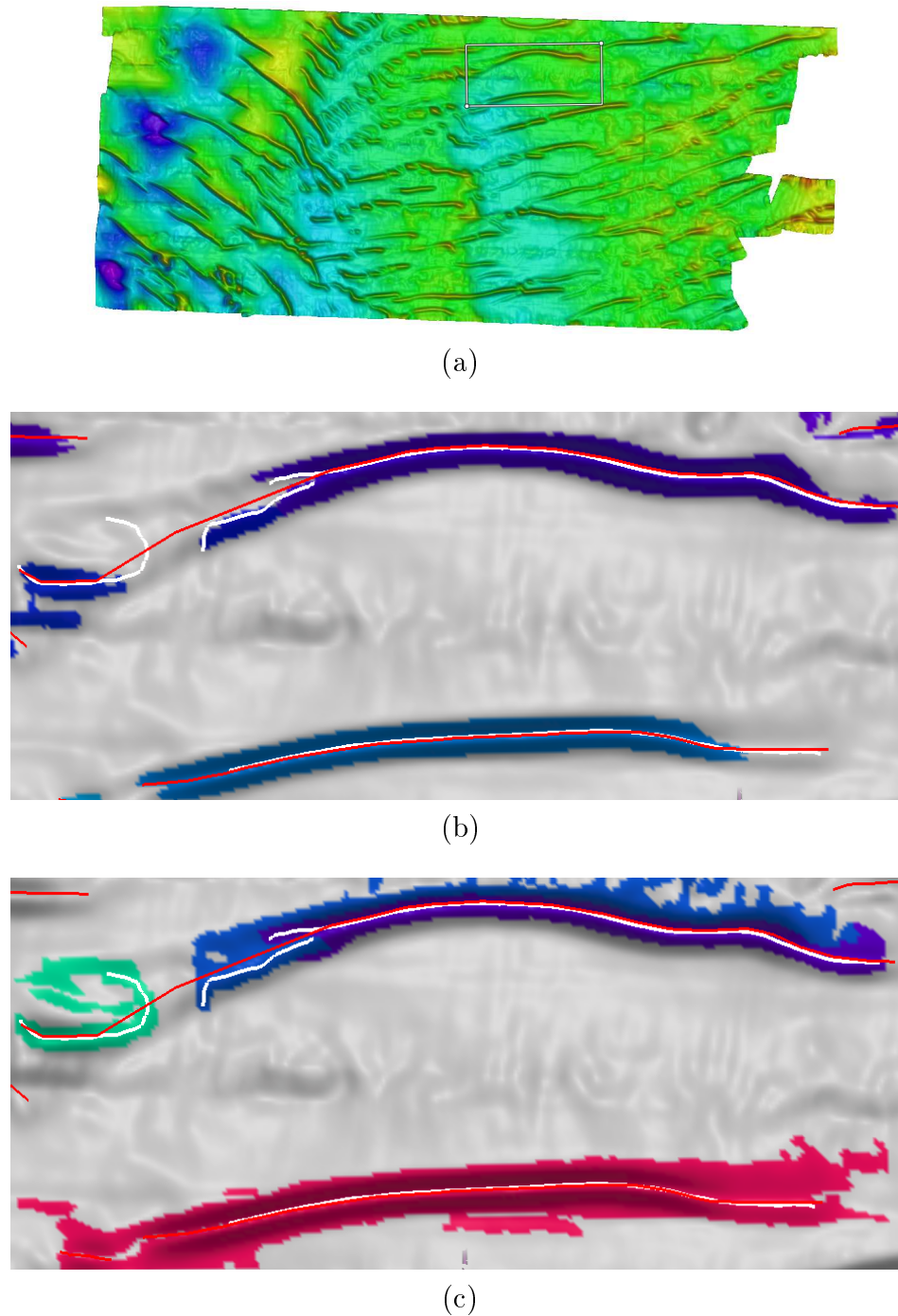


FIGURE 8.20: Comparisons between the new algorithm, the one presented in Chapter 4 and manually extracted crests. (a): Location of the area in SHOM zone 1; (b): Results of the first algorithm (c): Results of the new algorithm.

Yet, if the blue and purple dunes (extracted by the algorithm) in subfigure (c) were merged, the total dune would be a good approximation of the real dune. These dunes, especially the top one, are special in the sense that some parts of the crests are not higher than 0.5 to 1m above the rest of the seafloor. And, their width is approximately 250 m.

Therefore, the automatic detection of this dune and the extraction of its boundaries is challenging.

Despite the specifics (spatial extent, low height dunes, artifacts in the data) of this dunefield (SHOM zone 1), the new algorithm performs, at least as well as the original one that worked well on this area.

8.3.3 Periodic dunes

The capacity of the algorithm to properly extract periodic dunes had to be checked since it is a classical type of dune patterns. A $1\text{km}\times 1\text{km}$ region of SHOM zone 1 was selected for this test. The location of the selected patch (white square) in SHOM zone 1 is visible on Figure 8.21. The bathymetry of this region is composed of close, parallel dunes.

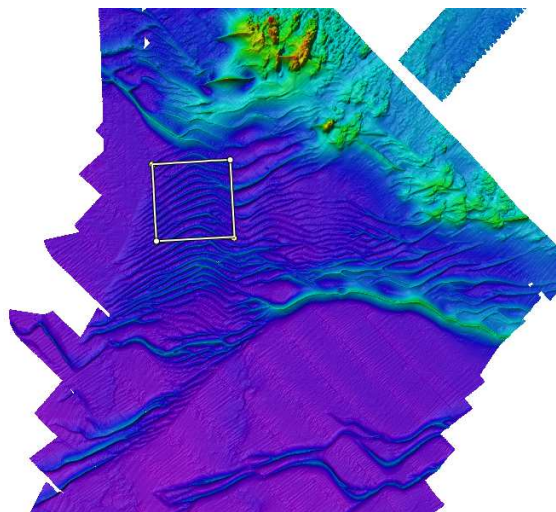


FIGURE 8.21: Location of the selected dataset in SHOM zone 1.

The results of the automatic extraction are shown on Figure 8.22. Thanks to the vertical exaggeration, it can be seen that the dunes are very well grown. In other words, the dune growth stopped where the seafloor starts to flatten. The functioning of the algorithm is very satisfying for this usual dune pattern. The tracing of the dune crests is accurate too.

Figure 8.23 is the plot of the height against the length of the dune extracted automatically (see Figure 8.22). These values are estimated by the algorithm. The dunes that cross the area are visible on the plot because of their length (approximately 1000 m). It can also be remarked that some dunes are twice as high as others (1.5 m

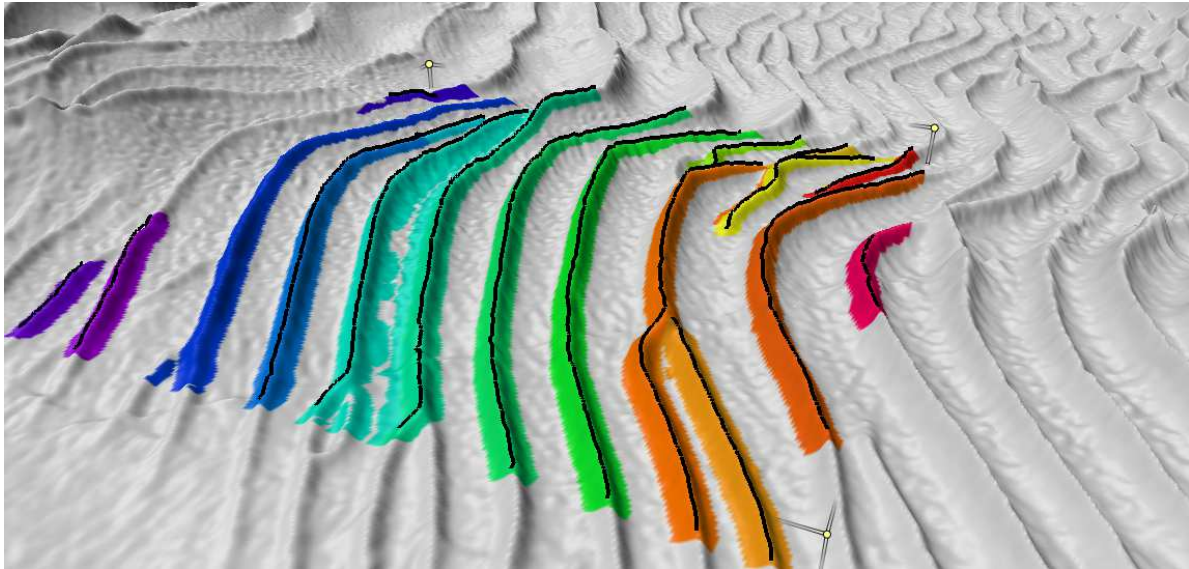


FIGURE 8.22: Extracted dunes on the area. $VE=10$.

vs 3 m). This plot provides little information as the area has a limited size and it only contains parts of dunes.

Nevertheless, this figure illustrates the type of plots that could be analyzed in order to study the morphology of dunes at the scale of the dunefield. The analysis of the morphological descriptors for an entire dunefield, or even database, will help in determining whether or not they are sufficient to quantitatively describe the dune types mentioned in Chapter 2.

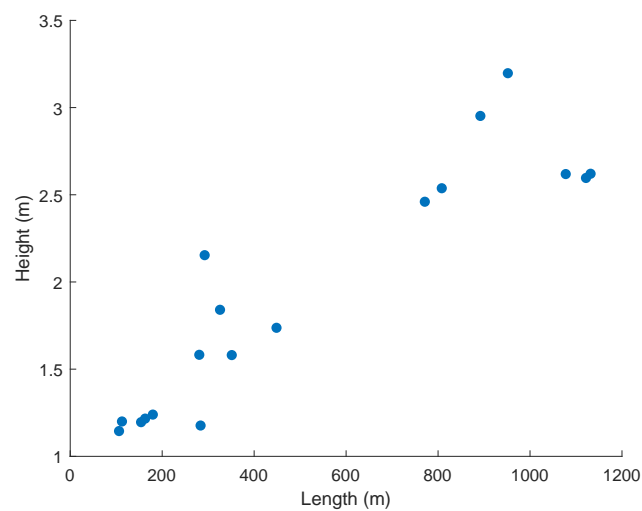


FIGURE 8.23: Plot of the estimated height against the length.

8.3.4 Dunes on Ouessant bank

One of the reasons requiring the design of a more sophisticated algorithm was that the slope used during the dune growing process is not only induced by dunes. In particular, this issue has been pointed out on Ouessant bank. The original algorithm had a tendency to extract overgrown dunes. Consequently, it is essential to verify if the new algorithm achieves better results.

The algorithm was used on a part of Ouessant bank (cf. Figure 8.24). As seen in the figure, the chosen area is located on the flank of the bank. From the top of the bank to the foot, the depth drops from 50 m to 95 m. The flank is around 600 m wide, while the dunes are approximately 3 m high. Their height is much smaller near the top of the bank (0.5 m), especially for the yellow dune (see Figure 8.25).

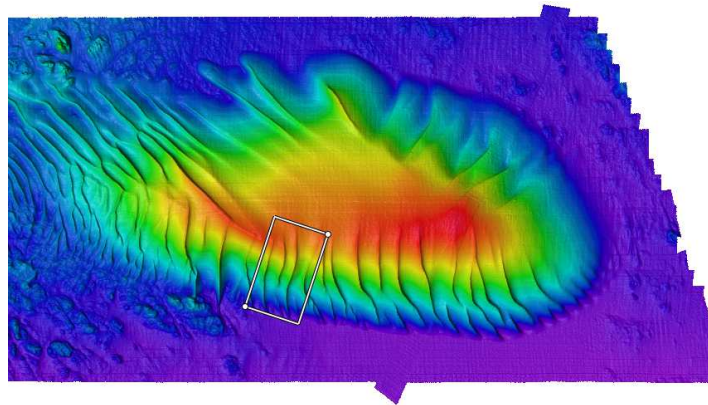


FIGURE 8.24: Location of the selected dataset with respect to Ouessant bank.

The algorithm's results are displayed in Figure 8.25. The top-view figure (left) shows that full length dunes are obtained despite a reduced height near the top of the bank. With the modifications brought to the new algorithm that account only for the slope component oriented towards the crest, the problem of overgrowing of the dunes is solved. The resulting dunes have an spatial extent coherent with what is visually expected. To conclude, the new algorithm is able to delineate dunes standing on steep sloping terrain. This is essential as this type of configurations is common.

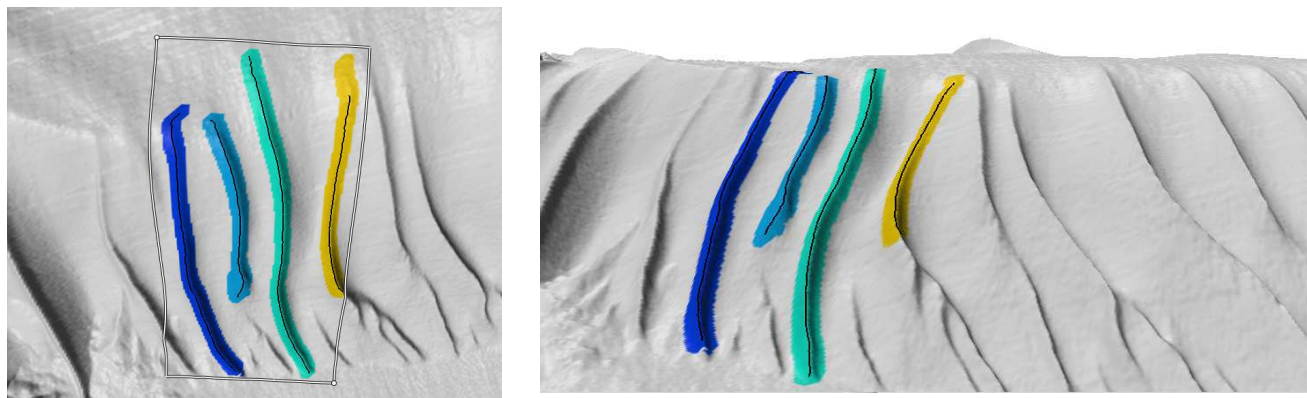


FIGURE 8.25: Extracted dunes on the flank of the bank. $VE=5$.

8.4 Conclusion

This chapter introduces our dune extraction algorithm. Its extractions yield to the estimation of the dune morphometrical descriptors. The extraction algorithm was built using the observations and the methods designed in the previous chapters (4,5,6,7). It is a semi-automatic region growing algorithm that uses detected crests as seed regions and a slope threshold to control their growth. The number of parameters was purposely kept low as only two were defined: (1) the minimum dune length; (2) the minimum dune width.

The internal parameters of the algorithm have been previously tuned for optimal results or been deliberately expressed from these two parameters. In fact, they provide insight on the shape of the dunes of the processed dataset. And, they are understandable by anyone without particular knowledge on the internal mechanisms of the algorithm. Therefore, this algorithm demands to input prior knowledge about the studied dunefield. Nevertheless, the setting of the parameters is rather flexible. A little change might have an impact on the detection of a few dunes but the extractions will not change drastically.

The proposed algorithm can be qualified as a user-friendly, robust, region growing, resolution adaptative algorithm. It has been successfully tested on diverse dune types and dunefields. Its performance is similar to these of the algorithm presented in Chapter 4 where this latter worked well. But, unlike the first, the new algorithm is capable of dealing with sand ripples and dunes lying on a sloping seafloor. More tests should be conducted on the amazingly rich dune database available at SHOM or Belgian continental service to check the behaviour of the algorithm in other cases.

The design of this algorithm is the first step towards the automation of the study of dune and dunefield morphology and dynamics. The objective behind this is to automatically estimate descriptive parameters of the morphology and dynamics of dunes. So far, only the classical morphometrical descriptors are computed, but more advanced ones could be added to the list if the current parameters prove insufficient or inappropriate to describe the variety of dune shapes.

Dune dynamics is an aspect that has often been omitted, especially in the classifications (cf. Section 2.2.4) or, at least, deserves more attention as it somehow reflects the hydrodynamics of the area and may be of importance for human activities at sea. The next chapter addresses the problem of automatically quantifying dune dynamics. The extraction algorithm presented in this chapter is the first important step to achieve this.

Chapter 9

Dune dynamics

Contents

9.1	Introduction	202
9.2	State of the art	203
9.2.1	Iconic algorithms	203
9.2.2	Symbolic algorithms	209
9.3	Proposed algorithm for the study of dune dynamics	212
9.3.1	Dune dynamics	212
9.3.2	Correspondence	216
9.3.3	Transformation estimation	218
9.3.4	Quantification of dune dynamics	219
9.4	Conclusion	227

9.1 Introduction

The study of dunes should not be reduced to the analysis of their morphology. To be complete, dune dynamics ought to be examined too. The quantification of dune morphology is generally addressed first as it naturally derives from the dune extraction. Yet, dune dynamics must not be neglected in order to get an overall picture of what dunes are, how they interact with the environment and each other, or how they change over time.

When examining dune dynamics, a distinction is to be made between deformation and migration. In 3D, migration can be reduced to six degrees of freedom (3 translations and 3 rotations)¹. Migration corresponds to the displacement of a rigid body. But, dunes are not rigid bodies. They deform. Although deformations are generally omitted, in most cases, a dune migrates and deforms at the same time. Therefore, a combination of the two components describes the dune dynamics. Other phenomena can be added to these two main dynamic mechanisms. For instance, the dynamics of ripples and megaripples superimposed onto the dunes or even dune mergings and splittings. The automatic estimation of dune dynamics would also be fundamental to answering controversial questions such as: Does the volume of a dune remain constant over time?

This chapter focuses on the automatic estimation of dune dynamics. It will take advantage of the results of our dune extraction algorithm. Now that the dune crests and boundaries may be automatically located in the seafloor topography, bathymetric data of the same area surveyed at different times may be analyzed to assess dune dynamics. The proposed algorithm will rely on these sets of extracted dunes to characterize their dynamics.

It is essential to note that dune migration cannot come down to crest or trough displacements as dunes are 3D objects. Therefore, the proposed algorithm must consider the morphological changes of the whole dune and not simply of its structural lines.

Our problem is close to these tackled in pattern recognition, shape matching, registration and related topics. The literature dealing with these problems is briefly reviewed. Then, an automatic technique for estimation of dune dynamics is presented.

1. The scaling coefficients are neglected.

9.2 State of the art

Pattern recognition, shape matching and registration are research topics that have a wide scope of applications (e.g., remote sensing (Gläser et al., 2013, Goldgof et al., 1989), medical imaging (Chui & Rangarajan, 2003, Pennec et al., 1999, Rueckert et al., 2001), computer vision (Hilaga et al., 2001, Johnson, 1997, Kim et al., 2013), Optical Character Recognition (OCR)², biometrics (Fingerprint matching (Hosseinbor et al., 2017), Face recognition, *etc*).

These algorithms were designed for the analysis of both images (Nicolas et al., 2016, Padfield, 2012, Yang et al., 2015, Zitová & Flusser, 2003) and 3D surfaces (Li et al., 2008). Image registration has been applied to fingerprint or facial recognition, terrain or seafloor registrations, 3D object reconstruction from stereo, *etc*. A survey of image registration methods may be found in Zitová & Flusser (2003). 3D problems have generally been studied in the medical domain as it often goes along with visualization and data interpretation (diagnosis) problems. 3D registration looks for the transformation between objects and shapes of various natures: human body tracking, brain, heart, eyes, scans of terrain or 3D objects, *etc*.

Registration algorithms can be divided into two main categories: (1) Pixel or voxel-based registration methods or (2) feature-based registration methods. In both cases, the registration problem can be reduced to an optimization problem. The optimal transformation is the one that minimizes an error/distance function or maximizes a similarity measure.

9.2.1 Iconic algorithms

The pixel or voxel-based registration methods are also called iconic methods; these techniques are referred to as area-based methods in Zitová & Flusser (2003). Images obtained under different conditions (e.g., sensor, acquisition time or viewpoint) are registered/aligned by testing possible transformations. For each transformation, a metric is computed to quantify the difference/similarity between one of the original images and the transformed image. The similarity metric is usually a correlation-like parameter.

2. OCR algorithms transform typed, handwritten or printed text into a text file.

The 2D cross-correlation of a $M \times N$ image I_1 , and a $P \times Q$ image, I_2 , is a matrix/image, C , of size $M+P-1$ by $N+Q-1$. Its elements are given by:

$$C(i, j) = \sum_{m=0}^{M-1} \sum_{n=0}^{N-1} I_1(m, n) I_2(m - i, n - j),$$

where $-(P - 1) \leq i \leq M - 1$, $-(Q - 1) \leq j \leq N - 1$.

The 2D cross-correlation is the simplest metric to measure the similarity between two images: one reference image and one that must be aligned with the reference.

The optimal transformation is derived from the analysis of the similarity metric (i.e., a search for the global similarity maximum). The similarity value associated with the optimal transformation is a natural estimator of the quality of the registration.

Iconic registration methods are strongly influenced by the image resolution, noise, dynamics and content. For example, a textured image is simpler to register than a homogeneous one. Another weakness of these methods is that the similarity metric must be calculated for a large number of transformations in order to determine the best, which is not computationally efficient.

Classically, the algorithms are seeking for the best rigid transformation. The hypothesis of rigid transformation, though simpler, showed its limits for some applications, especially in the domain of medical imaging. Non-rigidity was introduced in the models (e.g., elastic, viscous fluid) (Pennec et al., 1999).

The similarity metric or the type of model (e.g., number of translations and rotations, rigid or not) are not the only parameters that may be changed in order to better estimate the evolution of an image. Instead of testing all the possible transformations, gradient descent and equivalent methods were developed to accelerate the process and converge towards the global minimum of the difference measure hence providing the best transformation estimate. However, there are cases where these algorithms converge towards undesired local minimum. The sensitivity of these methods to the existence of local difference measure minima is variable. These approaches are been researched for preventing convergence to local minima (Pennec et al., 1999).

Other sophisticated techniques for choosing the optimal transformation have been developed. A possibility is to imitate the theory of evolution and its mechanisms (i.e., mutation, reproduction, crossover operators). Such methods are called Evolutionary Image registration methods and are reviewed in Santamaría et al. (2011).

Johnson (1997) introduced the notion of spin images, which are images generated by projecting a 3D object/surface onto planes from different viewpoints. They are used for object registration, recognition, classification.

A hybrid method called topology matching was examined in Hilaga et al. (2001). It is a hybrid as it aims to align two images by transforming them into graphs. It handles simultaneously the correspondence and pose estimation of 3D surfaces by using Reeb graphs, which are skeletons of a continuous scalar function (a height function in the paper). The graph construction is inspired from Morse theory³ by considering level sets of the scalar function. Thus, this method is half way between feature line registration (skeleton) and iconic (scalar function) methods.

Iconic methods have also been successful applied to range scanner images for the reconstruction of 3D object models. In Gläser et al. (2013), laser altimeter tracks are aligned with DTMs describing the surface of the Moon or Mars. A first set of transformations are tested to get a rough estimate of the best transformation. Then, the process is repeated to determine a fine transformation estimate. The degree of closeness between the laser profiles and the DTMs is quantified by computing the standard deviation of the height differences. Such an approach may be generalized for the localization of robots scanning their environment when this latter is known.

Registration is not necessarily done on the images themselves. In Padfield (2012), the cross-correlation of two images is calculated in the Fourier domain. The proposed algorithm has the advantage of being fast as it works in the Fourier domain and only one iteration is necessary to retrieve the optimal transformation. A masking option is added to discard parts of the image that are of little interest or that could skew the registration results. The MNCC map of images f_1 and f_2 with the masks m_1 and m_2 is estimated via the formula:

$$MNCC = \frac{F^{-1}(F_1 \cdot F_2^*) - \frac{F^{-1}(F_1 \cdot M_2^*) \cdot F^{-1}(M_1 \cdot F_2^*)}{F^{-1}(M_1 \cdot M_2^*)}}{\sqrt{F^{-1}(F(f_1 \cdot f_1) \cdot M_2^*)} \sqrt{F^{-1}(M_1 \cdot F(f_2' \cdot f_2')) - \frac{(F^{-1}(M_1 \cdot F_2^*))^2}{F^{-1}(M_1 \cdot M_2^*)}}}$$

The capital letters correspond to the Fourier transform of the images. The ' and * are respectively the symbol of transpose in the spatial and Fourier domain. The Fourier and inverse Fourier transforms are noted F and F^{-1} and \cdot is the element-wise product of matrices. Note that MNCC values range from 0 to 1.

3. In outline, Morse theory focuses on the study of the topology of surfaces. The surfaces are decomposed into level sets that contain information about the surface topology. For instance, a DTM can be divided into depth slices. Each component of the seafloor in a slice corresponds to a node in the graph. The nodes from adjacent slices are connected to obtain a graph of the seafloor.

This method has been adapted for the registration of sonar track (Nicolas et al., 2016). A block-matching approach is chosen to cope with the non-rigidity of seafloor changes. That is to say that the images are divided into smaller images. The proposed algorithm looks for the best rigid transformation on each small image. The problem of non-rigidity of the evolution of the seafloor is addressed by making the assumption that the evolution is rigid over small patches.

Although it was applied to Synthetic Aperture Sonar (SAS) imagery and not depth fields, this revealed interesting behaviour for the monitoring of seafloor changes. Therefore, Padfield's algorithm was implemented to assess its capacity, and more generally the capacity of iconic approaches, to estimate dune dynamics.

First, the algorithm was tested on simple geometric shapes to check on the validity of our code. Figure 9.1 illustrates the case of a 51×51 pixel image only containing a 10×10 pixel square (subfigure (a)) that was shifted in both x- and y-directions (subfigure (b): 20 and 6 pixels). The calculated MNCC map is shown in subfigure (c). The maximum of MNCC was found for a (20,6) translation, which is the exact translation.

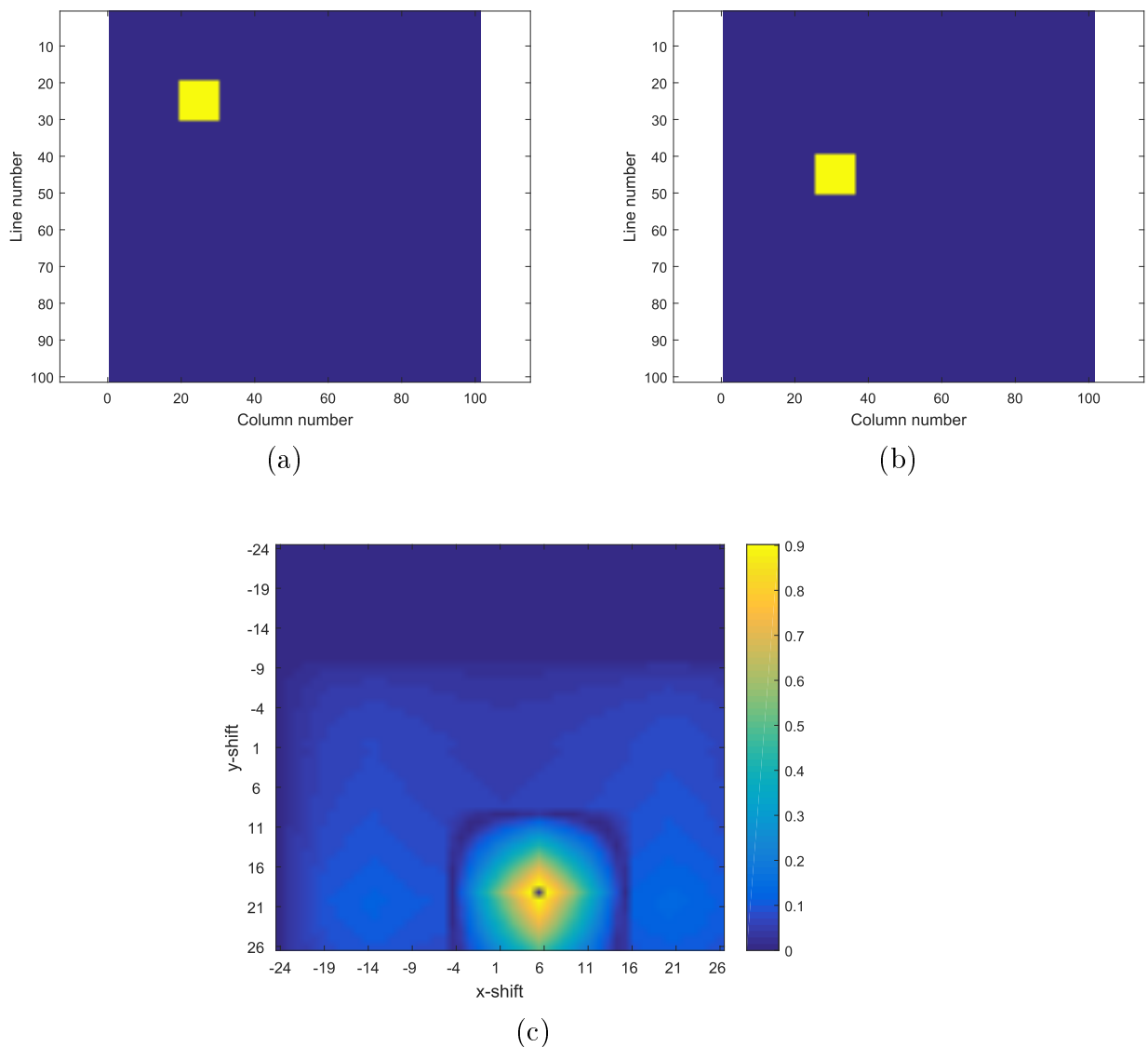


FIGURE 9.1: Test of the code validity with a simple image. Square translation: x: 20 pixels; y: 6 pixels. (a): initial image; (b): image with a shifted square and (c): resulting MNCC.

Then, the algorithm was tested on real data. Instead of matching two DTMs of the same area acquired at different times, it was decided to take the DTM of a small dune area (Figure 9.2) and to shift it by an arbitrarily-chosen number of pixels along the x- and y-axes. The estimates of MNCC for a $(-10,17)$ translation and no translation are presented on Figure 9.3). It may be seen that the correlation in the Fourier domain fails in recovering the correct translation value in both cases. For a $(0,0)$ shift, a MNCC peak would be expected in $(0,0)$. The estimation of cross-correlation in the Fourier domain might be straightforward but it is unsatisfactory for dune data.

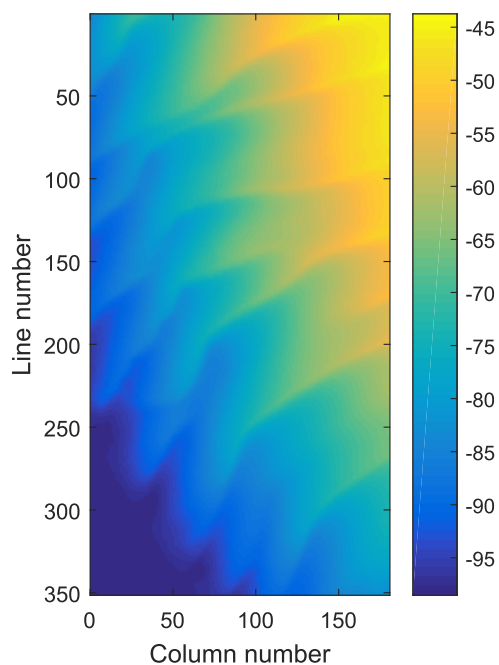


FIGURE 9.2: Part of a DTM of SHOM zone 2. Colored by depth (m).

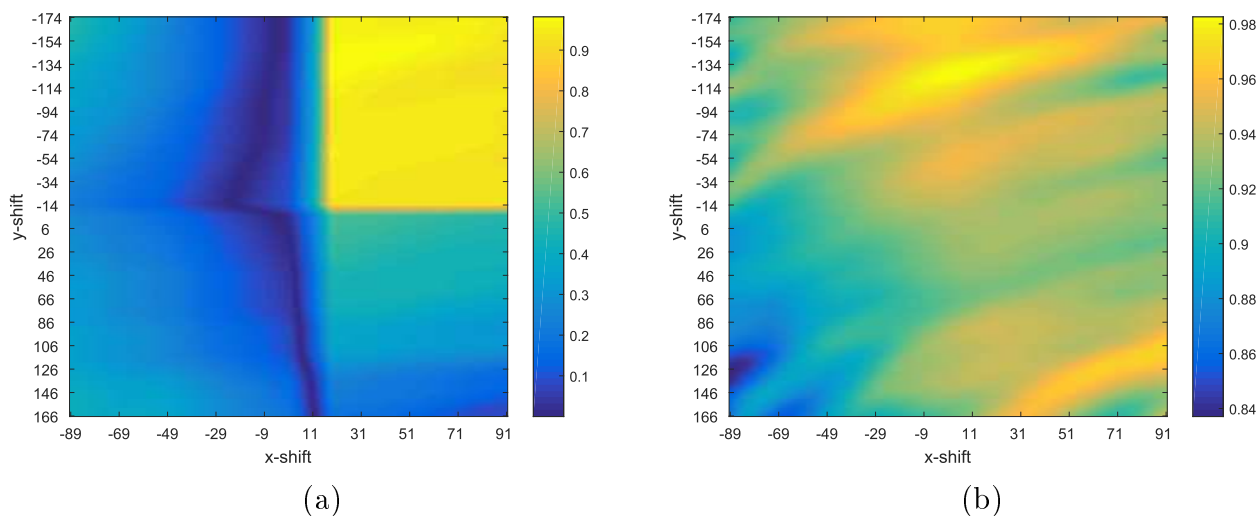


FIGURE 9.3: MNCC maps on real data with translations of: (a): $(-10, 17)$ pixels; (b): $(0,0)$ pixels.

Moreover, iconic methods estimating correlations in the spatial domain would be poorly adapted due to the periodic pattern of dunes. Indeed, the translations in the direction of dune crests or in the perpendicular direction by a multiple of dune spacing would give similar correlation values. Adding the fact that dunes deform between two acquisitions, the estimation of the global correlation maximum is even more difficult

when two DTMs of a same area surveyed at different times are considered. And, the global maximum might not correspond to the true translation according to the magnitude of the deformation.

When choosing an iconic approach, the assumption that the dynamics are constant over the registered image is made. In other words, even if non-rigid models exist (Pennec et al., 1999), the estimated transformation is valid at the scale of the image or of an image patch. It is, thus, not compatible with an estimation of the dynamics of each dune.

9.2.2 Symbolic algorithms

The methods of registration based on points, lines or meshes are called symbolic. In all three cases, they can be reduced to a point set matching problem. Lines and meshes may be seen as point sets with connectivity, neighborhood information brought by their specific structures (e.g., segments, edges, faces). The process of registration is divided into two principal steps: correspondence and pose estimation.

Some algorithms (Shapiro & Michael Brady, 1992) solely address one of the topics. These algorithms were not further studied as both aspects are essential for analyzing dune dynamics. In the following, only the approaches dealing with both aspects simultaneously are considered.

The correspondence step consists of finding pairs of equivalent points in the two point sets to align. Similarly to iconic methods, the pose estimation is an energy/-function optimization problem. The measure of closeness/matching relies on the distance between the pairs of points created during the correspondence step.

Most algorithms can manage the registration of point sets not containing the same number of points. Some are also capable of coping with noise and outliers (Kim et al., 2013). The use of scanning sensors gives point sets partially describing the same surface. Therefore, methods have been developed to manage partly overlapping point clouds (Li et al., 2008, Tevs et al., 2009).

A 3D rigid transformation is composed of scaling factors, translations and rotations. It is the simplest transformation model and is not appropriate to cases where the surface/object has deformed between two acquisitions. To resolve this limitation, non-rigid transformation models have been proposed using elastic, viscous fluid (Tevs et al., 2009) or isometric (Huang et al., 2008) models.

Statistical models of shape variability have been successfully applied to perform various image analysis tasks of 2D and 3D images. A free-form deformation (FFD) model based on B-splines is presented in Rueckert et al. (2001). A non-rigid model of deformation based on thin-plate splines (TPS) is another possibility (Chui & Rangarajan, 2003). In Wang et al. (2015), the registration of point sets is achieved with a non-rigid registration method based on a mixture of asymmetric Gaussian models (MoAG).

Isometric models (Ge, 2016, Sacharow et al., 2011) make the hypothesis that the geodesic distance between the points on a surface are preserved. The geodesic distance is the length of the shortest path on the surface between two points.

Registration may also include a downsampling step in order to reduce the number of points used for the estimation of the transformation (Ge, 2016, Kim et al., 2013). This is now commonly integrated in the registration procedure to manage denser point clouds due to improvements in scanning resolution.

The optimization function can simply quantify the spatial closeness of the two point sets or encompass local or global information. In Rusu et al. (2009), three features are estimated at several scales in the neighborhood of each point: the number of neighbors within a radius r , the surface normals, and their variations. Point Feature Histograms are computed from these features to help in obtaining more reliable correspondence pairs.

A global registration procedure for fingerprint matching is explained in Hosseinbor et al. (2017). During the correspondence process, a weight is assigned to each pair. This incorporates information about minutia attributes and local minutia features. In fingerprint analysis, minutia are the main features of a fingerprint (e.g, ridge ending, ridge bifurcation or merging, etc.) Similarly, a confidence weight is calculated for a global optimization of the correspondence in Li et al. (2008). The correspondence and pose are estimated at the same time.

A combination of neural network and statistical physics techniques is used in Gold et al. (1998) to design a new point set correspondence and matching algorithm, called softassign.

The Iterated Closest Point (ICP) algorithm (Besl & McKay, 1992) is probably the most famous and common 3D matching method. It is a local registration method. The correspondence pairs are built by calculating the Euclidian distance between the point sets. Each point is associated to the closest point in the other point set. The transformation that minimizes distance between the sets of pairs is calculated and applied.

Correspondence and pose estimations steps are repeated until the algorithm converges. This algorithm is not computationally efficient and very sensitive to outliers and to the initial positions of the point sets. If they are too far apart or deformed, the algorithm is not capable of correctly matching both point sets. In addition, it gets easily trapped in local minima of the distance function.

Numerous improved versions were next developed in the literature to overcome the weaknesses of the original ICP algorithm. For instance, an isometric version was designed for the analysis and compensation of form errors in production engineering (Sacharow et al., 2011). A modified ICP algorithm using the Levenberg–Marquardt algorithm for a non-linear minimization of the error function is presented in Fitzgibbon (2003). More recently, another ICP method using the Levenberg–Marquardt algorithm for the pose estimation was designed (Kim et al., 2013). It is a two-step global-to-local registration procedure. The PCA-based global registration is followed by a local registration technique that uses the ICP algorithm.

For mesh vertex matching, the correspondence procedure may be accelerated by using a point-to-plane technique (Li & Song, 2015). The common search for the closest point is replaced by the computation of the distance between the vertices of one mesh and the triangles of the other mesh. For each vertex, a correspondence point is inferred in the closest triangle.

Other original algorithms may be found. An algorithm for simultaneous pose and correspondence estimation inspired by genetic algorithms is described in Yang et al. (2015). Like Evolutionary Image registration methods (Santamaría et al., 2011), it imitates the processes of selection, crossover and mutation well-known in biology.

In Sclaroff & Pentland (1995), features are calculated for each vertex. The feature points are used to build a finite element model of the surface. Next, eigenmodes, that are sorts of symmetry axes of the model, are determined. They form an orthogonal object-centered frame. Feature correspondences and matching become simpler in this coordinate system.

The problem of non-rigidity of a surface/object is highly complex. To make it more accessible, it can be simplified to the sum of articulated rigid mappings. This approach is taken in Huang et al. (2008) and Ge (2016). To cope with large deformations, the surface to register is segmented and a non-rigid (isometric) registration method is applied to each segment. It has been successfully applied to articulated bodies.

Brown & Rusinkiewicz (2007) present a modified ICP method in order to support non-rigid registration of overlapping 3D datasets using thin-plate spline warps. The

objective is to account for the potential low-frequency distortion of the scans caused by the acquisition system. The results are compared to those obtained using a rigid method to illustrate the contributions of the spline warping.

In Budd et al. (2013), the authors address the problem of temporal alignment of mesh sequences. The objective is to align meshes of the same surface that changed between two acquisitions. This is particularly useful for the tracking of moving objects or beings. The non-rigid registration is achieved using a so called shape similarity matrix and a spanning tree structure.

Unlike most registration methods, the one described in Rouhani et al. (2014) does not necessitate the determination of point-to-point correspondences. Similar to isometric algorithms, this method simplifies the non rigid problem as the sum of local rigid transformations. Quadric functions are locally fitted to the set of points. These patches are then aligned with the reference point sets using affine transformations.

Zeng et al. (2010) looks at the non rigid registration problem from a different angle. Dense surface registration is mapped to a high-order graph matching. Meshes are replaced by graphs that can be matched.

Many methods for the registration of 3D surfaces have been proposed, but as the readers will see in the next section, a non-rigid registration method is probably the best option to quantify the complex dynamics of dunes.

9.3 Proposed algorithm for the study of dune dynamics

9.3.1 Dune dynamics

Before discussing the applicability of symbolic algorithms, dune dynamics have to be examined. After looking at bathymetric variations in dunefields, it may be noticed that dune dynamics are hard to visualize and even more difficult to manually estimate. In practice, they are visualized by toggling back and forth between DTMs, juxtaposing DTMs (Figure 9.4), superimposing DTMs (Figure 9.6), or computing DTMs differences (see Figure 2.12 in Chapter 2). Juxtaposition is used by dune experts to visualize the most obvious changes. Small variations may barely be noticed using this method. When the dunefield depicts a complex pattern, such as in Figure 9.4, the tracking of dunes is hard to achieve visually. It is not always easy to identify corresponding dunes on two

DTMs. Appreciating the changes between the two corresponding dunes is even more complicated.

However, superimposing DTMs (cf. Figure 9.6) can only be used to observe crest dynamics. Indeed, most of the time the displacements are small compared to the dune spacing, and most parts of the dune and its migrated version still overlap. Dune crests and their migrated versions are visible on both DTMs, so the superimposition of DTMs is suited when the migration is a pure translation (quantification with the crests) but not to visualize the dynamics of deforming dunes.

DTM differences are enough to determine whether or not a dunefield changes. But, the dune locations are lost. In other words, a depth difference map does not say where the dunes are. Consequently, it is difficult to analyze a difference map in terms of dynamics.

The comparisons of sets of crest lines are also common for the visualization and manual estimation of dune dynamics, but the reduction of a dune to its crest is too simplistic. Dunes are 3D features and the dynamics of the crests is not sufficient to fully describe the dune migration and deformation.

Dune dynamics may be studied at different timescales. Figure 9.4 illustrates the fact that dune morphological variations may be visible after a few months but the reliability of these observations must be balanced by the uncertainty of the bathymetric data. The time separation between two acquisitions necessary to determine the migration of dunes highly depends on the dunefield. Short-term observed changes are only relevant for shallow dunefields since the data uncertainty is, there, improved. For deep areas, long term trends may only be studied.

Several observations may be made from Figures 9.5, 9.6 and 9.7:

- Migration distance is generally small compared to the dune spacing. Actually, migration of tens of meters per year have been described in the literature and observed in our data but this value remains small in comparison with the width of a dune, which is classically several hundred meters.
- The dunes migrate roughly in the direction perpendicular to their crest.
- Each dune has unique dynamics. This means that they do not necessarily migrate in the same direction and at the same rate. This is particularly visible on Figure 9.6 where dunes at the top migrate to the left of the image and bottom dunes migrate to the right.

- The above remark is still true at the dune scale with dune parts not moving uniformly. Dunes are not rigid entities, they deform. In Figure 9.5, it may be seen that the dune crests are not perfectly parallel after migration. The dynamics of a dune is not a simple combination of translations and rotations.

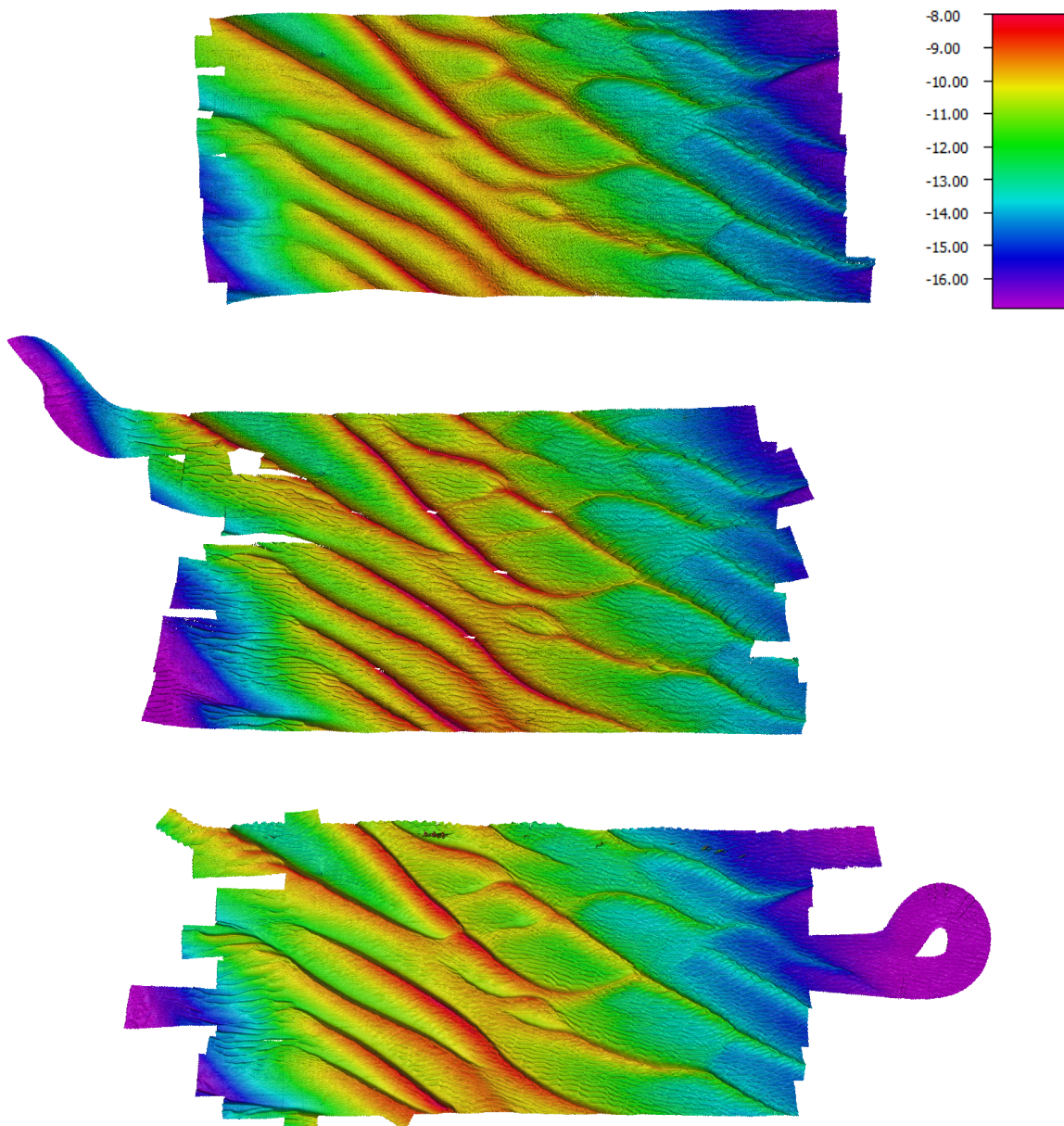


FIGURE 9.4: Juxtaposition of DTMs of Belgian zone R2 respectively surveyed in March 2012, September 2012 and March 2014.

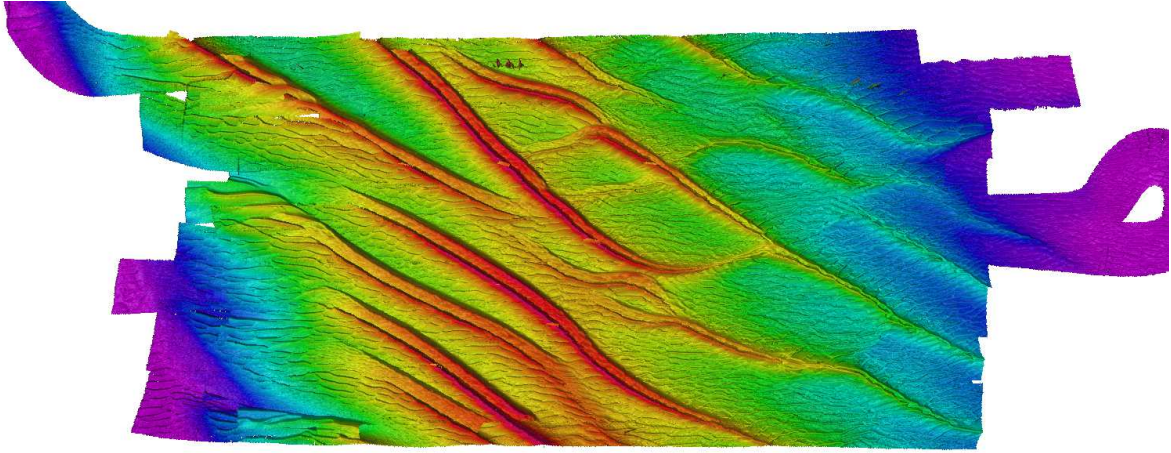


FIGURE 9.5: Simultaneous visualization of dunes in zone R2 acquired in March 2012 and 2014.

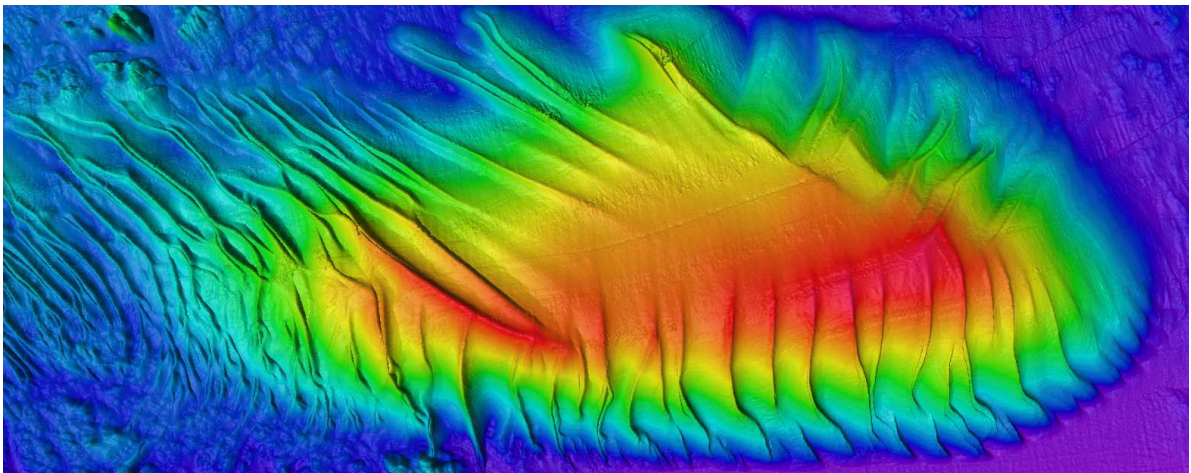


FIGURE 9.6: Simultaneous visualization of dunes in SHOM zone 2 acquired in 2012 and 2015.

Dunefields may be complicated patterns (Figure 9.7) that are hard to analyze even for the human eye. Even if some dunes are recognizable, others seem to have disappeared. This is due to mergings and splittings of dune or dune parts. This illustrates the complexity/non-uniformity of dune dynamics and its impact at the scale of a dunefield. In this context, the robustness of an automatic algorithm seem hard to guarantee for the most complex dunefields. Some dunefields should rather be considered as a single sedimentary, moving entity than as a sum of dunes not interacting with each other.

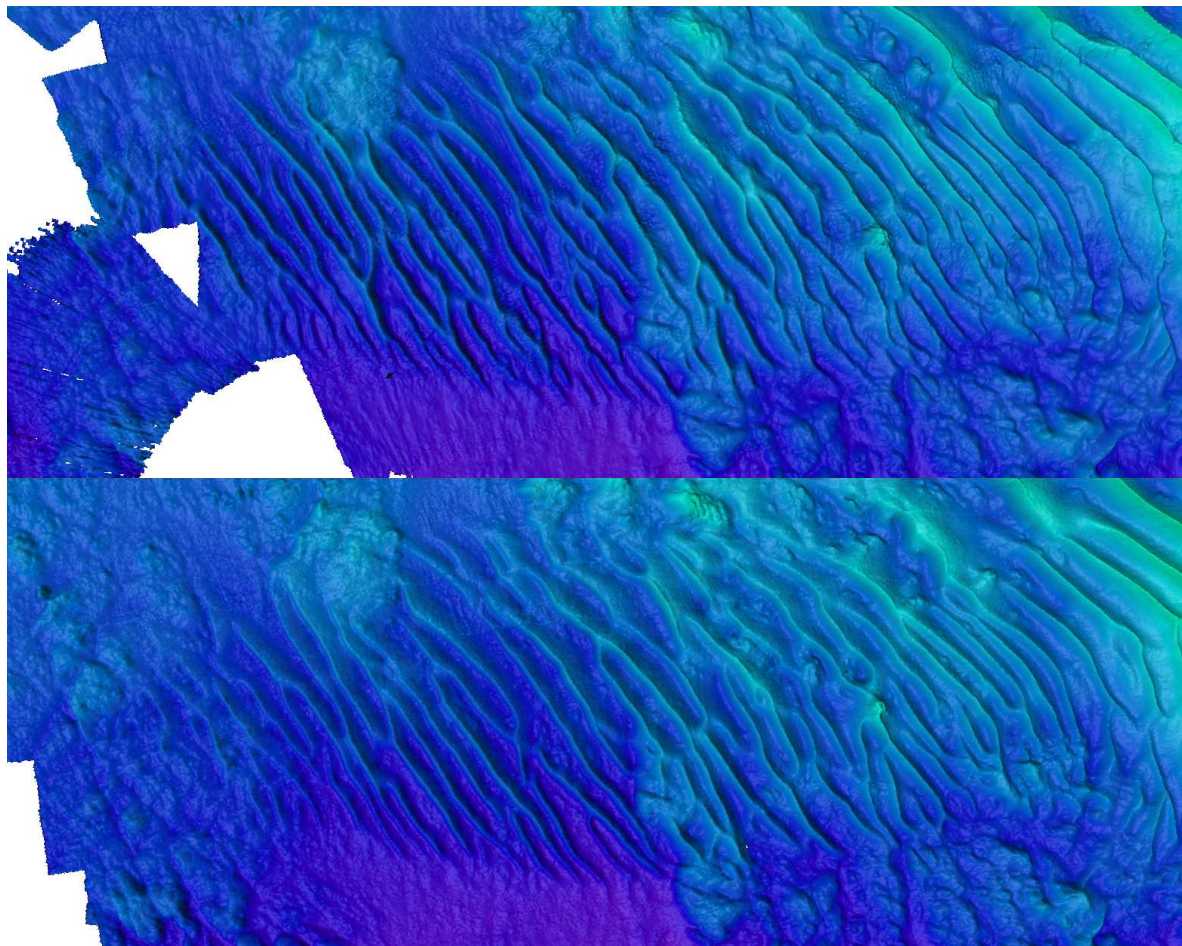


FIGURE 9.7: Comparative visualization of dunes in the flat seafloor part of SHOM zone 2.

9.3.2 Correspondence

In order to deal with the specificities of dunefields and dune dynamics discussed above, it seemed preferable to obtain dune-to-dune correspondences between two DTMs. In other words, we are looking for pairs of corresponding dunes in the datasets acquired at two different times and for the transformation between two corresponding dunes. The study of the dynamics of the dunes and dunefields could also be approached as a more complex dunefield to dunefield correspondence and matching problem. But, we chose to solve a relatively easier bipartite (dune with dune) matching problem rather than a more intractable graph (sets of dune with set of dunes) matching problem. An advantage of this approach is that dune dynamics are assessed at the dune scale instead of trying to match all dunes at once.

The automatic algorithm for the quantification of dune dynamics will work with the sets of dunes automatically extracted by the method introduced in the previous

chapter. This allows determination of the transformation allowing to pass from an initial dune to its equivalent in the dunefield acquired later. Although the dune migration is unknown, the crest orientation gives an idea of the migration direction. Researchers have noticed that the angle between the migration and the crest perpendicular orientations is almost always below 20° (Garlan, 2004). In theory, the crest asymmetry enables teasing out the migration direction. Yet, not all dunes are asymmetric. In practice, deducing migration direction from asymmetry is very heuristic. Nevertheless, migration is not totally unpredictable since dune crests provide information about their migration orientation.

This information is precious for the dune-to-dune correspondence step. Figure 9.8 illustrates how it is achieved. For each dune crest in the $t + dt$ dataset, a list of potential corresponding crests in the t dataset is created. These crests lie within a chosen maximum distance to the dune in the crest perpendicular direction.

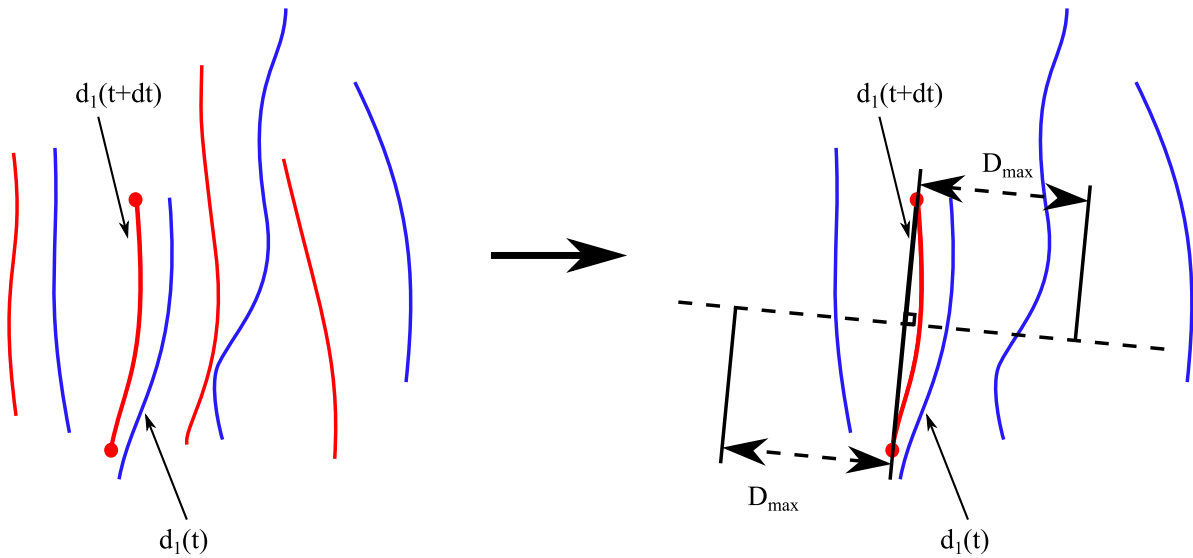


FIGURE 9.8: Dune correspondence process.

For each potential corresponding dune, a transformation is estimated using the transformation estimation process described in the next subsection. Along with the estimation of the dune dynamics, it provides a metric of the similarity between the initial dune and its potential match. The difference between dune d_{t+dt} and potential corresponding dune d_t after using the optimal transformation T may, for instance, be calculated as follows:

$$D(d_{t+dt}, d_t) = \sum_{i=0}^n d(t_i, T(s_i)),$$

where t_i are the vertices of dune d_{t+dt} , s_i are respectively the corresponding vertices on dune d_t and $d(\cdot, \cdot)$ is the Euclidian distance.

The best matched dune is taken. The confidence in the correspondence might be evaluated by comparing the similarity values for the best and second-best potential corresponding dunes. The ratio between these two similarity values would be a metric for the level of confidence of the algorithm in its dune-to-dune correspondences.

The dune-to-dune correspondence is controlled by the maximum distance parameter. This parameter is intuitive. If the maximum migration distance is unknown, the parameter can be set to a high value or to the dune spacing. However, if dunes have migrated by more than a dune spacing, it becomes difficult to determine reliable correspondences. Setting an arbitrarily high distance value would simply result in a slowing down of the algorithm as the list of potential corresponding dunes to be tested will be longer.

9.3.3 Transformation estimation

In our proposed approach, the transformation is essential in determining the correspondences. The ability of the algorithm presented in Huang et al. (2008) to cope with large deformation was interesting, and it seemed that it might be suited for the study of the complex dynamics of marine dunes. Consequently, it was decided to test it for dune registration. Huang's algorithm⁴ was integrated to our program and adapted to be applied on bathymetric data. Huang et al. (2008) is, to the best of our knowledge, one of the first isometric (i.e., providing conservation of the geodesic distances) registration algorithms and is a reference in the domain of non-rigid registration of 3D meshes.

To summarize, the algorithm is divided into four main stages⁵, which are depicted in Figure 9.9. The first step consists in downsampling the source and target meshes. The samples are obtained by a spatially uniform sampling of the surfaces, complemented by a uniform sampling on the Gauss map⁶ to preserve the surface features in spite of the sampling. Then, correspondences between the source and target samples are determined. Each source point is paired with a target point based on their closeness in the Euclidian space and feature space. The feature vector for each vertex contains values of the principal curvatures estimated at several scales. The correspondences are propagated from the samples to the other vertices of the source and target meshes taking care of the hypothesis of conservation of geodesic distances. Next, vertex clusters are

4. Our code is inspired by the code available at <https://github.com/huangqx>

5. For more details, the reader is referred to the publication: Huang et al. (2008)

6. See Section 5.2 for the exact definition. Essentially, it is a representation of the surface where each vertex is replaced by its corresponding surface normal.

created; the vertices of a cluster are supposed to be nearly coplanar. The final step aims at estimating, for each cluster, the optimal rigid transformation that brings the source vertices closer to their correspondences.

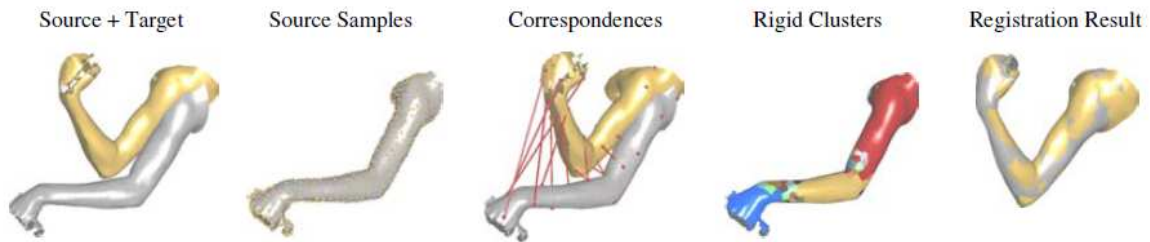


FIGURE 9.9: Diagram of the main steps of Huang's algorithm. The figure is drawn from the original paper.

The use of a registration algorithm for the quantification of dune dynamics is original as it is more interested in the alignment transformation than by the faithfulness of the registration. In other problems where a registration procedure is needed, the transformation is not further analyzed. The next subsection presents how these transformations can be used for the quantitative analysis of dune dynamics.

9.3.4 Quantification of dune dynamics

The presented algorithm can provide valuable information about dune dynamics and especially about their variability. The registration of dunes rather than dunefields is able to highlight the inter-dune differences from a dynamical standpoint. Therefore, the dynamics of dunefield might be compared in terms of homogeneity of the migration rate and direction as well as deformation. The segmentation of each dune in rigid clusters is suited for the quantification of dune deformation. The theoretical output of the algorithm at the dune scale are shown in Figure 9.10. For each cluster, three translations and three rotations are calculated. Horizontal translations are an approximation of the cluster migration (arrows with colors related to the clusters' in Figure 9.10). An important contribution of the clustering is that the divergence of these migration vectors may reveal shearing, internal dune deformation. This would be powerful information to quantify dune deformation or even to predict dune morphological changes. The transformation of linear dunes into barchanoidal dunes presented in Ernstsens et al. (2004) is a typical case where this set of migration vectors might be relevant.

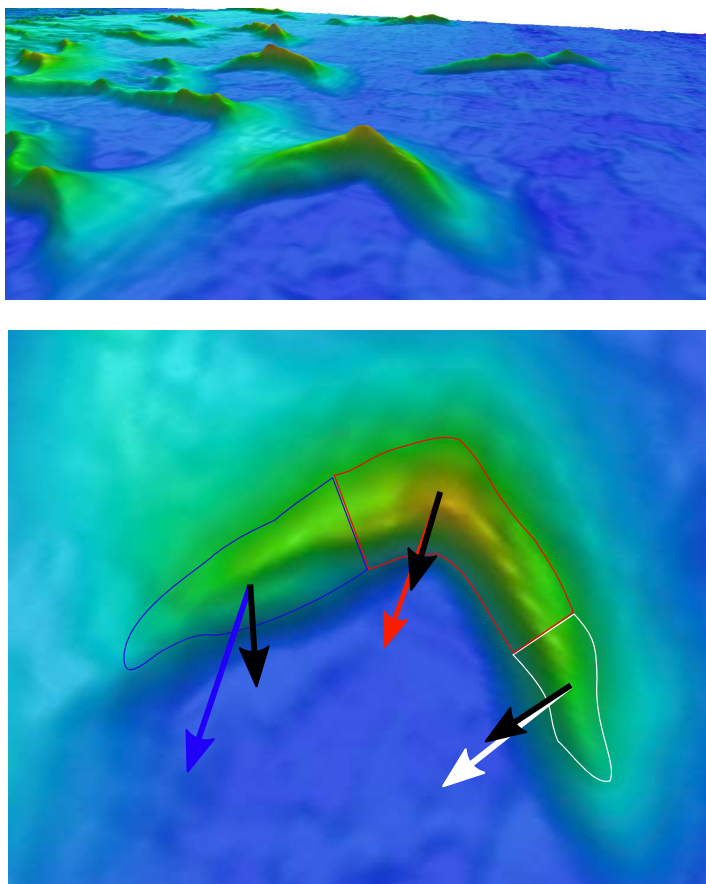


FIGURE 9.10: Dune segmentation and associated vectorial information.

The difference in the migration rate of dune parts is not the only deformation type that is measured by the algorithm. In fact, the rotation around the z -axis is also valuable information. If a part of a dune has rotated, it necessarily causes deformation of the overall dune, since independent rotations of the clusters can impact the global sinuosity of a dune. The rotations around the x - and y -axes might be considered if the estimated values are significant. The angles at which they start being significant are however hard to define. This is dependent of the accuracy of the dynamics required for the subsequent application.

The distribution and the number of clusters are clear indicators of the intensity of the deformation and complexity of the dynamics of a dune. Both flanks may have different dynamics or, perhaps, the flanks and the crest. These are examples where differences might show in the distribution of the clusters.

These signs of dune dynamics are a starting point for the development of metrics dedicated to the quantification of dune dynamics. These metrics could then be used in a classification scheme combining morphology and dynamics.

Additionally, the outputs of the algorithm would be very convenient for the visualization of dune dynamics. As illustrated in Figure 9.10, the information may be displayed as vectors and clusters. The z-rotation is transformed into a vector forming an angle equal to the rotation with respect to the migration vector (Black arrows on the Figure). The dune-to-dune correspondences also enables study of the variations of the morphological descriptors in time. This would be another way to quantify the time evolution of dune morphology.

The entire algorithm, inputting the sets of automatically extracted dunes and, then, evaluating correspondences and their dynamics has not been implemented. Yet, the use of an isometric registration procedure to study dune dynamics has been tested.

A zone of Ouessant bank was selected to verify the behaviour of Huang's algorithm applied to dunes. The location of this area with respect to Ouessant bank is shown in Figure 9.11. The DTMs constructed from 2012 and 2016 bathymetric datasets are simultaneously displayed to highlight the dynamics of the area. The description of the dynamics of the dune on its entire width requires extracting the bathymetry on a large spatial area in order to contain the 100 m wide dune in 2012 and in 2016 (with a 40 m shift). The arising issue is that the obtained meshes would describe the morphology of the dune and the morphology of the seafloor around it. But, we are only interested in the dynamics of the dune. Hence, it was decided to construct partly overlapping, rectangular (300×100 m) meshes from the 2012 and 2016 bathymetric datasets that describe the same part of the dune. Thus, the registration will only show the dynamics of the dune.

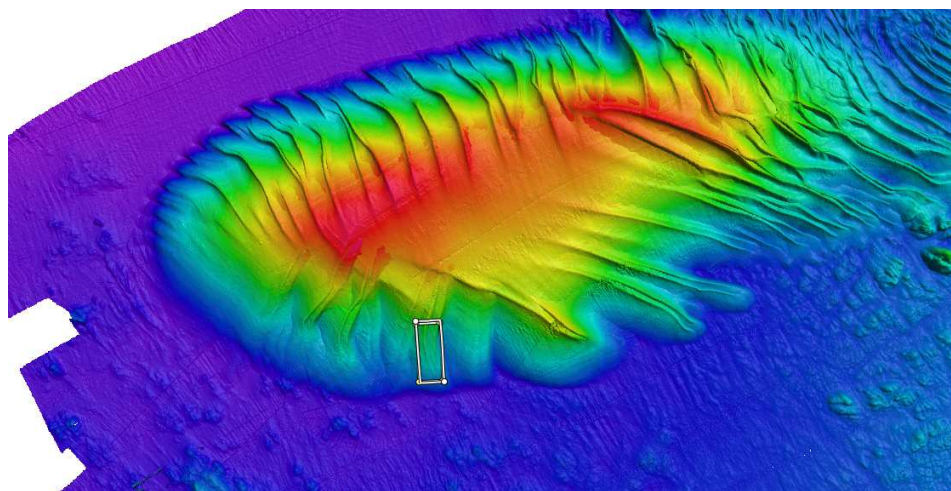


FIGURE 9.11: Area for the test of the dynamic algorithm in Ouessant bank. Data acquisitions: 2012 and 2016.

In order to correctly register two meshes, the first key point is to build robust vertex correspondences. A randomly-selected sample of the correspondences determined by the algorithm are depicted in Figure 9.12. The surface of 2012 is colored in gold and the silvery surface was acquired in 2016. The top-left figure shows that the algorithm tries to match vertices of the Stoss side of the dune in 2012 with vertices on the Stoss side of the dune in 2016. The top-right figure confirms the validity of the correspondences for the vertices of the Lee sides. The bottom figure is a plan image that shows that the correspondences are, effectively, made between vertices on the same side of the dune. In addition, the positions on the side of the dune are the same for corresponding vertices. For example, a vertex close to the dune crest is paired with a vertex that is also close to the crest on the other mesh.

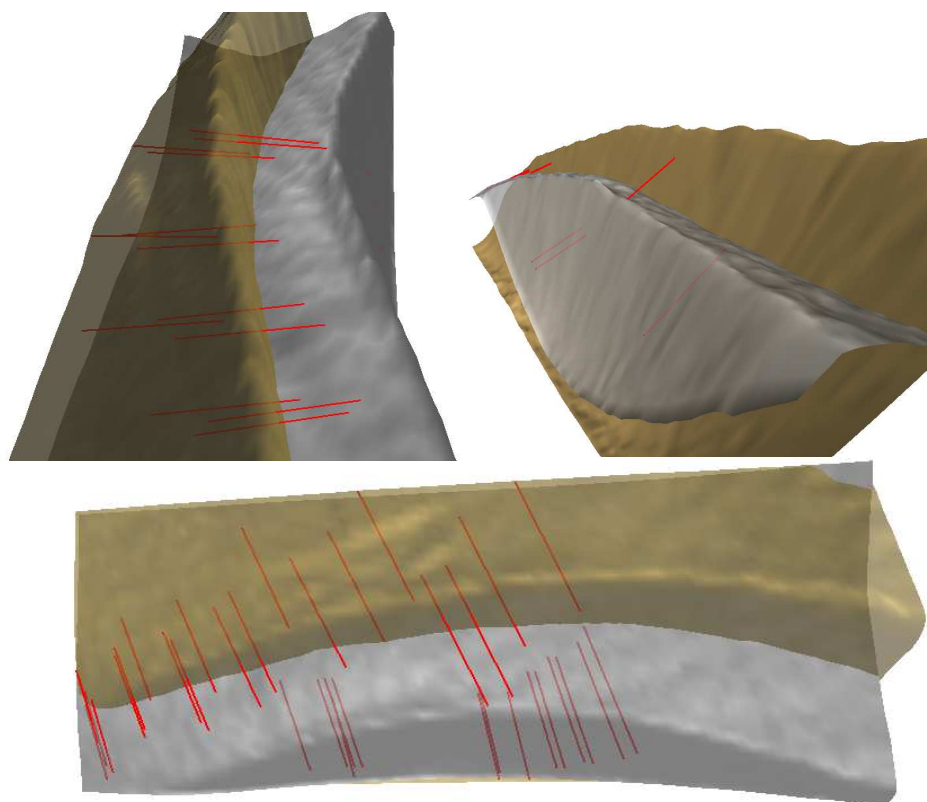


FIGURE 9.12: Sample of correspondences between two meshes.

When robust correspondences are made, the second main step is to estimate the transformations that will allow alignment of corresponding vertices. The results of the registration for our test dune are visible on Figure 9.13.

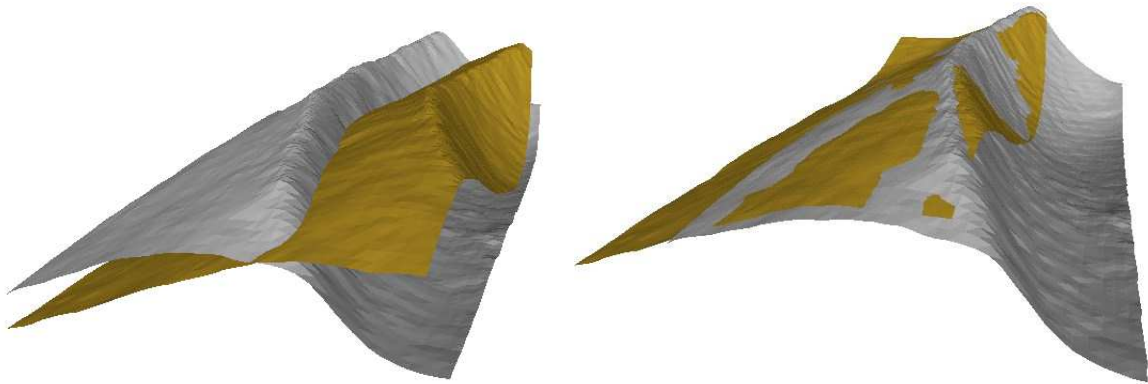


FIGURE 9.13: Simultaneous visualisation of the two meshes before and after the alignment procedure.

The left figure shows the two meshes before the registration. A significant migration (40 m) of the dune can be observed. The dune crest in 2016 stands where the foot of the Lee side was in 2012. The registered 2012 mesh and the 2016 mesh are simultaneously displayed on the right figure. The algorithm is capable to bring the two surfaces really close (average distance of 4m). The surfaces are so close that they intersect several times. This is particularly visible on the Stoss side. The crests are also correctly aligned.

The histograms of Figure 9.14 confirm that the registration algorithm is adapted to the dunes and quantify the registration error.

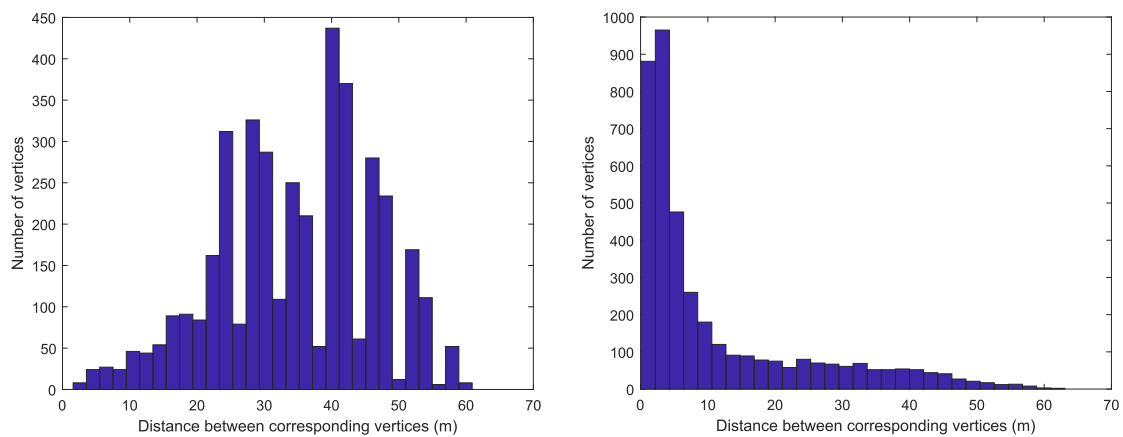


FIGURE 9.14: Histograms of the distances between the corresponding vertices before (left) and after (right) alignment.

The "before" histogram (left) should reflect the variation of the migration distance of the different parts of the dune. However, the distances between corresponding vertices vary from 0 to 60 m, and the visualization of the dune morphology does not show that parts of the dune did not move when others moved by 60m. These extreme distance values can be explained by the fact that some vertices of the 2012 mesh do not actually have a correspondence in the 2016 mesh. Yet, corresponding vertices are assigning to these vertices. This hypothesis is confirmed by Figure 9.15. In this figure, it can be seen that the vertices that are far from their corresponding vertex are located in parts of the dunes that are missing in the 2016 mesh. This is the case for the foot of the Lee side and one extremity of the crest. All these parts of the dunes common to the 2012 and 2016 meshes are colored in purple (distance ≤ 4 m) in the figure. The peak of the first histogram for a distance of 40 m corresponds to the real migration of the dune.

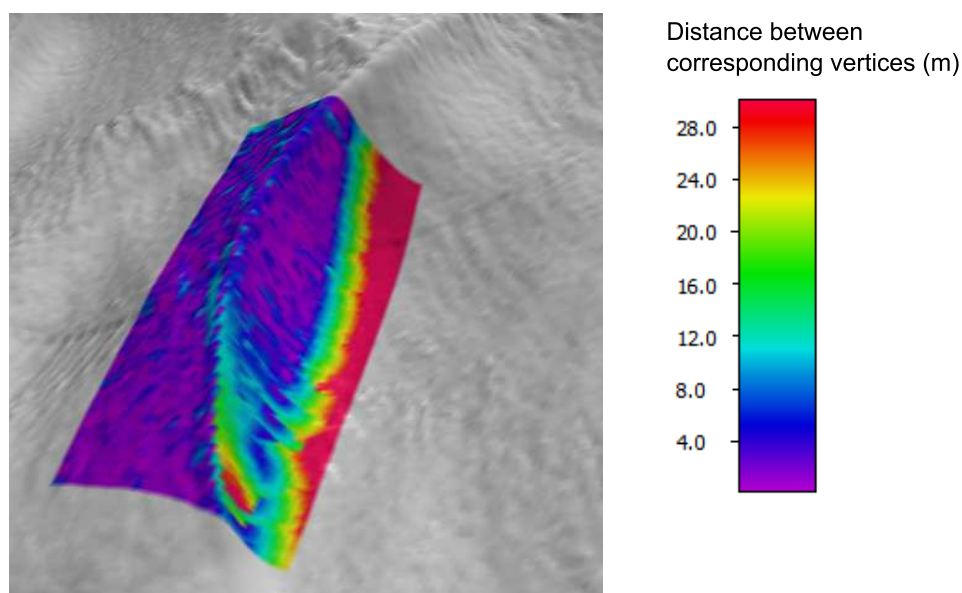


FIGURE 9.15: Map of distances between the vertex pairs after registration.

The histogram of the distances after registration has a peak between 0 and 5 m confirming the correct behaviour of the algorithm; and the tail of the histogram is due to the "incorrect" correspondences. The fact that some vertices had no correspondence in the fixed (2016) surface has not disturbed the algorithm. After registration, 25 percent of the corresponding distances are lower than 2.4 m, 50 percent are lower than 4.8 m, and 75 percent are lower 15.5 m. To determine significance, these values must be compared to the positioning uncertainties of the bathymetric models.

The International Hydrographic Organization (IHO) has set standards for the accuracy of bathymetric data. IHO standards for hydrographic surveys are presented in special publication S-44⁷. On the tested dune area (depth of 80m), IHO recommends that the vertical uncertainty of the depth measurements be below 60 cm and the horizontal uncertainty to be under 8 m (order 1a). The comparison of these values with the corresponding distances indicates that the algorithm is effectively able to align the two meshes. The quantification of the dynamics of the dune could be achieved using a isometric registration algorithm.

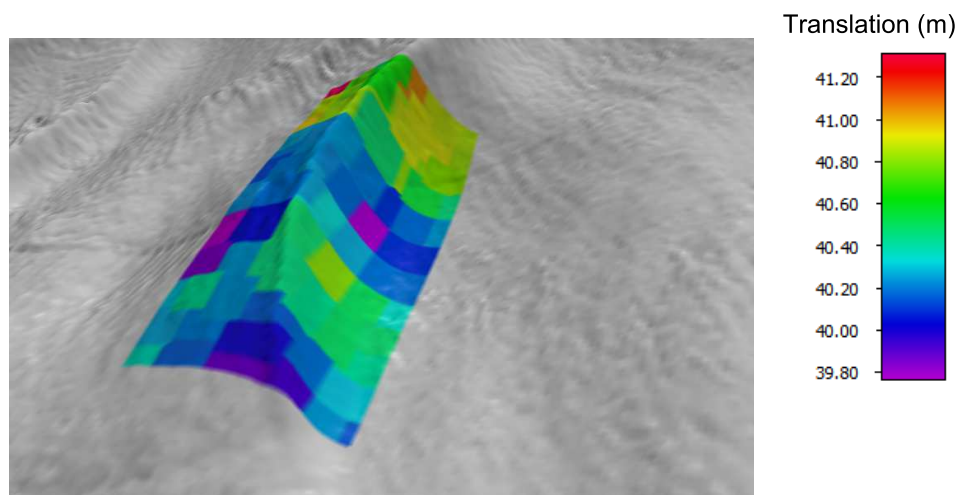


FIGURE 9.16: Vertex clusters colored by migrating distance.

Figure 9.16 illustrates the dynamics of the tested dune. Each vertex cluster is colored according to its estimated migration distance. The clusters located high on the side of the bank move faster than the rest of the dune (41 m). The central part of the dune is where the migration distance is the lowest (40 m). The analysis of the parts where the correspondences are not reliable is ignored. The 3D visualization of the DTMs also gives the impression that one part of the dune moves faster than the other. The algorithm helps quantifying this difference. However, it is important to bear in mind that this difference is small compared to the horizontal uncertainty of the data. In addition, the algorithm is "only" capable to move and deform the surfaces so that they are in average at 4m from one another. So it is delicate to give significance to the interpretation of the results in this case.

7. This document can be downloaded at https://www.iho.int/iho_pubs/standard/S-44_5E.pdf

As suggested previously (cf. Figure 9.10), deformation and migration vectors can be useful for the visualization of dune dynamics. The estimated dynamics-descriptive vectors for the tested dune are shown in Figure 9.17. One migration vector (blue) and one deformation vector (orange) are displayed for each cluster. In the figure, the clusters near the foot of the bank (bottom of the image) have larger z-rotation angles than the clusters closer to the top of the bank. This is the type of observations that can help dune specialists understanding how the morphology of dunes changes through time. Changes in the intensity or direction of the migration vectors are other potential indicators of this dynamics. These vectors quantify the dynamics of the dune. Furthermore, the vectors enable an enhanced visualization of the dynamics and, therefore, better understanding of it.

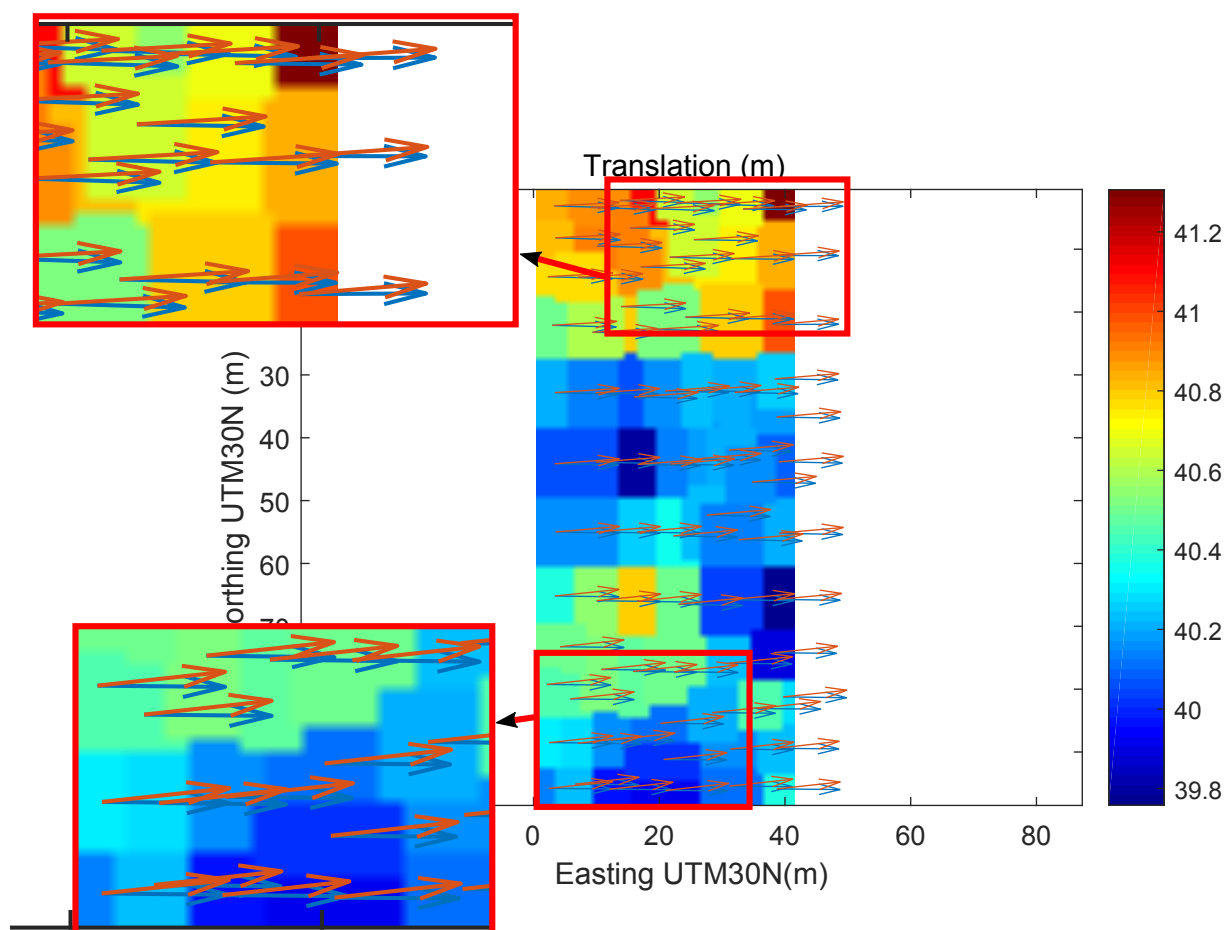


FIGURE 9.17: Migration and deformation vectors for each vertex cluster.

9.4 Conclusion

The automatic study of dune dynamics at the scale of a dune is a complex problem that, to the best of our knowledge, has not been tackled. Existing procedures are generally based on crest displacements or on the modeling of dunes as periodic patterns. Moreover, dune dynamics is often reduced to a simple migration, and structural deformation is omitted. Typically, the migration rate and direction are not estimated for each dune.

This problem may be thought of as a registration problem. The study of registration methods is the subject of numerous publications, because it finds applications in many domains. Two main types of registration algorithms are distinguished: the iconic and symbolic methods. The first category proved maladapted to the analysis of dune dynamics, but symbolic approaches appeared more suited.

An algorithm for the quantification of the dynamics of dunes has been sketched. This starts with a dune-to-dune correspondence procedure, introducing a new parameter, the maximum migration distance, for which the choice of parameters value is pretty loose and simple. A fine tuning would simply accelerate the computations.

The implementation of a non-rigid registration algorithm (Huang et al., 2008) showed that using symbolic algorithms is an encouraging possibility for the analysis of dune dynamics. It is capable of properly aligning two meshes representing the same dune, and allows a facilitated visualization of dune dynamics, and the definitions of new metrics for the quantification of this dynamics.

In addition, the dune-to-dune correspondence can support other dynamical descriptors derived from the changes of the values of the morphological descriptors. These results are promising, but the algorithm has still to be fully implemented and validated on entire dunefields. Improvements can be made to the registration part to adapt, even more, the results to the dune dynamics. For instance, the clustering of the dune made by the algorithm is very important for the visualization and the quantification of the dynamics. This step can certainly be adapted so that the number of clusters really reflected the dynamics of a dune.

Chapter 10

Conclusion

Contents

10.1 Summary of the thesis	230
10.2 Contributions	231
10.3 Future work	233

10.1 Summary of the thesis

The objective of this work is to design automated methods for the quantitative analysis of dune morphology and dynamics. Where our approach differs from existing automatic algorithms is that the estimation of the morphological and dynamical descriptors must be made for each dune. In order to achieve this goal, the work can be divided into two steps: a reliable extraction of crests and feet of dunes, and the quantification of dune shapes and their time evolution.

The two steps are achieved with automated tools. Currently, only manual delineation and analysis of dunes can provide descriptors for each dune. Compared to manual processing, automated tools reduce subjectivity, always handle the data in the same way and save valuable human time. Furthermore, if dunes have already been extracted and registered, the computations of new descriptors or of descriptors with a different definition is very fast. Manual processing would demand passing through each dune of the dataset. Therefore, the comparisons of the values of descriptors automatically estimated between dunes or between dunefields is more reliable.

A first dune extraction algorithm was developed. The results show that a geomorphometry-based, region-growing algorithm is a possible approach to extracting dunes. The extraction can be decomposed into two steps: a crest extraction and a growing phase. Problems at both levels were observed. The usual representation of the seafloor as a gridded DTM is not ideal in this context. It was advantageously replaced by 3D meshes in order to extract correctly dune crests that are the starting point of the region-growing process.

The extraction of dune crests requires the estimation of differential quantities (curvature and their derivatives). The comparisons of methods for the estimation of curvatures led to the conclusion that Casal's approach is the most suited method for dune crest extraction. To reach this conclusion, a quantitative comparison framework was proposed and applied to reference methods instead of the usual visual comparisons. However, others crests, especially of ripples, were extracted too. The notion of scale was introduced in geomorphometry to explain the fact that terrain structures are perceived differently according to the scale at which they are considered.

From this concept emerged the idea of adapting the mesh resolution in order to facilitate the extraction of the dune crests. A mesh simplification algorithm was designed to modify the resolution of the mesh so that the sets of extracted crests only contain dune crests. All these steps led to the implementation of a dune extraction algorithm that was successfully tested on a large benchmark.

Once dunes have been extracted, the morphology is known, but the dynamics have still to be quantified. Dune dynamics can be summarized as the changes in the location and shape of a dune. This is similar to a problem of registration that aims at best aligning two surfaces or images. The idea is to deform and move a dune so that its morphologies at different times match. The different morphologies are the results of step 1 (dune extraction). Two family of registration methods have been investigated : Iconic and Symbolic.

It was concluded that the use of iconic methods for dunes is inappropriate. Iconic methods were shown to be incapable of dealing with the complexity of the seafloor variations caused by dunes. Dunes can form periodic patterns and are very alike, which may cause an iconic method based on a correlation metrics to determine a wrong migration vector. In other cases, dunes do not migrate in the same direction at the same speed. The distances between the dunes having changed, an iconic method is unable to deal with various migrations. In addition, the best that could have been obtained is the registration of patches of bathymetry while the aim is to analyze the dynamics at the scale of a dune.

Symbolic methods perform better, as shown in Chapter 9. The tested non-rigid algorithm (Huang et al., 2008) enabled an improved visualization and the quantification of dune dynamics. On this basis, an algorithm directly using the results of dune extraction was outlined for the quantification of dune dynamics. Encouraging preliminary results on experimental data demonstrate that this approach is a good candidate for the analysis of dune dynamics.

10.2 Contributions

The main contribution of this thesis is a new method to automatically extract dunes. This algorithm has a major importance as the quantitative analyses of dune morphology and dynamics rely on it. The designed algorithm combines the observations and results of Chapters 4,5,6 and 7. The method first extracts dune crests and then extends normally (outwards) to delineate the feet of the dunes.

The second contribution of this thesis is to show that symbolic methods are better suited for monitoring dune dynamics than iconic. Although the presented algorithm for the analysis of dune dynamics has not been extensively tested on the full database, results on limited experimental data sets are very promising; the algorithm was able to register two representations of the same dune. The registration is achieved via a non-rigid (isometric) mesh registration method. The clustering step of the algorithm enables visualization and quantification of the internal dynamics of a dune. This automatic approach seems well suited for the quantitative monitoring of the time evolution of dune location and shape.

Automatic methods are controlled by parameters, but users do not always have the scientific background to understand their roles. Consequently, a particular effort has been made both in reducing the number of control (tuning) parameters and in making these parameters easily-understandable for the users. The set of user-friendly parameters has been reduced to two for the dune extraction algorithm: minimum dune length and minimum dune width.

Papers

This work resulted in three scientific articles in conferences and symposiums with peer reviewing:

- Ogor, J., Debese, N., Zerr, B., Garlan, T. (2015). Detection and description of sand dunes using geomorphometric approach. *Seabed and Sediment Acoustics: Measurements and Modelling, organized by the Underwater Acoustics Group of the Institute of Acoustics, University of Bath, UK 7-9 September 2015*
- Ogor, J., Zerr, B. (2016a). Towards the automation of sand dune detection in the bathymetry. *MARID (Marine and River Dune Dynamics) Conference V 2016, Bangor University, Bangor, Gwynedd, LL57 2DG (North Wales, UK)*
- Ogor, J., Zerr, B. (2016b). Comparisons of crest line extraction algorithms applied to marine dunes. *OCEANS'2016, MTS/IEEE, Monterey, California, USA – September 19-23, 2016*

Prior to the start of the thesis, I have been part of research on King scallops that led to the following publication:

Nicolle, A., Moitié, R., OGOR, J., Dumas, F., Foveau, A., Foucher E., and Thié-baut, E. Modelling larval dispersal of *Pecten maximus* in the English Channel: a tool for the spatial management of the stocks. *ICES Journal of Marine Science*, 74(6):1812–1825, July 2017.

10.3 Future work

The algorithms presented in the thesis are a great effort towards the automation of the quantitative dune analysis. But, these methods can be improved.

Although the dune extraction algorithm was tested on a large variety of cases (dune types, organization, mesh resolution), further tests on larger datasets are necessary to confirm its robustness. The designed algorithms ought to be used for the processing of the whole available database in the short term.

In order to improve the results of the algorithms, modifications can already be foreseen. The mesh simplification step can be improved to better preserve the features (*e.g.*, dune crests) of the surface. If observations on the quality of the extracted dune crests are made, procedures to merge, extend or split the crests might tackle the issues. The mesh simplification could also be applied more than once. In cases where dunes have varying dimensions, the mesh resolution might have to be modified so that the crests are extracted at appropriate scales.

The list of morphological descriptors computed by our algorithm is limited to the classic ones. Others can be added to this list. For instance, barkhan or trochoidal dunes could be differentiated from the others using descriptors of the shape of the crest. The scouring areas at the extremities of a trochoidal dune are a significant characteristic that might be quantified by a descriptor.

The dynamics algorithm must be implemented entirely and tested before considering any modifications. But, a potential improvement would be to end up with clusters that are significant from a dynamics perspective. The clustering of Huang's algorithm takes into account the flatness of the cluster which is not relevant for the study of dune dynamics. Similarly to the analysis of the morphology, the first proposed dynamics descriptors might be complemented or replaced by alternatives.

The problem of mesh construction is out of the scope of the thesis. Nevertheless, the construction of the meshes from DTMs is not ideal. Meshes can be constructed directly from the depth soundings. Methods of mesh construction are capable of generating surfaces where large terrain variations are described by numerous vertices and flat areas are covered by only a few vertices. This could help in preserving the dune crests while reducing the size of the output mesh. This would certainly facilitate the extraction of the dune. A great review of these techniques is made in Campos Dausa (2014).

Another aspect of the study of dunes that has not been addressed is the question of uncertainty. Since associating uncertainties to the morphological and dynamical descriptors estimated by the algorithms is not a trivial issue that might not be solved, but the uncertainty of the bathymetric data can, at least, be estimated. The problem of estimation of the uncertainty of soundings has been frequently discussed (Lurton, 2010). Several methods have been designed for this purpose (Hare et al., 2011, Lawes, 2013, Lucieer et al., 2016). The whole quantification of dune morphology and dynamics is based on the bathymetric data. Comparing the descriptor values to the uncertainties of the depth measurements is essential to conclude as to their reliability.

All these improvements would lead to a better analysis and quantification of dune morphology and its changes in time. The use of these automatic algorithms would enable consideration of both the morphology and the dynamics. This could yield conclusions on existing relationships between morphology and dynamics and the relevance of a new classification combining both aspects.

With the automatic algorithms, the analysis could be extended to dunefields. The dynamics and morphology of a dune may be compared with these of its neighbors in order to understand the mechanisms controlling the complex dunefields. The general idea is that automatic methods could help geoscientists making a major step forward in the understanding of dunes.

Bibliography

- Abdelmalek, N. N. (1990). Algebraic error analysis for surface curvatures and segmentation of 3-D range images. *Pattern Recognition*, 23(8), 807–817. 113
- Agarwal, P. K. & Desikany, P. K. (1997). An Efficient Algorithm for Terrain Simplification. In *SODA '97 Proceedings of the eighth annual ACM-SIAM symposium on Discrete algorithms*. 160, 163
- Albani, M., Klinkenberg, B., Andison, D. W., & Kimmins, J. P. (2004). The choice of window size in approximating topographic surfaces from digital elevation models. *International Journal of Geographical Information Science*, 18(6), 577–593. 72
- Andrews, B. D., Brothers, L. L., & Barnhardt, W. A. (2010). Automated feature extraction and spatial organization of seafloor pockmarks, Belfast Bay, Maine, USA. *Geomorphology*, 124(1), 55–64. 87
- Ashley, G. M. (1990). Classification of large-scale subaqueous bedforms; a new look at an old problem. *Journal of Sedimentary Research*, 60(1), 160–172. 27
- Barnard, P. L., Hanes, D. M., Rubin, D. M., & Kvitek, R. G. (2006). Giant sand waves at the mouth of San Francisco Bay. *Eos, Transactions American Geophysical Union*, 87(29), 285–289. 30, 37
- Bartholdy, J., Flemming, B. W., Bartholomä, A., & Ernstsen, V. B. (2005). Flow and grain size control of depth-independent simple subaqueous dunes. *J. Geophys. Res.*, 110(F4), F04S16. 15, 16, 30, 31
- Benz, U. C., Hofmann, P., Willhauck, G., Lingenfelder, I., & Heynen, M. (2004). Multi-resolution, object-oriented fuzzy analysis of remote sensing data for GIS-ready information. *ISPRS Journal of Photogrammetry and Remote Sensing*, 58(3–4), 239–258. 64
- Berger, M. & Gostiaux, B. (1987). *Géométrie différentielle: variétés, courbes et surfaces*. Presses universitaires de France. Google-Books-ID: bkPvAAAAMAAJ. 100

- Berti, M., Corsini, A., & Daehne, A. (2013). Comparative analysis of surface roughness algorithms for the identification of active landslides. *Geomorphology*, 182, 1–18. 66
- Besio, G., Blondeaux, P., Brocchini, M., Hulscher, S. J. M. H., Idier, D., Knaapen, M. A. F., Németh, A. A., Roos, P. C., & Vittori, G. (2008). The morphodynamics of tidal sand waves: A model overview. *Coastal Engineering*, 55(7–8), 657–670. 40
- Besio, G., Blondeaux, P., Brocchini, M., & Vittori, G. (2004). On the modeling of sand wave migration. *J. Geophys. Res.*, 109(C4), C04018. 14, 39
- Besl, P. J. & McKay, N. D. (1992). A method for registration of 3-d shapes. *IEEE Transactions on Pattern Analysis and Machine Intelligence*, 14(2), 239–256. 210
- Blondeaux, P., Brocchini, M., & Vittori, G. (2001). A model for sand waves generation. *University of Genova, Genova, Itália*. 14, 39
- Blondeaux, P. & Vittori, G. (2016). A model to predict the migration of sand waves in shallow tidal seas. *Continental Shelf Research*, 112, 31–45. 39
- Boothroyd, J. C. & Hubbard, D. K. (1974). *Bed Form Development and Distribution Pattern, Parker and Essex Estuaries, Massachusetts*. Technical report, MASSACHUSETTS UNIV AMHERST COASTAL RESEARCH CENTER, MASSACHUSETTS UNIV AMHERST COASTAL RESEARCH CENTER. 27
- Boothroyd, J. C. & Hubbard, D. K. (1975). Genesis of bedforms in mesotidal estuaries. In L. E. Cronin (Ed.), *Geology and Engineering* (pp. 217–234). Academic Press. DOI: 10.1016/B978-0-12-197502-9.50018-6. 27
- Borsje, B. W., Besio, G., Hulscher, S., Blondeaux, P., & Vittori, G. (2008). Exploring biological influence on offshore sandwave length. In *Marine and River Dune Dynamic III, International Workshop* (pp. 1–3). 40
- Boubekeur, T. & Alexa, M. (2009). Mesh simplification by stochastic sampling and topological clustering. *Computers & Graphics*, 33(3), 241–249. 162
- Brown, B. & Rusinkiewicz, S. (2007). Global non-rigid alignment of 3-D scans. *ACM Transactions on Graphics (Proc. SIGGRAPH)*, 26(3). 211
- Budd, C., Huang, P., Klaudiny, M., & Hilton, A. (2013). Global non-rigid alignment of surface sequences. *International Journal of Computer Vision*, 102(1), 256–270. 212

- Burrough, P. A., van Gaans, P. F. M., & MacMillan, R. A. (2000). High-resolution landform classification using fuzzy k-means. *Fuzzy Sets and Systems*, 113(1), 37–52. 79
- Calder, B. & Rice, G. (2011). Design and Implementation of an Extensible Variable Resolution Bathymetric Estimator. *U.S. Hydrographic Conference*. 46
- Calder, B. R. & Mayer, L. A. (2003). Automatic processing of high-rate, high-density multibeam echosounder data. *Geochemistry, Geophysics, Geosystems*, 4(6), 1048. 46
- Calder, B. R. & Wells, D. E. (2006). Cube user guide. (pp. 46). 46
- Campos Dausa, R. (2014). *Surface Reconstruction Methods for Seafloor Modelling*. PhD thesis, University of Girona. 234
- Carling, Williams, Götz, & Kelsey (2000). The morphodynamics of fluvial sand dunes in the River Rhine, near Mainz, Germany. II. Hydrodynamics and sediment transport. *Sedimentology*, 47(1), 253–278. 14, 29, 39
- Cataño-Lopera, Y. A., Abad, J. D., & García, M. H. (2009). Characterization of bedform morphology generated under combined flows and currents using wavelet analysis. *Ocean Engineering*, 36(9–10), 617–632. 14, 36
- Cazals, F., Faugere, J.-C., Pouget, M., & Rouillier, F. (2008). Ridges and umbilics of polynomial parametric surfaces. In *Geometric modeling and algebraic geometry* (pp. 141–159). Springer. 126, 127
- Cazals, F., Faugère, J.-C., Pouget, M., & Rouillier, F. (2006). The implicit structure of ridges of a smooth parametric surface. *Computer Aided Geometric Design*, 23(7), 582–598. 126, 127, 128
- Cazals, F. & Pouget, M. (2004). Ridges and umbilics of a sampled smooth surface: a complete picture gearing toward topological coherence. 145
- Cazals, F. & Pouget, M. (2005a). Estimating differential quantities using polynomial fitting of osculating jets. *Computer Aided Geometric Design*, 22(2), 121–146. 112, 113, 121
- Cazals, F. & Pouget, M. (2005b). Topology driven algorithms for ridge extraction on meshes. 132, 142
- Chen, X. & Schmitt, F. (1992). Intrinsic surface properties from surface triangulation. In *Computer Vision—ECCV'92* (pp. 739–743).: Springer. 111, 113, 117

- Chui, H. & Rangarajan, A. (2003). A new point matching algorithm for non-rigid registration. *Computer Vision and Image Understanding*, 89(2-3), 114–141. 203, 210
- Cignoni, P., Montani, C., & Scopigno, R. (1998). A comparison of mesh simplification algorithms. *Computers & Graphics*, 22(1), 37–54. 161, 164
- Cohen-steiner, D. & Morvan, J.-m. (2003). Restricted Delaunay triangulations and normal cycle. In *In: ACM Symposium on Computational Geometry*. 108
- Csákány, P. & Wallace, A. M. (2000). Computation of local differential parameters on irregular meshes. In *The mathematics of surfaces IX* (pp. 19–33). Springer. 114
- Cutter Jr, G. R., Rzhanov, Y., & Mayer, L. A. (2003). Automated segmentation of seafloor bathymetry from multibeam echosounder data using local Fourier histogram texture features. *Journal of Experimental Marine Biology and Ecology*, 285, 355–370. 66, 79
- de Berg, M. & Dobrindt, K. T. (1995). On levels of detail in terrains, Department of Computer Science, Utrecht University, PO Box 80.089, 3508 TB Utrecht, the Netherlands. 159, 160
- De Moor, G. (2002). Évaluation de la morphodynamique sous-marine en Mer du Nord méridionale au cours de la période 1985-1995/Evaluation of sea-floor sediment dynamics in the Flemish Banks (southern North Sea) between 1985 and 1995. *Géomorphologie: relief, processus, environnement*, 8(2), 135–150. 37
- Debese, N., Jacq, J.-J., & Garlan, T. (2016). Extraction of sandy bedforms features through geodesic morphometry. *Geomorphology*, 268, 82–97. 126, 129
- Debese, N., Moitié, R., & Seube, N. (2012). Multibeam echosounder data cleaning through a hierarchic adaptive and robust local surfacing. *Computers & Geosciences*, 46(Supplement C), 330–339. 46
- DeCarlo, D., Finkelstein, A., Rusinkiewicz, S., & Santella, A. (2003). Suggestive contours for conveying shape. *ACM Transactions on Graphics (TOG)*, 22(3), 848–855. 126
- Degrendele, K., Roche, M., Schotte, P., Van Lancker, V. R., Bellec, V. K., & Bonne, W. M. (2010). Morphological evolution of the Kwinte Bank central depression before and after the cessation of aggregate extraction. *Journal of Coastal Research*, (pp. 77–86). 31, 37

- Desbrun, M., Meyer, M., & Alliez, P. (2002). Intrinsic parameterizations of surface meshes. In *Computer Graphics Forum*, volume 21 (pp. 209–218).: Wiley Online Library. 110
- Desbrun, M., Meyer, M., Schröder, P., & Barr, A. H. (2000). Discrete differential-geometry operators in nD. *preprint, the Caltech Multi-Res Modeling Group*. 110, 113, 114, 116
- Di Angelo, L. & Di Stefano, P. (2010). continuities detection in triangular meshes. *Computer-Aided Design*, 42(9), 828–839. 130
- Dikau, R., Heidelberg, Mark, R. K., Pike, R. J., Park, M., & Brabb, E. E. (1995). Morphometric landform analysis of New Mexico. 79
- Diop, E. H. S., Boudraa, A. O., Khenchaf, A., Thibaud, R., & Garlan, T. (2008). Multiscale characterization of bathymetric images by empirical mode decomposition. *MARID III, Leeds, UK*. 35
- Do Carmo, M. P. (1976). *Differential geometry of curves and surfaces*, volume 2. Prentice-hall Englewood Cliffs. xvii, 100, 106, 107
- Dodd, N., Blondeaux, P., Calvete, D., De Swart, H. E., Falqués, A., Hulscher, S. J., Różyński, G., & Vittori, G. (2003). Understanding coastal morphodynamics using stability methods. *Journal of coastal research*, (pp. 849–865). 28
- Dohmen-Janssen, C. M. & Hulscher, S. J. M. H. (2008). *River, coastal, and estuarine morphodynamics: RCEM 2007 : proceedings of the 5th IAHR Symposium on River, Coastal, and Estuarine Morphodynamics, Enschede, the Netherlands, 17-21 September 2007*. London; New York: Taylor & Francis. 14, 39
- dOleire Oltmanns, S., Eisank, C., Dragut, L., & Blaschke, T. (2013). An Object-Based Workflow to Extract Landforms at Multiple Scales From Two Distinct Data Types. *IEEE Geoscience and Remote Sensing Letters*, 10(4), 947–951. 86
- Dorst, L. L. (2004). geodetic deformation analysis: new method for the estimation of seabed dynamics. In *Proceedings of MARID II Conference*. 34
- Dorst, L. L., Roos, P. C., & Hulscher, S. (2007). ESTIMATION OF SAND WAVE DYNAMICS IN THE SOUTHERN NORTH SEA. In *Proceedings of the 30th International Conference of Coastal Engineering (ICCE), San Diego, California, USA, 3-8 September 2006*. 34, 38

- Douros, I. & Buxton, B. F. (2002). Three-Dimensional Surface Curvature Estimation using Quadric Surface Patches. In *Presented at: Scanning 2002 Proceedings. (2002)*. 111
- Dragut, L. & Eisank, C. (2011). Object representations at multiple scales from digital elevation models. *Geomorphology*, 129(3), 183–189. 64, 86
- Drăguț, L. & Blaschke, T. (2006). Automated classification of landform elements using object-based image analysis. *Geomorphology*, 81(3-4), 330–344. 86
- Drăguț, L., Tiede, D., & Levick, S. R. (2010). ESP: a tool to estimate scale parameter for multiresolution image segmentation of remotely sensed data. *International Journal of Geographical Information Science*, 24(6), 859–871. 64
- Duffy, G. P. & Hughes-Clarke, J. E. (2005). Application of spatial cross correlation to detection of migration of submarine sand dunes. *J. Geophys. Res.*, 110(F4), F04S12. 38
- Dyer, K. R. & Huntley, D. A. (1999). The origin, classification and modelling of sand banks and ridges. *Continental Shelf Research*, 19(10), 1285–1330. 28
- Dymond, J. R., Derose, R. C., & Harmsworth, G. R. (1995). Automated mapping of land components from digital elevation data. *Earth Surf. Process. Landforms*, 20(2), 131–137. 79
- Dyn, N., Hormann, K., Kim, S.-J., & Levin, D. (2001). *Mathematical methods for curves and surfaces: Oslo 2000*. Innovations in applied mathematics. Nashville: Vanderbilt University Press, 1st ed edition. 108, 109, 113, 116
- Ehsani, A. H. & Quiel, F. (2008). Geomorphometric feature analysis using morphometric parameterization and artificial neural networks. *Geomorphology*, 99(1–4), 1–12. 79
- Eisank, C., Smith, M., & Hillier, J. (2014). Assessment of multiresolution segmentation for delimiting drumlins in digital elevation models. *Geomorphology*, 214, 452–464. 64, 86
- Ernstsen, V. B., Noormets, R., Winter, C., Bartholomä, A., Flemming, B. W., & Bartholdy, J. (2004). Development of subaqueous barchan dunes due to lateral grain size variability. In *Hulscher JMH, Garlan T. & Idier D.(Eds), Marine Sandwave and River Dune Dynamics, International Workshop. Enschede (Pays-Bas)* (pp. 80–87). 14, 30, 37, 219

- Evans, I. S. (1972). General geomorphometry, derivatives of altitude, and descriptive statistics. (pp. 17–90). 61
- Evans, I. S. (1980). An integrated system of terrain analysis and slope mapping. *Zeitschrift für Geomorphologie, Supplementband*, (pp. 274–295). 67
- Evans, I. S. (2012). Geomorphometry and landform mapping: What is a landform? *Geomorphology*, 137(1), 94–106. 61
- Farin, G. (2001). *Curves and Surfaces for CAGD: A Practical Guide*. Elsevier. Google-Books-ID: 0GFWCkvpobcC. 100
- Ferret, Y., Le Bot, S., Tessier, B., Garlan, T., & Lafite, R. (2010). Migration and internal architecture of marine dunes in the eastern English Channel over 14 and 56 year intervals: the influence of tides and decennial storms. *Earth Surf. Process. Landforms*, 35(12), 1480–1493. 14, 30
- Fisher, P., Wood, J., & Cheng, T. (2004). Where is Helvellyn? Fuzziness of multi-scale landscape morphometry. *Transactions of the Institute of British Geographers*, 29(1), 106–128. 64, 79
- Fitzgibbon, A. W. (2003). Robust registration of 2d and 3d point sets. *Image and Vision Computing*, 21(13–14), 1145–1153. 211
- Flemming, B. W. (2000). The role of grain size, water depth and flow velocity as scaling factors controlling the size of subaqueous dunes. In *Marine Sandwave Dynamics, International Workshop* (pp. 23–24). 30
- Florinsky, I. V. (1998). Accuracy of local topographic variables derived from digital elevation models. *International Journal of Geographical Information Science*, 12(1), 47–62. 64
- Flynn, P. & Jain, A. (1989). On reliable curvature estimation. In , *IEEE Computer Society Conference on Computer Vision and Pattern Recognition, 1989. Proceedings CVPR '89* (pp. 110–116). 110
- Franzetti, M., Le Roy, P., Delacourt, C., Garlan, T., Cancouët, R., Sukhovich, A., & Deschamps, A. (2013). Giant dune morphologies and dynamics in a deep continental shelf environment: Example of the banc du four (Western Brittany, France). *Marine Geology*, 346(Supplement C), 17–30. 19, 30, 37, 38

- Gafeira, J., Long, D., & Diaz-Doce, D. (2012). Semi-automated characterisation of seabed pockmarks in the central North Sea. *Near Surface Geophysics*, 10(4), 303–314. 87
- Garcia, M. H. & Best, J. L. (2012). *Characterization of Bed Morphodynamics Using Multibeam Echo Sounding (MBES) and Wavelet Transform (WT) Analysis*. Technical report, DTIC Document. 36
- Garlan, T. (2004). *Apports de la modélisation dans l'étude de la sédimentation marine récente*. PhD thesis, Université de Lille. 217
- Garlan, T. (2009). Gis and mapping of moving marine sand dunes. *Proceedings ICC2009, Santiago, Chili*. 28, 31
- Garlan, T., Cartier, A., Franzetti, M., Le Roy, P., Duarte, J., Pombo, J., Peix, M., Guyomard, P., Le Faou, Y., Gabelotaud, I., & others (2013). Complex morphology and organisation of dunes in a giant dunes field. *Proceedings of MARID 2013*, (pp. 113–118). 30
- Garland, M. (1999). *Quadric-based polygonal surface simplification*. PhD thesis, Georgia Institute of Technology. 160, 162, 163
- Gatzke, T. D. & Grimm, C. M. (2006). Estimating curvature on triangular meshes. *International journal of shape modeling*, 12(01), 1–28. 114, 123, 124
- Ge, X. (2016). Non-rigid registration of 3d point clouds under isometric deformation. *ISPRS Journal of Photogrammetry and Remote Sensing*, 121, 192–202. 210, 211
- Gläser, P., Haase, I., Oberst, J., & Neumann, G. A. (2013). Co-registration of laser altimeter tracks with digital terrain models and applications in planetary science. *Planetary and Space Science*, 89, 111–117. 203, 205
- Gold, S., Rangarajan, A., Lu, C.-P., Pappu, S., & Mjolsness, E. (1998). New algorithms for 2d and 3d point matching: pose estimation and correspondence. *Pattern Recognition*, 31(8), 1019–1031. 210
- Goldfeather, J. & Interrante, V. (2004). A novel cubic-order algorithm for approximating principal direction vectors. *ACM Transactions on Graphics (TOG)*, 23(1), 45–63. 110, 111, 112, 113, 114, 121

- Goldgof, D. B., Huang, T. S., & Lee, H. (1989). A curvature-based approach to terrain recognition. *IEEE Transactions on Pattern Analysis and Machine Intelligence*, 11(11), 1213–1217. 203
- González, C., Gumbau, J., Chover, M., Ramos, F., & Quirós, R. (2009). User-assisted simplification method for triangle meshes preserving boundaries. *Computer-Aided Design*, 41(12), 1095–1106. 167
- Graff, L. H. (1992). *Automated classification of basic-level terrain features in digital elevation models*. Technical report, DTIC Document. 86
- Grosse, P., van Wyk de Vries, B., Euillades, P. A., Kervyn, M., & Petrinovic, I. A. (2012). Systematic morphometric characterization of volcanic edifices using digital elevation models. *Geomorphology*, 136(1), 114–131. 83
- Guala, M., Singh, A., BadHeartBull, N., & Foufoula-Georgiou, E. (2014). Spectral description of migrating bed forms and sediment transport. *Journal of Geophysical Research: Earth Surface*, 119(2), 123–137. 35
- Guo, Y.-w., Peng, Q.-s., Hu, G.-f., & Wang, J. (2005). Smooth feature line detection for meshes. *Journal of Zhejiang University SCIENCE*, 6A(5), 460–468. 126
- Gutierrez, R. R., Abad, J. D., Parsons, D. R., & Best, J. L. (2013). Discrimination of bed form scales using robust spline filters and wavelet transforms: Methods and application to synthetic signals and bed forms of the Río Paraná, Argentina. *J. Geophys. Res. Earth Surf.*, 118(3), 1400–1418. 36
- Guyonic, S., Mory, M., Wever, T. F., Arduin, F., & Garlan, T. (2007). Full-Scale Mine Burial Experiments in Wave and Current Environments and Comparison With Models. *IEEE Journal of Oceanic Engineering*, 32(1), 119–132. 40
- Hagbi, N. & El-Sana, J. (2010). Carving for topology simplification of polygonal meshes. *Computer-Aided Design*, 42(1), 67–75. 160
- Hamann, B. (1993). Curvature Approximation for Triangulated Surfaces. In P. D. G. Farin, P. D. H. Noltemeier, P. D. H. Hagen, & P. D. W. Knödel (Eds.), *Geometric Modelling*, number 8 in Computing Supplementum (pp. 139–153). Springer Vienna. DOI: 10.1007/978-3-7091-6916-2_10. 111, 113, 118, 121
- Hamann, B. (1994). A data reduction scheme for triangulated surfaces. *Computer Aided Geometric Design*, 11(2), 197 – 214. 161, 164

- Hammond, E. H. (1964). Analysis of properties in land form geography: an application to broad-scale land form mapping. *Annals of the Association of American Geographers*, 54, 11–19. 65, 70
- Hardy, R., Shugar, D., Parsons, D., Lane, S., Orfeo, O., Best, J., & Kostaschuk, R. (2006). Morphology, flow and sediment transport over a natural 3d dune field: Rio parana, argentina. In E. Alves, A. Cardoso, J. Leal, & R. Ferreira (Eds.), *River Flow 2006*. Taylor & Francis. DOI: 10.1201/9781439833865.ch105. 14, 29, 30
- Hare, R., Eakins, B., & Amante, C. (2011). Modelling bathymetric uncertainty. *The International Hydrographic Review*, (6). 234
- Heckbert, P. S. & Garland, M. (1997). *Survey of polygonal surface simplification algorithms*. Technical report, DTIC Document. 160, 161, 162
- Heckbert, P. S. & Garland, M. (1999). Optimal triangulation and quadric-based surface simplification. *Computational Geometry*, 14(1), 49–65. 160, 163
- Hesse, M. & Gavrilova, M. L. (2003). An efficient algorithm for real-time 3d terrain walkthrough. In *International Conference on Computational Science and Its Applications* (pp. 751–761): Springer. 159
- Hilaga, M., Shinagawa, Y., Kohmura, T., & Kunii, T. L. (2001). Topology matching for fully automatic similarity estimation of 3d shapes. In *Proceedings of the 28th annual conference on Computer graphics and interactive techniques* (pp. 203–212): ACM. 203, 205
- Hildebrandt, K. & Polthier, K. (2004). Anisotropic Filtering of Non-Linear Surface Features. In *Computer Graphics Forum*, volume 23 (pp. 391–400): Wiley Online Library. 110
- Hildebrandt, K., Polthier, K., & Wardetzky, M. (2005). Smooth Feature Lines on Surface Meshes. In *Symposium on geometry processing* (pp. 85–90). 131
- Hoppe, H. (1996). Progressive meshes. In *Proceedings of the 23rd annual conference on Computer graphics and interactive techniques* (pp. 99–108): ACM. 160, 162
- Horn, B. K. P. (1981). Hill shading and the reflectance map. *Proceedings of the IEEE*, 69(1), 14–47. 69

- Hosseinbor, A. P., Zhdanov, R., & Ushveridze, A. (2017). A New Point-set Registration Algorithm for Fingerprint Matching. *arXiv:1702.01870 [cs]*. arXiv: 1702.01870. 203, 210
- Huang, Q.-X., Adams, B., Wicke, M., & Guibas, L. J. (2008). Non-Rigid Registration Under Isometric Deformations. *Computer Graphics Forum*, 27(5), 1449–1457. 209, 211, 218, 227, 231
- Hubeli, A. & Gross, M. (2001). Multiresolution feature extraction for unstructured meshes. In *Visualization, 2001. VIS '01. Proceedings* (pp. 287–294). 129
- Hulscher, S. J. M. H., de Swart, H. E., & de Vriend, H. J. (1993). The generation of offshore tidal sand banks and sand waves. *Continental Shelf Research*, 13(11), 1183–1204. 14, 39
- Hunter, G. J. & Goodchild, M. F. (1997). Modeling the Uncertainty of Slope and Aspect Estimates Derived from Spatial Databases. *Geographical Analysis*, 29(1), 35–49. 64
- Idier, D. (2002). *Dynamique des bancs et dunes de sable du plateau continental : observation in-situ et modélisation numérique*. PhD thesis. Thèse de doctorat dirigée par Astruc, Dominique Sciences de la Terre et environnement Toulouse, INPT 2002. 14, 39
- Interrante, V., Fuchs, H., & Pizer, S. (1995). Enhancing transparent skin surfaces with ridge and valley lines. In *Proceedings of the 6th conference on Visualization'95* (pp. 52): IEEE Computer Society. 126
- Ismail, K., Huvenne, V. A., & Masson, D. G. (2015). Objective automated classification technique for marine landscape mapping in submarine canyons. *Marine Geology*, 362, 17–32. 79
- Iuricich, F., Fugacci, U., & De Floriani, L. (2015). Topologically-consistent simplification of discrete Morse complex. *Computers & Graphics*, 51, 157–166. 158
- Iwahashi, J. & Pike, R. J. (2007). Automated classifications of topography from DEMs by an unsupervised nested-means algorithm and a three-part geometric signature. *Geomorphology*, 86(3–4), 409–440. 78, 79
- Jenny, B., Jenny, H., & Hurni, L. (2011). Terrain Generalization with Multi-scale Pyramids Constrained by Curvature. *Cartography and Geographic Information Science*, 38(2), 110–116. 60

- Jiang, L., Tang, G., Liu, K., & Yang, J. (2013). Extraction of drainage network from grid terrain datasets using parallel computing. In *Computational Intelligence and Design (ISCID), 2013 Sixth International Symposium on*, volume 1 (pp. 240–243).: IEEE. 83
- Johnson, A. E. (1997). *Spin-images: a representation for 3-D surface matching*. PhD thesis, Citeseer. 203, 204
- Johnson, A. E. & Hebert, M. (1998). Control of Polygonal Mesh Resolution for 3-D Computer Vision. *Graphical Models and Image Processing*, 60(4), 261–285. 158, 165
- Kalogerakis, E., Nowrouzezahrai, D., Simari, P., & Singh, K. (2009). Extracting lines of curvature from noisy point clouds. *Computer-Aided Design*, 41(4), 282–292. 126
- Kim, C., Son, H., & Kim, C. (2013). Fully automated registration of 3d data to a 3d CAD model for project progress monitoring. *Automation in Construction*, 35, 587–594. 203, 209, 210, 211
- Kim, S.-J., Kim, C.-H., & Levin, D. (2002). Surface simplification using a discrete curvature norm. *Computers & Graphics*, 26(5), 657–663. 161, 163
- Kim, S.-K. & Kim, C.-H. (2005). Finding ridges and valleys in a discrete surface using a modified MLS approximation. *Computer-Aided Design*, 37(14), 1533–1542. 130, 145
- Kleinhans, M. (2004). Experimental dune trough scour in sediment mixtures. *Proc. of Marine Sandwave and River Dune Dynamics, 1-2 April 2004, Enschede, the Netherlands*. 27
- Klingseisen, B., Metternicht, G., & Paulus, G. (2008). Geomorphometric landscape analysis using a semi-automated GIS-approach. *Environmental Modelling & Software*, 23(1), 109–121. 78
- Knaapen, M. A. F. (2004). Measuring sand wave migration in the field. Comparison of different data sources and an error analysis. In *Proceedings of the 2nd international workshop on Marine Sand Wave and River Dune Dynamics, Enschede, The Netherlands, University of Twente, Enschede, The Netherlands*. 38
- Knaapen, M. a. F. (2005). Sandwave migration predictor based on shape information. *J. Geophys. Res.*, 110(F4), F04S11. 19, 38
- Knaapen, M. a. F., Henegouw, C. N. v. B., & Hu, Y. Y. (2005). Quantifying bedform migration using multi-beam sonar. *Geo-Mar Lett*, 25(5), 306–314. 38

- Kobbelt, L., Campagna, S., & Seidel, H.-P. (1998). A general framework for mesh decimation. In *Graphics interface*, volume 98 (pp. 43–50). 163
- Kobbelt, L., Vorsatz, J., & Seidel, H.-P. (1999). Multiresolution hierarchies on unstructured triangle meshes. *Computational Geometry*, 14(1), 5–24. 162
- Kudelski, D. (2011). *Détection automatique d'objets géologiques à partir de données numériques d'affleurements 3D*. PhD thesis, Aix Marseille 1. 126, 132
- Lawes, G. (2013). Architecture independent vertical tpu estimation for multibeam sonar processing. In *Proceedings of U.S. hydro 2013 Conference*. 234
- Le Bot, S., Idier, D., Garlan, T., Trentesaux, A., & Astruc, D. (2000). Dune dynamics: from field measurements to numerical modelling. Application to bathymetric survey frequency in the Calais-Dover Strait. *Marine Sandwave Dynamics*, (pp. 101–108). 39, 40
- Lecours, V., Lucieer, V. L., Dolan, M. F. J., & Micallef, A. (2015). An ocean of possibilities: applications and challenges of marine geomorphometry. *Geomorphometry for geosciences, International Society for Geomorphometry, Poznań, Poland*, (pp. 23–26). 60
- Lee, A. W., Sweldens, W., Schröder, P., Cowsar, L., & Dobkin, D. (1998). MAPS: Multiresolution adaptive parameterization of surfaces. In *Proceedings of the 25th annual conference on Computer graphics and interactive techniques* (pp. 95–104).: ACM. 158, 163
- Lee, C. H., Varshney, A., & Jacobs, D. W. (2005). Mesh saliency. In *ACM transactions on graphics (TOG)*, volume 24 (pp. 659–666).: ACM. 161
- Lee, H. & Kyung, M.-H. (2016). Parallel mesh simplification using embedded tree collapsing. *The Visual Computer*, 32(6-8), 967–976. 165
- Lefebvre, A. & Lyons, A. (2011). Quantification of roughness for seabed characterization. In *Proc. of 4th Intern. Conf. and Exhib. on UAM, Kos Island, Greece, 20-24 June 2011, 8 p.* 36, 66
- Lesage, P. L. & Visvalingam, M. (2002). Towards sketch-based exploration of terrain. *Computers & Graphics*, 26(2), 309–328. 126

- Li, H., Sumner, R. W., & Pauly, M. (2008). Global Correspondence Optimization for Non-Rigid Registration of Depth Scans. *Computer Graphics Forum*, 27(5), 1421–1430. 203, 209, 210
- Li, W. & Song, P. (2015). A modified ICP algorithm based on dynamic adjustment factor for registration of point cloud and CAD model. *Pattern Recognition Letters*, 65, 88–94. 211
- Lindenbergh, R. (2004). Parameter estimation and deformation analysis of sand waves and mega ripples. In *Proceedings of the 2nd international workshop on Marine Sand Wave and River Dune Dynamics, Enschede, The Netherlands, University of Twente, Enschede, The Netherlands*. 34
- Lindstrom, P. & Pascucci, V. (2002). Terrain simplification simplified: A general framework for view-dependent out-of-core visualization. *IEEE Transactions on Visualization and Computer Graphics*, 8(3), 239–254. 159
- Lisimenka, A. & Kubicki, A. (2017). Estimation of dimensions and orientation of multiple riverine dune generations using spectral moments. *Geo-Marine Letters*, 37(1), 59–74. 36
- Lisimenka, A. & Rudowski, S. (2013). Bedform characterization in river channel through 2d spectral analysis. In *MARID Conference IV, in Bruges (Belgium)*. 29, 35
- Little, J. J. & Shi, P. (2014). Structural Lines, TINs, and DEMs. *Algorithmica*, 30(2), 243–263. 126
- Lucieer, V., Huang, Z., & Siwabessy, J. (2016). Analyzing uncertainty in multibeam bathymetric data and the impact on derived seafloor attributes. *Marine Geodesy*, 39(1), 32–52. 234
- Lurton, X. (2010). *An Introduction to Underwater Acoustics: Principles and Applications*. Springer Praxis Books. Springer Berlin Heidelberg. 234
- Lévy, B., Petitjean, S., Ray, N., & Maillot, J. (2002). Least squares conformal maps for automatic texture atlas generation. In *ACM Transactions on Graphics (TOG)*, volume 21 (pp. 362–371).: ACM. 126
- Lyons, A., Fox, W., Hasiotis, T., & Pouliquen, E. (2002). Characterization of the two-dimensional roughness of wave-rippled sea floors using digital photogrammetry. *IEEE Journal of Oceanic Engineering*, 27(3), 515–524. 35

- Ma, X., Keates, S., Jiang, Y., & Kosinka, J. (2015). Subdivision surface fitting to a dense mesh using ridges and umbilics. *Computer Aided Geometric Design*, 32, 5–21. 162
- Max, N. (1999). Weights for Computing Vertex Normals from Facet Normals. *Journal of Graphics Tools*, 4(2), 1–6. 111
- Maximo, A., Velho, L., & Siqueira, M. (2014). Adaptive multi-chart and multiresolution mesh representation. *Computers & Graphics*, 38, 332–340. 158, 160
- McAdoo, B. G., Pratson, L. F., & Orange, D. L. (2000). Submarine landslide geomorphology, US continental slope. *Marine Geology*, 169(1), 103–136. 60
- McIvor, A. M. & Valkenburg, R. J. (1997). A comparison of local surface geometry estimation methods. *Machine Vision and Applications*, 10(1), 17–26. 114
- McKee, E. D. (1979). *A study of global sand seas*. USGS Numbered Series 1052, U.S. Govt. Print. Off.,. 26
- Meek, D. S. & Walton, D. J. (2000). On surface normal and Gaussian curvature approximations given data sampled from a smooth surface. *Computer Aided Geometric Design*, 17(6), 521–543. 108, 109, 113, 116
- Mehnert, A. & Jackway, P. (1997). An improved seeded region growing algorithm. *Pattern Recognition Letters*, 18(10), 1065–1071. 86
- Melis, M. T., Mundula, F., Dessì, F., Cioni, R., & Funedda, A. (2014). Tracing the boundaries of Cenozoic volcanic edifices from Sardinia (Italy): a geomorphometric contribution. *Earth Surface Dynamics*, 2(2), 481–492. 83
- Meng, M. & He, Y. (2016). Consistent quadrangulation for shape collections via feature line co-extraction. *Computer-Aided Design*, 70, 78–88. 162
- Miliaresis, G. & Argialas, D. (1998). Physiographic feature extraction from moderate resolution digital elevation data. In *24th International Conference of the Remote Sensing Society, Greenwich (UK), Sept* (pp. 9–11). 86
- Minár, J. & Evans, I. S. (2008). Elementary forms for land surface segmentation: The theoretical basis of terrain analysis and geomorphological mapping. *Geomorphology*, 95(3), 236–259. 77

- Mohrig, B. M. D. & Blom, A. (2008). Determining Characteristic Scales for the Dynamics and Geometry of Sandy Bedforms. *Proceedings of MARID, 1-3 April 2008, Leeds, UK*. 32, 38
- Monga, O., Benayoun, S., & Faugeras, O. D. (1992). From partial derivatives of 3-D density images to ridge lines. In *1992 IEEE Computer Society Conference on Computer Vision and Pattern Recognition, 1992. Proceedings CVPR '92* (pp. 354–359). 130
- Monier, P. (1997). *Caractérisation du terrain en vue de son traitement numérique. Application à la généralisation de l'orographie*. PhD thesis, Louis Pasteur, Strasbourg. 60
- Mosher, D. C., Thomson, R. E., & others (2000). Massive submarine sand dunes in the eastern Juan de Fuca Strait, British Columbia. In *Marine Sandwave Dynamics, International Workshop, Université de Lille 1, 23-24 mars 2000* (pp. 131–142). 14, 30, 37
- Nabi, M. A. (2008). Three-dimensional model of detailed hydrodynamics for simulation of subaqueous dunes. *Marine and River Dune Dynamics III, edited by DR Parsons et al*, (pp. 235–240). 14, 39
- Nicolas, F., Arnold-Bos, A., Quidu, I., & Zerr, B. (2016). Fast fourier-based block-matching algorithm for non-rigid sonar tracks registration in a multi-resolution framework. In *MOQESM - Quantitative Monitoring of Underwater Environment, Brest, France*. 203, 206
- Németh, A. A., Hulscher, S. J., & de Vriend, H. J. (2000). Migration of sand waves in shallow shelf seas. *Proceedings of MARID Conference, Lille, 2000*. 14, 39
- Németh, A. A., Hulscher, S. J. M. H., & de Vriend, H. J. (2002). Modelling sand wave migration in shallow shelf seas. *Continental Shelf Research*, 22(18–19), 2795–2806. 39
- O'Callaghan, J. F. & Mark, D. M. (1984). The extraction of drainage networks from digital elevation data. *Computer Vision, Graphics, and Image Processing*, 28(3), 323–344. 83
- Oksanen, J. (2006). *Digital elevation model error in terrain analysis*. PhD thesis, University of Helsinki, Faculty of Science, Department of Geography and Finnish Geodetic Institute. 64

- Oksanen, J. & Sarjakoski, T. (2005). Error propagation of DEM-based surface derivatives. *Computers & Geosciences*, 31(8), 1015–1027. 64
- Padfield, D. (2012). Masked Object Registration in the Fourier Domain. *IEEE Transactions on Image Processing*, 21(5), 2706–2718. 203, 205
- Pajarola, R. & Gobbetti, E. (2007). Survey of semi-regular multiresolution models for interactive terrain rendering. *The Visual Computer*, 23(8), 583–605. 162
- Pauly, M., Keiser, R., & Gross, M. (2003). Multi-scale Feature Extraction on Point-Sampled Surfaces. *Computer Graphics Forum*, 22(3), 281–289. 129
- Payan, F., Roudet, C., & Sauvage, B. (2015). Semi-Regular Triangle Remeshing: A Comprehensive Study. *Computer Graphics Forum*, 34(1), 86–102. 162
- Pennec, X., Ayache, N., & Thirion, J.-P. (2000). Landmark-based registration using features identified through differential geometry. In I. Bankman (Ed.), *Handbook of Medical Imaging - Processing and Analysis. I.* (pp. 499–513). Academic Press. 126
- Pennec, X., Cachier, P., & Ayache, N. (1999). Understanding the “Demon’s Algorithm”: 3d Non-rigid Registration by Gradient Descent. In *Medical Image Computing and Computer-Assisted Intervention – MICCAI’99* (pp. 597–605).: Springer, Berlin, Heidelberg. 203, 204, 209
- Petitjean, S. (2002). A Survey of Methods for Recovering Quadrics in Triangle Meshes. *ACM Comput. Surv.*, 34(2), 211–262. 113
- Pike, R. (1995). Geomorphometry - progress, practice and prospect. *Zeitschrift für Geomorphologie*, Supplementband 101, 221–238. 60
- Pike, R. J. (1988). The geometric signature: Quantifying landslide-terrain types from digital elevation models. *Math Geol*, 20(5), 491–511. 62, 64
- Pike, R. J., Evans, I. S., & Hengl, T. (2009). Geomorphometry: A brief guide. *Developments in Soil Science*, 33, 3–30. 62, 64, 65
- Porter-Smith, R., Lyne, V. D., Kloser, R. J., & Lucieer, V. L. (2012). Catchment-based classification of Australia’s continental slope canyons. *Marine Geology*, 303, 183–192. 84
- Pouget, M. (2005). *Geometry of surfaces: from the estimation of local differential quantities to the robust extraction of global differential*. PhD thesis, INRIA Sophia Antipolis. 132

- Pratson, L. F. & Ryan, W. B. (1996). Automated drainage extraction in mapping the Monterey submarine drainage system, California margin. *Marine Geophysical Researches*, 18(6), 757–777. 84
- P.W. Cazenave, D. L. & Dix, J. (2008). Quantitative bedform analysis using decimetre resolution swath bathymetry. 33, 35, 36
- Raper, J. (1989). *Three Dimensional Applications In GIS*. CRC Press. 79
- Reeve, D. E., Horrillo-Caraballo, J. M., & Magar, V. (2008). Statistical analysis and forecasts of long-term sandbank evolution at Great Yarmouth, UK. *Estuarine, Coastal and Shelf Science*, 79(3), 387–399. 35
- Reinhard, K. (1998). Multiresolution representations for surfaces meshes based on the vertex decimation method. *Computers & Graphics*, 22(1), 13–26. 158, 160, 161, 163
- Robert W. Dalrymple, R. J. K. & Lambiase, J. J. (1978). Bedforms and their hydraulic stability relationships in a tidal environment, Bay of Fundy, Canada. *Nature*, (pp. 100–104). 27
- Roche, M., Degrendele, K., De Mol, L., Milano, R., Van den Branden, R., & De Schep- per, G. (2013). Essential facts of the monitoring of the sand extraction and its impact on the Flemish banks on the Belgian continental shelf from 2003 to 2012. *Marine and River Dune Dynamics–MARID IV–15 &*, 16, 223–230. 31
- Romstad, B. a. (2001). Improving relief classification with contextual merging. In *ScanGIS* (pp. 3–13): Citeseer. 78
- Rossl, C., Kobbelt, L., & Seidel, H.-P. (2000). Extraction of feature lines on triangulated surfaces using morphological operators. In *Proceedings of the AAAI Symposium on Smart Graphics* (pp. 71–75). 130
- Rouhani, M., Boyer, E., & Sappa, A. D. (2014). Non-rigid registration meets surface reconstruction. In *2014 2nd International Conference on 3D Vision*, volume 1 (pp. 617–624). 212
- Rowbotham, D. N. & Dudycha, D. (1998). GIS modelling of slope stability in Phewa Tal watershed, Nepal. *Geomorphology*, 26(1–3), 151–170. 60
- Rueckert, D., Frangi, A. F., & Schnabel, J. A. (2001). Automatic Construction of 3d Statistical Deformation Models Using Non-rigid Registration. In *Medical Image Computing and Computer-Assisted Intervention – MICCAI 2001* (pp. 77–84): Springer, Berlin, Heidelberg. 203, 210

- Rusinkiewicz, S. (2004). Estimating curvatures and their derivatives on triangle meshes. In *3D Data Processing, Visualization and Transmission, 2004. 3DPVT 2004. Proceedings. 2nd International Symposium on* (pp. 486–493).: IEEE. 113, 119
- Rusu, R. B., Blodow, N., & Beetz, M. (2009). Fast Point Feature Histograms (FPFH) for 3d registration. In *2009 IEEE International Conference on Robotics and Automation* (pp. 3212–3217). 210
- Sacharow, A., Balzer, J., Biermann, D., & Surmann, T. (2011). Non-rigid isometric ICP: A practical registration method for the analysis and compensation of form errors in production engineering. *Computer-Aided Design*, 43(12), 1758–1768. 210, 211
- Santamaría, J., Cordon, O., & Damas, S. (2011). A comparative study of state-of-the-art evolutionary image registration methods for 3d modeling. *Computer Vision and Image Understanding*, 115(9), 1340–1354. 204, 211
- Schmidt, J. & Andrew, R. (2005). Multi-scale landform characterization. *Area*, 37(3), 341–350. 64, 79
- Schmidt, J. & Hewitt, A. (2004). Fuzzy land element classification from DTMs based on geometry and terrain position. *Geoderma*, 121(3–4), 243–256. 79
- Schnur, S., Escartin, J., Purves, R. S., Frueh-Green, G. L., & Soule, S. A. (2011). Automatic Fault Extraction at Mid-Ocean Ridges: Effects of Bathymetry Resolution and Extraction Method. In *AGU Fall Meeting Abstracts*, volume 1 (pp.08). 83
- Schnur, S. R. (2011). *Assessing the Effects of Extraction Method and Resolution on the Accuracy of Automatic Fault Extraction at Mid-Ocean Ridges*. PhD thesis, Geographisches Institut der Universität Zürich. 83
- Schroeder, W. J., Zarge, J. A., & Lorensen, W. E. (1992). Decimation of Triangle Meshes. In *Proceedings of the 19th Annual Conference on Computer Graphics and Interactive Techniques*, SIGGRAPH '92 (pp. 65–70). New York, NY, USA: ACM. 161, 163
- Scalaroff, S. & Pentland, A. P. (1995). Modal matching for correspondence and recognition. *IEEE Transactions on Pattern Analysis and Machine Intelligence*, 17(6), 545–561. 211
- Shapiro, L. S. & Michael Brady, J. (1992). Feature-based correspondence: an eigenvector approach. *Image and Vision Computing*, 10(5), 283–288. 209

- Shary, P. A., Sharaya, L. S., & Mitusov, A. V. (2002). Fundamental quantitative methods of land surface analysis. *Geoderma*, 107(1–2), 1–32. 65
- Smith, D. P., Kvitek, R., Iampietro, P. J., & Wong, K. (2007). Twenty-nine months of geomorphic change in upper Monterey Canyon (2002–2005). *Marine Geology*, 236(1), 79–94. 37
- Southard, J. B. & Boguchwal, L. A. (1990). Bed configuration in steady unidirectional water flows; Part 2, Synthesis of flume data. *Journal of Sedimentary Research*, 60(5), 658–679. 27
- Stokely, E. & Wu, S. (1992). Surface parametrization and curvature measurement of arbitrary 3-D objects: five practical methods. *IEEE Transactions on Pattern Analysis and Machine Intelligence*, 14(8), 833–840. 108, 109
- Strobl, J. (1999). *Angewandte geographische Informationsverarbeitung Beiträge zum AGIT-Symposium Salzburg 1999*. Heidelberg: Wichmann. 86
- Stylianou, G. & Farin, G. (2004). Crest lines for surface segmentation and flattening. *IEEE Transactions on Visualization and Computer Graphics*, 10(5), 536–544. 126, 130, 134
- Tang, H., Shu, H. Z., Dillenseger, J. L., Bao, X. D., & Luo, L. M. (2007). Moment-based metrics for mesh simplification. *Computers & Graphics*, 31(5), 710–718. 163
- Taubin, G. (1995). Estimating the tensor of curvature of a surface from a polyhedral approximation. In , *Fifth International Conference on Computer Vision, 1995. Proceedings* (pp. 902–907). 112, 113
- Tevs, A., Bokeloh, M., Wand, M., Schilling, A., & Seidel, H. P. (2009). Isometric registration of ambiguous and partial data. In *2009 IEEE Conference on Computer Vision and Pattern Recognition* (pp. 1185–1192). 209
- Thakur, A., Banerjee, A. G., & Gupta, S. K. (2009). A survey of CAD model simplification techniques for physics-based simulation applications. *Computer-Aided Design*, 41(2), 65–80. 162
- Thibaud, R., Del Mondo, G., Garlan, T., Mascaret, A., & Carpentier, C. (2013). A Spatio-Temporal Graph Model for Marine Dune Dynamics Analysis and Representation. *Transactions in GIS*, 17(5), 742–762. 29, 38

- Thirion, J.-P. (1996). New Feature Points Based on Geometric Invariants for 3d Image Registration. *Int. J. Comput. Vision*, 18(2), 121–137. 126
- Trevisani, S., Cavalli, M., & Marchi, L. (2012). Surface texture analysis of a high-resolution DTM: Interpreting an alpine basin. *Geomorphology*, 161–162, 26–39. 79
- Tribe, A. (1992). Problems in automated recognition of valley features from digital elevation models and a new method toward their resolution. *Earth Surf. Process. Landforms*, 17(5), 437–454. 84
- Tubau, X., Lastras, G., Canals, M., Micallef, A., & Amblas, D. (2013). Significance of the fine drainage pattern for submarine canyon evolution: The Foix Canyon System, Northwestern Mediterranean Sea. *Geomorphology*, 184, 20–37. 84
- van Asselen, S. & Seijmonsbergen, A. C. (2006). Expert-driven semi-automated geomorphological mapping for a mountainous area using a laser DTM. *Geomorphology*, 78(3–4), 309–320. 86
- van der Mark, C. F. & Blom, A. (2007). *A new & widely applicable bedform tracking tool*. Technical report, CE&M Research Report 2007R-003/WEM-002., Faculty of Engineering Technology, University of Twente. 32, 35
- Van Dijk, T. A. G. P. & Lindenbergh, R. C. (2017). Methods for Analysing Bedform Geometry and Dynamics. In J. Guillén, J. Acosta, F. L. Chiocci, & A. Palanques (Eds.), *Atlas of Bedforms in the Western Mediterranean* (pp. 7–13). Cham: Springer International Publishing. DOI: 10.1007/978-3-319-33940-5_2. 32
- van Dijk, T. A. G. P., Lindenbergh, R. C., & Egberts, P. J. P. (2008). Separating bathymetric data representing multiscale rhythmic bed forms: A geostatistical and spectral method compared. *J. Geophys. Res.*, 113(F4), F04017. 35
- Van Lancker, V. R., Bonne, W., Velegrakis, A. F., & Collins, M. B. (2010). Aggregate extraction from tidal sandbanks: Is dredging with nature an option? Introduction. *Journal of Coastal Research*, (pp. 53–62). 31
- Van Landeghem, K., Besio, G., Niemann, H., Mellett, C., Huws, D., Steinle, L., O'Reilly, S., Croker, P., Hodgson, D., Williams, D., & others (2013). Amplified Sediment waves in the Irish Sea (AmSedIS). In *Van Lancker, V. and Garlan, T. Ed., 4th Conference MARID. Bruges, Belgium, VLIZ Special Publication*, volume 65 (pp. 338p). 14, 30

- Vera, R. M., Bonne, W., Garel, E., Degrendele, K., Roche, M., Van den Eynde, D., Bellec, V., Brière, C., Collins, M. B., & Velegrakis, A. F. (2010). Recommendations for the sustainable exploitation of tidal sandbanks. *Journal of Coastal Research*, (pp. 151–164). 31
- Vidal, V., Wolf, C., & Dupont, F. (2011). Robust feature line extraction on CAD triangular meshes. In *International Conference on Computer Graphics Theory and Applications* Algarve, Portugal. 129
- W. Hallinan, P., Gordon, G., Yuille, A. L., Giblin, P., & Mumford, D. (1999). Two- and Three-Dimensional Patterns of the Face. 126
- Wang, D., Laffan, S. W., Liu, Y., & Wu, L. (2010). Morphometric characterisation of landform from DEMs. *International Journal of Geographical Information Science*, 24(2), 305–326. 79
- Wang, G., Wang, Z., Chen, Y., & Zhao, W. (2015). A robust non-rigid point set registration method based on asymmetric gaussian representation. *Computer Vision and Image Understanding*, 141, 67–80. 210
- Watanabe, K. & Belyaev, A. G. (2001). Detection of Salient Curvature Features on Polygonal Surfaces. *Computer Graphics Forum*, 20(3), 385–392. 130, 134
- Weber, C., Hahmann, S., & Hagen, H. (2010). Sharp feature detection in point clouds. In *Shape Modeling International Conference (SMI), 2010* (pp. 175–186). 128
- Wood, J. (1996). *the geomorphological characterisation of Digital Elevation Models*. PhD thesis, University of Lancaster, UK. 64, 67, 80
- Xu, J., Wong, F. L., Kvittek, R., Smith, D. P., & Paull, C. K. (2008). Sandwave migration in Monterey Submarine Canyon, Central California. *Marine Geology*, 248(3-4), 193–212. 19, 37
- Yang, H., Wang, F., Li, Z., & Dong, H. (2015). Simultaneous Pose and Correspondence Estimation Based on Genetic Algorithm. *International Journal of Distributed Sensor Networks*, 11(11), 828241. 203, 211
- Yoshizawa, S., Belyaev, A., Yokota, H., & Seidel, H.-P. (2008). Fast, robust, and faithful methods for detecting crest lines on meshes. *Computer Aided Geometric Design*, 25(8), 545–560. 132

- Zeng, Y., Wang, C., Wang, Y., Gu, X., Samaras, D., & Paragios, N. (2010). Dense non-rigid surface registration using high-order graph matching. In *2010 IEEE Computer Society Conference on Computer Vision and Pattern Recognition* (pp. 382–389). 212
- Zevenbergen, L. W. & Thorne, C. R. (1987). Quantitative analysis of land surface topography. *Earth Surface Processes and Landforms*, 12(1), 47–56. 69, 70
- Zhang, K., Yang, F., Zhao, C., & Feng, C. (2016). Using robust correlation matching to estimate sand-wave migration in Monterey Submarine Canyon, California. *Marine Geology*, 376, 102–108. 38
- Zheng, P., Belaton, B., Liao, I. Y., & Rajion, Z. A. (2011). The Gradient of the Maximal Curvature Estimation for Crest Lines Extraction. In H. B. Zaman, P. Robinson, M. Petrou, P. Olivier, T. K. Shih, S. Velastin, & I. Nyström (Eds.), *Visual Informatics: Sustaining Research and Innovations*, number 7066 in Lecture Notes in Computer Science (pp. 196–205). Springer Berlin Heidelberg. 130
- Zhou, Q. & Liu, X. (2004). Analysis of errors of derived slope and aspect related to DEM data properties. *Computers & Geosciences*, 30(4), 369–378. 64
- Zitová, B. & Flusser, J. (2003). Image registration methods: a survey. *Image and Vision Computing*, 21(11), 977–1000. 203